UNIVERSITY OF CALIFORNIA, SAN DIEGO

Postsynthetic Modification of Metal-Organic Frameworks

A dissertation submitted in partial satisfaction of the

requirements for the degree Doctor of Philosophy

in

Chemistry

by

Kristine Kimie Tanabe

Committee in charge:

Professor Seth M. Cohen, Chair
Professor Michael J. Sailor
Professor Jan B. Talbot
Professor F. Akif Tezcan
Professor Roger Y. Tsien

2011

The Dissertation of Kristine Kimie Tanabe is approved, and it is acceptable in quality and form for publication on microfilm and electronically:

_____

_____

_____

_____

_____

Chair

University of California, San Diego

2011

DEDICATION

To Mariano

Thank you for always being by my side.

TABLE OF CONTENTS

LIST OF SYMBOLS AND ABBREVIATIONS

α	Alpha
Å	Angstrom
$Å^3$	Cubic Ångstrøm
AA	Atomic Absorption
acac	Acetylacetonate
AM	Amide
Ar	Argon
atm	atmosphere (1 atm = 101.325 kPa)
β	Beta
BET	Brunauer-Emmett-Teller
BDC	Benzenedicarboxylic acid
Bn	Benzyl
BTB	4,4′,4″-benzene-1,3,5-triyl-tribenzoic acid
°C	Degrees Celsius
ca.	Calculated
CAT	Catechol
$CDCl_3$	Deuterated chloroform
$CHCl_3$	Chloroform
CD_2Cl_2	Deuterated methylene chloride
CH_2Cl_2	Methylene chloride
CH_4	Methane
CH_3CN	Acetonitrile

CO_2	Carbon Dioxide
δ	Chemical shift; ppm
°	Degree
d	Doublet (NMR)
d^6-DMSO	Deuterated DMSO
DABCO	1,4-Diazabicyclo[2.2.2]octane
DCl	Deuterated hydrochloric acid
DEF	Diethylformamide
DMF	Dimethylformamide
DMOF	DABCO-MOF
DMSO	Dimethylsulfoxide
ESI-MS	Electrospray Ionization mass spectrometry
Et_2O	Diethyl ether
γ	Gamma
g	Gram
h	Hour
H_2	Hydrogen
ΔH_{ads}	Heat of adsorption
HCl	Hydrochloric acid
H_2O	Water, hydrate
H_2SO_4	Sulfuric acid
Hz	Hertz
J	Coupling constant

K	Kelvin
κ	kappa
K_2CO_3	Potassium Carbonate
KOH	Potassium Hydroxide
λ	Lambda; wavelength; nm
m	Multiplet
M	Molar; mol L-1
mg	Miligram
μL	Microliter
μm	Micrometers
mL	Mililiter
mm	Milimeter
mmol	Milimol
mmHg	Milimeters mercury
MHz	MegaHertz
MeOH	Methanol
MIL	Material Institut Lavoisier
MOF	Metal-Organic Framework
MS	Mass spectrometry
MTV	Multivariate
$MgSO_4$	Magnesium Sulfate
N_2	Dinitrogen
$NaHCO_3$	Sodium Bicarbonate

NaOH	Sodium Hydroxide
nm	Nanometer
NMR	Nuclear Magnetic Resonance spectroscopy
PCP	Porous coordination polymer
Ph	Phenyl
PSD	Postsynthetic deprotection
PSM	Postsynthetic modification
pz	Pyrazine
PXRD	Powder X-ray diffraction
RT	Room temperature
s	Singlet (NMR)
sal	Salicylate
SBU	Secondary Building Uni
SiO_2	Silica
θ	Theta
t	Triplet
TGA	Thermal gravimetric analysis
THF	Tetrahydrofuran
TLC	Thin Layer Chromatography
UMCM	University of Michigan Crystalline Material
UV/VIS	Ultra-Violet/Visible
wt%	Weight percent
XRD	X-ray diffraction

LIST OF FIGURES

LIST OF SCHEMES

LIST OF TABLES

ACKNOWLEDGEMENTS

For the record, I am not very good with words. In this case, words would not be able to fully express how grateful I am.

First, I would like to thank my advisor, Prof. Seth Cohen. Thank you for letting me join your lab and for giving me a chance. I know I haven't shown it or said it much over the years, but I appreciate all that you have done for me. You've always pushed (and nagged) me to do my best, and at the same time, you left me alone and trusted me to get the work done. I'd like to think a good balance was achieved in the end.

I would also like to thank all the past and present Cohen lab members who have helped me throughout the years. I am honored to have worked with a very talented group of individuals. Jana, Faith, Misha, Jay, Vishakha, Loi, and Sara, thank you for all your help and friendship during the early years. Min, Phuong, Kevin, Jamie, Dave, and Corinne, thank you for bringing amusement to the lab. Arpita, Sergio, Rick, Joe, Christophe, Matthieu, Jen, and Jody, thank you for your input as scientists and company as friends. It has been great to work with a group of people who are passionate about what they do and believe in. I'll always have great memories of our coffee walks and lively conversations that left me flabbergasted to laughing until my sides hurt. I'd like to especially thank Rick for teaching me anything and everything about MOFs. I wouldn't be where I am today without your guidance and patience. I'd like to also thank Arpita for being a great friend and work spouse from the very beginning, and Joe for always taking time to help me out and lending an ear to listen.

I would like to thank those who helped me get to grad school and helped me with my research. Thank you Prof. Patrick Farmer for taking me on as an undergraduate

research student. I owe a big thanks to Dr. Szeman 'Z' Ng for taking the time to train me and for encouraging me to go to grad school. Thank you Prof. Arnie Rheingold, Dr. Antonio DiPasquale and Dr. Curtis Moore for assisting me with X-ray crystallography. Thank you Dr. Y Su for all your help with mass spectrometry and instrument troubleshooting.

Lastly, I would like to thank my family and friends for sticking by me all these years and for their support. To my family, thank you for your love and for putting up with my scatterbrained habits. To my friends, thank you for your encouragement and for making me laugh even when I was down. Kelly, thank you for all those times you listened to me ramble and for keeping my spirits up. Mariano, words can't describe how lucky I am to have you in my life. You've been my biggest fan throughout all of grad school, even if it meant you had to come second to research. It means a lot to me. I am beyond excited to start the next phase of our lives together.

Text, schemes, and figures in Chapters 1, 2, 3, 4, 5, 6, in part, are reprints of the materials published in the following papers: Tanabe K. K., Wang, Z., Cohen, S. M. "Systematic Functionalization of a Metal-Organic Framework via a Postsynthetic Modification Approach" *J. Am. Chem. Soc*. **2008**, *130*, 8508-8517; Wang, Z., Tanabe K. K., Cohen, S. M. "Accessing Postsynthetic Modification in a Series of Metal-Organic Frameworks and the Influence of Framework Topology on Reactivity" *Inorg. Chem.* **2009**, *48*, 296-306; Wang, Z., Tanabe K. K., Cohen, S. M. "Tuning Hydrogen Sorption Properties of Metal-Organic Frameworks by Postsynthetic Covalent Modification" *Chem. Eur. J.* **2010**, *16*, 212 – 217; Tanabe, K. K., Cohen, S. M. "Engineering a Metal–Organic Framework Catalyst by using Postsynthetic Modification" *Angew. Chem. Int. Ed.* **2009**,

48, 7424-7427; Tanabe, K. K., Cohen, S. M. “Modular, Active, Robust Lewis Acid Catalyst supported on a Metal-Organic Framework.” *Inorg. Chem.* **2010**, *49*, 6766-6774; Tanabe, K. K., Allen, C. A., Cohen, S. M. "Photochemical Activation of a Metal–Organic Framework to Reveal Functionality” *Angew. Chem. Int. Ed.* **2010**, *49*, 9730-9733; and Tanabe, K. K., Cohen, S. M. “Postsynthetic Modification of Metal-Organic Frameworks – A Progress Report.” *Chem. Soc. Rev.* **2011**, *40*, 498-519. The dissertation author was the primary researcher and either primary or co-author for the data presented. The co-authors listed in these publications also participated in the research. The permissions to reproduce these papers were granted by the American Chemical Society, Wiley-VCH Verlag GmbH & Co. KGaA, Weinheim, and the Royal Society of Chemistry.

VITA AND PUBLICATIONS

Education

2011	Doctor of Philosophy, Chemistry, University of California, San Diego, La Jolla, CA
2007	Master of Science, Chemistry, University of California, San Diego, La Jolla, CA
2005	Bachelor of Science, Chemistry, University of California, Irvine, Irvine, CA

Research Awards and Affliations

2011	ACS Division of Inorganic Chemistry Young Investigator Award recipient
2004-2005	Undergraduate Research Opportunities Program (UROP) award recipient, University of California, Irvine, Advisor: Patrick J. Farmer
2002-present	American Chemical Society Member

Publications

1. **Tanabe, K. K.**, Cohen, S. M. "Postsynthetic Modification of Metal-Organic Frameworks – A Progress Report." *Chem. Soc. Rev.* **2011**, *40*, 498-519.

2. **Tanabe, K. K.**, Allen, C. A., Cohen, S. M. "Photochemical Activation of a Metal-Organic Framework to Reveal Functionality." *Angew. Chem. Int. Ed.* **2010**, *49*, 9730-9733 (selected as a 'Hot Article' by *Angew. Chem. Int. Ed*. and highlighted by *Chemical and Engineering News* Nov. 22, 2010)

3. **Tanabe, K. K.**, Cohen, S. M. "Modular, Active, Robust Lewis Acid Catalyst supported a Metal-Organic Framework." *Inorg. Chem.* **2010**, *49*, 6766-6774

4. Nguyen, J. G., **Tanabe, K. K.**, Cohen, S. M. "Postsynthetic Diazeniumdiolate Formation and NO Release from MOFs" *CrystEngComm* **2010**, *12*, 2335-2338 (invited contribution, highlighted in *Highlights in Chemical Technology* Apr. 13, 2010)

5. **Tanabe, K. K.**, Cohen, S. M. "Engineering a Metal–Organic Framework Catalyst by using Postsynthetic Modification" *Angew. Chem. Int. Ed.* **2009**, *48*, 7424-7427

(selected as a 'Hot Article' by *Angew. Chem. Int. Ed*.; highlighted in *Chemistry World* Sept. 7, 2009)

6. Wang, Z., **Tanabe K. K.**, Cohen, S. M. "Tuning Hydrogen Sorption Properties of Metal-Organic Frameworks by Postsynthetic Covalent Modification" *Chem. Eur. J.* 2010, *16*, 212 – 217

7. Garibay, S. J., Wang, Z., **Tanabe K. K.**, Cohen, S. M. "Postsynthetic Modification: A Versatile Approach Toward Multifunctional Metal-Organic Frameworks" *Inorg. Chem.* 2009, *48*, 7341-7349

8. Wang, Z., **Tanabe K. K.**, Cohen, S. M. "Accessing Postsynthetic Modification in a Series of Metal-Organic Frameworks and the Influence of Framework Topology on Reactivity" *Inorg. Chem.* **2009**, *48*, 296-306

9. **Tanabe K. K.**, Wang, Z., Cohen, S. M. "Systematic Functionalization of a Metal-Organic Framework via a Postsynthetic Modification Approach" *J. Am. Chem. Soc*. **2008**, *130*, 8508-8517

ABSTRACT OF THE DISSERTATION

Postsynthetic Modification of Metal-Organic Frameworks

By

Kristine Kimie Tanabe

Doctor of Philosophy in Chemistry

University of California, San Diego, 2011

Professor Seth M. Cohen, Chair

Metal-organic frameworks (MOFs) are porous crystalline materials that are built from metal ions or metal ion clusters and organic ligands. There has been much interest in designing functionalized MOFs with enhanced host-guest interactions for potential applications in gas storage, catalysis, and separation. However, it has remained a challenge to synthesize functionalized MOFs directly through traditional MOF synthesis. This dissertation focuses on the development of postsynthetic modification (PSM) as a method for functionalizing MOFs. A systematic overview of PSM will be presented to highlight PSM as a general, versatile approach for enhancing the physical and chemical properties of MOFs.

In the first half of this dissertation, IRMOF-3, an amino-containing MOF, is modified with a series of alkyl anhydrides, and the effects of reagent size on modification

extent are explored. In the next chapter, other amino-containing MOFs systems (DMOF-1-NH_2 and UMCM-1-NH_2) are synthesized and modified using PSM. Through this study, PSM is shown to be a practical approach for functionalizing MOFs, and also indicates MOF topology can influence the modification outcome. The second half of this dissertation focuses on using PSM to develop MOFs for gas storage and catalysis applications. IRMOF-3, DMOF-1-NH_2, and UMCM-1-NH_2 are modified and tested for H_2 storage. The MOFs are modified with certain functionalities (e.g., alkyl vs. aromatic) to determine if H_2 uptake and heat of adsorption is improved. In a separate study, UMCM-1-NH_2 is modified with metal binding substituents, and is metallated with different metal ions to generate a series of potential Lewis acid MOF catalysts. The metallated UMCM MOFs are tested for the Mukaiyama aldol reaction and for epoxide ring opening catalysis, and the catalytic results are presented.

Lastly, a new functionalization technique, named postsynthetic deprotection (PSD), is introduced. Two new BDC ligands are synthesized with photolabile protecting groups and are incorporated into MOFs. The MOFs are then exposed to UV light, which results in the removal of the photolabile groups to produce MOFs with free, uncoordinated hydroxyl groups. This is the first example of using light to unmask functionalities in a MOF, and presents a novel route for obtaining MOFs with more complex functionalities.

Chapter 1 Introduction

1.1 Metal-Organic Frameworks

Metal-organic frameworks (MOFs) are 2D or 3D porous, crystalline materials that consist of metal ions or metal ion clusters and multidentate organic ligands.[1,2] MOFs, which are also referred to as porous coordination polymers (PCPs)[3], generally have uniform pores, exhibit high surface areas, and have good thermal stability.[4-8] Many MOFs have been constructed using metals across the periodic table (e.g., alkali,[9,10] transition metals,[4,7,11] group 13,[12] lanthanides[13]) and a wide variety of ligands with different metal binding groups (e.g., cyanides, pyridyls, carboxylates, sulfonates, phosphates, and imidazoles[14-16]). Coordination complexes (e.g., dipyrrins[17], porphyrins[18]) and ligands with pendant substituents (e.g., -Br, $-NH_2$, $-CH_3$)[11] have also been explored to create MOFs with unique topologies and functionalities. Within the last two decades, a wide range of topologically diverse MOFs have been synthesized with varying pore sizes and pore volumes from the different combinations of metals and ligands.

MOFs are commonly prepared from one-pot, solvothermal reactions with the metal ion and organic ligand dissolved in a high-boiling, polar solvent. IRMOF-1 (Isoreticular Metal-Organic Framework-1), otherwise known as MOF-5, is among the most widely studied MOFs and is generally synthesized via a prototypical solvothermal synthesis.[5,19] In a typical IRMOF-1 reaction, 1,4-benzenedicarboxylic acid (BDC) and $Zn(NO_3)_2$ are dissolved in diethylformamide (DEF) and heated in a sealed vessel to 100 °C (Figure 1). During synthesis, the metal ions (nodes) and organic ligands (struts) generate coordinate covalent bonds to form metal ion clusters that are referred to as secondary building units (SBUs), which will produce the connecting nodes of the

framework.[20] The overall SBU shape, which influences the framework topology, is determined by the coordination geometry preference of the metal, the size and shape of the ligand, and the reaction conditions (e.g., concentration, solvent, temperature, time).[21-25] For IRMOF-1, BDC and Zn^{2+} ions react together in DEF to form Zn_4O clusters coordinated by six BDC ligands, resulting in an octahedral SBU. The octahedral SBUs assemble to form a 3D, porous cubic lattice that is manifest as the precipitation of colorless block-shaped crystals of IRMOF-1. In most cases, MOFs produced from solvothermal methods either form as single crystals or crystalline powders that can subsequently be characterized using single crystal X-ray diffraction (XRD), powder X-ray diffraction (PXRD), thermal gravimetric analysis (TGA), and gas sorption analysis in order to determine the topology, thermal stability and solvent content, and porosity of the framework, respectively.

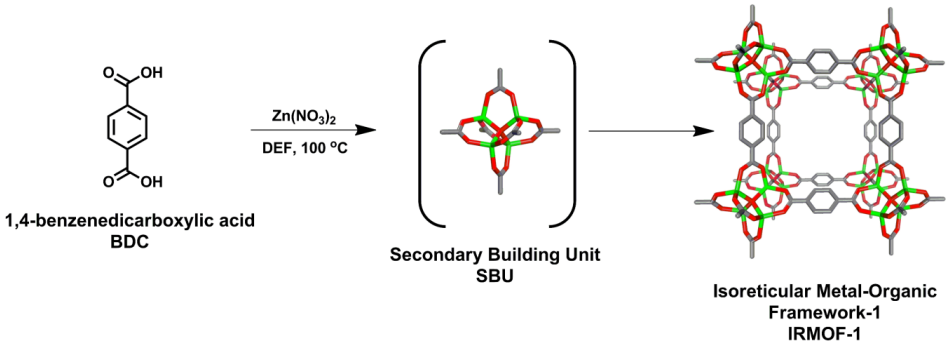

Figure 1-1. Solvothermal synthesis of Isoreticular Metal-Organic Framework-1 (IRMOF-1) using 1,4-benzenedicarboxylic acid (BDC) and $Zn(NO_3)_2$ dissolved in diethylformamide (DEF). Color scheme: Zn, green; O, red; C, gray.

1.2 MOF applications

Within the last decade, MOFs have emerged as attractive materials in the areas of gas sorption,[26] catalysis,[27,28] separation,[29] and biomedical applications.[30,31] MOFs encompass the best features of traditional inorganic (e.g., zeolites) and organic (e.g., carbon nanotubes) materials and have several advantages over both systems. Zeolites are constructed from tetrahedral aluminosilicate building blocks and cations (e.g., Na^{+}, K^{+}, Ca^{2+}).[16,32] Zeolites have been widely explored for petrochemical cracking, catalysis, ion exchange, and separation applications due to their high chemical stability and size selective micropores; however, zeolites are not chemically tunable and have smaller pore channels and pore volumes.[33] Zeolites are restricted to Si^{4+}, Al^{3+}, and O^{2-} ions as their building blocks and can only be functionalized via their cations, which overall limits control over designing zeolites with specific pore sizes, pore volumes, and functionalities. Carbon nanotubes are cylindrical graphite tubes that have been explored for their electronic and mechanical capabilities.[34] In contrast to zeolites, carbon nanotubes are more chemically diverse because their walls can be functionalized using organic chemistry. Ironically though, carbon nanotubes are only modifiable at their defect sites and are not well-ordered crystalline materials. MOFs, on the other hand, are robust, crystalline materials like zeolites, yet can be functionalized similarly to carbon nanotubes based on the choice of ligand. Due to their hybrid inorganic-organic nature, MOFs are highly tunable materials that can be physically and chemically modulated for storage, catalysis, and separation applications, which is otherwise a limitation of zeolites and carbon nanotubes.

Gas storage and separation has been the most popular applications for MOFs. There has been a lot of interest in developing cost-effective methods for storing H_2 and CH_4 as alternative energy sources and capturing CO_2 for sequestration in order to mitigate emissions of this global-warming gas.[35,36] MOFs have shown promise as storage and separation devices because they exhibit good reversibility of guest uptake and release, remain permanently porous upon guest removal, and have exceptional pore volumes.[26,29] Moreover, because MOFs can readily be tuned to have specific topologies (e.g., pore sizes and shapes) and pore functionalities, they can be optimized for guest uptake and interactions based on size, shape, and polarity. Several studies have indicated MOFs with unsaturated metal centers show stronger guest interactions with increased heat of adsorption (ΔH_{ads}), while other studies have indicated that MOFs with substituents (e.g., amines) decorating the pore channels display a preference for CO_2 capture from a mixture of CO_2/CH_4.[36,37]

In addition to gas storage and separation applications, MOFs have also been explored extensively as heterogeneous catalysts. MOFs are the ideal platform system because they can be designed to have the benefits of both homogeneous and heterogeneous catalysts.[27,28,38,39] Homogeneous catalysts lack thermal stability, can undergo self-degradation, and are not easy to isolate and reuse.[40] Heterogeneous catalysts are more robust, yet have poor mass transport and are not chemically tunable.[41,42] MOFs are able to overcome the limitations of homogeneous and heterogeneous catalysts because they are thermally robust, porous materials that can be easily isolated and reused. Their large pores allow for fast transport of substrates while the uniformity of MOFs prevents self-degradation of the active sites. Moreover, careful

selection of the metal ion and organic ligand can produce MOFs with chiral topologies, specific pore apertures, unsaturated metal centers, therefore resulting in MOFs that act as either enantioselective or size selective Lewis acid[43,44] and organocatalysts.[45]

Lastly, MOFs have been studied for drug delivery and bio-imaging applications. Given the wide range of building blocks that are available, MOFs can be synthesized with active metal centers (e.g., Gd^{3+} MOFs doped with Eu^{3+} or Tb^{3+}) for bio-imaging,[46,47] biologically active ligands (e.g., nicotinic acid) that can be released upon framework degradation, and with low toxicity metals and ligands in order to form a framework that can effectively deliver drugs within a biological system.[31] Preliminary drug delivery studies have indicated that MOFs are able to accommodate higher drug storage capacities with better rates of release for both solid (e.g., ibuprofen) and gaseous (e.g., nitric oxide) therapeutics. MOFs have great potential as drug delivery vessels because they can be designed with specific pore sizes and shapes, which can influence the rate of drug release based on the size and shape of the drug.[48] Additionally, the framework pores can be functionalized with substituents to improve uptake, delivery, and release of drugs that may not be easy to transport across the cell membrane or consumed too quickly.

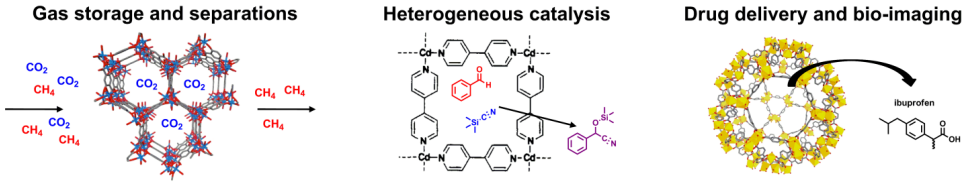

Figure 1-2. Examples of MOFs for gas storage and separations, heterogeneous catalysis, and drug delivery and bio-imaging applications. CO_2 capture with MOF-74[37] (left), cyanosilylation of aldehydes with Cd^{2+} bipyridine framework[49] (middle), and ibuprofen drug delivery with MIL-101[50] (right).

1.3 Prefunctionalization of MOFs

There has been interest in tailoring, or functionalizing, the MOF pores to improve host-guest interactions for catalysis, separation applications, and gas storage. The choice of metal and ligand can greatly affect the uptake and host-guest interactions in the framework, which in turn can affect the performance of MOFs (Figure 2).[42,51-53] Traditionally, functionalized MOFs have been synthesized through a 'prefunctionalization' approach (Figure 3). Prefunctionalization describes the solvothermal synthesis of a functionalized MOF using a specific metal ion and functionalized ligand (e.g., organic ligand with functional group substituents) combination. Many functionalized MOFs have been synthesized via the prefunctionalization approach with different metal centers and various functional groups (e.g., -Br, $-NH_2$, $-CH_3$) decorating the framework pores.[11,54,55]

The IRMOF series is one well-known system of functionalized MOFs that have been synthesized via the prefunctionalization route. As mentioned previously, IRMOF-1 is a cubic framework with Zn_4O SBUs coordinated by BDC ligands. In the IRMOF series, all the MOFs contain Zn_4O SBUs, but are linked by different BDC derivatives. Such BDC derivatives include 2-bromo-1,4-benzenedicarboxylic acid (Br-BDC), 2-amino-1,4-benzenedicarboxylic acid (NH_2-BDC), and 2,5-dipropoxy-1-4-benzenedicarboxylic acid (dp-BDC), which have been used to form IRMOF-2, IRMOF-3, and IRMOF-4, respectively.[11] As implied by their name, the IRMOFs are isostructural to one another, yet they are all functionally diverse frameworks with different pore volumes and surface areas. Recently, prefunctionalization has been used to develop Multivariate MOFs (MTV-MOFs), which are multi-functionalized versions of IRMOFs.[56]

MTV-MOFs are structurally similar to IRMOFs, but they are constructed from multiple BDC derivatives instead of one BDC derivative. Different combinations of BDC derivatives (-Br, -NH_2, -$(Cl)_2$, -NO_2, -$(CH_3)_2$, -C_4H_4, -$(OC_3H_5)_2$, -$OC_7H_7)_2$) have been successfully mixed together in one-pot reactions to yield MTV-MOFs with up to eight functional groups within a single framework.

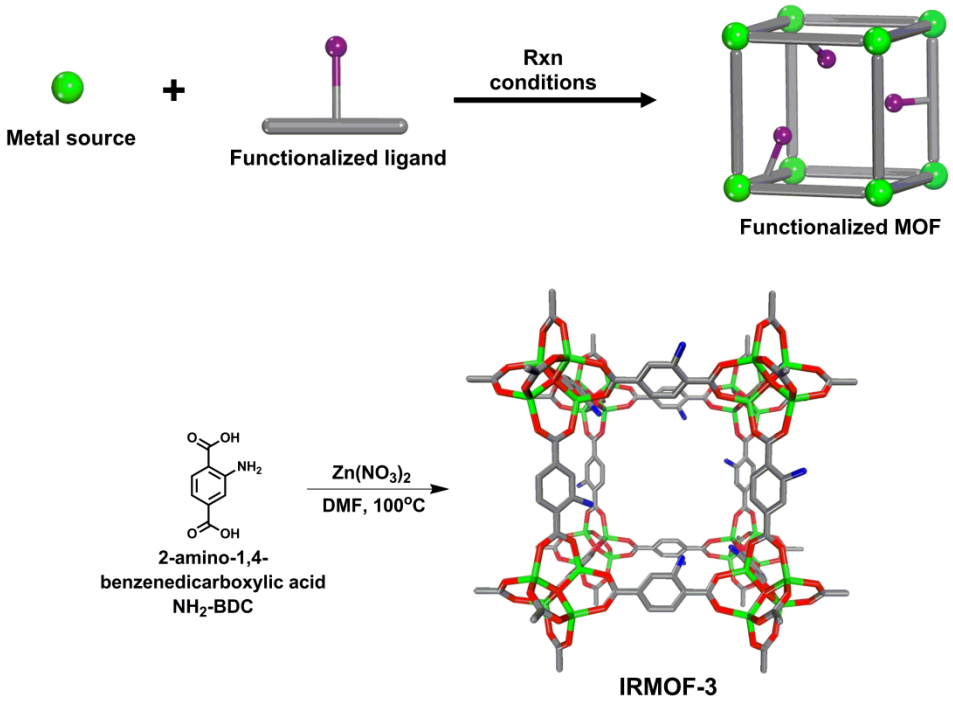

Figure 1-3. Synthesis of a functionalized MOF using the prefunctionalization route (top). Synthesis of IRMOF-3 from 2-amino-1,4,-benzenedicarboxylic acid (NH_2-BDC) and $Zn(NO_3)_2$ in DMF (bottom). Color scheme: Zn, green; O, red; C, gray; N, blue.

1.4 Postsynthetic modification of MOFs

Although many different functionalized MOFs have been developed via the prefunctionalization route, there are limitations with the types of functional groups that can be directly incorporated into the framework. The prefunctionalization route assumes

that functionality is preserved during and after synthesis and has no effect on the framework topology. However, the type of functional group can greatly influence the structural and chemical outcome of a solvothermal reaction. Some functional groups are not stable under the standard solvothermal conditions, which require high temperatures and pressures. Other functional groups are not compatible in terms of polarity, solubility, and sterics. Metal-binding groups, such as hydroxyls and carboxylic acids, are especially difficult to incorporate into MOFs because they can interfere with framework formation and chelate metal ions in the process. As a result, the overall product may result in either an undesired crystalline phase or the functionality is compromised. Another challenge with prefunctionalization involves incorporating multiple functionalities within the MOF. MTV-MOFs contain multiple functional groups, but the overall ratio of functionalities within the framework cannot be easily controlled. As seen with each MTV-MOF synthesis, the functional group outcome is overall unpredictable despite starting with equivalent ratios of each ligand. In one synthesis, a 1:1 starting ratio of BDC:NH_2-BDC results in a framework containing 1:0.57 ratio of BDC:NH_2-BDC. Depending on the functional group, the ligands may compete with one another during synthesis and form products at different rates, which would make it difficult to achieve a MOF with a specified ratio of functionalities.

An alternative functionalization route is by postsynthetic modification (PSM). In 1990, Hoskins and Robson observed that, "Relatively unimpeded migration of species throughout the lattice may allow chemical functionalization of the rods subsequent to construction of the framework."[57] Rather than trying to produce a functionalized MOF directly from a functionalized ligand, Hoskins and Robson proposed that the framework

be formed first and modified in a heterogeneous fashion afterwards. Surprisingly, though, there were no attempts made to chemically modify MOFs for almost a decade despite the fact that the observation was made during the early years of MOF research.

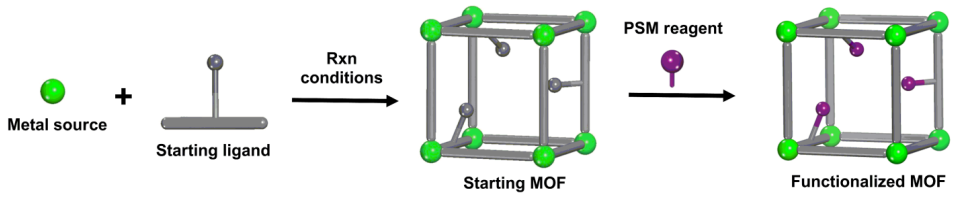

Figure 1-4. Synthetic schematic for postsynthetic modification (PSM) of a MOF.

In 1999, Lee and coworkers synthesized a series of 2D coordination polymers from Ag(OTf) and 2,4,6-tris(4-ethynylbenzonitrile)benzene derivatives.[58] Several ligands were produced with different pendant groups off the central benzene ring, including $-CH_3$, $-CH_2{=}CH_2$, and $-OCH_2CH_2OH$ (Figure 5). Lee and coworkers observed that one of the Ag^+ coordination polymers, which was built using (2,4,6-tris(4-ethynylbenzonitrile)phenoxy)ethanol, had a alcohol group that could undergo chemical modification (Figure 5). As a proof of concept, they successfully modified the pendant alcohol group with trifluoroacetic anhydride and converted this pendant group into an ester. Solid-state IR analysis, in addition to solution state ^1H NMR analysis upon dissolving the coordination polymer in d^6-acetone, confirmed the successful transformation of the alcohol into the ester. No significant structural changes were observed for the coordination polymer, as observed by powder X-ray diffraction. The following year, Kim and coworkers prepared D-POST-1, a 2D MOF with Zn^{2+} trimer

SBUs and a chiral tartaric pyridine derivative (Figure 5).[45] During their studies with D-POST-1, Kim and coworkers discovered that D-POST-1 was an active catalyst for transesterification of alcohols. It was proposed that the catalytic activity was due to free, uncoordinated pyridyl groups located within the pores of the framework. To confirm the pyridyl groups were the catalytic source, the MOF was exposed to iodomethane (and iodohexane) in DMF to alkylate the pyridyl groups. In order to characterize the modification, N-alkylated D-POST-1 was analyzed by ^{1}H NMR and powder X-ray diffraction. The N-alkylated product was dissolved in CF_3COOD in D_2O and the newly modified substituent was observed in the spectra. Powder X-ray diffraction of the modified MOF confirmed the framework remained stable after alkylation. Once the identity and integrity of N-alkylated D-POST-1 was established, the MOF was retested for catalysis. As predicted, the newly alkylated MOF did not show any catalytic activity.

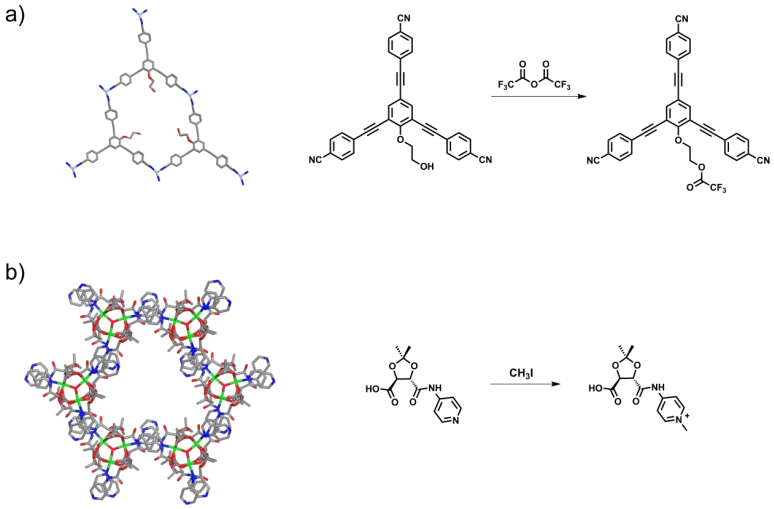

Figure 1-5. Ag^{+} 2D coordination polymer with (2,4,6-tris(4-ethynylbenzonitrile)phenoxy)ethanol undergoing postsynthetic modification with trifluoroacetic anhydride (top). D-POST-1, constructed from Zn^{2+} and chiral tartaric pyridine derivative, undergoing postsynthetic modification with iodomethane (bottom). Color scheme: Zn, green; O, red; C, gray; N, blue; Ag, light blue.

1.5 PSM of IRMOF-3

Although Lee and Kim successfully performed PSM on MOFs, neither group further pursued any additional PSM studies. PSM has been frequently utilized to functionalize other solid-state materials such as organosilicates (sulfonation)[59,60] and carbon nanotubes (carboxylation activation, amide couplings, esterification, halogenation, thiolation, hydrogenation, carbene addition, and cycloadditions).[34,61] However, no further work was pursed with MOFs. In 2007, Wang and Cohen investigated the PSM of MOFs in a more systematic, deliberate approach and coined the term 'postsynthetic modification' by analogy to the posttranslational modification of proteins.[62] Posttranslational modification of proteins refers to the covalent modification of side-chains on proteins that have been translated from RNA. The side-chains of proteins undergo various modifications, including acylation, phosophorylation, carboxylation, and O-glycosylation. Herein, the term PSM was adapted after post-translational modification with respect to the same concept of modification. With Hoskins and Robson's initial proposal in mind, Wang and Cohen formally defined PSM as the chemical modification of a MOF after construction of the framework.[63]

Given the lack of PSM studies since Lee and Kim's work, Wang and Cohen pursued a simple PSM reaction on a well-characterized MOF system. The initial target was IRMOF-3, a highly porous MOF built from Zn_4O SBUs and NH_2-BDC (Figure 1-3).[11,64] IRMOF-3, which is isostructural to IRMOF-1, was chosen because it contains free, uncoordinated amino groups within the framework pores. As a simple proof of concept, the amino groups of IRMOF-3 were exposed to acetic anhydride in an effort to convert these groups into amide functionalities. Single crystals of IRMOF-3 were

suspended in a CH_2Cl_2 solution of acetic anhydride and were left to react at RT. After 3 days, IRMOF-3 was successfully converted into its amide version, denoted as IRMOF-3-AM1 (AM = amide), in a single-crystal-to-single-crystal (SCSC) reaction.[63]

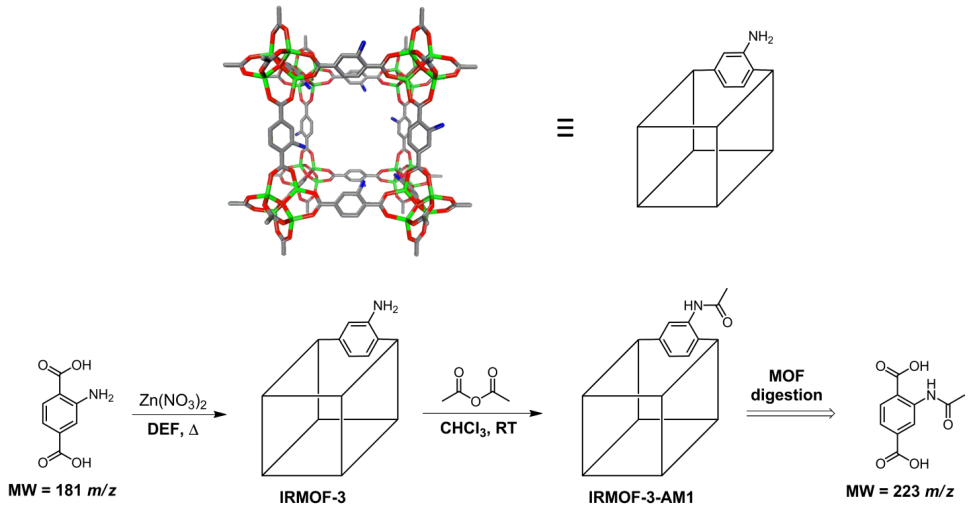

Figure 1-6. PSM of IRMOF-3 with acetic anhydride into IRMOF-3-AM1 (AM = amide).

No visible differences could be discerned between unmodified IRMOF-3 and IRMOF-3-AM1 crystals. Thermogravimetric analysis (TGA) and powder X-ray diffraction (PXRD) confirmed that the modification had no effect on the thermal stability or structure of the framework when compared to the parent MOF (IRMOF-3). Single crystal X-ray diffraction also provided additional evidence that the framework topology remained intact. Unfortunately, the modified substituent could not be located within the structure due to a positional disorder over all four equivalent positions of the central benzene ring of the BDC ligand. To quantify the degree of modification, single crystals of IRMOF-3-AM1 were dried and digested using dilute acid (35% DCl/D_2O in d^6-DMSO) and analyzed by solution ^1H NMR (Figure 1-7). Distinct shifts within the

aromatic region and the emergence of a new peak corresponding to the methyl group in the upfield region were clearly observed and found to be consistent with the new amide functionality. Using these spectral changes, ^{1}H NMR of the digested sample confirmed the successful modification of IRMOF-3 into IRMOF-3-AM1, which was determined to be ~80%. Based on these results, Wang and Cohen were able to show IRMOF-3 could be functionalized using PSM without affecting its overall thermal and structural stability. This simple experiment demonstrated that a functionalized MOF could be readily obtained as a high yielding, pure product under mild chemical conditions, thus opening the possibilities of developing a variety of functionalized MOFs that could not otherwise be obtained through prefunctionalization.

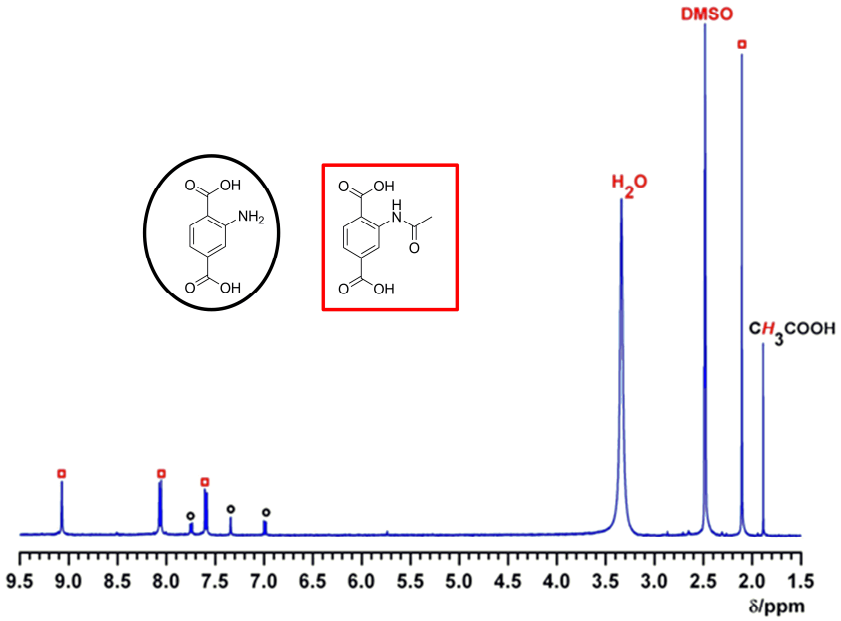

Figure 1-7. ^{1}H NMR spectra of digested IRMOF-3-AM-1 crystals in d^{6}-DMSO/DCl/D_2O. Unmodified IRMOF-3 peaks are indicated by black circles and modified IRMOF-3-AM1 peaks are indicated by red squares.

The following thesis work explores the development of PSM of MOFs through various stages. During the course of these investigations, there have been many reports published on the PSM of MOFs including two reviews solely focusing on PSM.[65,66] The main focus of this thesis is to showcase the early advancements made with PSM developed in the Cohen laboratory. Initial studies on how MOF modification and porosity is affected by reagent size will be reported in Chapter 2. In Chapter 3, new topologically MOFs are synthesized and examined by PSM to understand if PSM is applicable to different MOF systems and how topology can affect modification. This work will then move in the direction of designing MOFs for applications in gas storage and catalysis. Chapter 4 focuses on the development of MOFs for H_2 storage while Chapter 5 focuses on the design and synthesis of new Lewis acid MOF catalysts. Preliminary results regarding the advantages of using PSM for improving host-guest interactions for H_2 storage and Lewis acid catalysis will be reported. Finally, Chapter 6 introduces a new modification technique called postsynthetic deprotection (PSD), which allows for more complex functionalities to be incorporated into MOFs and highlights the overall advantages of using a postsynthetic approach for designing functionalized MOFs.

1.6 Acknowledgements

Chapter 1 contains material, in part, as it appears in Tanabe, K. K., Cohen, S. M. "Postsynthetic Modification of Metal-Organic Frameworks – A Progress Report." *Chem. Soc. Rev.* **2011**, *40*, 498-519. The dissertation author was the primary researcher and author for the data presented. The co-authors listed in these publications also participated

in the research. The permissions to reproduce these papers were granted by the Royal Society of Chemistry, copyright 2011.

1.7. References

(1) Kitagawa, S.; Kondo, M. *Bull. Chem. Soc. Jpn.* **1998**, *71*, 1739-1753.

(2) Yaghi, O. M.; Li, H. L.; Davis, C.; Richardson, D.; Groy, T. L. *Acc. Chem. Res.* **1998**, *31*, 474-484.

(3) Kitagawa, S.; Kitaura, R.; Noro, S.-i. *Angew. Chem. Int. Ed.* **2004**, *43*, 2334-2375.

(4) Chui, S. S.-Y.; Lo, S. M.-F.; Charmant, J. P. H.; Orpen, A. G.; Williams, I. D. *Science* **1999**, *283*, 1148-1150.

(5) Li, H.; Eddaoudi, M.; O'Keeffe, M.; Yaghi, O. M. *Nature* **1999**, *402*, 276-279.

(6) Chae, H. K.; Siberio-Pérez, D. Y.; Kim, J.; Go, Y.; Eddaoudi, M.; Matzger, A. J.; O'Keeffe, M.; Yaghi, O. M. *Nature* **2004**, *427*, 523-527.

(7) Férey, G.; Mellot-Draznieks, C.; Serre, C.; Millange, F.; Dutour, J.; Surblé, S.; Margiolaki, I. *Science* **2005**, *309*, 2040-2042.

(8) Koh, K.; Wong-Foy, A. G.; Matzger, A. J. *J. Am. Chem. Soc.* **2009**, *131*, 4184–4185.

(9) Zou, R. Q.; Sakurai, H.; Xu, Q. *Angew. Chem., Int. Ed.* **2006**, *45*, 2542-6.

(10) Smaldone, R. A.; Forgan, R. S.; Furukawa, H.; Gassensmith, J. J.; Slawin, A. M. Z.; Yaghi, O. M.; Stoddart, J. F. *Angew. Chem. Int. Ed.* **2010**, *49*, 8630–8634.

(11) Eddaoudi, M.; Kim, J.; Rosi, N.; Vodak, D.; Wachter, J.; O'Keeffe, M.; Yaghi, O. M. *Science* **2002**, *295*, 469-472.

(12) Volkringer, C.; Meddouri, M.; Loiseau, T.; Guillou, N.; Marrot, J.; Ferey, G.; Haouas, M.; Taulelle, F.; Audebrand, N.; Latroche, M. *Inorg. Chem.* **2008**, *47*, 11892-11901.

(13) Reineke, T. M.; Eddaoudi, M.; O'Keeffe, M.; Yaghi, O. M. *Angew. Chem. Int. Ed.* **1999**, *38*, 2590-2594.

(14) Yaghi, O. M.; O'Keeffe, M.; Ockwig, N. W.; Chae, H. K.; Eddaoudi, M.; Kim, J. *Nature* **2003**, *423*, 705-714.

(15) Shimizu, G. K. H.; Vaidhyanathan, R.; Taylor, J. M. *Chem. Soc. Rev.* **2009**, *38*, 1430-1449.

(16) Park, K. S.; Ni, Z.; Cote, A. P.; Choi, J. Y.; Huang, R. D.; Uribe-Romo, F. J.; Chae, H. K.; O'Keeffe, M.; Yaghi, O. M. *Proc. Natl. Acad. Sci. USA* **2006**, *103*, 10186-10191.

(17) Halper, S. R.; Cohen, S. M. *Inorg. Chem.* **2005**, *44*, 486-488.

(18) Smithenry, D. W.; Wilson, S. R.; Suslick, K. S. *Inorg. Chem.* **2003**, *42*, 7719-7721.

(19) Kaye, S. S.; Dailly, A.; Yaghi, O. M.; Long, J. R. *J. Am. Chem. Soc.* **2007**, *129*, 14176-14177.

(20) Eddaoudi, M.; Moler, D. B.; Li, H.; Chen, B.; Reineke, T. M.; O'Keeffe, M.; Yaghi, O. M. *Acc. Chem. Res.* **2001**, *34*, 319-330.

(21) Robson, R. *J. Chem. Soc., Dalton Trans.* **2000**, 3735-3744.

(22) Ockwig, N. W.; Delgado-Friedrichs, O.; O'Keeffe, M.; Yaghi, O. M. *Acc. Chem. Res.* **2005**, *38*, 176-182.

(23) Tranchemontagne, D. J.; Mendoza-Cortes, J. L.; O'Keeffe, M.; Yaghi, O. M. *Chem. Soc. Rev.* **2009**, *38*, 1257-1283.

(24) Halper, S. R.; Do, L.; Stork, J. R.; Cohen, S. M. *J. Am. Chem. Soc.* **2006**, *128*, 15255-15268.

(25) Perry IV, J. J.; Perman, J. A.; Zaworotko, M. J. *Chem. Soc. Rev.* **2009**, *38*, 1400-1417.

(26) Murray, L. J.; Dinca, M.; Long, J. R. *Chem. Soc. Rev.* **2009**, *38*, 1294-1314.

(27) Lee, J.; Farha, O. K.; Roberts, J.; Scheidt, K. A.; Nguyen, S. T.; Hupp, J. T. *Chem. Soc. Rev.* **2009**, *38*, 1450-1459.

(28) Ma, L.; Abney, C.; Lin, W. *Chem. Soc. Rev.* **2009**, *38*, 1248-1256.

(29) Li, J.-R.; Kuppler, R. J.; Zhou, H.-C. *Chem. Soc. Rev.* **2009**, *38*, 1477-1504.

(30) Huxford, R. C.; Rocca, J. D.; Lin, W. *Curr. Opinion Chem. Biol.* **2010**, *14*, 262-268.

(31) McKinlay, A. C.; Morris, R. E.; Horcajada, P.; Ferey, G.; Gref, R.; Couvreur, P.; Serre, C. *Angew. Chem. Int. Ed.* **2010**, *49*, 6260-6266.

(32) Baerlocher, C.; McCusker, L. B. 2008.

(33) Eddaoudi, M.; Eubank, J. F. In *Metal-Organic Frameworks: Design and Application*; MacGillivray, L. R., Ed.; John Wiley & Sons, Inc.: Hoboken, N. J., 2010, p 37-89.

(34) Hirsch, A. *Angew. Chem. Int. Ed.* **2002**, *41*, 1853-1859.

(35) Collins, D. J.; Ma, S.; Zhou, H.-C. In *Metal-Organic Frameworks: Design and Application*; MacGillivray, L. R., Ed.; John Wiley & Sons, Inc.: Hoboken, N. J., 2010, p 249-266.

(36) D'Alessandro, D. M.; Smit, B.; Long, J. R. *Angew. Chem. Int. Ed.* **2010**, *49*, 6058-6082.

(37) Britt, D.; Furukawa, H.; Wang, B.; Glover, T. G.; Yaghi, O. M. *Proc. Natl. Acad. Sci. USA* **2009**, *106*, 20637-20640.

(38) Farrusseng, D.; Aguado, S.; Pinel, C. *Angew. Chem. Int. Ed.* **2009**, *48*, 7502 - 7513.

(39) Corma, A.; Garcia, H.; Llabres i Xamena, F. X. *Chem. Rev.* **2010**, *110*, 4606-4655.

(40) Li, C. *Catal. Rev. Sci. Eng.* **2004**, *46*.

(41) Forster, P. M.; Cheetham, A. K. *Topics in Catalysis* **2003**, *24*, 79-86.

(42) Czaja, A. U.; Trukhan, N.; Muller, U. *Chem. Soc. Rev.* **2009**, *38*, 1284-1293.

(43) Wu, C.-D.; Hu, A.; Zhang, L.; Lin, W. *J. Am. Chem. Soc.* **2005**, *127*, 8940-8941.

(44) Cho, S.-H.; Ma, B.; Nguyen, S. T.; Hupp, J. T.; Albrecht-Schmitt, T. E. *Chem. Commun.* **2006**, 2563-2565.

(45) Seo, J. S.; Whang, D.; Lee, H.; Jun, S. I.; Oh, J.; Jeon, Y. J.; Kim, K. *Nature* **2000**, *404*, 982-986.

(46) Allendorf, M. D.; Bauer, C. A.; Bhakta, R. K.; Houk, R. J. T. *Chem. Soc. Rev.* **2009**, *38*, 1330-1352.

(47) Della Rocca, J.; Lin, W. *Eur. J. Inorg. Chem.* **2010**, 3725-3734.

(48) Horcajada, P.; Chalati, T.; Serre, C.; Gillet, B.; Sebrie, C.; Baati, T.; Eubank, J. F.; Heurtaux, D.; Clayette, P.; Kreuz, C.; Chang, J.-S.; Hwang, Y. K.; Marsaud, V.; Bories, P.-N.; Cynober, L.; Gil, S.; Férey, G.; Couvreur, P.; Gref, R. *Nat. Mater.* **2009**, *13*, 172-178.

(49) Fujita, M.; Kwon, Y. J.; Washizu, S.; Ogura, K. *J. Am. Chem. Soc.* **1994**, *116*, 1151-1152.

(50) Horcajada, P.; Serre, C.; Vallet-Regi, M.; Sebban, M.; Taulelle, F.; Ferey, G. *Angew. Chem. Int. Ed.* **2006**, *45*, 5974–5978.

(51) Janiak, C. *Dalton Trans.* **2003**, 2781-2804.

(52) Férey, G. *Chem. Soc. Rev.* **2008**, *37*, 191-214.

(53) Kitagawa, S.; Noro, S.-i.; Nakamura, T. *Chem. Commun.* **2006**, 701-707.

(54) Devic, T.; Horcajada, P.; Serre, C.; Salles, F.; Maurin, G.; Moulin, B.; Heurtaux, D.; Clet, G.; Vimont, A.; Greneche, J.-M.; Ouay, B. L.; Moreau, F.; Magnier, E.; Filinchuk, Y.; Marrot, J.; Lavalley, J.-C.; Daturi, M.; Ferey, G. *J. Am. Chem. Soc.* **2010**, *132*, 1127–1136.

(55) Garibay, S. J.; Cohen, S. M. *Chem. Commun.* **2010**, *46*, 7700-7702.

(56) Deng, H.; Doonan, C.; Furukawa, H.; Ferreira, R. B.; Towne, J.; Knobler, C. B.; Wang, B.; Yaghi, O. M. *Science* **2010**, *327*, 846 - 850.

(57) Hoskins, B. F.; Robson, R. *J. Am. Chem. Soc.* **1990**, *112*, 1546-1554.

(58) Kiang, Y.-H.; Gardner, G. B.; Lee, S.; Xu, Z.; Lobkovsky, E. B. *J. Am. Chem. Soc.* **1999**, *121*, 8204-8215.

(59) Inagaki, S.; Guan, S.; Ohsuna, T.; Terasaki, O. *Nature* **2002**, *416*, 304-307.

(60) Yang, Q.; Kapoor, M. P.; Inagaki, S. *J. Am. Chem. Soc.* **2002**, *124*, 9694-9695.

(61) Hirsch, A.; Vostrowsky, O. *Top Curr. Chem.* **2005**, *245*, 193-237.

(62) Walsh, C. T.; Garneau-Tsodikova, S.; Gatto, G. J., Jr. *Angew. Chem., Int. Ed.* **2005**, *44*, 7342-72.

(63) Wang, Z.; Cohen, S. M. *J. Am. Chem. Soc.* **2007**, *129*, 12368-12369.

(64) Rowsell, J. L. C.; Yaghi, O. M. *J. Am. Chem. Soc.* **2006**, *128*, 1304-1315.

(65) Wang, Z.; Cohen, S. M. *Chem. Soc. Rev.* **2009**, *38*, 1135-1329.

(66) Tanabe, K. K.; Cohen, S. M. *Chem. Soc. Rev.* **2011**, *40*, 498-519.

Chapter 2 Systematic Functionalization of IRMOF-3

2.1 Introduction

Back in 1990, Hoskins and Robson proposed the idea of PSM and described how a MOF could be synthesized first and chemically modified afterwards.[1] In 2007, Wang and Cohen formally coined the term PSM and introduced PSM as a strategy for functionalizing MOFs after the framework had been synthesized.[2] In their study, they exposed single crystals of IRMOF-3, which contains pendant amino groups, to a solution of acetic anhydride and successfully converted IRMOF-3[3,4] into IRMOF-3-AM1, a MOF with amide functionalities (Figure 2-1). By TGA and PXRD analysis, IRMOF-3-AM1 showed no distinct thermal or structural differences from unmodified IRMOF-3, therefore implying the modification had no deleterious effect on the framework. Single crystal X-ray diffraction analysis of IRMOF-3-AM1 confirmed the TGA and PXRD results and revealed the expected cubic lattice; however, no suitable electron density was present for the modified amide substituent to justify the new functionality. To confirm the modification did occur, single crystals of IRMOF-3-AM1 were digested and analyzed by ^{1}H NMR, which distinctly showed IRMOF-3 was successfully modified with >80% of the amino groups converted into amides. Here, Wang and Cohen were able to obtain a functionalized MOF by modifying the framework after it had been synthesized and clearly demonstrated the feasibility of PSM.

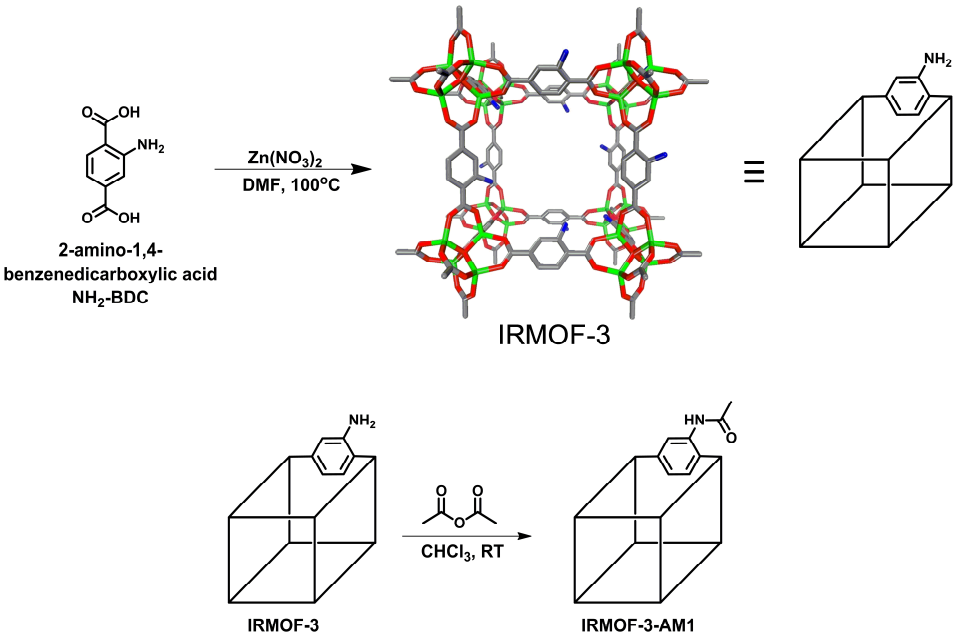

Figure 2-1. Synthesis of IRMOF-3 from NH_2-BDC and $Zn(NO_3)_2$ in DMF (top). Synthesis of IRMOF-3-AM1 by modifying IRMOF-3 with acetic anhydride (bottom).

Although the modification of IRMOF-3 was a simple, yet profound result, it became apparent that several aspects of PSM needed to be addressed before fully exploiting PSM to functionalize MOFs, especially given the lack of PSM studies within the last twenty years.[5,6] We sought to perform a systematic study to understand the following: (a) could larger reagents be used; (b) how would the physical properties (e.g., thermal stability, surface area, etc) be affected after modification; and (c) is PSM a general functionalization approach. To answer these questions, a thorough study of PSM was conducted using IRMOF-3 as a model system. IRMOF-3 was modified with ten alkyl anhydrides of varying chain lengths, $(CH_3(CH_2)_nCO)_2O$, where n = 1 to 18), and analyzed by a variety of characterization techniques (^{1}H NMR, ESI-MS, TGA, PXRD, single-crystal X-ray analysis, and Brunauer-Emmett-Teller (BET) surface area

measurements)[7] to determine the modification extent, stability, and microporosity of the modified IRMOFs (Scheme 2-1).

2.2 Results and Discussion

2.2.1 Modification of IRMOF-3 with Alkyl Anhydrides.

Two different methods (denoted as denoted as 'Method 1' and 'Method 2') were used to study the effects of PSM on IRMOF-3. 'Method 1' involves taking $CHCl_3$ soaked samples of IRMOF-3 and drying them under vacuum with heat to remove solvent from the pores of the framework prior to PSM. 'Method 2' uses $CHCl_3$ soaked samples of IRMOF-3, but without drying prior to modification. Both methods were used to study different features of the modified IRMOFs and to compare the effects of modification based on sample preparation.

Method 1 samples were primarily used to study the rates of reactivity of each alkyl anhydride. When IRMOF-3 was exposed to acetic anhydride, acetic acid was observed as a byproduct upon acylation of the amino groups.[2] ^{1}H NMR analysis of the reaction supernatant showed the distinct appearance of acetic acid and disappearance of acetic anhydride, which provided indirect evidence that the amino groups were modified. Similar experiments were performed with IRMOF-3 and the ten alkyl anhydrides to examine how alkyl chain length affected the rate of modification (Figure 2-2). IRMOF-3 samples (prepared using Method 1) were soaked in $CDCl_3$ with their respective anhydrides and the $CDCl_3$ supernatant was monitored by ^{1}H NMR every 24 h for a total of 5 days. The carboxylic acid byproduct has a distinct α-CH_2 peak from the anhydride,

which made it easy to observe whether or not the anhydride was undergoing a reaction with IRMOF-3 (Figure 2-3).

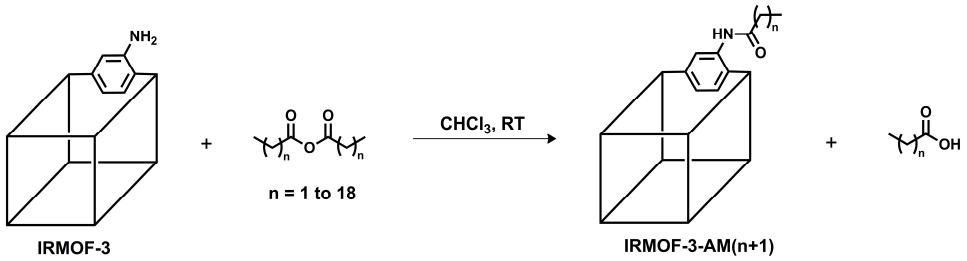

Figure 2-2. Modification of IRMOF-3 with alkyl anhydrides $(CH_3(CH_2)_nCO)_2O$, where n = 1 to 18)

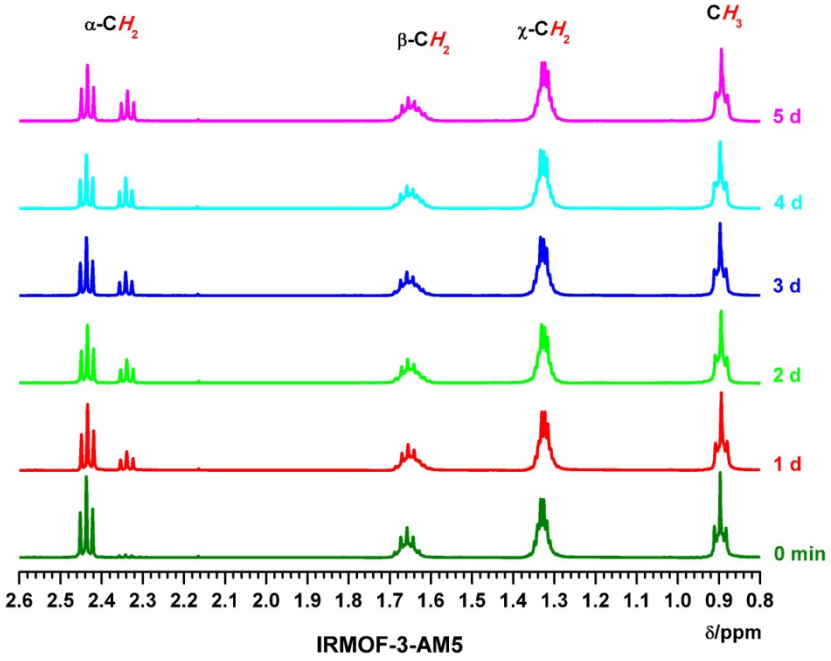

Figure 2-3. ^{1}H NMR spectra of the reaction mixture of IRMOF-3 modified with hexanoic anhydride (n = 4) collected between 0 and 5 days. Reaction conditions: rt, $CDCl_3$ (1.00 mL), IRMOF-3 crystals (Method 1, 0.10 mmol equiv of -NH_2), and anhydride (0.20 mmol).

^{1}H NMR spectra of the reaction supernatant with each alkyl anhydride were compiled to compare the ratio of anhydride to acid byproduct over the 5 day period (Figure 2-3). At the beginning of the reaction, only the anhydride is observed in the supernatant. After 24 h, a new triplet peak begins to appear in the spectra, which corresponds to the α-CH_2 peak for the carboxylic acid byproduct. Analysis of all ten alkyl anhydride supernatants revealed the amount of carboxylic acid byproduct produced was dependent on alkyl chain length. The smaller alkyl anhydrides ($n < 8$) were found to be more reactive, as indicated by the continuous growth of the α-CH_2 peak every 24 h, which suggested that high percent conversions were achieved with IRMOF-3. In contrast, the larger alkyl anhydrides ($n > 8$) were found to produce smaller amounts of acid byproduct and hence lower modifications (see below).

After sampling the supernatant for 5 days, the modified IRMOF-3 samples were washed with $CHCl_3$, dried under vacuum, and digested (35% DCl in D_2O/ DMSO) for ^{1}H NMR analysis. Unmodified IRMOF-3 and modified IRMOF-3 have distinct aromatic proton shifts from each other, which allows for easy quantification of modification. Percent conversion was determined by taking the integration of the aromatic singlet resonance, which is the proton adjacent to the amine/amide group at the C3 position on the BDC ligand, and dividing it over the summation of unmodified and modified IRMOF-3 aromatic singlet integrations (Figure 2-4). ^{1}H NMR analysis of the ten samples revealed IRMOF-3 had undergone modification with all the alkyl anhydrides to generate a series of long alkyl chain functionalized MOFs, denoted as IRMOF-3-AM(n+1), where n = 1 to 18 and corresponds to the number of methylene groups present in the alkyl chain.

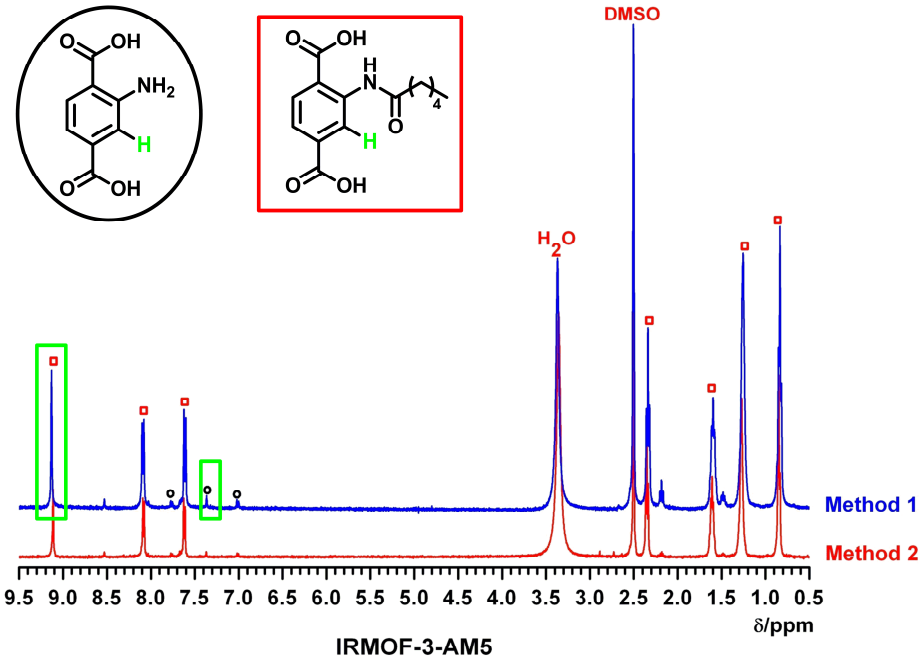

Figure 2-4. ^{1}H NMR spectra of digested IRMOF-3 modified with hexanoic anhydride (*n* = 4) via Method 1 (5 days) and Method 2 (3 days). Labeled peaks represent NH_2-BDC (black circles) and the acylated reaction product (red squares). Percent conversion was determined by taking the integration of the proton at the C3 position on NH_2-BDC (highlighted in green). The proton integration of the modified singlet (red square) was divided by the summation of the unmodified singlet integration (black circle) and modified singlet integration (red square).

Percent conversion was found to range from 97% (IRMOF-3-AM2) to 11% (IRMOF-3-AM19).[8] Under identical reaction concentrations and times (using Method 1), the degree of modification was determined to be inversely proportional to the alkyl chain length. As expected, the percent conversion correlated directly with the amount of carboxylic acid byproduct produced between IRMOF-3 and the respected alkyl anhydride (Figure 2-5). The effect of alkyl chain length on percent conversion can be simply rationalized by the relationship between number of atoms per alkyl chain and the amount of free space available in IRMOF-3. When IRMOF-3 undergoes modification, additional substituents are incorporated into the pores, which may prevent more alkyl anhydride

from diffusing into the pores and reacting with other available amino sites. Alternatively, the reactivity of the anhydride may decrease as the alkyl chains increases under these reaction conditions. Regardless, modification extent is a function of reagent size, which is clearly reflected as increasing alkyl chain length results in lower modifications. The relationship between modification and alkyl chain length is supported by the pronounced difference in percent conversion between IRMOF-3-AM7 and IRMOF-3-AM9, IRMOF-3-AM9 and IRMOF-3-AM13, and IRMOF-3-AM16 and IRMOF-3-AM19 where the percent conversions noticeably drop 20-30% upon the addition of 2-3 methylene groups.

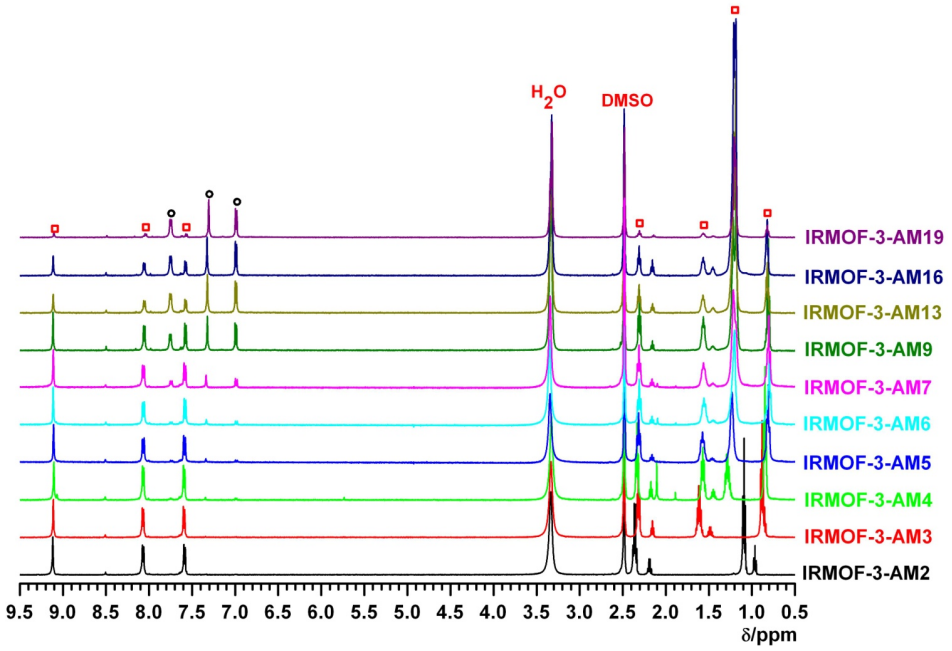

Figure 2-5. ^{1}H NMR spectra of digested IRMOF-3 samples (Method 1). Each spectra was normalized either to the singlet at 9.1 ppm ($n \leq 8$) or to the singlet at 7.3 ppm ($n > 8$). Reaction conditions: r.t., 5 d, $CDCl_3$ (1.00 mL), IRMOF-3 crystals (0.10 mmol equiv of -NH_2), and anhydride (0.20 mmol). Each sample (5 mg) was dried at 90 °C for 8 h and digested in 500 µL of d^6-DMSO and 100 µL of DCl solution (23 µL of 35% DCl in D_2O and 1 mL of d^6-DMSO) with sonication.

MOFs prepared using Method 2 were examined to determine if sample preparation (e.g., drying vs. no drying) had an effect on modification. The reaction conditions for Method 2 were optimized in order to obtain the best single crystal samples for single crystal X-ray diffraction and gas sorption analysis. Although Method 1 samples maintained their bulk crystallinity, as determined by PXRD, the single crystallinity of the modified MOFs was mediocre. Single crystals of IRMOF-3, which were not dried prior to modification, were subjected to daily exchanges of fresh anhydride solutions (0.05 M to 0.1 M) over a 3-day period. All modified IRMOF-3 samples visually maintained their single crystallinity and were determined to have similar percent conversions as Method 1, with conversion ranging from ~99% (IRMOF-3-AM2) to 7% (IRMOF-3-AM19) (Figure 2-4, Table 2-1). Overall, Method 1 and Method 2 results suggest modification extent appears to be more dependent on reagent size than sample preparation. However, it is possible to achieve higher conversions by adjusting the reaction conditions (e.g., concentration and time) accordingly based on the reagent size and reactivity.[9]

Table 2-1. Percent conversions of IRMOF-3 with different anhydrides as determined by ^{1}H NMR. Values listed are an average (with standard deviations) of at least three independent experiments for Method 1 and four independent experiments for Method 2.

IRMOF-3	-AM2	-AM3	-AM4	-AM5	-AM6	-AM7	-AM9	-AM13	-AM16	-AM19
n =	1	2	3	4	5	6	8	12	15	18
Method 1 [b]	97±3%	98±3%	97±3%	94±5%	90±5%	81±5%	51±5%	31±5%	30±2%	11±1% [a]
Method 2 [c]	~99%	~99%	98±3%	96±3%	90±3%	80±5%	46±7%	32±5%	20±1%	7±1% [a]

[a] 0.8 equiv. of anhydride was used (instead of 2 equiv) due to low solubility of the reagent; [b] total reaction time of five days; [c] total reaction time of three days

2.2.2 Thermal and Structural Stability of modified IRMOFs

IRMOF-3- AM2 to IRMOF-3-AM19 (prepared by Method 1) were analyzed by thermal gravimetric analysis (TGA) and powder X-ray diffraction (PXRD) to determine the thermal and structural stability of the modified IRMOF-3. All modified IRMOF-3 were found to remain stable up to 430 °C, which was comparable to unmodified IRMOF-3 (Figure 2-6). PXRD indicated that the bulk crystallinity of all modified IRMOF-3 samples was maintained and all 2θ peaks were consistent with as-synthesized IRMOF-3 (Figures 2-7 and 2-8) The uniformity of all 2θ peaks for each modified IRMOF-3 sample, along with unmodified IRMOF-3, showed that modification has no effect on the overall structural integrity of the framework.

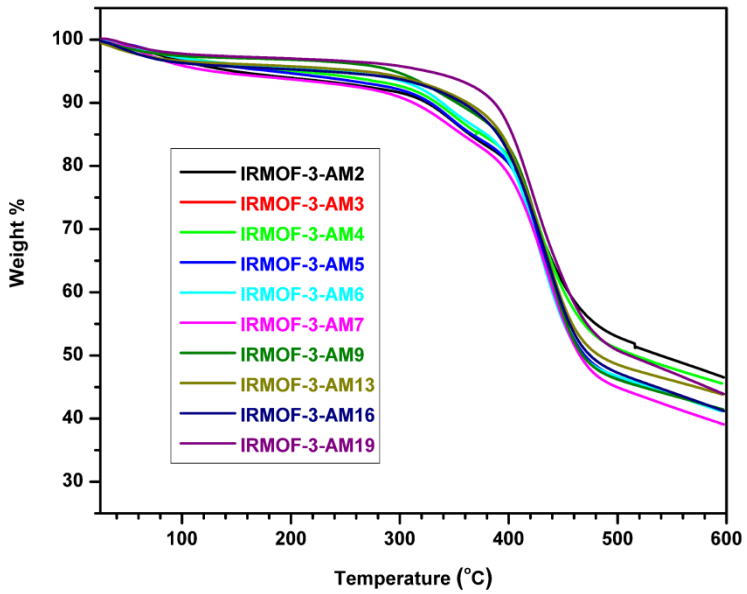

Figure 2-6. Thermogravimetric analysis (TGA) of modified IRMOF-3 samples. All samples were previously dried at 90 °C under vacuum for 8 h. Modified IRMOF-3 (10-12 mg) was heated at a scan rate of 5 °C/min from 25 °C to 600 °C.

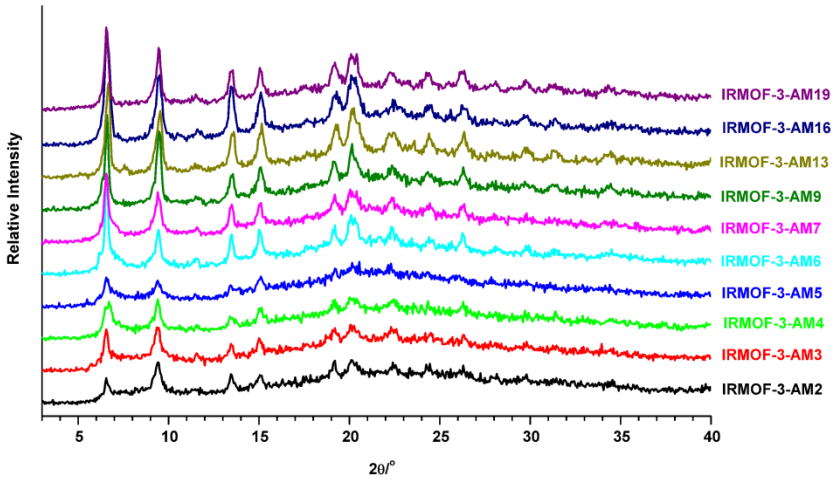

Figure 2-7. Powder X-ray diffraction (PXRD) patterns of modified IRMOF-3 samples (Method 1). Modified IRMOF-3 samples were soaked and exchanged with fresh $CHCl_3$ for 2 days. After decanting off the solvent, the samples were left drying in air for an hour prior to PXRD analysis.

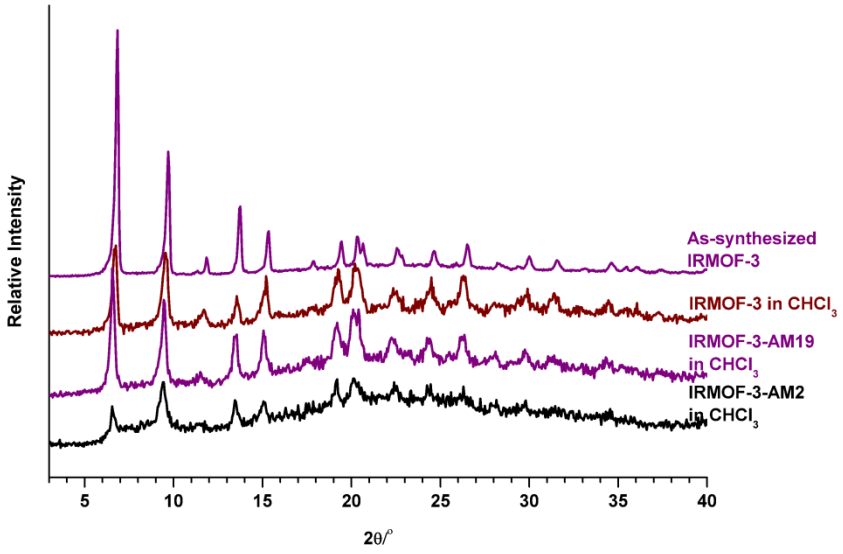

Figure 2-8. PXRD comparisons of as-synthesized IRMOF-3 (gray, prepared from DMF), IRMOF-3 (magenta, dried as per Method 1), IRMOF-3-AM19 (green, prepared as per Method 1), and IRMOF-3-AM2 (black, prepared as per Method 1). IRMOF-3-AM19 and -AM2 were soaked and washed with fresh $CHCl_3$ for 2 days after the reaction with anhydride. The solvent was decanted from the vials containing as-synthesized IRMOF-3, IRMOF-3, -AM19, and -AM2, and the samples were left drying in air prior to PXRD analysis.

IRMOF-3-AM2 to IRMOF-3-AM19 did not show any visual signs of degradation or changes in morphology after being exposed to alkyl anhydride for several days (Figure 2-9). As further proof, Method 2 samples were analyzed by single crystal X-ray diffraction to confirm that the crystallinity was indeed preserved. Complete X-ray diffraction data were collected for IRMOF-3-AM4, -AM6, -AM13, and -AM19 while unit cell determinations were obtained for the remaining modified IRMOFs. IRMOF-3 is a cubic structure (space group *Fm*-3m with $a = b = c = 25.7465(14)$ Å, $\alpha = \beta = \gamma = 90°$, and a unit cell volume of 17066.0(16) Å^3. All modified samples underwent single-crystal to single-crystal transformation with retention of the same crystal system and cell setting (cubic, *F* centered) with $a = b = c \approx 25$ Å, $\alpha = \beta = \gamma = 90°$, and unit cell volumes of ~17000 Å^3 (Tables 2-2 and 2-3).

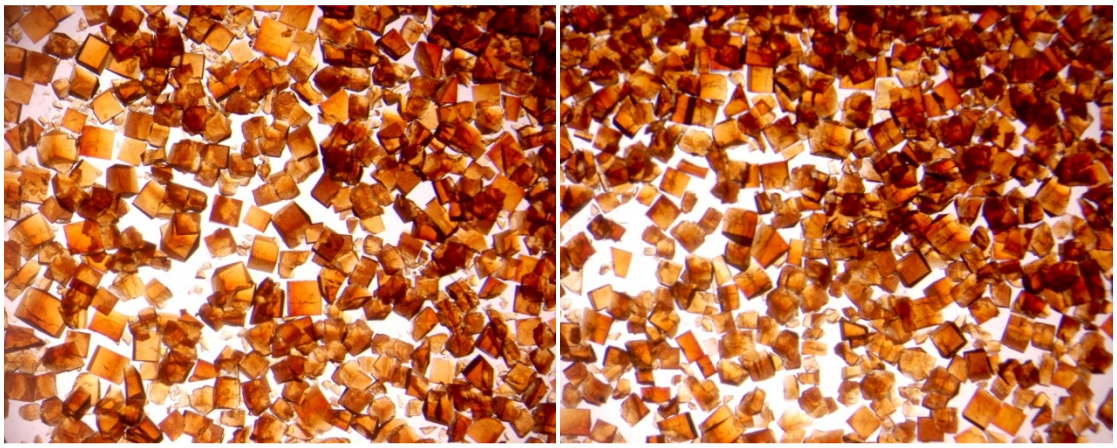

Figure 2-9. IRMOF-3 (right) and modified IRMOF-3 (left) as prepared with hexanoic anhydride ($n = 4$) via Method 2.

The data sets for IRMOF-3-AM4, -AM6, -AM13, and -AM19 revealed that the IRMOF lattice was retained after exposure to the alkyl anhydrides. Although high quality data sets were collected for the four modified IRMOFs, the modified amide

substituents could not be located due to disorder over all four positions on the BDC ligand. However, to confirm the presence of the modified substituent, each single crystal was removed from the diffractometer and digested in either H_2O or MeOH and analyzed by negative mode ESI-MS. All single crystals showed the expected amide-modified BDC ligand and verified the crystal contained the appropriate modified substituent (Figure 2-10).

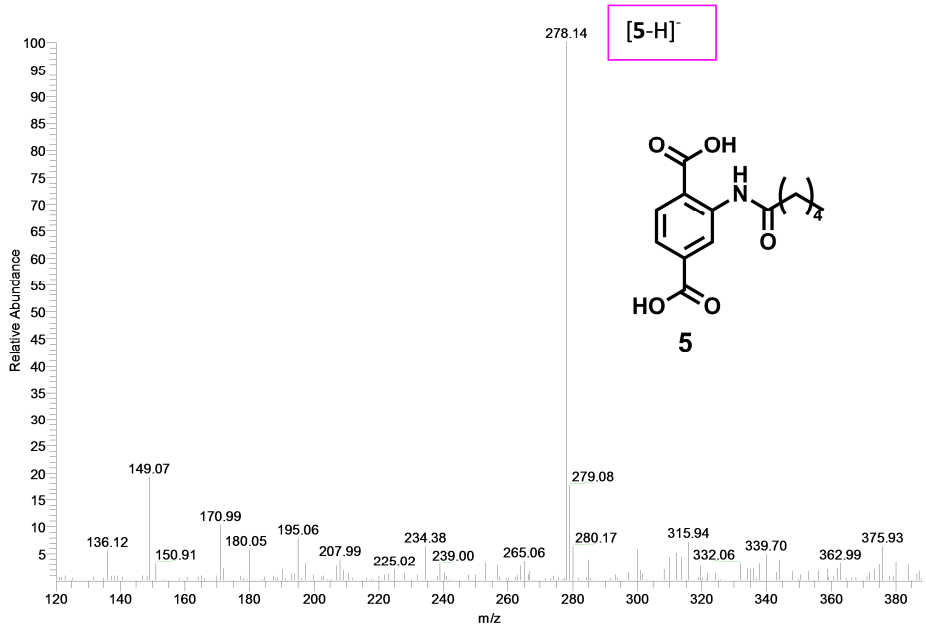

Figure 2-10. ESI-MS (negative mode) of the digested IRMOF-3-AM5 (*n* = 4) single crystal.

Table 2-2. Unit cell determinations and mass spectrometry data for modified IRMOF-3 single crystals.

IRMOF-3	-AM2	-AM3	-AM5	-AM7	-AM9	-AM16
Morphology	Block	Block	Block	Block	Block	Block
Size (mm)	0.33 0.31 0.31	0.40 0.33 0.28	0.33 0.31 0.25	0.50 0.35 0.34	0.51 0.27 0.20	0.30 0.30 0.25
Cell setting	Cubic *F*	Cubic *F*	Cubic *F*	Cubic *F*	Cubic *F*	Cubic *F*
$a = b = c$	25.53	25.74	25.65	25.73	25.68	25.97
$\alpha = \beta = \gamma$	90°	90°	90°	90°	90°	90°
Volume ($Å^3$)	16639	17054	16876	17036	16943	17519
ESI-MS(-) $[M-H]^-$	236	250	278	306	334	432

Table 2-3. Structure determination parameters and mass spectrometry data for modified IRMOF-3 single crystals.

IRMOF-3	-AM4	-AM6	-AM13	-AM19
Formula	$C_{45}H_{45}C_{l18}$ $N_3O_{16}Zn_4$	$C_{47.90}H_{52.40}C_{l15}$ $N_3O_{15.70}Zn_4$	$C_{45.30}H_{50.70}C_{l13.50}$ $N_3O_{14.20}Zn_4$	$C_{35.40}H_{29.91}C_{l22.50}$ $N_3O_{13.21}Zn_4$
Morphology	Block	Block	Block	Block
Color	Amber	Amber	Amber	Amber
Size (mm)	0.30 0.20 0.20	0.34 0.32 0.27	0.43 0.39 0.29	0.41 0.32 0.24
Crystal System	Cubic	Cubic	Cubic	Cubic
Space Group	Fm-3m	Fm-3m	Fm-3m	Fm-3m
a = b = c	25.7386(6)	25.7228(6)	25.7691(17)	25.7786(7)
$\alpha = \beta = \gamma$	90°	90°	90°	90°
Volume ($Å^3$)	17051.2(7)	17019.8(7)	17112(2)	17130.8(8)
T, K	200(2)K	200(2)K	200(2)K	200(2)K
Reflns measured	6694	6551	3216	9407
Data/restraints/parameters	935 / 0 / 28	845 / 0 / 28	701 / 0 / 30	832 / 0 /28
Independent Reflns [R(int)]	935 [R(int) = 0.0361]	845 [R(int) = 0.0193]	701 [R(int) = 0.0178]	832 [R(int) = 0.0289]
Final R indices [I>2σ(I)]a	R1 = 0.0304, wR2 = 0.0814	R1 = 0.0349, wR2 = 0.1047	R1 = 0.0368, wR2 = 0.1140	R1 = 0.0351, wR2 = 0.1035
R indices (all data, F^2 refinement)a	R1 = 0.0387, wR2 = 0.0849	R1 = 0.0395, wR2 = 0.1081	R1 = 0.0407, wR2 = 0.1207	R1 = 0.0405, wR2 = 0.1078
GOF on F^2	0.918	1.082	1.165	1.071
Largest diff. peak and hole , $e/Å^3$	0.357 and -0.207	0.297 and -0.278	0.474 and -0.287	0.522 and -0.267
ESI-MS(-) $[M-H]^-$	264	292	390	474

2.2.3 Gas Sorption Analysis of Modified IRMOF-3

Brunauer-Emmett-Teller (BET) surface area measurements were collected for each modified IRMOF-3 (using Method 2) at 77 K using dinitrogen (N_2). All modified IRMOF-3 samples were found to retain their microporosity regardless of their modification extent and alkyl chain length. IRMOF-3-AM2 to IRMOF-3-AM6, which have high conversions > 90%, had lower BET surface areas than the parent IRMOF-3, which has an initial surface area of 2400 m^2/g. The BET surface areas were found to range from 1641 m^2/g (IRMOF-3-AM2) to 1165 m^2/g (IRMOF-3-AM6). Interestingly, the BET surface areas for IRMOF-3-AM7 to IRMOF-3-AM19, which have conversions < 90%, exhibited a reverse trend where surface area increased from 1185 m^2/g (IRMOF-3-AM7) to 2164 m^2/g (IRMOF-3-AM19).

When BET surface area is plotted versus alkyl chain length, a distinct "well-shaped" curve is observed and MOF porosity decreases from IRMOF-3-AM2 to -AM6, but increases from -AM7 to -AM19 (Figure 2-11). IRMOF-3-AM3 and IRMOF-3-AM13, which have conversions of ~99% and 32%, respectively, have comparable BET surfaces areas (1487 vs 1438 m^2/g), but their alkyl chain lengths differ by 10 methylene groups. Interestingly, IRMOF-3-AM19 has a very high surface area (2162 m^2/g, close to the unmodified IRMOF-3) despite having been modified with C19 chains. It would seem intuitively obvious that microporosity should decrease upon the inclusion of additional atoms into the pores of the framework based on a surface area per mass basis.[10] To determine the effects of sample mass on surface area, the modified IRMOF surface area (cm^3/g) was converted to molar surface area ($m^2/mmol$) and plotted against alkyl chain

length (Figure 2-12). The same well-shaped curve was observed for molar surface area vs alkyl chain, therefore ruling out sample mass influences surface area.

Based on these results, the microporosity appears to be influenced by a combination of alkyl chain length and percent conversion. To develop a better understanding of how alkyl chain length and percent conversion affects surface area, the number of newly incorporated atoms per unit cell was calculated for each modified IRMOF. For example, IRMOF-3-AM5 is 96% modified and its modified substituent consists of 7 non-hydrogen atoms total: one N atom for the amide, two atoms for the carbonyl group (C and O), four C atoms for the methylenes, and one C atom for the methyl group. Each IRMOF-3 unit cell consists of three amino groups based on the formula unit of $Zn_4O(L)_3$, where L = NH_2-BDC or modified NH_2-BDC. By taking simple calculations into account, IRMOF-3-AM5 has ~20 additional atoms per unit cell and a corresponding BET of 1201 m^2/g (Table 2-4). The additional atom value falls well within reason with the other modified IRMOFs. IRMOF-3-AM2, which has a BET of 1641 m^2/g and a percent conversion of ~99%, has ~12 additional atoms and IRMOF-3-AM19, which has a BET of 2162 m^2/g and percent conversion of 7%, has ~4 additional atoms. The surface area of the modified IRMOFs correlates inversely with the number of additional atoms per unit volume, therefore indicating the surface area is influenced by percent conversion and reagent size (Figure 2-13).

Table 2-4. Comparison of BET surface area and determination of the number of additional atoms (excluding hydrogen atoms) included per unit cell due to modification.

IRMOF-3	-AM2	-AM3	-AM4	-AM5	-AM6	-AM7	-AM9	-AM13	-AM16	-AM19
n	1	2	3	4	5	6	8	12	15	18
# of additional atoms per chain (n+3) [a]	4	5	6	7	8	9	11	15	18	21
% conversion (Table 1, Method 2)	0.99	0.99	0.98	0.96	0.90	0.80	0.46	0.32	0.20	0.07
# of additional atoms per unit cell [b]	11.88	14.85	17.64	20.16	21.60	21.60	15.18	14.40	10.80	4.41
BET Surface Area (m^2/g)	1641	1487	1424	1201	1165	1185	1243	1438	1581	2164

[a] The number of atoms added per modified ligand were calculated by including one carbonyl oxygen, one carbonyl carbon, one methyl carbon, and n methylene carbons (only non-hydrogen atoms). [b] Obtained from the formula: (n+3)×(percent conversion)×3, where 3 is the number of unique amino groups per unit cell.

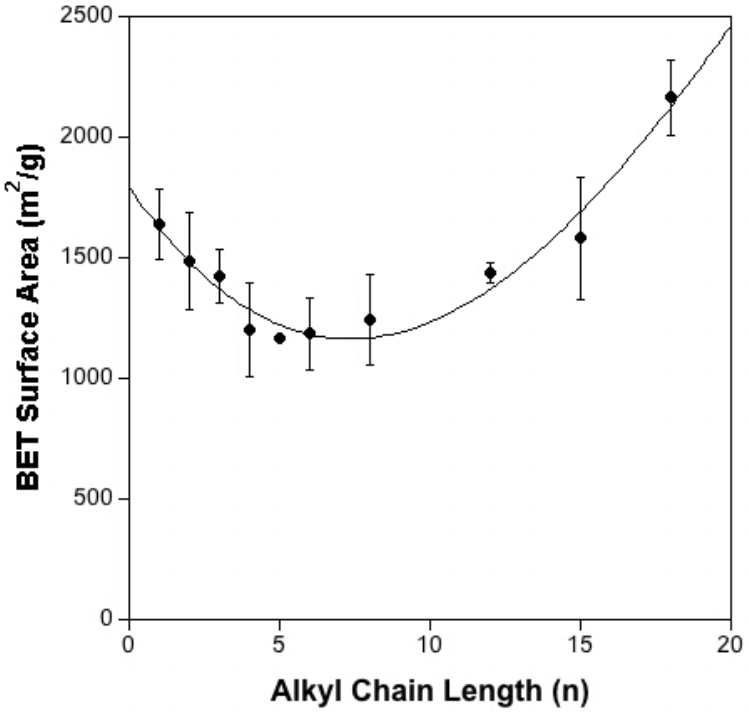

Figure 2-11. Plot of BET surface area of modified IRMOF-3 as a function of alkyl chain length.

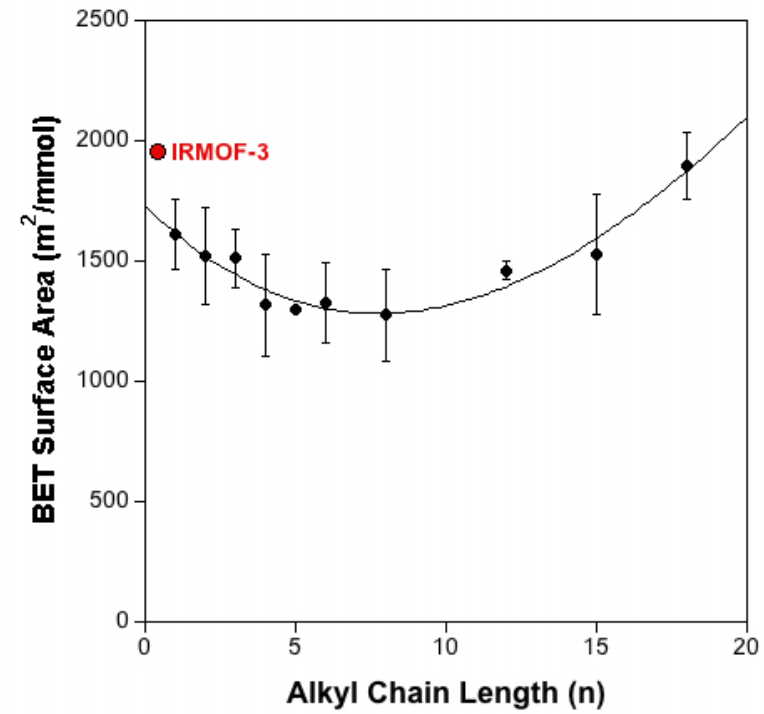

Figure 2-12. Plot of BET surface area (in m^2/mmol of MOF) of modified IRMOF-3 as a function of alkyl chain length. The value for unmodified IRMOF-3 is indicated with a red circle.

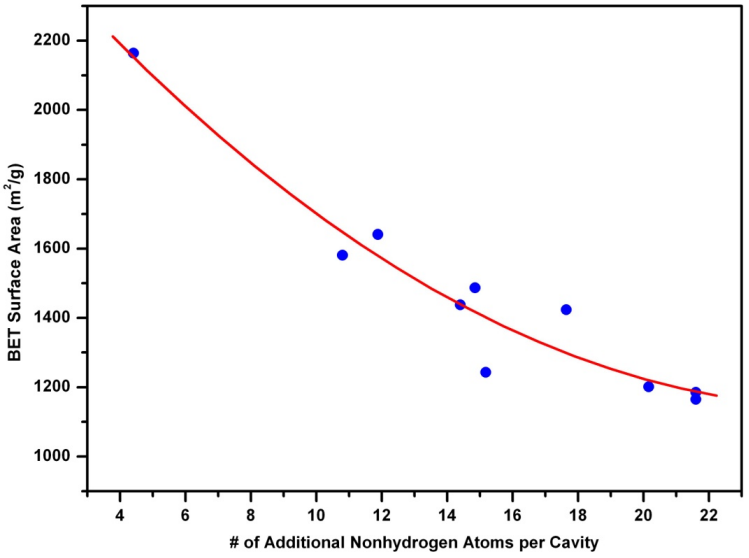

Figure 2-13. Plot of BET surface area (in m^2/mmol of MOF) of modified IRMOF-3 as a function of the number of additional non-hydrogen atoms per cavity (see Table 2-4, row 5).

2.3 Conclusions

IRMOF-3 was modified with ten alkyl anhydrides with varying chain lengths, resulting in a series of isostructural, but chemically distinct IRMOFs. Controlling the reaction conditions (e.g., concentration and time) resulted in highly crystalline modified IRMOFs with comparable thermal and structural stabilities as the original IRMOF-3. The microporosity of each modified framework was also found to be preserved. Closer analysis of the modified IRMOF system revealed a correlation between alkyl chain length and percent conversion where increasing alkyl chain length resulted in lower conversions. Additionally, the combination of alkyl chain length and percent conversion were found to influence BET surface area measurements. Overall, these results implicate that postsynthetic modification is a versatile, valuable technique for obtaining MOFs with unique functionalities and porosities.

2.4 Experimental Section

General. Starting reagents and solvents were purchased and used without further purification from commercial suppliers (Sigma-Aldrich, Alfa Aesar, EMD, TCI, Cambridge Isotope Laboratories, Inc., and others).

Synthesis of IRMOF-3. IRMOF-3 was synthesized and activated according to a modified procedure from literature.[4] $Zn(NO_3)_2 \cdot 4H_2O$ (6.00 g, 22.9 mmol) and 2-aminobenzenedicarboxylic acid (1.50 g, 8.30 mmol) were dissolved in 200 mL of DMF. The solution was divided into 10 mL portions and transferred to 20 scintillation vials (20 mL capacity). The vials were placed in a sand bath, and the bath was transferred to a programmable oven and heated at a rate of 2.5 °C/min from 35 to 100 °C. The

temperature was held for 18 h, and then the oven was cooled at a rate of 2.5 °C/min to a final temperature of 35 °C. This procedure generated amber block crystals of IRMOF-3. The mother liquor from each vial was decanted, and the crystals were washed with dry DMF (3 × 12 mL) (dried over molecular sieves) followed by one rinse with 12 mL of $CHCl_3$. The crystals were then soaked in 12 mL of $CHCl_3$ for 3 days with fresh $CHCl_3$ added every 24 h. After 3 days of soaking the crystals were stored in the last $CHCl_3$ solution until needed. The average yield of dried IRMOF-3 per vial was determined to be approximately 55-60 mg (~50%).

Method 1. Postsynthetic Modification Using Dry IRMOF-3. For each alkyl anhydride examined, five 4 mL dram vials were prepared in order to monitor the reactivity of IRMOF-3 over a period of five days. The $CHCl_3$ storage solution of IRMOF-3 was decanted, and the crystals were dried at 75 °C under vacuum for 12 h. Dried IRMOF-3 (27 mg, ca. 0.10 mmol equiv of $-NH_2$) was suspended in 1.0 mL of $CDCl_3$ in a 4 mL dram vial. Alkyl anhydride (2 equiv, 0.20 mmol for n) 1 to 15; 0.8 equiv, 0.08 mmol for n = 18) was added to the $CDCl_3$ solution, and the mixture was left to react at room temperature. The $CDCl_3$ solution was removed from one vial every 24 h and set aside for 1H NMR analysis of the soluble reaction byproducts (vide infra). After removal of the $CDCl_3$ solution, the modified IRMOF-3 crystals were washed with CH_2Cl_2 (3 × 2 mL) and left to soak in 2 mL of CH_2Cl_2 for 3 days, with fresh CH_2Cl_2 added every 24 h. After 3 days, the CH_2Cl_2 solution was decanted and the modified IRMOF-3 crystals were dried at 90 °C under vacuum for 8 h. Samples prepared in this fashion were analyzed using 1H NMR, ESI-MS, TGA, and PXRD.

Method 2. Postsynthetic Modification Using Wet IRMOF-3. Approximately 55-60 mg of IRMOF-3 (ca. 0.2 mmol equiv of $-NH_2$) were placed in a vial with 2 equiv (0.4 mmol for n = 1 to 15) or 0.8 equiv (0.16 mmol for n = 18) of alkyl anhydride dissolved in either 8 mL (n = 1, 2, 3) or 4 mL (n = 4, 5, 6, 8, 12, 15, 18) of $CHCl_3$. The different dilutions (i.e., anhydride concentrations) were used in order to best preserve the single crystallinity of the samples. After allowing the sample (n = 1 to 12) to stand at room temperature for 24 h, the solution was decanted and the crystals were washed with $CHCl_3$ (3 × 5 mL). A fresh solution of the anhydride was added to the vial, and the crystals were left to stand for an additional 24 h. The aforementioned procedure was repeated (washing followed by treatment with anhydride), with the only difference that some anhydrides (n = 1, 2, 3) were replenished at half the original concentration (1 equiv, 0.2 mmol in 8 mL of $CHCl_3$ for n = 1, 2, 3), giving a total reaction time of 3 days. Other samples (n = 15, 18) were treated for 3 days without replacing the anhydride solution. The $CHCl_3$ solution was decanted, and the crystals were washed with $CHCl_3$ (3 × 5 mL) before soaking in 5 mL of pure $CHCl_3$ for 3 days, with fresh $CHCl_3$ added every 24 h. After 3 days of soaking the crystals were stored in the last $CHCl_3$ solution until needed. Samples prepared in this fashion were analyzed using ^{1}H NMR, ESI-MS, gas sorption, and single crystal X-ray diffraction (when applicable).

Digestion and Analysis by ^{1}H NMR. ^{1}H NMR spectra were recorded on Varian FT-NMR spectrometers (400 and 500 MHz). Approximately 5 mg of IRMOF-3 modified using either Method 1 or Method 2 were digested by sonication in 500 μL of d^6-DMSO and 100 μL of dilute DCl (23 μL of 35% DCl in D_2O diluted with 1 mL of d^6-

DMSO). Upon complete dissolution of the crystals, this solution was used for ^{1}H NMR analysis.

Digestion and Analysis by MS. Electrospray ionization mass spectrometry (ESI-MS) was performed using a ThermoFinnigan LCQ-DECA mass spectrometer, and the data were analyzed using the Xcalibur software suite. Samples for analysis by ESI-MS were prepared by digesting the single crystal from X-ray analysis (vide infra) in 200-300 μL of H_2O or MeOH and were analyzed in negative ion mode.

Thermal Analysis. Approximately 10-12 mg of IRMOF-3 modified using Method 1 were used for TGA measurements. Samples were analyzed under a stream of dinitrogen using a TA Instrument Q600 SDT running from 25 to 600 °C with a scan rate of 5 °C/min.

PXRD Analysis. Approximately 15 mg of IRMOF-3 modified using Method 1 were soaked in 2 mL of fresh $CHCl_3$ for 2 days prior to analysis. Powder X-ray diffraction (PXRD) data were collected at ambient temperature on a Rigaku Miniflex II diffractometer at 30 kV, 15 mA for Cu Kα (λ = 1.5418 Å), with a scan speed of 5°/min and a step size of 0.05° in 2θ.

BET Surface Analysis. Approximately 60-75 mg of modified IRMOF-3 using Method 2 were evacuated under vacuum overnight. The modified IRMOF-3 was transferred to a preweighed sample tube and degassed at 30 °C for approximately 24 h on an ASAP 2020 or until the outgas rate was <5 μmHg. The sample tube was reweighed to obtain a consistent mass for the degassed modified IRMOF-3. BET surface area (m^2/g) measurements were collected at 77 K by dinitrogen on an ASAP 2020.

Single-Crystal X-ray Diffraction. Single crystals of modified IRMOF-3 soaking in $CHCl_3$ were mounted on nylon loops with Paratone oil and placed under a nitrogen cold stream (200 K). Data were collected on Bruker Apex diffractometers using Mo Kα radiation (λ = 0.71073 Å) controlled using the APEX 2.0 software package. Cell determinations were performed on all modified IRMOF-3, and full data sets were collected on four modifications of IRMOF-3 (-AM4, -AM6, -AM13, and -AM19). A semiempirical method utilizing equivalents was employed to correct for absorption.[11] All data collections were solved and refined using the SHELXTL suite. All non-hydrogen atoms were refined anisotropically. IRMOF-3-AM4, -AM6, -AM13, and -AM19 were treated with the "squeeze" protocol in PLATON[12] to account for electron density associated with the disordered alkyl substituent $-CO(CH_2)_nCH_3$ and for partially occupied or disordered solvent (e.g., $CHCl_3$) within the porous framework. The empirical formulas were adjusted to accommodate the appropriate ratio of unmodified NH_2–BDC to modified alkyl amide BDC ligand; solvent was not included, but was noted in the CIF.

2.5. Appendix

Table 2-5. Dinitrogen adsorption data at 77 K for IRMOF-3-AM2 to -AM19.

Relative pressure (P/Po)	**Adsorption Amount (cm^3/g STP)**							
	IRMOF-3-AM2		***IRMOF-3-AM3***		***IRMOF-3-AM4***		***IRMOF-3-AM5***	
	Trial 1	Trial 2	Trial 1	Trial 2	Trial 1	Trial 2	Trial 1	Trial 2
0.0048	385.0362	339.4204	297.5063	362.9429	338.2423	300.6941	238.6291	300.1054
0.0164	428.2287	375.3302	330.1062	400.4342	369.8939	330.3262	259.9708	327.6479
0.0253	437.7898	384.9125	337.7557	410.1403	379.0805	337.9172	267.2965	336.1665
0.0379	445.7125	392.2222	344.0044	417.4627	385.7779	343.8072	271.9618	342.2888
0.0511	451.1152	397.0214	348.2652	422.2262	390.1440	347.7886	275.2938	346.2941
0.0574	453.1615	398.7867	349.9092	424.1120	391.7670	349.2816	276.3899	347.6850
0.0678	455.9922	401.3263	352.0626	426.5162	394.0771	351.5025	278.2047	349.7984
0.0784	458.4007	403.4816	353.8862	428.6611	395.9804	353.2742	279.8326	351.5819
0.0890	460.4355	405.3429	355.3669	430.5051	397.6582	354.8381	281.1183	353.1444
0.0995	462.2335	406.9217	356.7270	431.9596	399.0661	356.1252	282.2063	354.4339
0.1096	463.7465	408.2899	357.9323	433.3189	400.2911	357.3076	283.1177	355.6199
0.1199	465.1551	409.5316	359.0075	434.4610	401.3764	358.3406	283.9724	356.6429
0.1301	466.3508	410.7127	359.9322	435.5456	402.3590	359.2856	284.8023	357.5918
0.1404	467.4916	411.7397	360.7889	436.5232	403.2941	360.1346	285.5224	358.4363
0.1507	468.5397	412.7151	361.5816	437.3769	404.1295	360.9280	286.1919	359.2260

Table 2-5 (continued). Dinitrogen adsorption data at 77 K for IRMOF-3-AM2 to -AM19.

Relative pressure (P/Po)	Adsorption Amount (cm^3/g STP)							
	IRMOF-3-AM6		***IRMOF-3-AM7***		***IRMOF-3-AM9***		***IRMOF-3-AM13***	
	Trial 1	Trial 2	Trial 1	Trial 2	Trial 1	Trial 2	Trial 1	Trial 2
0.0048	261.6644	264.7282	290.5899	238.8475	303.3731	241.8078	308.5140	319.3071
0.0164	285.8177	286.5337	317.0612	261.2192	336.3821	268.9478	342.2816	358.1553
0.0253	293.2842	294.1965	324.5582	269.9378	344.1327	277.1175	352.3142	367.2194
0.0379	298.3172	299.2741	330.1390	275.0589	350.4995	282.7333	359.5771	374.1722
0.0511	301.6836	302.4158	333.7840	278.3658	354.8681	286.3838	364.0752	378.9030
0.0574	302.9406	303.5523	335.0873	279.8734	356.6059	287.6591	365.7780	380.7023
0.0678	304.7989	305.3117	337.1448	281.7249	358.9167	289.5631	368.1412	383.1365
0.0784	306.3676	306.7288	338.8630	283.2783	360.8073	291.2192	370.0392	385.1681
0.0890	307.7412	308.0186	340.3910	284.6263	362.4884	292.6292	371.7875	386.9294
0.0995	308.9400	309.0686	341.6377	285.8759	363.9449	293.8180	373.2989	388.4377
0.1096	309.9403	309.9927	342.7810	286.8336	365.1972	294.8703	374.5631	389.6949
0.1199	310.9389	310.7933	343.7939	287.7404	366.2696	295.8039	375.7132	390.8327
0.1301	311.7821	311.5825	344.7268	288.5644	367.2796	296.6914	376.7324	391.8872
0.1404	312.6116	312.2193	345.5522	289.3316	368.2045	297.4786	377.6256	392.8459
0.1507	313.0887	312.8352	346.3303	290.0039	369.0413	298.2661	378.5070	393.7036

Table 2-5 (continued). Dinitrogen adsorption data at 77 K for IRMOF-3-AM2 to -AM19.

Relative pressure (P/Po)	**Adsorption Amount (cm^3/g STP)**			
	IRMOF-3-AM16		***IRMOF-3-AM19***	
	Trial 1	Trial 2	Trial 1	Trial 2
0.0048	382.7407	300.8550	484.4784	438.3383
0.0164	430.7469	339.8272	553.1148	499.5813
0.0253	441.1123	349.2001	572.0869	513.3464
0.0379	449.6682	356.3142	580.7649	523.9642
0.0511	455.3345	360.7979	587.9451	530.7334
0.0574	457.4333	362.4933	591.1616	533.1069
0.0678	460.3087	364.9315	594.9064	536.5307
0.0784	462.7736	367.0075	598.0290	539.3141
0.0890	464.8548	368.7879	600.7028	541.7086
0.0995	466.6147	370.2564	602.9324	543.8157
0.1096	468.1561	371.5303	604.8355	545.5605
0.1199	469.5560	372.7148	606.5549	547.1145
0.1301	470.7660	373.7735	608.0542	548.5181
0.1404	471.9341	374.7988	609.4676	549.7733
0.1507	472.9869	375.6667	610.7388	550.9405

Table 2-6. Comparison of BET surface area, evaluated by mass and per mole of MOF, and determination of the number of additional atoms (excluding hydrogen atoms) included per unit cell due to modification.

IRMOF-3	Unmodified	-AM2	-AM3	-AM4	-AM5	-AM6	-AM7	-AM9	-AM13	-AM16	-AM19
n	NA	1	2	3	4	5	6	8	12	15	18
# of additional atoms per chain (n+3) [a]	NA	4	5	6	7	8	9	11	15	18	21
conversion (Table 1, Method 2)	1.00	0.99	0.99	0.98	0.96	0.90	0.80	0.46	0.32	0.2	0.07
# of additional atoms per cavity [b]	NA	11.88	14.85	17.64	20.16	21.6	21.6	15.18	14.4	10.8	4.41
Idealized FW [c] (g/mol)	815.03	983.22	1025.3	1067.38	1109.46	1151.54	1193.62	1277.78	1446.1	1572.33	1698.57
Actual FW [d] (g/mol)	815.03	981.54	1023.20	1062.33	1097.68	1117.89	1117.90	1027.90	1016.97	966.49	876.88
BET Surface Area (m^2/g)	2408	1641	1487	1424	1201	1165	1185	1243	1438	1581	2164
Error Bar (m^2/g)	99	146	199	114	192	1	148	186	40	256	157
BET Surface Area (m^2/mmol)	1963	1611	1521	1513	1318	1302	1325	1278	1462	1528	1898
Error Bar (m^2/mmol)	81	144	204	121	211	1	165	191	40	247	138

[a] The number of atoms added per modified ligand were calculated by including one carbonyl oxygen, one carbonyl carbon, one methyl carbon, and n methylene carbons (only non-hydrogen atoms). [b] Obtained from the formula: (n+3)×(percent conversion)×3, where 3 is the number of unique amino groups per unit cell. [c] Formula weight of MOF based on fully modified BDC ligand. [d] Formula weight of MOF based on the following formula FW = (idealized formula weight)×(*r*)+(formula weight of IRMOF-3)(1-*r*), where r = percent conversion.

2.6 Acknowledgements

Text, schemes, and figures in this chapter, in part, are reprints of the materials published in the following papers: Tanabe K. K., Wang, Z., Cohen, S. M. "Systematic Functionalization of a Metal-Organic Framework via a Postsynthetic Modification Approach" *J. Am. Chem. Soc*. **2008**, *130*, 8508-8517. The dissertation author was the primary researcher and author for the data presented. The co-authors listed in these publications also participated in the research. The permissions to reproduce these papers were granted by the American Chemical Society, copyright 2008.

2.7 References

(1) Hoskins, B. F.; Robson, R. *J. Am. Chem. Soc.* **1990**, *112*, 1546-1554.

(2) Wang, Z.; Cohen, S. M. *J. Am. Chem. Soc.* **2007**, *129*, 12368-12369.

(3) Eddaoudi, M.; Kim, J.; Rosi, N.; Vodak, D.; Wachter, J.; O'Keeffe, M.; Yaghi, O. M. *Science* **2002**, *295*, 469-472.

(4) Rowsell, J. L. C.; Yaghi, O. M. *J. Am. Chem. Soc.* **2006**, *128*, 1304-1315.

(5) Kiang, Y.-H.; Gardner, G. B.; Lee, S.; Xu, Z.; Lobkovsky, E. B. *J. Am. Chem. Soc*. **1999**, *121*, 8204-8215.

(6) Seo, J. S.; Whang, D.; Lee, H.; Jun, S. I.; Oh, J.; Jeon, Y. J.; Kim, K. *Nature* **2000**, *404*, 982-986.

(7) Walton, K. S.; Snurr, R. Q. *J. Am. Chem. Soc.* **2007**, *129*, 8552-8556.

(8) Assuming the crystals have an idealized cubic shape with sides of length l, the total exposed surface area for each crystal would be $6\times l^2$. A cubic unit cell on the other hand would have a surface area of $6\times a^2$ (a being the unit cell edge dimension). Because the total number of unit cells present in each crystal is l^3/a^3, the percent of exposed crystal surfaces vs. total unit cell surfaces can be estimated to be $(6\times l^2)/[(l^3/a^3)(6\times a^2)]=a/l$. For a typical IRMOF-3 crystal (l ~ 0.25 mm; a~ 26 Å), modification of only the crystal surface would give rise to a percent conversion far less than 1%.

(9) Wang, Z.; Cohen, S. M. *Angew. Chem. Int. Ed.* **2008**, *47*, 4699-702.

(10) The caveat to this assumption is that if a specific modification significantly increased sorption capacity (e.g. through stronger energetics of gas binding) then the antcipated drop in surface area would not necessarily be observed.

(11) Sheldrick, G. M.; version 2.10 ed.; Bruker AXS, Inc.: Madison, WI, 2004, p The semiempirical method used is based on a method of Blessing, R. H. *Acta Crystallogr*. **1995**, *A51*, 33.

(12) Spek, A. L. *J.Appl.Cryst.* **2003**, *36*, 7-13.

Chapter 3 Influence of Metal-Organic Framework Topology on Postsynthetic Modification

3.1 Introduction

After finishing our systematic PSM study with IRMOF-3[1], we[2,3] and others[4-9] began testing new PSM reactions to produce new functionalized MOFs. As a follow-up to our IRMOF-3 study, we modified IRMOF-3 with a range of isocyanates to generate urea modified IRMOFs (IRMOF-3-UR, UR = urea) with alkyl, aromatic, and olefin substituents (Figure 3-1).[2] In a separate study, IRMOF-3 was shown to undergo tandem modification with two different reagents via two routes (Figure 3-2). In the first route, IRMOF-3 was modified with both an alkyl and olefin substituent using acetic anhydride and crotonic anhydride in a two step process. The second route consisted of modifying IRMOF-3 with crotonic anhydride to produce an IRMOF with olefin substituents and transform the olefins into alkyl halides through bromination. In addition to using anhydrides and isocyanates, other groups modified IRMOF-3 and various amino containing MOFs with aldehydes to produce imine functionalities within the framework (Figure 3-3).[5,8] Non-amino containing MOF systems (e.g., IRMOF-1), were also examined for PSM and were modified with unique functionalities such as organometallic complexes ($Cr(CO)_3$)[9] (Figure 3-3).

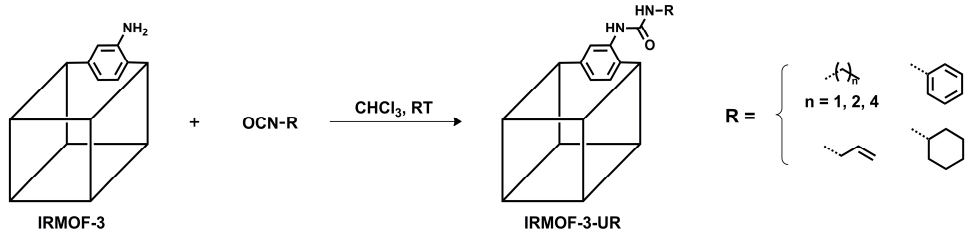

Figure 3-1. Modification of IRMOF-3 with isocyanates.

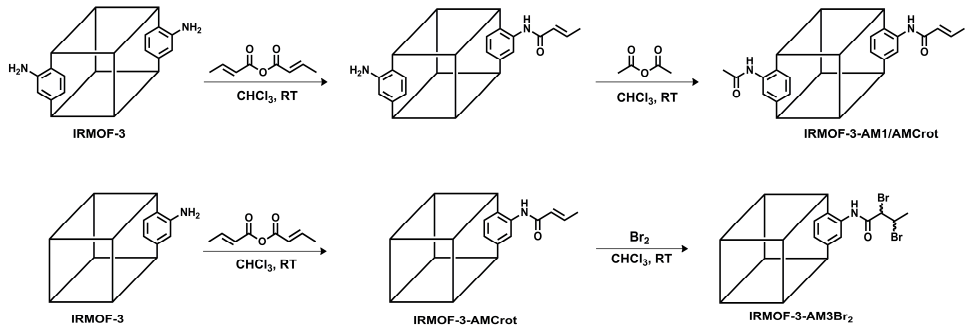

Figure 3-2. Tandem modification of IRMOF-3 via two modification pathways: modification with crotonic anhydride followed by acetic anhydride (top), and modification with crotonic anhydride and bromide (bottom).

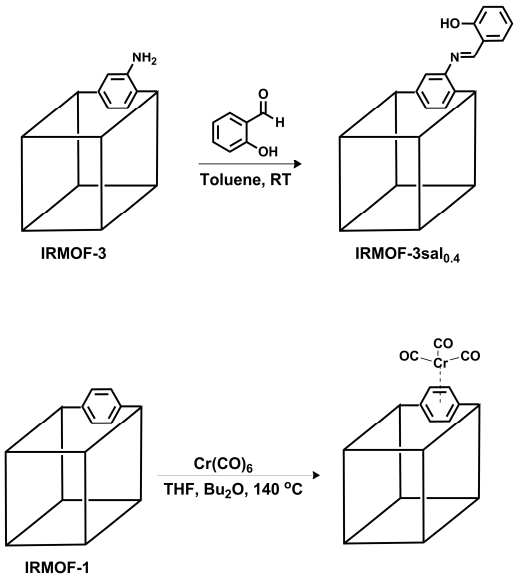

Figure 3-3. Modification of IRMOF-3 with salicylaldehyde (top) and modification of IRMOF-1 with $Cr(CO)_6$ **(**bottom).

Although PSM was proving to be a useful functionalization approach, it became apparent there was no clear understanding about what types of MOFs would be suitable for PSM and how MOF topology (e.g., pore size and shape), in conjunction with reagent size and shape, would affect modification. One, not all MOFs can undergo chemical modification, which may present an issue if the MOF has a desirable topology but has no modifiable component. Two, there were no reports studying the effects of reagent shape

with PSM aside from our previous study with reagent size. Lastly, topologically diverse MOFs (e.g., different pore sizes and shapes) might have different modification outcomes even when treated under similar conditions. Therefore, another systematic study on MOF topology and PSM was needed, especially to address several important issues.

Given the success with the IRMOF-3 system, the next strategy was to target other MOFs that had NH_2-BDC as their organic component, modify the amino groups via PSM, and compare and contrast the results with IRMOF-3. However, there were few other well-established NH_2-BDC frameworks to test for PSM. Despite the lack of NH_2-BDC containing MOFs, there were in fact many topologically diverse MOFs containing the BDC ligand. Moreover, Yaghi and coworkers had reported that they could obtain isostructural MOFs (e.g., IRMOF-1 and IRMOF-3) by either using BDC or NH_2-BDC, respectively.[10,11] Theoretically, NH_2-BDC containing MOF analogs could be synthesized by simply replacing BDC with NH_2-BDC, therefore giving new MOF topologies that could be tested for PSM and compared with IRMOF-3. In this chapter, two new NH_2-BDC containing MOFs (denoted as DMOF-1-NH_2 and UMCM-1-NH_2) were synthesized based on the previously reported DMOF-1 (DABCO-MOF-1)[12,13] and UMCM-1 (University of Michigan Crystalline Material-1)[14] MOFs, which contain BDC (Scheme 3-1). IRMOF-3, DMOF-1-NH_2, and UMCM-1-NH_2 were modified with linear alkyl anhydrides ($(CH_3(CH_2)_nCO_2)O$, where n = 0, 2, 4, 8, 12, 18) and branched alkyl anhydrides (trimethylacetic anhydride and isobutyric anhydride). ^{1}H NMR and ESI-MS were used to confirm the modification for each modified sample and all modified samples were analyzed by TGA, PXRD, single-crystal X-ray diffraction, and Brunauer-Emmett-Teller (BET) surface areas.

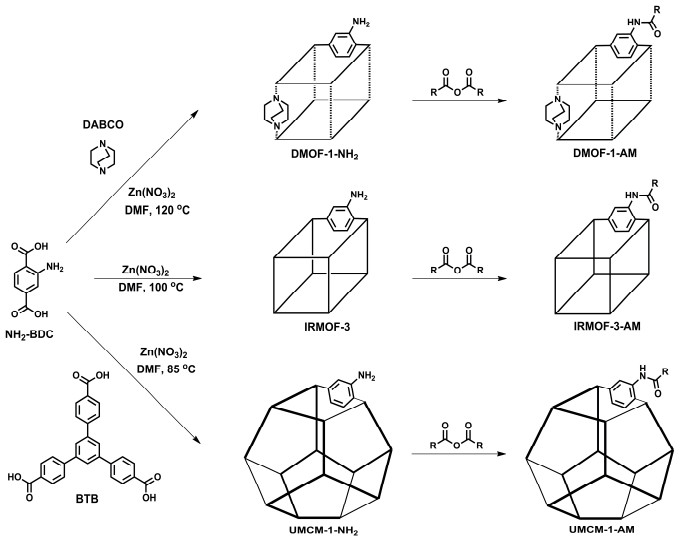

Scheme 3-1. Synthesis and Postsynthetic Modification of Three MOFs: DMOF-1-NH_2, IRMOF-3, and UMCM-1-NH_2. For DMOF-1-NH_2 and UMCM-1-NH_2, DABCO and BTB ligands are represented by dashed and bold lines in the scheme, respectively.

3.2 Results and Discussion

3.2.1 Synthesis and characterization of DMOF-1-NH_2

DMOF-1-NH_2 was adapted from DMOF-1, a 3D MOF constructed from Zn^{2+} paddlewheel SBUs that are equatorially coordinated by BDC ligands and axially coordinated by DABCO (1,4-diazabicyclo[2.2.2]octane) (Figure 3-4).[12,13] By slightly modifying the reaction conditions of DMOF-1, as well as replacing BDC with NH_2-BDC, DMOF-1-NH_2 was produced as beige, plate-like crystals from DMF after 12 h at 120 °C. Initial attempts were made to collect and solve the single crystal X-ray structure of DMOF-1-NH_2, but only unit cell parameters were obtained due to the weak diffraction quality of the crystals. The unit cell parameters for DMOF-1-NH_2 (tetragonal P, $a = b =$ 15.02 Å, c = 19.25 Å, $\alpha = \beta = \gamma$ = 90 °, V = 4341 $Å^3$) were found to be similar to DMOF-1 (tetragonal I, $a = b$ = 15.15 Å, c = 19.41 Å, $\alpha = \beta = \gamma$ = 90 °, V = 4455 $Å^3$), suggesting that DMOF-1-NH_2 was isostructural to DMOF-1. As further proof DMOF-1-NH_2 was

isostructural to DMOF-1, both DMOFs were analyzed and compared by PXRD, TGA, and gas sorption analysis. DMOF-1 and DMOF-1-NH_2 exhibited similar PXRD patterns and both were found to decompose between 300-350 °C (Figure 3-5). Dinitrogen (N_2) sorption analysis of DMOF-1-NH_2 revealed its BET surface area to be ~1510 m^2/g, which falls within the report range for DMOF-1 (1450 m^2/g to 1794 m^2/g). As further proof, DMOF-1-NH_2 was digested and analyzed by ^1H NMR (Figure 3-6), which showed the presence of NH_2-BDC and DABCO in a 1:0.6 ratio based on ^1H NMR integration of the NH_2-BDC and DABCO peaks (1:0.5 ratio expected). As evidenced by XRD, TGA, gas sorption analysis, and ^1H NMR, DMOF-1-NH_2 is an analog of DMOF-1.

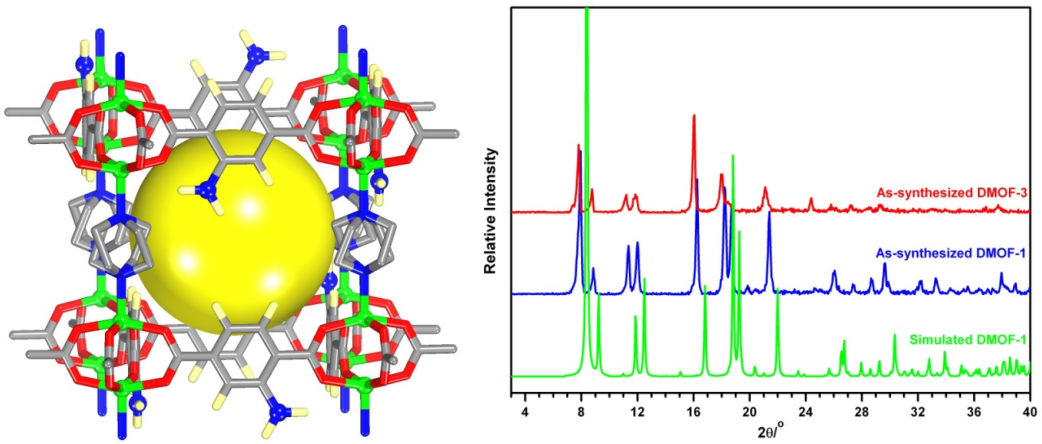

Figure 3-4. Proposed structural model for DMOF-1-NH_2 ($Zn_2(NH_2\text{-BDC})_2(DABCO)$) (left), based on the reported structure of DMOF-1. Color scheme: green, Zn; red, O; grey, C; blue, N; gold, H. DABCO molecules are shown with disorder as reported for DMOF-1. The yellow sphere illustrates estimated free space. PXRD (right) of the as-synthesized DMOF-1-NH_2 (red), as-synthesized DMOF-1 (blue), and simulated DMOF-1 (green) derived from ref. 13.

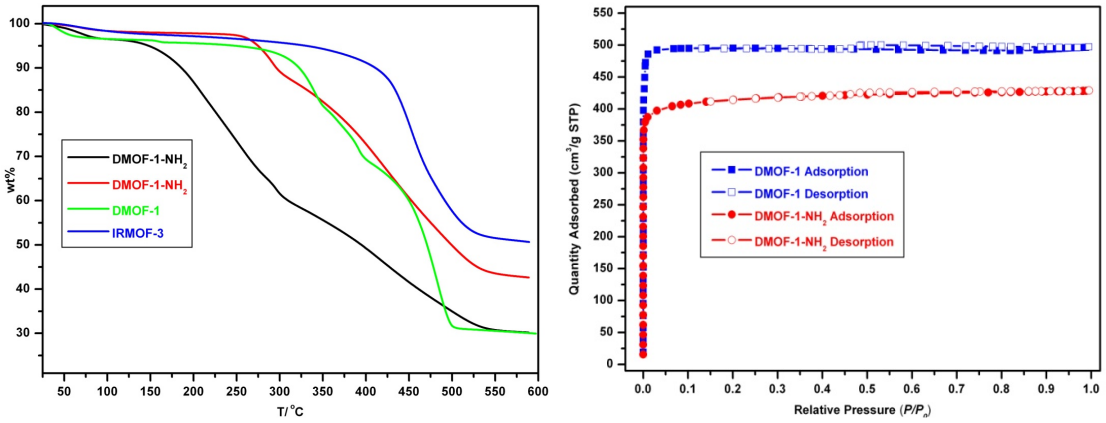

Figure 3-5. TGA trace (left) for as-synthesized DMOF-1-NH_2 (black), dried DMOF-1-NH_2 (red), dried DMOF-1 (green), and dried IRMOF-3 (blue). N_2 isotherm analysis (right) of DMOF-1 and DMOF-1-NH_2 at 77 K.

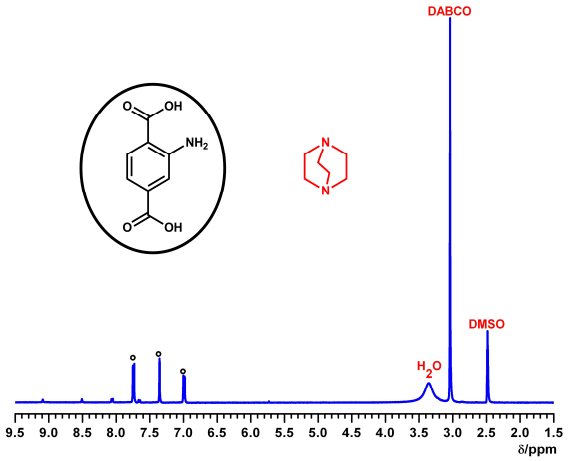

Figure 3-6. ^{1}H NMR of digested DMOF-1-NH_2. Resonances associated with NH_2-BDC are highlighted with black circles.

3.2.2 Synthesis and characterization of UMCM-1-NH_2

UMCM-1-NH_2 was modified from a published report of UMCM-1 by Matzger and coworkers.[14] UMCM-1 contains Zn_4O SBUs that are octahedrally coordinated by BTB and 4,4′,4″-benzene-1,3,5-triyl-tribenzoic acid) and BDC ligands, which results in an unique 3D lattice with two types of pores: a small pore bordered by BTB and BDC and a large 1D hexagonal pores bordered primarily by the BTB ligand. Matzger and

coworkers discovered the synthesis of UMCM-1, as well as its phase purity, was dependent on the ratio of BDC:BTB. Increasing the BDC ratio resulted in the formation of IRMOF-1 as colorless block-like crystals, while increasing the BTB ratio resulted in the formation of MOF-177, which forms as colorless polyhedral crystals. By controlling the BDC:BTB ratio between 3:2 to 1:1, UMCM-1 was obtained as a single phase crystalline material in the form of colorless needles from DEF after 3 days at 85 °C. After exploring different ratios of NH_2-BDC:BTB, UMCM-1-NH_2 was synthesized from a ratio of 2.5:1 NH_2-BDC:BTB in DMF after 2 days at 85 °C. An excess of NH_2-BDC was needed in order to avoid forming MOF-177. Although NH_2-BDC and BTB are chemically similar, the reactivity of BTB is much faster than NH_2-BDC, especially in a 1:1 ratio. With the exception of UMCM-1 and UMCM-2, other UMCM systems have required an excess of BDC ligand to BTB ligand in order to successfully form the mixed ligand MOF as a pure phase.[14-16]

UMCM-1, IRMOF-3, and MOF-177 were prepared as control samples to confirm the composition and phase purity of UMCM-1-NH_2. The morphology of UMCM-1-NH_2 was comparable with UMCM-1, but clearly distinct from IRMOF-3 and MOF-177 for both morphology and color (Figure 3-7). ^{1}H NMR analysis of all four MOF samples revealed UMCM-1-NH_2 contained both NH_2-BDC and BTB in the expected 2:1 ratio. TGA analysis of UMCM-1-NH_2 showed the MOF had comparable thermal stability (~450 °C) as UMCM-1 and IRMOF-3 (MOF-177 not shown), which are stable up to 450 °C. PXRD analysis confirmed the overall bulk crystallinity of UMCM-1-NH_2 resembled UMCM-1 (Figure 3-8) and was not a mixture of IRMOF-3 or MOF-177 (data not shown).

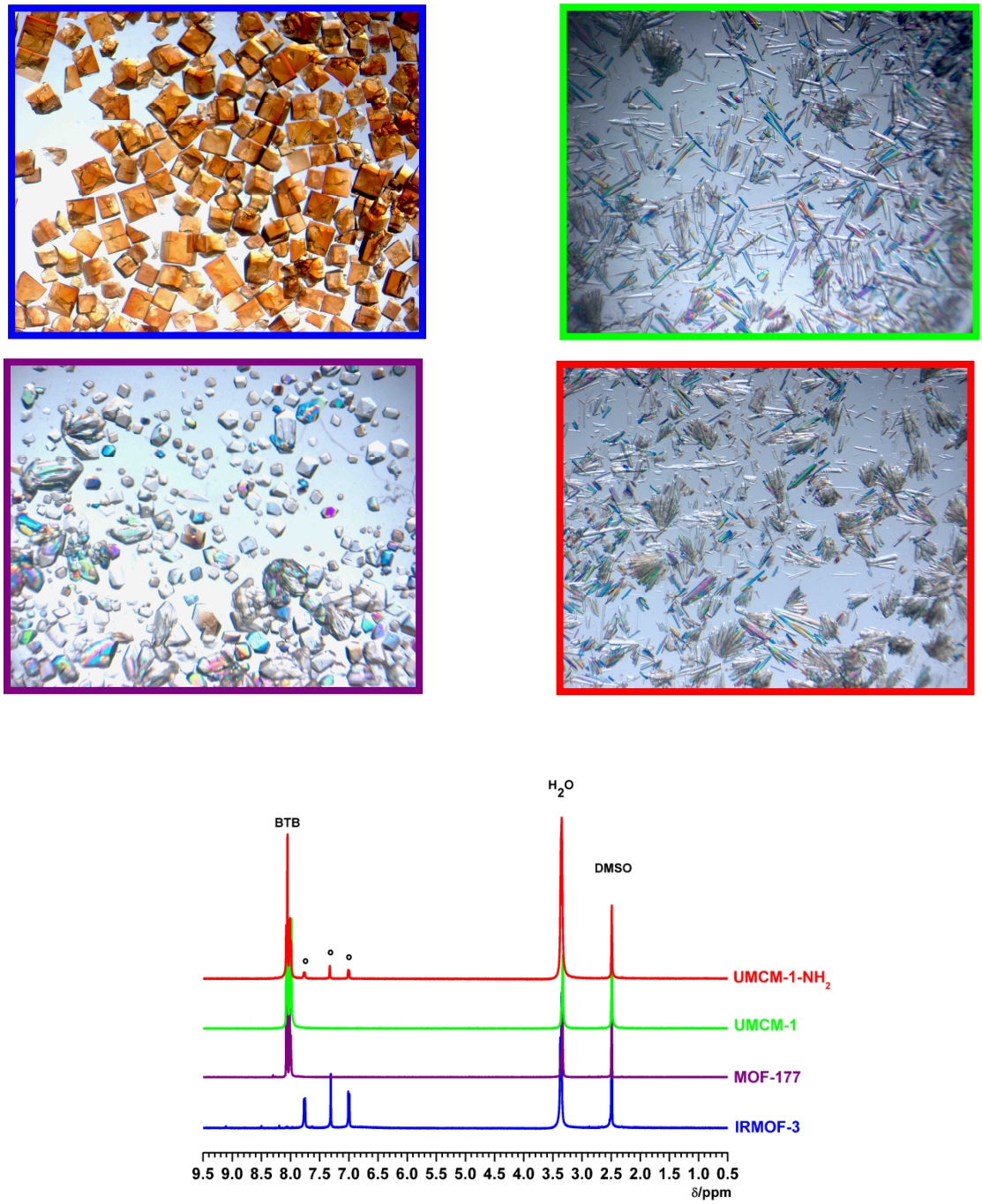

Figure 3-7. Photographs (top) of IRMOF-3 (blue border), MOF-177 (purple border), UMCM-1 (green border), and UMCM-1-NH_2 (red border). ^{1}H NMR spectra (bottom) of IRMOF-3 (blue), MOF-177 purple), UMCM-1 (green), and UMCM-1-NH_2 (red) samples digested in DCl/D_2O and DMSO-d^6. Resonances associated with NH_2-BDC are highlighted with black circles.

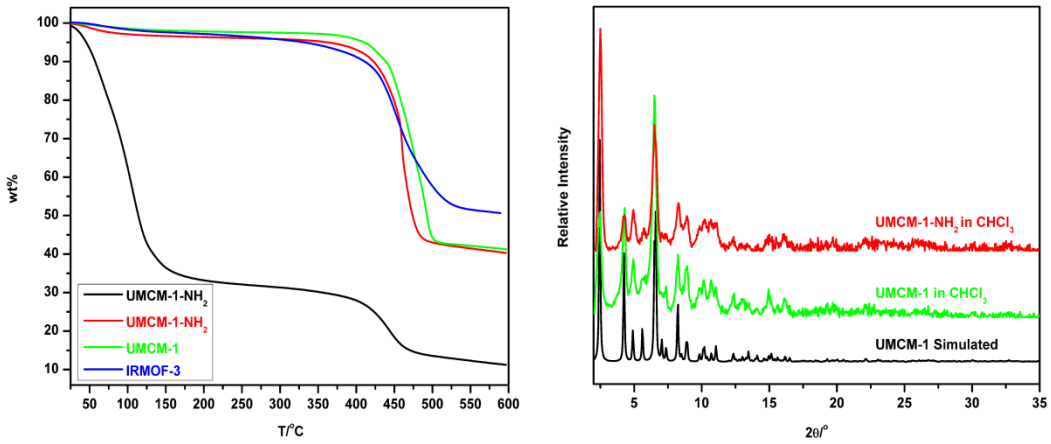

Figure 3-8. TGA trace (left) for as-synthesized UMCM-1-NH_2 (black), dried UMCM-1-NH_2 (red), dried UMCM-1 (green), and dried IRMOF-3 (blue). PXRD analysis (right) of UMCM-1 (simulated, black), UMCM-1 ($CHCl_3$ exch., green), and UMCM-1-NH_2 ($CHCl_3$ exch., red).

Single crystal X-ray diffraction of UMCM-1-NH_2 provided definite proof that UMCM-1-NH_2 was isostructural to UMCM-1. The original UMCM-1 structure is hexagonal ($P6_3/m$) with $a = b = 41.5262(8)$ Å, $c = 17.4916(5)$ Å with a unit cell volume of 26129 $Å^3$.[14] UMCM-1-NH_2 was found to crystallize with the same unit cell parameters as UMCM-1. Suitable atomic positions were found and assigned for three Zn^{2+} ions, 31 carbon atoms, and 8 oxygen atoms in the asymmetric unit, which corresponds to one Zn_4O SBU, 3 BTB ligands, and one NH_2-BDC ligand (Figure 3-9). Unfortunately, no suitable electron density could be located for the amino group due to disorder over all four positions on the phenyl ring and due to the weak diffraction quality of the crystal. To prove NH_2-BDC was present, the single crystal was taken directly from the difffractometer, digested in MeOH, and analyzed by ESI-MS. Both NH_2-BDC and BTB were detected by ESI-MS (data not shown). After solving the structure, UMCM-1-NH_2 was found to be a 3D framework containing 1D hexagonal pores bordered by the

BTB ligands and smaller pores constructed from a combination of six NH_2-BDC and five BTB linkers (Figure 3-10). N_2 sorption analysis of UMCM-1-NH_2 provided additional support of the framework topology. UMCM-1 has a reported BET of 4160 m^2/g and exhibits a distinct step in its isotherm, which indicates the presence of two different pores sizes. UMCM-1-NH_2 was determined to have a slightly lower BET of 3973 m^2/g, as expected due to the presence of amino groups, and also displayed the two-step in its isotherm. Based on single crystal X-ray and BET surface area alone, the data verifies UMCM-1-NH_2 is the amino version of UMCM-1.

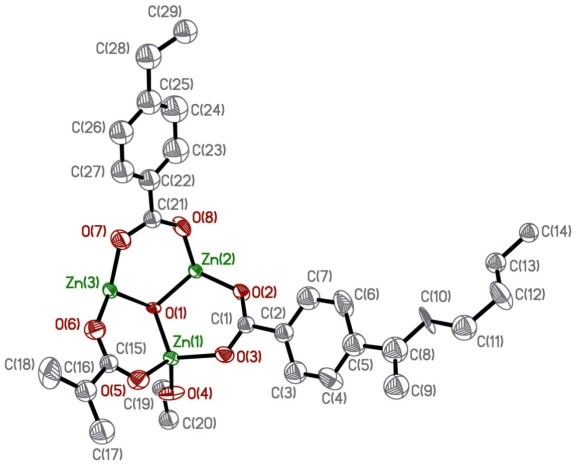

Figure 3-9. Asymmetric unit of UMCM-1-NH_2 with 50% probability ellipsoids and atom numbering scheme.

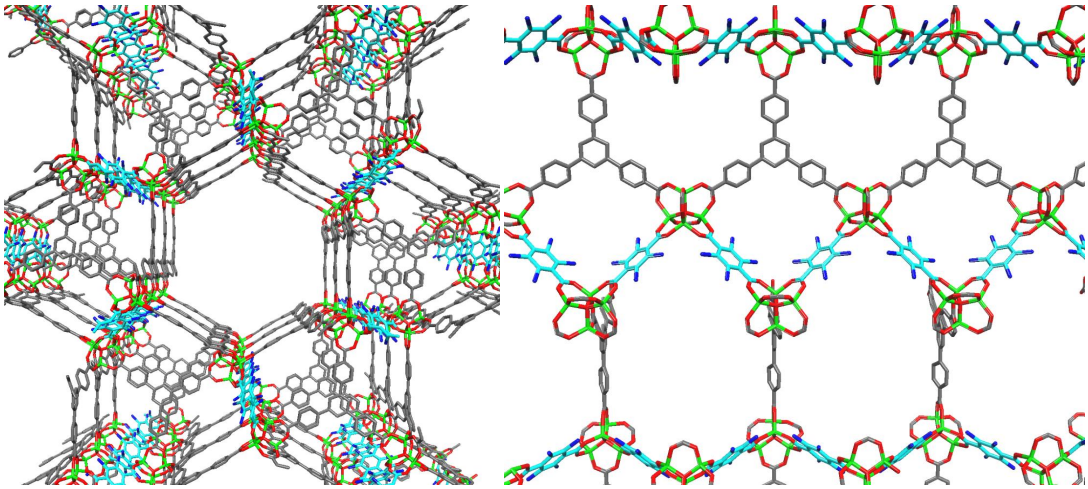

Figure 3-10. Structure of UMCM-1-NH_2 ($Zn_4O(BTB)_{4/3}(NH_2\text{-BDC})$) determined by single-crystal X-ray diffraction (two views). Color scheme: green, Zn; red, O; grey, C; blue, N. Amino groups have been modeled in all four possible positions of the NH_2-BDC ring, but were not found in the difference map. The NH_2-BDC ligands are highlighted in cyan.

3.2.3 Method 1: Modification of IRMOF-3, DMOF-1-NH_2, and UMCM-1-NH_2

To properly assess the relationship between MOF topology and PSM, IRMOF-3, DMOF-1-NH2, and UMCM-1-NH_2 were prepared using Method 1 (e.g., dried under vacuum) and examined under identical reaction conditions. Each MOF was reacted with 6 long chain alkyl anhydrides ($(CH_3(CH_2)_nCO)_2$, where n = 0, 2, 4, 8, 12, 18) and two branched anhydrides (trimethylacetic anhydride and isobutyric anhydride) in $CHCl_3$. Both linear and branched anhydrides were used to explore how reagent shape could affect modification. After treating the MOFs with the eight anhydrides, the MOFs were washed extensively with $CHCl_3$, dried under vacuum, digested using $DCl/D_2O/d^6$-DMSO, and analyzed by ^1H NMR to determine their percent conversions.

Similar to IRMOF-3, both DMOF-1-NH_2 and UMCM-1-NH_2 underwent modification with the anhydrides, which indicated that PSM could be applied to different framework topologies. ^1H NMR analysis of the MOFs revealed that, under identical

conditions, the extent of modification was dependent on a combination of reagent size and MOF topology. On average, UMCM-1-NH_2 had the highest degree of modification, followed by IRMOF-3 in the middle, and then DMOF-1-NH_2, which had the lowest conversions overall (Table 3-1, Figure 3-11). This modification trend appeared to be consistent since UMCM-1-NH_2 has larger pores than IRMOF-3 and DMOF-1-NH_2, and DMOF-1-NH_2 has smaller pores in respect to IRMOF-3. UMCM-1-NH_2 and IRMOF-3 were found to have similar percent conversions with the smaller linear anhydrides ($n \leq 4$); however, their differences in pore size and surface area was clearly reflected when longer linear anhydrides were used. In our original IRMOF-3 study with alkyl anhydrides, the percent conversion was found to be inversely proportional to the alkyl anhydride chain length.[1] This trend was also observed with both UMCM-1-NH_2 and DMOF-1-NH_2 and found to be independent of their pore sizes. Interesting results were obtained when branched anhydrides were examined with the MOFs instead of linear anhydrides. For trimethylacetic anhydride, which is the bulkiest reagent used, very low conversions (<10%) were achieved for all three MOFs. In contrast, isobutyric anhydride, which is less bulky, had very different results between all three MOFs. In particular, IRMOF-3 had the highest conversion of 84%, followed by UMCM-1-NH_2 with 48%, and DMOF-1-NH_2 with 10%. The conversions suggest a different relationship exists between reagent shape and pore size, especially since IRMOF-3 had the highest modification extent even though it has smaller pores than UMCM-1-NH_2.

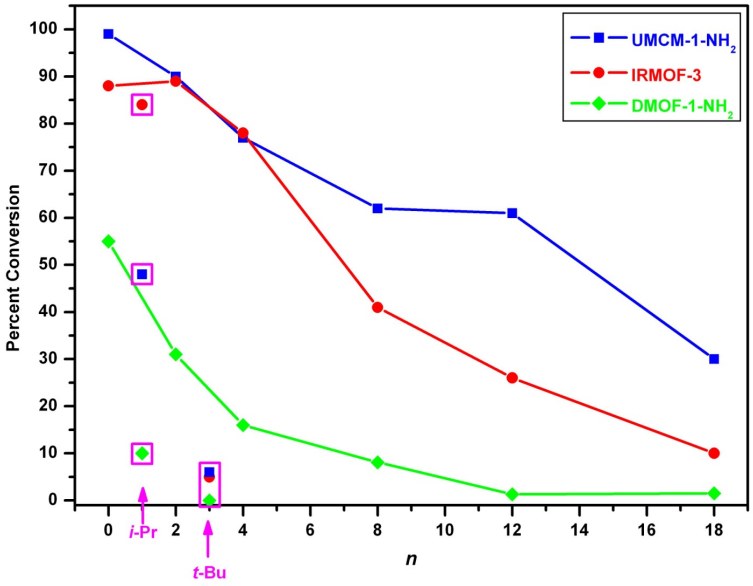

Figure 3-11. Plots of percent conversion vs length of linear anhydrides (*n*) for IRMOF-3 (red), DMOF-1-NH_2 (green), and UMCM-1-NH_2 (blue) based on Method 1. Data for trimethylacetic anhydride and isobutyric anhydride are also included for comparison.

Table 3-1. Percent conversions of postsynthetic modification reactions with IRMOF-3, DMOF-1-NH_2, and UMCM-1-NH_2 with different anhydrides as determined by ^{1}H NMR. Values are given for reactions performed under identical (Method 1) and MOF-specific, optimized (Method 2) conditions. Values listed are an average (with standard deviations) of at least three independent experiments.

MOF		-AM1	-AM3	-AM5	-AM9	-AM13	-AM19	-AM*i*Pr	-AM*t*Bu
n =		0	2	4	8	12	18	n/a	n/a
Method 1	DMOF-1	55±13%	31±3%	17±3%	8±3%	~1%	~1%	10±2%	0%
	IRMOF-3	88±3%	89±6%	78±2%	41±1%	26±3%	10±3%	84±5%	5±1%
	UMCM-1	~99%	90±5%	77±5%	62±4%	61±3%	30±2%	48±9%	6±3%
Method 2	DMOF-1	~99%	~99%	67±3%	34±4%	11±2%	~2%	63±9%	~1%
	IRMOF-3[a]	~99%	~99%	96±3%	46±7%	32±5%	7±1%	n.d. [b]	n.d. [b]
	UMCM-1	~99%	~99%	93±1%	89±5%	84±7%	28±4%	49±4%	~1%

[a] from reference 1. [b] not determined.

3.2.4 Method 2: DMOF-1-NH_2 modification and characterization

Attempts were made to improve the percent conversions for DMOF-1-NH_2 by using heat to drive modification of the framework. Preliminary tests at 55 °C with acetic anhydride (n = 0) resulted in a dramatic increase in percent conversion for DMOF-1-AM1 from 55% to ~99%. By using a combination of heat, daily washings with $CHCl_3$, and daily exchanges with fresh anhydride solutions, the modification conditions were greatly improved for DMOF-1-NH_2 (Table 3-1, Figure 3-12) showing both higher yields and a high degree of crystallinity. On average, DMOF-1-AM1 and DMOF-1-AM3 were quantitatively modified (~99%) while DMOF-1-AM5, -AM9, and -AM*i*Pr had significantly improved conversions (Table 3-1). By taking a closer look at the DMOF-1-NH_2 lattice, the orientation of the NH_2-BDC ligands and position of the amino group appears to play a significant role with modification. Unlike IRMOF-3 and UMCM-1-NH_2, the smaller pore size of DMOF-1-NH_2 increases the probability that the NH_2-BDC ligands may orientate in an edge-to edge manner, which places one NH_2-BDC ligand in close proximity to another. This potentially limits the accessibility of the amino groups for modification with the anhydrides. Under Method 1, DMOF-1-NH_2 had very low modifications even with the smaller alkyl anhydrides (e.g., acetic anhydride). However, upon applying heat with Method 2, DMOF-1-NH_2 undergoes high modifications, suggesting that the NH_2-BDC rings can undergo free rotation and avoid interfering with one another. This observation can only be applied to the smaller alkyl anhydrides, though. Unfortunately, higher conversions could not be achieved for DMOF-1-AM13, -AM19, and -AM*t*Bu, which suggests the alkyl substituents are too bulky overall for the DMOF-1-NH_2 channels.

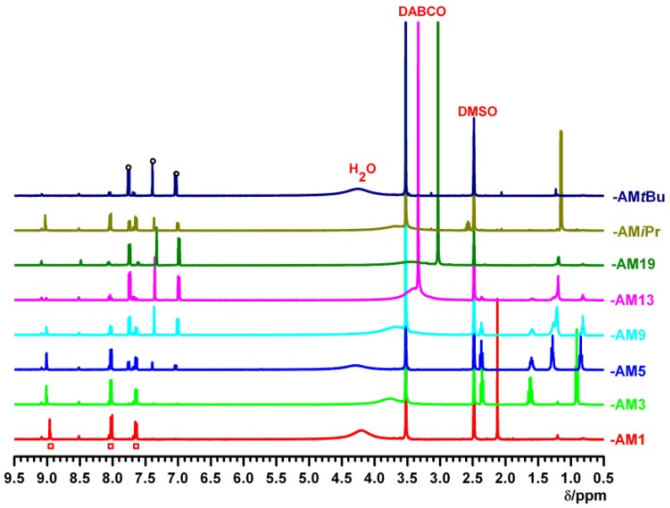

Figure 3-12. ^{1}H NMR spectra of modified DMOF-1-NH_2 samples (Method 2) digested in DCl/D_2O and DMSO-d^6 (left). Red squares and black circles represent signals of modified and unmodified NH_2-BDC, respectively.

Modified DMOF-1-NH_2 samples were analyzed by optical microscopy, TGA, PXRD, and gas sorption experiments to confirm the overall stability of the modified materials. No apparent degradation of the modified DMOF-1-NH_2 samples was observed visually after the crystals were exposed to anhydride (Figure 3-13). By TGA, the modified samples maintained similar thermal stability as unmodified DMOF-1-NH_2, and PXRD analysis showed good agreement between the most intense reflections of unmodified and modified DMOF-1-NH_2, showing the overall structural integrity was preserved (Figure 3-14). The modified DMOF-1-NH_2 samples were then analyzed by BET surface area measurements under N_2 at 77 K and were found to remain microporous. Full isotherm analysis of DMOF-1-AM5, which is 67% modified, showed a Type I isotherm as DMOF-1-NH_2, and was determined to have a BET surface area of ~740 m^2/g with a median pore width of 5.35 Å based on the Horvath-Kawazoe (H-K)

model (Figure 3-15). As expected, the isotherm type and measurements are lower than unmodified DMOF-1-NH_2 (1510 m^2/g and 5.58 Å, respectively).

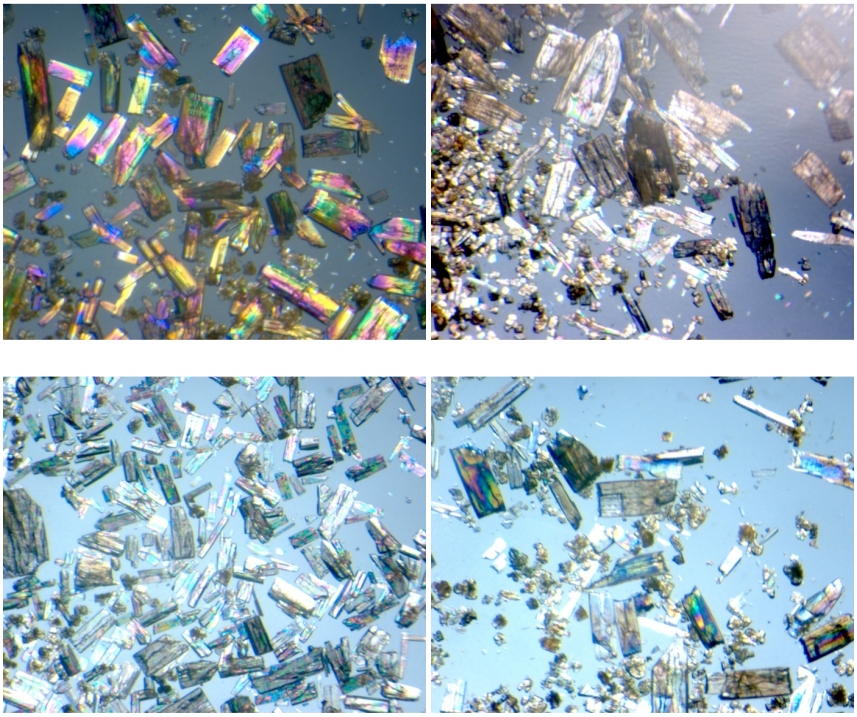

Figure 3-13. Photographs of unmodified DMOF-1-NH_2 (upper left), DMOF-1-AM5 (upper right), DMOF-1-AM9 (lower left), and DMOF-1-AM13 (lower right) as prepared via Method 2.

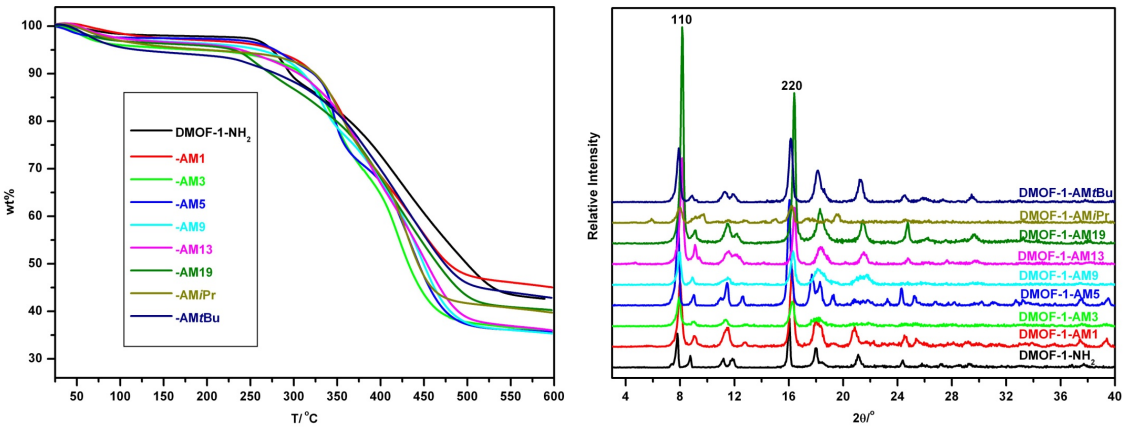

Figure 3-14. TGA trace (left) and PXRD analysis (right) of modified DMOF-1-NH_2 samples.

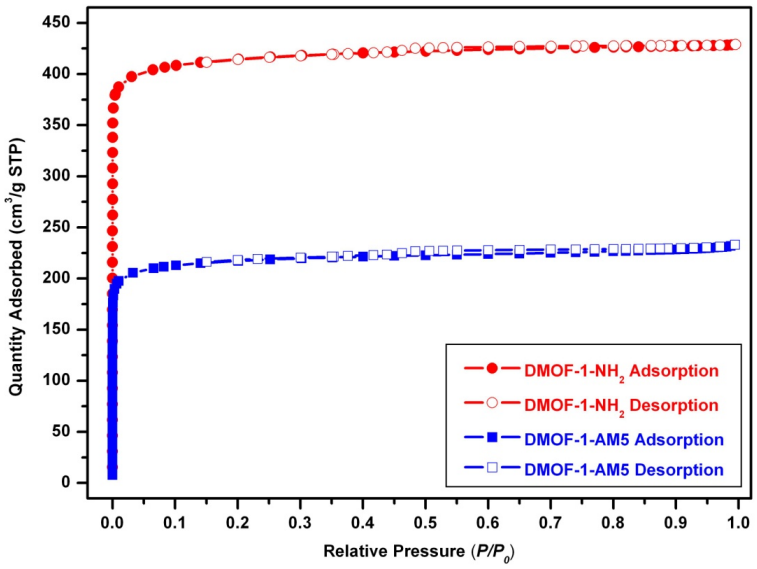

Figure 3-15. N_2 isotherms of DMOF-1-NH_2 and DMOF-1-AM5 at 77 K (right).

3.2.5 Method 2: UMCM-1-NH_2 modification and characterization

Given UMCM-1-NH_2 has large pores and showed moderate conversions with the longer alkyl anhydrides, UMCM-1-NH_2 was exposed to higher anhydride concentrations to improve the extent of modification. UMCM-1-NH_2 is tolerant to higher concentrations of anhydride than IRMOF-3 with respect to preservation of crystallinity (Figure 3-16). By using higher anhydride concentrations (0.2 M, 8 eq. of anhydride), UMCM-1-AM3 to UMCM-1-AM13 were achieved with > 80% on average, with a distinct 20% increase for UMCM-1-AM5, -AM9, and –AM13 from the Method 1 results (Table 3-1, Figure 3-17). UMCM-1-AM1 and UMCM-1-AM19 did not show any change in percent conversion (~99% for n = 0 and ~28% for n =18), and no improvements were seen with UMCM-1-AM*t*Bu (~1%) and UMCM-1-AM*i*Pr (~49%). While higher anhydride concentrations appeared to improve the percent modification of the linear alkyl chains, use of a higher anhydride concentration had no effect on the formation of UMCM-1-AM*i*Pr. This suggests the shape and bulkiness of the isobutyric anhydride is not very compatible with

the UMCM topology. Under identical reaction conditions (Method 1), IRMOF-3-AM*i*Pr had higher modification over UMCM-1-AM*i*Pr even though IRMOF-3 has lower porosity overall. By looking at structural models, the pore size and cavities adjacent to the amino substituents in UMCM-1-NH_2 appear to be smaller than in IRMOF-3 (Figure 3-18). As a result, modification with branched anhydrides is more dependent on the size and shape constraints of the framework in contrast with linear anhydrides.

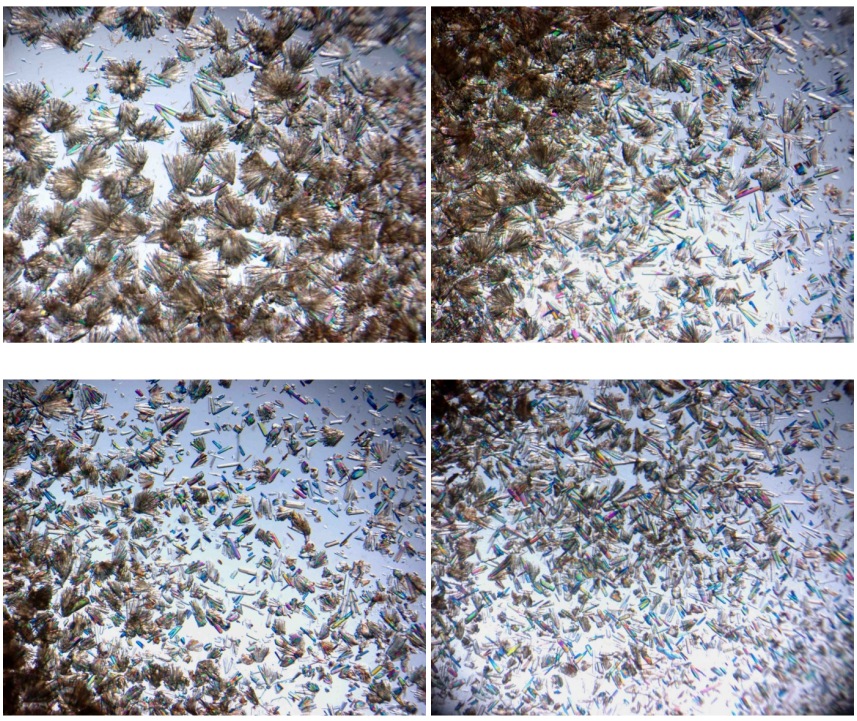

Figure 3-16. Photographs of unmodified UMCM-1-NH_2 (upper left), UMCM-1-AM5 (upper right), UMCM-1-AM9 (lower left), and UMCM-1-AM13 (lower right) as prepared via Method 2.

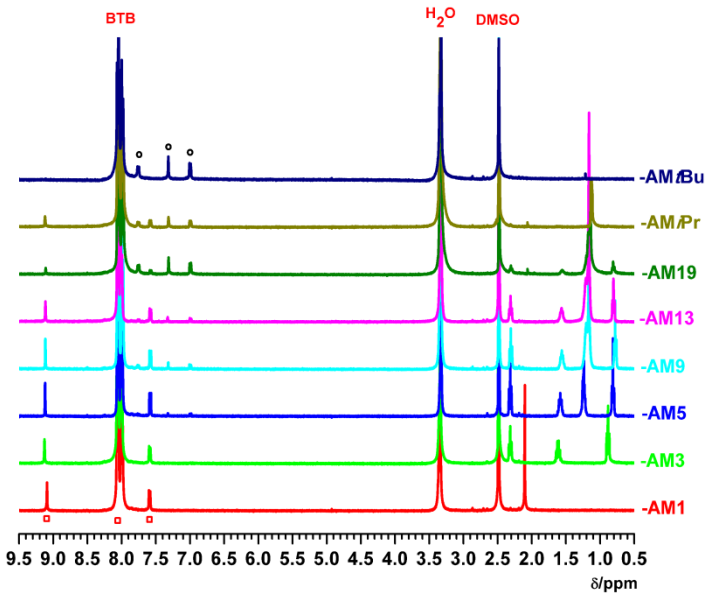

Figure 3-17. ^{1}H NMR spectra of modified UMCM-1-NH_2 samples (Method 2) digested in DCl/D_2O and DMSO-d^6 (left). Red squares and black circles represent signals of modified and unmodified NH_2-BDC, respectively.

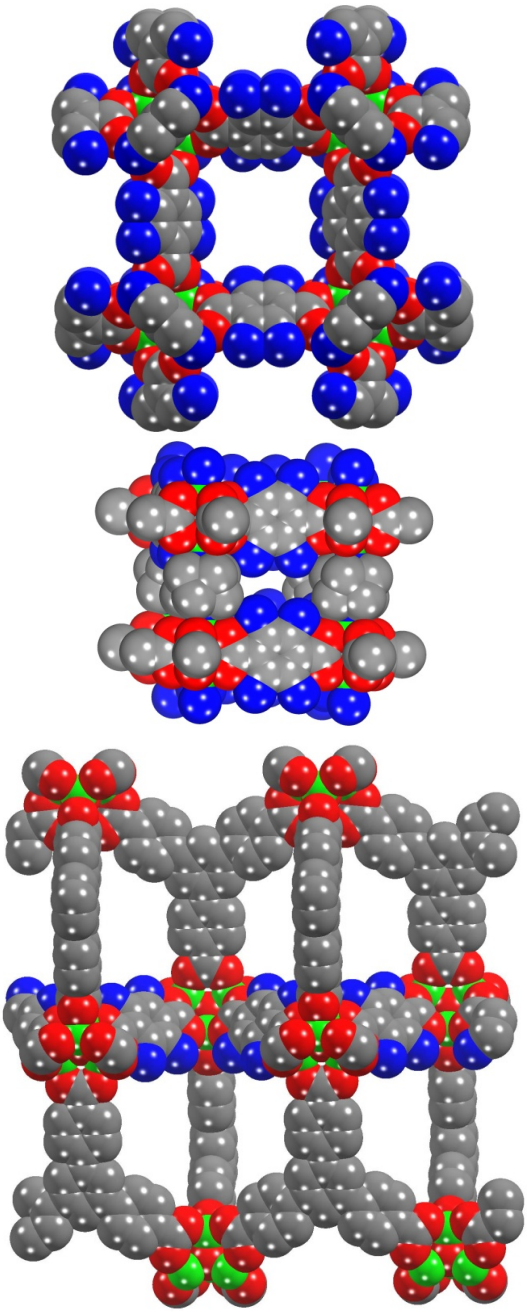

Figure 3-18. CPK representations highlighting the NH_2-BDC groups in IRMOF-3 (top), DMOF-1-NH_2 (middle), and UMCM-1-NH_2 (bottom). All four possible amino group positions are highlighted in blue.

All modified UMCM-1-NH_2 were found to maintain thermal and structural stability after being treated via Method 2 (Figure 3-19). Each modified UMCM-1-NH_2

remained stable up to ~450 °C and the structural integrity of each modified UMCM-1-NH_2 remained intact based on PXRD analysis. As additional support, a single crystal X-ray structure was collected and solved for UMCM-1-AM5, which was determined to be 93% modified by ^{1}H NMR analysis. UMCM-1-AM5 was found to have similar cell parameters as UMCM-1-NH_2. Three Zn^{2+} ions, 29 carbon atoms, and 8 oxygen atoms were located and assigned in the asymmetric unit, and those atoms corresponded with the Zn_4O cluster, three BTB ligands, and one modified NH_2-BDC ligand (Figure 3-20). Unfortunately, due to a combination of disorder over all four positions of the benzene ring and weak diffraction quality of the UMCM-1-AM5 crystal, suitable atomic positions could not be located for the modified alkyl-amide substituent; however, the framework structure of UMCM-1-AM5 framework was found to be identical to UMCM-1 and UMCM-1-NH_2 (Figure 3-20). To prove UMCM-1-AM5 was in fact the modified version of UMCM-1-NH_2, the single crystal was taken directly off the diffractometer, digested by sonication in MeOH, and submitted for ESI-MS analysis. The modified NH_2-BDC ligand was detected as the base peak in the spectrum (*m/z* 278 $[M-H]^-$).

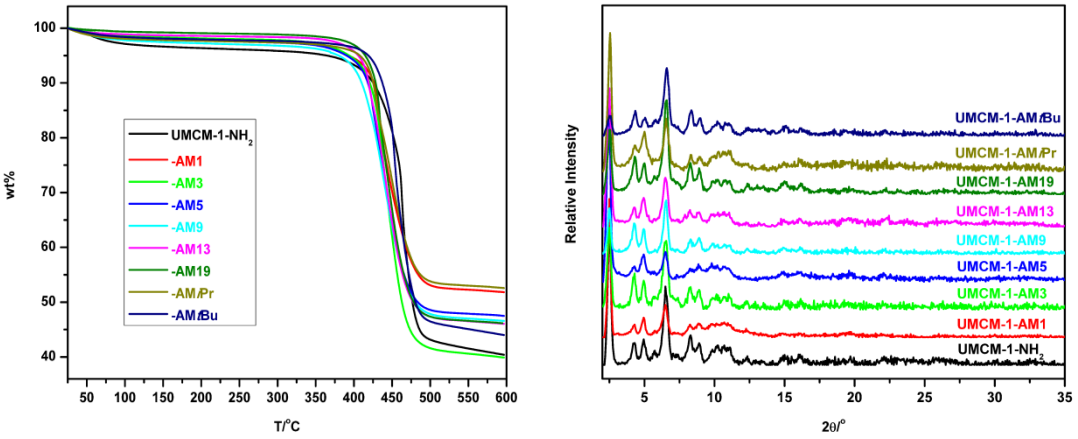

Figure 3-19. TGA (left) and PXRD analysis of modified UMCM-1-NH_2.

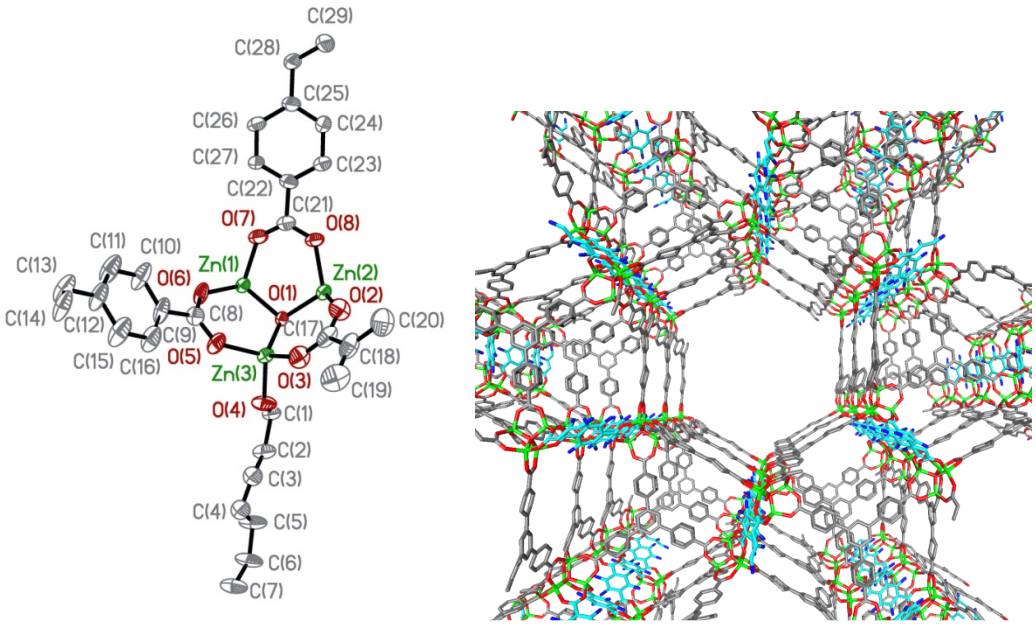

Figure 3-20. Structure of UMCM-1-AM5 determined by single-crystal X-ray diffraction. Asymmetric unit (left) and view of framework with NH_2-BDC highlighted in cyan (right).

BET surface area measurements were also collected for the modified UMCM-1-NH_2 to determine the effects of modification on porosity. Analysis of the modified UMCM-1-NH_2 samples under N_2 at 77 K revealed the MOFs remained highly porous with the BET surface areas ranged from as low as ~2800 m^2/g (UMCM-1-AM13) to as high as ~3800 m^2/g (UMCM-1-AM*t*Bu)). As proposed from our IRMOF-3 study, the low BET surface area for UMCM-1-AM13 is influenced by a combination of high conversion (84%) and long alkyl chains (C13) that are occupying the pores of the framework. Similarly, the high BET surface area for UMCM-1-AM*t*Bu is acceptable since it has extremely low modification and very few atoms occupying the framework channels. To further justify the modified MOFs did not undergo any structural changes, a full isotherm was collected for UMCM-1-AM5, which is 93% modified and has a BET

surface area of 3300 m^2/g. UMCM-1-AM5 was found to have a similar isotherm as unmodified UMCM-1-NH_2 and displayed the same step in the isotherm (Figure 3-21).

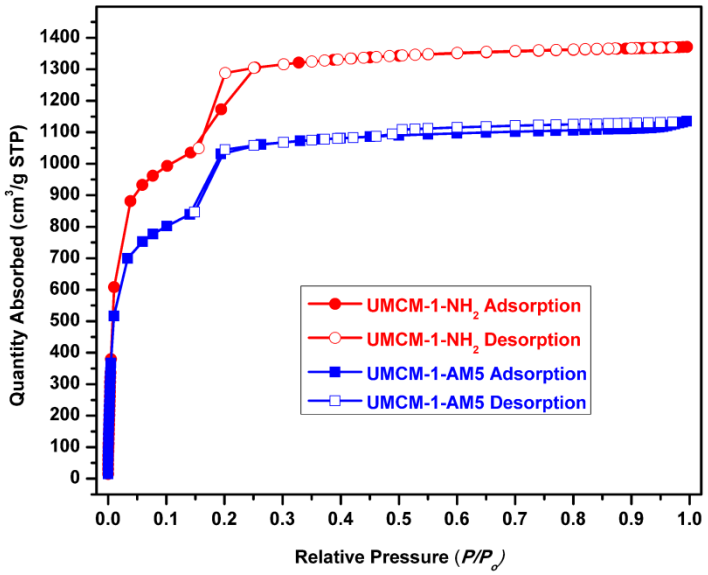

Figure 3-21. N_2 isotherms of UMCM-1-NH_2 and UMCM-1-AM5 at 77 K.

Closer observation of the modified UMCM surface areas indicated that high surface areas could be obtained even with high modification with the longer alkyl anhydrides. In particular, all the modified MOFs still have higher surface areas over other known MOFs, such as IRMOF-3, which has a surface area of 2400 m^2/g. While it has been established that surface area is influenced by a combination of modification extent and reagent size, the framework topology seems to dictate how modification affects the surface area. UMCM-1-NH_2 has two types of pores, a large hexagonal 1D pore that is bordered primarily by BTB and a smaller pore lined by NH_2-BDC and BTB ligands. Based on the location of the amino groups, there is a high probability the smaller pore is occupied by the modified substituents, leaving the larger hexagonal pores

relatively untouched. Here, the modified UMCM represent a unique class of materials that remain highly porous even after modification.

3.3 Conclusions

We have demonstrated topologically diverse frameworks can be developed with similar building block components (e.g., NH_2-BDC) and targeted for modification. Here, we were able to show the BDC component of MOFs (e.g., DMOF-1 and UMCM-1) can be replaced with NH_2-BDC to produce isostructural, amino-containing analogs (e.g., DMOF-1-NH_2 and UMCM-1-NH_2). Our controlled modification performed on three structurally diverse MOFs (IRMOF-3, DMOF-1-NH_2, UMCM-1-NH_2) not only confirmed PSM is possible, but also has identified several key concepts that are important for understanding and using postsynthetic modification, including: (1) the overall porosity of MOFs largely determines the degree of modification and reactivity with reagents; (2) framework topology and the local environment surrounding the targeted reactive groups (e.g., -NH_2) both play an important role that affects modification; and, (3) the size and shape of reagents both play a crucial role in influencing the modification outcome. Based on our results, we believe these concepts can serve as practical guidelines for PSM of other MOFs, and therefore lead to a better understanding about the types of MOFs that can undergo modification and the choice of reagent, based on size and shape, that can be used to effectively functionalize the framework.

3.4 Experimental Methods

General. Starting materials and solvents were purchased and used without further purification from commercial suppliers (Sigma-Aldrich, Alfa Aesar, EMD, TCI, Cambridge Isotope Laboratories, Inc., and others). IRMOF-3 was synthesized and activated as described previously.[1] 4,4′,4″-benzene-1,3,5-triyl-tribenzoic acid (BTB) synthesis was adapted from a published procedure.[17]

Preparation of DMOF-1-NH_2. $Zn(NO_3)_2 \cdot 4H_2O$ (1.56 g, 6.00 mmol) and 2-amino-1,4-benzenedicarboxylic acid (NH_2-BDC, 1.10 g, 6.07 mmol) were dissolved in 150 mL of dimethylformamide (DMF). 1,4-Diazabicyclo[2.2.2]octane (DABCO, 1.08 g, 9.63 mmol) was then added to the solution, which immediately generated a large amount of white precipitate. The mixture was filtered using a 60 mL PYREX glass funnel of fine porosity. The filtrate was collected, and the solution was diluted to a volume of 150 mL with DMF before being divided into 15 mL portions and transferred to 10 scintillation vials (20 mL capacity each). The vials were placed in a sand bath, and the bath was transferred to a programmable oven and heated at a rate of 2.5 °C/min from 35 to 120 °C. The temperature was held at 120 °C for 12 h, and then the oven was cooled at a rate of 2.5 °C/min to a final temperature of 35 °C. This procedure generated yellowish rod-shaped crystals of DMOF-1-NH_2. The mother liquor from each vial was decanted, and the crystals were washed with 3 × 6 mL of DMF followed by 3 × 6 mL of $CHCl_3$. The crystals were then soaked in 10 mL of $CHCl_3$ for 3 days with fresh $CHCl_3$ added every 24 h. After 3 days of soaking the crystals were stored in the last $CHCl_3$ solution until needed. The average yield of dried DMOF-1-NH_2 per vial was determined to be approximately 57 mg (0.20 mmol -NH_2 equiv., 33% based on starting $Zn(NO_3)_2 \cdot 4H_2O$).

Substituting NH_2-BDC with BDC (1.02 g, 0.60 mmol) using an identical procedure led to the generation of DMOF-1 crystals.[12,13]

Synthesis of 1,3,5-tribenzeneacetophenone. 1,3,5-tribenzenacetophenone was modified from a published procedure.[17] $AlCl_3$ (16.4 g, 123 mmol) was dissolved in acetyl chloride (88 mL) and placed in an ice bath to cool down to 0 °C under N_2. 1,3,5-triphenylbenzene (4.6 g, 15 mmol) was dissolved in CH_2Cl_2 (100 mL) and was added to the $AlCl_3$/acetyl chloride solution. The deep red solution was left stirring at 0 °C for 10 min and was stirred at RT for an additional 80 min. During the 80 minute period, the solution color became cloudy and lighter in color. The mixture was **slowly** poured to a 500 mL Erlenmeyer flask packed 2/3rds with ice. The cloudy red solution became yellow-brown upon addition to ice. More ice was added to the Erlenmeyer flask to keep the reaction cool until the transfer was complete. The mixture was then left to stir overnight at RT. CH_2Cl_2 was added to dissolve the crude beige solid and the solution was transferred to a separatory funnel. The layers were allowed to separate and the organic layer was isolated. Sat. $NaHCO_3$ was then slowly added to the organic layer (with vigorous stirring) in order to neutralize any remaining acid byproduct. During the addition of sat. $NaHCO_3$, the solution underwent a color change from brown to yellow. The solution was transferred to a separatory funnel and was allowed to separate into two layers **without** any shaking involved. The organic layer was recovered and sat. $NaHCO_3$ was added to the organic layer again until all the acid byproduct was neutralized. After separating the organic layer again, the solution was dried over $MgSO_4$, filtered, and concentrated to yield a yellowish white solid. The solid was washed with benzene to remove any unreacted 1,3,5-triphenylbenzene and the white product was dried on the

house vacuum. Yield: (5.1 g, 78%). ^{1}H NMR (400 MHz, $CDCl_3$, 25 °C): δ 8.11 (d, 6H, *J* = 8 Hz), 7.88 (s, 3H), 7.82 (d, 6H, *J* = 8.4 Hz), 2.68 (s, 9H). ESI-MS(+): *m/z* 433.27 $[M+H]^+$.

Synthesis of 4,4′,4′′-benzene-1,3,5-triyl-tribenzoic acid (BTB). 4,4',4''-benzene-1,3,5-triyl-tribenzoic acid was modified from a published procedure.[17] NaOH (17.6 g, 44 mmol) was dissolved in 118 mL of H_2O and cooled in an ice bath to 0 °C. Bromine (8 mL) was added 1 mL at a time to the NaOH solution, resulting in an orange solution. The NaOBr solution was left stirring at 0 °C for 15 minutes and was added in small portions to a suspension of 1,3,5-acetophenone (5.0 g, 11.6 mmol) in 240 mL of dioxane. The mixture was then transferred to a preheated oil bath at 60 °C and was left stirring for 2 h. During the 2 h, the solid eventually was dissolved, resulting in a pale yellow solution. After letting the solution completely cool to RT, an aqueous solution of $Na_2S_2O_3{\cdot}5H_2O$ (2.0 g in 40 mL H_2O) was added to the reaction to quench NaOBr, which resulted in the solution becoming less yellow. The solution was transferred to a separatory funnel and allowed to separate into two layers. The bottom layer was collected, filtered to remove any undissolved starting material, and acidified with conc. HCl. A white solid precipitated from solution and was isolated by vacuum filtration. After washing the solid with copious amounts of H_2O, the solid was left drying in air and was eventually dried under vacuum with heat overnight. Yield: 4.9 g (96%). ^{1}H NMR (400 MHz, d^6-DMSO) : δ 8.09 (s, 3H), 8.06 (s, 12H). ESI-MS(-): *m/z* 437.10 $[M-H]^-$.

Preparation of UMCM-1-NH_2. $Zn(NO_3)_2{\cdot}4H_2O$ (2.83 g, 10.8 mmol), NH_2-BDC (0.490 g, 2.7 mmol), and 4,4′,4′′-benzene-1,3,5-triyl-tribenzoic acid (BTB, 0.424 g, 0.97 mmol) were dissolved in 100 mL of DMF. The solution was divided into 10 mL portions

and transferred to 10 scintillation vials (20 mL capacity each). The vials were placed in a sand bath, and the bath was transferred to an isothermal oven heated at 85 °C. After 48 h, the vials were removed from the oven and left to cool to room temperature. Beige, crystalline needle clusters were present in every vial. The mother liquor was decanted, and crystals were washed with 3 × 12 mL of DMF and soaked in $CHCl_3$ (12 mL) for 24 h. The crystals were then rinsed 3 × 10 mL of $CHCl_3$ and left to soak for 3 days with fresh $CHCl_3$ added every 24 h. After 3 days of soaking the crystals were stored in the last $CHCl_3$ solution until needed. The average yield of dried UMCM-1-NH_2 per vial was determined to be approximately 56 mg (0.05mmol -NH_2 equiv, ~56% based on BTB).

Method 1 Modification of MOFs. The $CHCl_3$ storage solution of each MOF was decanted, and the crystals were dried at 75 °C under vacuum for at least 12 h. The freshly dried MOF sample (~15 mg, 0.050 mmol equiv of -NH_2 of DMOF-1-NH_2; 52 mg, 0.050 mmol equiv of -NH_2 of UMCM-1-NH_2; 14 mg, 0.050 mmol equiv of -NH_2 of IRMOF-3) was placed into a dram vial (4 mL capacity) with 1.0 mL of solvent ($CDCl_3$ or $CHCl_3$) and 2 equiv (0.10 mmol) of anhydride. The samples were left to react for 3 days at room temperature, and the reaction was quenched by decanting the solvent. The samples were rinsed with 3 × 2 mL of CHCl3 and soaked in 2 mL of $CHCl_3$ overnight. The rinsing and soaking were repeated for a total of 3 days, and the samples were left in fresh $CHCl_3$. Each vial was dried under vacuum at room temperature or at 90 °C overnight and used for ^{1}H NMR analysis.

Method 2 Modification of DMOF-1-NH_2. Approximately 57 mg of DMOF-1-NH_2 (0.20 mmol, equiv of -NH_2) was placed in a vial with 2 equiv (0.4 mmol) of alkyl anhydride dissolved in either 8 mL (for n = 0, 2) or 4 mL (for n = 4, 8, 12, 18; isobutyric

anhydride, trimethylacetic anhydride) of $CHCl_3$. The samples were heated in an oven at 55 °C for 24 h, after which the solution was decanted (except for *n* = 12 and 18, vide infra) and the crystals were washed with 3 × 6 mL of $CHCl_3$. A fresh solution of the anhydride was added to the vial, and the mixtures were heated for an additional 24 h. The aforementioned procedure was repeated two more times, giving a total reaction time of 4 days. For samples where *n* = 12 or 18, the mixtures were heated at 55 °C for 4 days without replacing the anhydride solution, but the volume was adjusted to 4 mL every 24 h by adding fresh $CHCl_3$ (some solvent loss occurred because of evaporation). After the reaction was complete, the $CHCl_3$ solution was decanted, and the crystals were washed with 3 × 6 mL of $CHCl_3$ before soaking in 10 mL of pure $CHCl_3$ (i.e., without anhydride) for 3 days, with fresh $CHCl_3$ added every 24 h. After 3 days of soaking the crystals were stored in the last $CHCl_3$ solution until analyzed.

Method 2 Modification of UMCM-1-NH_2. One vial of UMCM-1-NH_2 (~56 mg, ca. 0.050 mmol equiv of -NH_2) was combined with 4 equiv (0.20 mmol for *n* = 0, 18) or 8 equiv (0.40 mmol for *n* = 2, 4, 8, 12, isobutyric anhydride, trimethylacetic anhydride) of alkyl anhydride in 2 mL of $CHCl_3$. The reduced equivalents/concentration (0.1 M vs 0.2 M) used for *n* = 0 and *n* = 18 were due to the high reactivity (*n* = 0) and low solubility (*n* = 18) of these anhydrides. After allowing the sample to stand at room temperature for 3 days, the solution was decanted, and the crystals were washed with 3 × 10 mL of $CHCl_3$ before soaking in 10 mL of $CHCl_3$ for 24 h. After repeating the washes and soaks for 3 days, the crystals were stored in the last $CHCl_3$ solution until analyzed.

Digestion and Analysis by ^{1}H NMR. ^{1}H NMR spectra were recorded on Varian FT-NMR spectrometer (400 MHz). Approximately 5 mg of MOF (DMOF-1-NH_2,

UMCM-1-NH_2, or IRMOF-3) modified using either Method 1 or Method 2 was dried under vacuum at room temperature or at 90 °C overnight and digested with sonication in 500 μL of DMSO-d^6 and 100 μL of dilute DCl (23 μL of 35% DCl in D_2O diluted with 1.0 mL of DMSO-d^6).

Digestion and Analysis by ESI-MS. ESI-MS was performed using a ThermoFinnigan LCQ-DECA mass spectrometer, and the data was analyzed using the Xcalibur software suite. Crystals of modified DMOF-1-NH_2 and UMCM-1-NH_2 (0.1~1 mg) were digested in 1 mL of MeOH (or H_2O) with sonication.

Thermal Analysis. Approximately 10-20 mg of IRMOF-3, DMOF-1-NH_2, or UMCM-1-NH_2 modified using Method 2 was used for TGA measurements. Samples were analyzed under a stream of dinitrogen using a TA Instrument Q600 SDT running from room temperature to 600 °C with a scan rate of 5 °C/min.

PXRD Analysis. Approximately 15 mg of DMOF-1-NH_2 (typically soaked in DMF) or UMCM-1-NH_2 (typically soaked in $CHCl_3$) modified using Method 2 were air-dried before PXRD analysis. PXRD data were collected at ambient temperature on a Rigaku Miniflex II diffractometer at 30 kV, 15 mA for Cu Kα (λ = 1.5418 Å), with a scan speed of 1°/min or 5°/min, a step size of 0.05° in 2θ, and a 2θ range of 3-40° and 2-35° for DMOF-1-NH_2 samples and UMCM-1-NH_2 samples, respectively. The experimental backgrounds were corrected using the Jade 5.0 software package. The simulated PXRD patterns were calculated from the single crystal diffraction data using Mercury CSD 2.0.

BET Surface Area Analysis. Approximately 80-100 mg of modified DMOF-1-NH_2 or 40-60 mg of modified UMCM-1-NH_2 (prepared using Method 2) was evacuated on a vacuum line for 5-18 h. The sample was then transferred to a preweighed sample

tube and degassed at 105 °C for approximately 24 h on an ASAP 2020 or until the outgas rate was <5 μm Hg/min. The sample tube was reweighed to obtain a consistent mass for the degassed modified DMOF-1-NH_2 or UMCM-1-NH_2. BET surface area (m^2/g) measurements were collected at 77 K by dinitrogen on an ASAP 2020 using volumetric technique.

Single-Crystal X-ray Diffraction. Single crystals of UMCM-1-NH_2 and UMCM-1-AM5 in $CHCl_3$ were mounted on nylon loops with Paratone oil and placed under a nitrogen cold stream (200 K). Data was collected on a Bruker Kappa Apex II diffractometer using Cu Kαradiation (λ = 1.54178 Å) controlled using the APEX 2.0 software package. A semiempirical method utilizing equivalents was employed to correct for absorption. All data collections were solved and refined using the SHELXTL suite. The Zn^{2+} ions, O atoms, and several of the C atoms were refined anisotropically while the rest of the C atoms were refined isotropically for UMCM-1- NH_2. All non-hydrogen atoms, except for atoms C3 and C4, were refined anisotropically for UMCM-1-AM5. UMCM-1-NH_2 and UMCM-1-AM5 were treated with the “squeeze” protocol in PLATON to account for electron density associated with the amino and alkyl-amide substituents and for partially occupied or disordered solvent (e.g., $CHCl_3$) within the porous framework.

3.5 Appendix

Table 3-2. Preliminary crystallographic data for DMOF-1-NH_2 in comparison with those of DMOF-1.

Entry	MOF	Crystal System	Cell Setting	*a, b* (Å)	*c* (Å)	*α, β, γ* (°)	*V* (Å^3)	Ref.
1	*DMOF-1*	tetragonal	*I*	15.063	19.247	90	4367.1	Kim *et al*, *Angew. Chem. Int. Ed.* **2004**, *43*, 5033
2	*DMOF-1*	tetragonal	*P*	14.8999	19.1369	90	4248.4	Li *et al*, *Adv. Funct. Mater.* **2007**, *17*, 1255
3	*DMOF-1*	tetragonal	*P*	15.15	19.41	90	4455	This work
4	*DMOF-1-NH_2*	tetragonal	*I*	15.02	19.25	90	4341	This work

Table 3-3. Structure determination parameters and mass spectrometry data for UMCM-1-NH_2 and UMCM-1-AM5 single crystals.

MOF	UMCM-1-NH_2	UMCM-1-AM5
Formula	$C_{44}H_{25}NO_{13}Zn_4$	$C_{49.50}H_{34.30}NO_{13.90}Zn_4$ [a]
Morphology	Needle	Needle
Color	Beige	Beige
Size (mm)	0.38 0.15 0.14	0.55 0.25 0.20
Crystal System	Hexagonal	Hexagonal
Space Group	*P*6(3)*/m*	*P*6(3)*/m*
$a = b$, c	41.2555(8) Å, 17.5091(9) Å	41.2685(10) Å, 17.5342(11) Å
$\alpha = \beta$, γ	90°, 120°	90°, 120°
Volume (Å^3)	25808.2(15)	25861.5(18)
T, K	200(2)K	200(2)K
Reflns measured	11730	64158
Data/restraints/parameters	3967/0/217	15699/0/306
Independent Reflns [R(int)]	3967[*R*(int) =0.0660]	15699[*R*(int) = 0.2054]
Final *R* indices [I>2σ(I)]a	*R*1 =0.0584 *wR*2 = 0.1587	*R*1 = 0.0711 *wR*2 = 0.1471
R indices (all data, F^2 refinement)a	*R*1 = 0.0677 *wR*2 = 0.1648	*R*1 = 0.1369 *wR*2 = 0.1643
GOF on F^2	0.995	0.786
Largest diff. peak and hole , e/ Å ^{3}	0.574 and -0.798e/Å^{-3}	0.541 and -1.747 e/Å $^{-3}$
ESI-MS(-) $[M-H]^-$	180	278

[a] The empirical formulas reflect the ratio of unmodified amino-BDC to modified alkyl amide BDC ligand as determined by ^{1}H NMR.

Table 3-4. BET surface area measurements (m^2/g) for DMOF-1-NH_2 and UMCM-1-NH_2. Results shown are from two independent N_2 adsorption experiments at 77 K.

	Unmodified	-AM1	-AM3	-AM5	-AM9	-AM13	-AM19	-AM*i*Pr	-AM*t*Bu
DMOF-1	1510 ± 28	271 ± 68	778 ± 15	741 ±84	70 ± 9	1076 ± 105	1275 ± 57	284 ± 81	1289 ± 53
UMCM-1	3974 ± 30	3493 ± 6	3508 ± 132	3292 ± 98	2975 ± 260	2786 ± 134	3464 ± 169	3528 ± 102	3733 ± 172

DMOF-1-NH$_2$				***DMOF-1-AM1***			
Trial 1		*Trial 2*		*Trial 1*		*Trial 2*	
Relative Pressure (P/Po)	**Adsorption Amount (cm^3/g STP)**	**Relative Pressure (P/Po)**	**Adsorption Amount (cm^3/g STP)**	**Relative Pressure (P/Po)**	**Adsorption Amount (cm^3/g STP)**	**Relative Pressure (P/Po)**	**Adsorption Amount (cm^3/g STP)**
0.005075	370.6918784	0.005124	381.2556856	0.005182	77.95502	0.004787	53.78076
0.017067	381.8410501	0.015592	391.5233848	0.015701	80.42338	0.016451	55.79453
0.028133	386.2866401	0.026569	396.2462242	0.028676	81.68193	0.02912	56.73798
0.040618	389.5734724	0.039286	399.7421103	0.040979	82.53897	0.041272	57.36033
0.052938	392.0718698	0.05189	402.2774448	0.046429	82.87812	0.053311	57.76846
0.057487	392.8592449	0.057814	403.2421917	0.057139	83.39909	0.057074	57.94717
0.067766	394.4040638	0.067811	404.7403375	0.067689	83.83414	0.067584	58.28038
0.078348	395.7397307	0.078453	406.0646461	0.077914	84.1891	0.077922	58.56656
0.088759	396.8825152	0.088931	407.2071707	0.088367	84.52744	0.088248	58.82913
0.098974	397.9438274	0.099118	408.223126	0.098645	84.83808	0.098687	59.08199
0.109419	398.6846477	0.109433	409.1520592	0.109058	85.10429	0.109004	59.31589
0.119508	399.5807786	0.119706	410.0025328	0.119394	85.36981	0.119371	59.53195
0.129798	400.4425275	0.129968	410.7628321	0.129736	85.60338	0.129674	59.69799
0.14016	401.2053904	0.140339	411.4653009	0.140041	85.81056	0.140035	59.89566
0.150512	401.9086725	0.150598	412.1540933	0.150343	86.04104	0.150329	60.03815

Table 3-4 (continued). BET surface area measurements (m^2/g) for DMOF-1-NH_2 and UMCM-1-NH_2. Results shown are from two independent N_2 adsorption experiments at 77 K.

DMOF-1-AM3				***DMOF-1-AM5***			
Trial 1		*Trial 2*		*Trial 1*		*Trial 2*	
Relative Pressure (P/Po)	**Adsorption Amount (cm^3/g STP)**	**Relative Pressure (P/Po)**	**Adsorption Amount (cm^3/g STP)**	**Relative Pressure (P/Po)**	**Adsorption Amount (cm^3/g STP)**	**Relative Pressure (P/Po)**	**Adsorption Amount (cm^3/g STP)**
0.005689	11.0999	0.005516	37.12931	0.004891	192.4484	0.005209	163.8425
0.015054	27.39079	0.016137	39.6525	0.01581	200.3077	0.016896	170.5962
0.025082	124.7122	0.025859	111.4784	0.026876	203.8834	0.02787	173.5022
0.042612	169.7339	0.038236	151.4929	0.03965	206.5054	0.040259	175.6001
0.050167	177.9312	0.047463	162.3247	0.052122	208.3057	0.052555	177.1183
0.055407	183.4301	0.058943	173.8212	0.057317	208.9629	0.057274	177.6637
0.068864	190.2778	0.065858	178.0929	0.067699	210.0752	0.06771	178.6091
0.078353	193.8977	0.078057	183.993	0.078178	211.0752	0.078009	179.4819
0.088702	196.9446	0.088537	187.7897	0.088758	211.8997	0.088628	180.2147
0.0991	199.7823	0.099047	190.7314	0.099239	212.6355	0.098973	180.869
0.109786	201.289	0.109679	193.0777	0.109353	213.3017	0.109184	181.4845
0.120042	203.6147	0.120124	195.2919	0.11954	213.9143	0.119471	182.0273
0.130366	205.0492	0.130475	197.2744	0.129919	214.4736	0.12989	182.5275
0.140832	206.3619	0.140783	199.1166	0.140246	214.975	0.140161	183.0523
0.150796	207.2458	0.151423	200.2265	0.150562	215.4665	0.150489	183.4762

Table 3-4 (continued). BET surface area measurements (m^2/g) for DMOF-1-NH_2 and UMCM-1-NH_2. Results shown are from two independent N_2 adsorption experiments at 77 K.

DMOF-1-AM9				***DMOF-1-AM13***			
Trial 1		*Trial 2*		*Trial 1*		*Trial 2*	
Relative Pressure (P/Po)	**Adsorption Amount (cm^3/g STP)**	**Relative Pressure (P/Po)**	**Adsorption Amount (cm^3/g STP)**	**Relative Pressure (P/Po)**	**Adsorption Amount (cm^3/g STP)**	**Relative Pressure (P/Po)**	**Adsorption Amount (cm^3/g STP)**
0.005307	14.60539	0.005149	17.20854	0.00508	286.1482	0.004755	248.6462
0.017318	15.0216	0.017306	17.91216	0.015818	294.1454	0.016395	256.2681
0.029865	15.30209	0.029472	18.30711	0.027072	297.8566	0.027841	259.4043
0.041552	15.5464	0.041557	18.63724	0.039775	300.504	0.040199	261.6466
0.046629	15.64977	0.046578	18.77308	0.052252	302.4039	0.052553	263.2928
0.057057	15.8088	0.057255	18.98187	0.05763	303.1281	0.057441	263.9011
0.06745	15.97345	0.067413	19.16633	0.067857	304.2921	0.067817	264.9233
0.077907	16.07557	0.077815	19.33693	0.078312	305.2953	0.078292	265.8262
0.088078	16.20769	0.088144	19.49145	0.088783	306.1886	0.088654	266.6041
0.09853	16.31825	0.098545	19.66601	0.099066	306.9734	0.098949	267.3205
0.108902	16.46107	0.108875	19.81475	0.109344	307.6992	0.109233	267.9266
0.119254	16.56431	0.119294	19.94402	0.119527	308.324	0.119575	268.4944
0.129582	16.68678	0.12963	20.08718	0.12993	308.912	0.12981	269.0118
0.140021	16.78048	0.14003	20.1962	0.14021	309.4582	0.140181	269.5037
0.150365	16.87052	0.150377	20.31786	0.15058	309.9639	0.150486	269.9342

Table 3-4 (continued). BET surface area measurements (m^2/g) for DMOF-1-NH_2 and UMCM-1-NH_2. Results shown are from two independent N_2 adsorption experiments at 77 K.

DMOF-1-AM19				***DMOF-1-AMiPr***			
Trial 1		*Trial 2*		*Trial 1*		*Trial 2*	
Relative Pressure (P/Po)	**Adsorption Amount (cm^3/g STP)**	**Relative Pressure (P/Po)**	**Adsorption Amount (cm^3/g STP)**	**Relative Pressure (P/Po)**	**Adsorption Amount (cm^3/g STP)**	**Relative Pressure (P/Po)**	**Adsorption Amount (cm^3/g STP)**
0.00518	327.6454	0.004954	306.8141	0.005093	72.37978027	0.004804	51.52385
0.016253	336.7131	0.015987	315.7232	0.014785	77.45600513	0.01536	54.22455
0.027061	340.6883	0.027268	319.6891	0.027511	81.09223481	0.02868	55.83799
0.039736	343.668	0.039884	322.5163	0.040311	83.26392785	0.041168	56.77486
0.052248	345.8465	0.052409	324.5626	0.052592	84.91790945	0.053065	57.4876
0.057694	346.6134	0.057676	325.3149	0.05698	85.44724595	0.057158	57.73296
0.067842	347.9011	0.067804	326.5255	0.067606	86.40139479	0.067598	58.17421
0.078301	349.0746	0.078229	327.6345	0.07807	87.16733134	0.077911	58.58459
0.08882	350.1104	0.088655	328.5964	0.088246	87.92283281	0.088316	58.96291
0.099137	350.991	0.09905	329.4566	0.098802	88.53957127	0.09878	59.31788
0.1094	351.7937	0.109261	330.2005	0.109005	89.29317863	0.108975	59.64077
0.119765	352.5418	0.119573	330.918	0.119644	89.82555371	0.119528	59.96728
0.13004	353.1928	0.129922	331.5302	0.129906	90.29617973	0.129796	60.21243
0.140285	353.8228	0.140148	332.1219	0.140168	90.74061173	0.140085	60.44559
0.150574	354.42	0.150431	332.7028	0.150431	91.16496975	0.150421	60.69451

Table 3-4 (continued). BET surface area measurements (m^2/g) for DMOF-1-NH_2 and UMCM-1-NH_2. Results shown are from two independent N_2 adsorption experiments at 77 K.

DMOF-1-AMtBu				***UMCM-1-NH_2***			
Trial 1		*Trial 2*		*Trial 1*		*Trial 2*	
Relative Pressure (P/Po)	**Adsorption Amount (cm^3/g STP)**	**Relative Pressure (P/Po)**	**Adsorption Amount (cm^3/g STP)**	**Relative Pressure (P/Po)**	**Adsorption Amount (cm^3/g STP)**	**Relative Pressure (P/Po)**	**Adsorption Amount (cm^3/g STP)**
0.004815	329.7311	0.004988	310.3247	0.004786	377.9176	0.004771	369.473
0.016002	339.4235	0.016062	319.6563	0.014912	697.9455	0.015016	691.6707
0.027053	343.5277	0.027147	323.6526	0.024813	811.2059	0.025832	810.7077
0.039704	346.5298	0.039785	326.5806	0.03456	866.9682	0.036252	865.1752
0.052336	348.6856	0.052142	328.6798	0.04452	900.513	0.048761	902.66
0.057742	349.5094	0.057673	329.4629	0.059255	933.9071	0.057968	922.3684
0.067876	350.7981	0.067738	330.7687	0.065763	945.5757	0.065701	936.1853
0.078318	351.9635	0.078429	331.9171	0.07805	964.2869	0.078132	954.9237
0.088751	352.9568	0.088759	332.9277	0.088432	977.9836	0.088611	968.4285
0.099111	353.9004	0.099064	333.8025	0.09905	990.5831	0.099152	980.8507
0.109362	354.6944	0.109306	334.5639	0.109649	1002.312	0.109821	992.2712
0.119722	355.422	0.119552	335.317	0.120152	1013.313	0.120351	1003.25
0.129945	356.1139	0.130134	335.9727	0.130714	1024.284	0.130956	1013.844
0.140199	356.7316	0.140315	336.592	0.141333	1034.982	0.14151	1024.076
0.150555	357.3228	0.150539	337.1701	0.151729	1045.973	0.151745	1034.412

Table 3-4 (continued). BET surface area measurements (m^2/g) for DMOF-1-NH_2 and UMCM-1-NH_2. Results shown are from two independent N_2 adsorption experiments at 77 K.

UMCM-1-AM1				***UMCM-1-AM3***			
Trial 1		*Trial 2*		*Trial 1*		*Trial 2*	
Relative Pressure (P/Po)	**Adsorption Amount (cm^3/g STP)**	**Relative Pressure (P/Po)**	**Adsorption Amount (cm^3/g STP)**	**Relative Pressure (P/Po)**	**Adsorption Amount (cm^3/g STP)**	**Relative Pressure (P/Po)**	**Adsorption Amount (cm^3/g STP)**
0.004777	375.9893	0.004772	376.948	0.00477	392.8221	0.004771	377.4966
0.014881	623.3404	0.01515	625.8643	0.015005	646.8145	0.01465	609.9947
0.024717	717.0907	0.02462	715.0023	0.02564	747.1152	0.024875	703.5668
0.036172	768.259	0.036951	768.8074	0.03737	797.0804	0.036347	751.6235
0.044351	790.4858	0.045038	789.9408	0.045314	818.4018	0.044358	772.5205
0.060613	821.5263	0.060783	819.4467	0.054562	837.4554	0.054111	792.0652
0.066187	829.9369	0.066274	827.7618	0.06512	855.1277	0.064819	809.0287
0.077797	845.5387	0.07799	843.3252	0.078081	872.9489	0.078048	826.5201
0.088339	857.9003	0.088372	855.4775	0.088397	885.3934	0.088479	838.4676
0.098828	869.0973	0.098917	866.8543	0.099055	896.9619	0.099065	849.4611
0.109319	879.5958	0.109411	877.3466	0.109636	907.5675	0.109574	859.7873
0.119851	889.7299	0.119916	887.5363	0.120143	917.7916	0.120067	869.7098
0.130374	899.4819	0.130372	897.4541	0.130675	927.7306	0.130564	879.4897
0.140934	909.3953	0.140875	907.3609	0.141136	937.6324	0.141089	889.3039
0.151342	919.4084	0.151279	917.4004	0.151577	947.6194	0.151461	899.1416

Table 3-4 (continued). BET surface area measurements (m^2/g) for DMOF-1-NH_2 and UMCM-1-NH_2. Results shown are from two independent N_2 adsorption experiments at 77 K.

UMCM-1-AM5				***UMCM-1-AM9***			
Trial 1		*Trial 2*		*Trial 1*		*Trial 2*	
Relative Pressure (P/Po)	**Adsorption Amount (cm^3/g STP)**	**Relative Pressure (P/Po)**	**Adsorption Amount (cm^3/g STP)**	**Relative Pressure (P/Po)**	**Adsorption Amount (cm^3/g STP)**	**Relative Pressure (P/Po)**	**Adsorption Amount (cm^3/g STP)**
0.004793	379.4085	0.004794	366.2318	0.004754	330.5608	0.004769	378.4561
0.014672	611.6668	0.014621	584.846	0.015164	518.7819	0.014813	591.4863
0.025007	697.7966	0.025015	666.7427	0.025133	578.573	0.024695	660.8653
0.034783	736.2691	0.034529	702.5798	0.035614	610.0823	0.035264	697.225
0.044309	760.7289	0.048655	735.3077	0.047481	633.1681	0.04514	719.544
0.054997	781.2393	0.058332	751.639	0.054641	644.0627	0.055201	736.9357
0.065244	797.2372	0.065789	762.3593	0.065369	657.9108	0.065523	751.6573
0.078066	813.9257	0.077871	777.5869	0.077861	671.643	0.077912	766.5601
0.088441	825.6844	0.088364	789.1898	0.088236	681.8634	0.088355	777.6397
0.098903	836.5674	0.098832	799.8847	0.098774	691.5473	0.098831	787.9137
0.109386	846.8905	0.109347	810.0368	0.109163	700.7231	0.109371	797.6461
0.119958	856.712	0.119727	819.7605	0.119584	709.7214	0.119866	807.0053
0.130453	866.32	0.130157	829.5055	0.129888	718.6984	0.130332	816.1135
0.140888	875.7842	0.140545	839.3755	0.140136	728.0882	0.140739	825.3025
0.151337	885.4176	0.150784	849.6724	0.150267	737.934	0.151135	834.6155

Table 3-4 (continued). BET surface area measurements (m^2/g) for DMOF-1-NH_2 and UMCM-1-NH_2. Results shown are from two independent N_2 adsorption experiments at 77 K.

UMCM-1-AM13				***UMCM-1-AM19***			
Trial 1		*Trial 2*		*Trial 1*		*Trial 2*	
Relative Pressure (P/Po)	**Adsorption Amount (cm^3/g STP)**	**Relative Pressure (P/Po)**	**Adsorption Amount (cm^3/g STP)**	**Relative Pressure (P/Po)**	**Adsorption Amount (cm^3/g STP)**	**Relative Pressure (P/Po)**	**Adsorption Amount (cm^3/g STP)**
0.004769	337.8202	0.004768	314.7768	0.004797	356.0304	0.00476	376.9502
0.01499	528.0332	0.015316	492.7963	0.014925	599.5303	0.01503	643.1859
0.025404	597.1742	0.025387	553.5961	0.025263	688.7329	0.025012	736.0495
0.034922	629.1209	0.036249	586.4143	0.036869	736.1951	0.03738	790.0746
0.046726	654.1685	0.046105	605.6974	0.04502	756.7774	0.045429	811.7188
0.054505	666.642	0.0553	619.5813	0.054267	775.0007	0.054362	830.3425
0.065091	680.9349	0.065588	632.5387	0.064921	791.6983	0.064992	848.2664
0.077953	695.418	0.07788	645.7485	0.078057	808.7764	0.07806	866.3718
0.088357	705.8592	0.088282	655.8083	0.088534	820.6123	0.088425	878.8528
0.098819	715.5007	0.09868	665.269	0.099101	831.4691	0.098984	890.4735
0.109308	724.7023	0.109161	674.3061	0.109653	841.5829	0.109474	901.2918
0.119806	733.5416	0.119522	683.055	0.1202	851.2407	0.120016	911.6786
0.130217	742.3747	0.129869	691.9686	0.130665	860.7768	0.130529	921.8347
0.140731	751.2408	0.140111	700.9942	0.141279	870.0909	0.141022	931.9592
0.150998	760.1795	0.150382	710.473	0.15149	879.3947	0.151425	942.1509

Table 3-4 (continued). BET surface area measurements (m^2/g) for DMOF-1-NH_2 and UMCM-1-NH_2. Results shown are from two independent N_2 adsorption experiments at 77 K.

UMCM-1-AMiPr				***UMCM-1-AMtBu***			
Trial 1		*Trial 2*		*Trial 1*		*Trial 2*	
Relative Pressure (P/Po)	**Adsorption Amount (cm^3/g STP)**	**Relative Pressure (P/Po)**	**Adsorption Amount (cm^3/g STP)**	**Relative Pressure (P/Po)**	**Adsorption Amount (cm^3/g STP)**	**Relative Pressure (P/Po)**	**Adsorption Amount (cm^3/g STP)**
0.004795	373.9367	0.004801	372.1312	0.00476	366.9539	0.004761	355.5972
0.014889	637.3434	0.014979	617.0614	0.015023	675.9722	0.014644	651.25
0.024889	736.433	0.024973	708.7616	0.024925	783.573	0.02569	766.8113
0.036127	788.9026	0.034307	751.5235	0.035773	840.9226	0.036438	819.6924
0.048929	822.8626	0.049214	789.9121	0.048372	877.9782	0.04428	843.5674
0.058142	840.4714	0.059048	807.6228	0.057701	897.6179	0.054047	865.8868
0.065669	852.6047	0.066149	818.5405	0.065562	911.3913	0.064795	885.0348
0.077995	869.6132	0.07798	834.0748	0.078053	929.8463	0.078028	904.2456
0.088413	882.1413	0.088354	846.2486	0.088497	943.1793	0.08853	917.2999
0.098962	893.7276	0.098826	857.4843	0.099025	955.3345	0.098973	929.1866
0.109502	904.5099	0.109375	867.8975	0.109608	966.6872	0.109587	940.2614
0.12003	914.8459	0.11995	878.1836	0.120086	977.589	0.120136	950.8382
0.130497	924.977	0.130291	888.0498	0.130628	988.2702	0.130616	961.2177
0.141018	935.1054	0.140733	898.221	0.141047	999.0032	0.14109	971.5925
0.151493	945.5448	0.150963	908.6077	0.151362	1009.971	0.151426	982.0732

Table 3-5. Full N_2 isotherm measurements for DMOF-1-NH_2, DMOF-1-AM5, UMCM-1-NH_2, and UMCM-1-AM5.

DMOF-1-NH_2		***DMOF-1-AM5***		***UMCM-1-NH_2***		***UMCM-1-AM5***	
Relative Pressure (P/Po)	**Adsorption Amount (cm^3/g STP)**	**Relative Pressure (P/Po)**	**Adsorption Amount (cm^3/g STP)**	**Relative Pressure (P/Po)**	**Adsorption Amount (cm^3/g STP)**	**Relative Pressure (P/Po)**	**Adsorption Amount (cm^3/g STP)**
6.65E-06	15.43181	3.86E-06	7.807951	2.1E-05	15.23029	1.28E-05	14.80768
7.02E-06	30.8705	1.86E-06	15.62555	4.22E-05	30.36619	2.6E-05	29.55663
8.44E-06	46.30461	1.85E-06	23.44427	7.96E-05	45.31122	5.15E-05	44.17213
9.75E-06	61.73464	2.2E-06	31.26104	0.000145	59.9048	9.57E-05	58.55868
1.09E-05	77.16162	2.66E-06	39.07622	0.000249	73.82536	0.000164	72.60343
1.19E-05	92.58598	3.21E-06	46.89064	0.000393	87.24925	0.000258	86.18824
1.29E-05	108.0077	3.81E-06	54.70339	0.000559	99.90282	0.000373	99.21773
1.4E-05	123.4264	4.5E-06	62.51358	0.000729	111.7901	0.000505	111.6027
1.49E-05	138.8421	5.25E-06	70.3231	0.000956	126.7885	0.000647	123.4309
1.59E-05	154.2551	6.13E-06	78.12989	0.001185	141.7777	0.000793	134.6002
1.7E-05	169.6654	7.14E-06	85.9338	0.001416	156.7535	0.000999	149.1603
1.81E-05	185.0721	8.31E-06	93.73666	0.001646	171.728	0.001217	163.6952
1.95E-05	200.4754	9.68E-06	101.533	0.001873	186.7049	0.00144	178.2129
2.1E-05	215.8748	1.14E-05	109.3264	0.0021	201.6853	0.001667	192.72
2.3E-05	231.2681	1.37E-05	117.1129	0.002325	216.663	0.001898	207.2174
2.57E-05	246.6541	1.68E-05	124.8941	0.002551	231.6424	0.002133	221.7081
2.94E-05	262.0295	2.16E-05	132.6623	0.002778	246.6168	0.002372	236.1895
3.51E-05	277.3879	2.95E-05	140.4082	0.003004	261.5914	0.002613	250.6657
4.45E-05	292.7176	4.39E-05	148.1156	0.003233	276.5625	0.00286	265.1289
6.16E-05	307.995	7.31E-05	155.7398	0.003459	291.5339	0.003112	279.5803
9.69E-05	323.1584	0.000137	163.1787	0.003685	306.5089	0.00337	294.0229
0.000181	338.0423	0.000278	170.1985	0.003911	321.5397	0.003635	308.4495
0.000408	352.1301	0.000554	176.3633	0.004142	336.5567	0.003906	322.8668
0.001266	366.707	0.001372	183.5484	0.004803	379.7256	0.004187	337.3274
0.004155	379.2615	0.003143	189.8396	0.010235	608.4577	0.004809	367.2386
0.004808	380.692	0.00648	194.9255	0.038479	881.4473	0.01	516.7533

Table 3-5 (continued). Full N_2 isotherm measurements for DMOF-1-NH_2, DMOF-1-AM5, UMCM-1-NH_2, and UMCM-1-AM5.

DMOF-1-NH_2		***DMOF-3-AM5***		***UMCM-1-NH_2***		***UMCM-1-AM5***	
Relative Pressure (P/Po)	**Adsorption Amount (cm^3/g STP)**	**Relative Pressure (P/Po)**	**Adsorption Amount (cm^3/g STP)**	**Relative Pressure (P/Po)**	**Adsorption Amount (cm^3/g STP)**	**Relative Pressure (P/Po)**	**Adsorption Amount (cm^3/g STP)**
0.009793	387.3796	0.009672	197.6072	0.05885	932.7766	0.0335	699.4293
0.030348	397.4544	0.032593	205.5901	0.076829	962.0096	0.059194	752.8862
0.064598	404.1871	0.065556	210.079	0.101508	992.9032	0.077241	776.7087
0.083464	406.5373	0.081797	211.5708	0.142026	1035.384	0.100961	801.8739
0.101821	408.3409	0.10124	212.9427	0.194377	1172.856	0.14049	839.0643
0.140594	411.2979	0.140434	215.0071	0.252869	1305.273	0.193857	1030.857
0.201145	414.5676	0.200924	217.2208	0.32788	1321	0.262823	1061.356
0.252259	416.6391	0.251758	218.6562	0.387711	1330.059	0.330267	1072.587
0.302567	418.2295	0.302059	219.7619	0.418122	1333.987	0.367965	1077.451
0.351568	419.4933	0.35122	220.6945	0.450212	1337.703	0.399818	1081.086
0.400294	420.5531	0.400183	221.4887	0.500404	1342.61	0.450258	1085.905
0.450212	421.5308	0.450052	222.1782	0.550204	1346.877	0.5	1090.061
0.500358	422.3775	0.500131	222.7899	0.600348	1350.572	0.550205	1093.548
0.550268	423.1319	0.549975	223.3762	0.650384	1353.591	0.599859	1096.612
0.600327	423.8675	0.600059	223.9286	0.699919	1356.549	0.650014	1099.387
0.650435	424.5476	0.64996	224.4869	0.740321	1358.709	0.700045	1101.822
0.70029	425.1656	0.699863	225.1021	0.770242	1360.243	0.739942	1103.641
0.74038	425.6123	0.739948	225.6847	0.800204	1361.634	0.769914	1105.022
0.77029	425.9374	0.769905	226.1625	0.82025	1362.634	0.800007	1106.32
0.800488	426.2171	0.799842	226.6593	0.840436	1363.508	0.819859	1107.207
0.820408	426.4294	0.819861	227.0051	0.860174	1364.347	0.839935	1108.074
0.840398	426.6561	0.83986	227.3545	0.875216	1365.081	0.859933	1108.98
0.860402	426.8899	0.859874	227.6792	0.890295	1365.669	0.874931	1109.689
0.875315	427.0893	0.874742	227.9286	0.900201	1366.149	0.890159	1110.428
0.890474	427.2803	0.889793	228.1941	0.907077	1366.468	0.900245	1111.029
0.900427	427.3555	0.899781	228.4046	0.913891	1366.744	0.907022	1111.522
0.925937	427.5523	0.906613	228.5641	0.920642	1367.072	0.913775	1111.96
0.927551	427.6177	0.913335	228.7058	0.927527	1367.35	0.920491	1112.452
0.93458	427.6713	0.920113	228.8877	0.934263	1367.68	0.927227	1113.144
0.9598	427.8227	0.926905	229.0535	0.940973	1367.961	0.934174	1113.93
0.980035	428.1082	0.933647	229.2477	0.947763	1368.26	0.940872	1114.838
0.981921	428.2161	0.940462	229.4688	0.95465	1368.612	0.947593	1116.097
0.988913	428.4414	0.947165	229.6797	0.961417	1368.961	0.954414	1117.736
0.995317	428.8403	0.953925	229.907	0.968111	1369.355	0.961145	1119.981

Table 3-5 (continued). Full N_2 isotherm measurements for DMOF-1-NH_2, DMOF-1-AM5, UMCM-1-NH_2, and UMCM-1-AM5.

DMOF-1-NH$_2$		***DMOF-3-AM5***		***UMCM-1-NH$_2$***		***UMCM-1-AM5***	
Relative Pressure (P/Po)	**Adsorption Amount (cm^3/g STP)**	**Relative Pressure (P/Po)**	**Adsorption Amount (cm^3/g STP)**	**Relative Pressure (P/Po)**	**Adsorption Amount (cm^3/g STP)**	**Relative Pressure (P/Po)**	**Adsorption Amount (cm^3/g STP)**
0.970428	428.1489	0.960744	230.1956	0.975033	1369.696	0.968124	1122.834
0.949679	428.0055	0.967576	230.4643	0.981732	1370.032	0.974831	1125.972
0.929342	427.8989	0.974178	230.8171	0.988582	1370.403	0.981839	1129.139
0.90892	427.8423	0.981031	231.2467	0.995368	1370.984	0.988357	1131.868
0.888474	427.7686	0.987653	231.884	0.970278	1369.852	0.995061	1134.796
0.875481	427.7449	0.994354	232.9417	0.949733	1368.997	0.970586	1132.277
0.860462	427.7455	0.970135	231.1796	0.929203	1368.225	0.949739	1130.991
0.821767	427.6368	0.948979	230.4611	0.908803	1367.492	0.929174	1130.029
0.820455	427.6132	0.928397	230.0334	0.907294	1367.25	0.908853	1129.188
0.800429	427.5606	0.907967	229.7167	0.900012	1367.053	0.888367	1128.419
0.751692	427.3906	0.887448	229.4713	0.871825	1366.086	0.875238	1127.954
0.740457	427.365	0.87454	229.3545	0.860345	1365.61	0.860304	1127.419
0.70064	427.0657	0.859543	229.2202	0.840405	1364.839	0.840299	1126.677
0.65013	426.772	0.840214	229.0734	0.820517	1363.963	0.820266	1125.91
0.600406	426.404	0.820231	228.9633	0.800424	1363.142	0.800196	1125.149
0.55031	425.9373	0.800214	228.8635	0.770547	1361.833	0.770264	1123.882
0.528025	425.7162	0.770273	228.6858	0.740449	1360.386	0.740261	1122.568
0.505772	425.4596	0.740227	228.5468	0.700369	1358.286	0.700317	1120.747
0.483637	425.0627	0.700263	228.3617	0.650449	1355.359	0.650313	1118.208
0.462323	423.0289	0.650316	228.053	0.600482	1351.851	0.600314	1115.293
0.438545	421.479	0.600226	227.7476	0.550333	1347.997	0.550253	1111.927
0.416951	420.7931	0.550354	227.3895	0.528059	1346.133	0.527917	1110.244
0.376032	419.8176	0.527933	227.1956	0.505871	1344.168	0.505829	1108.452
0.35342	419.2707	0.505829	227.0177	0.483924	1341.606	0.488772	1094.554
0.350283	419.1757	0.483748	226.6684	0.461207	1338.983	0.461031	1086.728
0.300566	417.8835	0.462371	224.9139	0.439271	1336.577	0.421396	1082.997
0.25068	416.2295	0.438163	223.4874	0.417229	1333.928	0.398452	1080.672
0.200301	414.1798	0.41678	222.8745	0.394884	1330.93	0.394678	1080.176
0.150472	411.528	0.375803	222.0335	0.372425	1327.836	0.372336	1077.692
		0.353327	221.5474	0.350361	1324.573	0.350533	1075.031
		0.350309	221.4337	0.30186	1315.987	0.301633	1067.923
		0.300445	220.5589	0.250666	1304.286	0.250628	1058.358
		0.231933	219.0368	0.201339	1287.986	0.201022	1045.101
		0.20021	218.1102	0.155928	1049.612	0.148608	846.3113
		0.150283	216.3216				

3.6 Acknowledgements

Text, schemes, and figures in this chapter, in part, are reprints of the materials published in the following papers: Wang, Z., Tanabe K. K., Cohen, S. M. "Accessing Postsynthetic Modification in a Series of Metal-Organic Frameworks and the Influence of Framework Topology on Reactivity" *Inorg. Chem.* **2009**, *48*, 296-306. The dissertation author was the primary researcher and co-author for the data presented. The co-authors listed in these publications also participated in the research. The permissions to reproduce these papers were granted by the American Chemical Society, copyright 2009.

3.7 References

(1) Tanabe, K. K.; Wang, Z.; Cohen, S. M. *J. Am. Chem. Soc.* **2008**, *130*, 8508-8517.

(2) Dugan, E.; Wang, Z.; Okamura, M.; Medina, A.; Cohen, S. M. *Chem. Commun.* **2008**, 3366-8.

(3) Wang, Z.; Cohen, S. M. *Angew. Chem. Int. Ed.* **2008**, *47*, 4699-702.

(4) Costa, J. S.; Gamez, P.; Black, C. A.; Roubeau, O.; Teat, S. J.; Reedijk, J. *Eur. J. Inorg. Chem* **2008**, 1551–1554.

(5) Haneda, T.; Kawano, M.; Kawamichi, T.; Fujita, M. *J. Am. Chem. Soc.* **2008**, *130*, 1578-1579.

(6) Hwang, Y. K.; Hong, D.-Y.; Chang, J.-S.; Jhung, S. H.; Seo, Y.-K.; Kim, J.; Vimont, A.; Daturi, M.; Serre, C.; Férey, G. *Angew. Chem. Int. Ed.* **2008**, *47*, 4144-4148.

(7) Ingleson, M. J.; Barrio, J. P.; Bacsa, J.; Dickinson, C.; Park, H.; Rosseinsky, M. J. *Chem. Commun.* **2008**, 1287-9.

(8) Ingleson, M. J.; Barrio, J. P.; Guilbaud, J. B.; Khimyak, Y. Z.; Rosseinsky, M. J. *Chem. Commun.* **2008**, 2680-2682.

(9) Kaye, S. S.; Long, J. R. *J. Am. Chem. Soc.* **2008**, *130*, 806–807.

(10) Eddaoudi, M.; Kim, J.; Rosi, N.; Vodak, D.; Wachter, J.; O'Keeffe, M.; Yaghi, O. M. *Science* **2002**, *295*, 469-472.

(11) Rowsell, J. L. C.; Yaghi, O. M. *J. Am. Chem. Soc.* **2006**, *128*, 1304-1315.

(12) Dybtsev, D. N.; Chun, H.; Kim, K. *Angew. Chem. Int. Ed.* **2004**, *43*, 5033-5036.

(13) Lee, J. Y.; Olson, D. H.; Pan, L.; Emge, T. J.; Li, J. *Advanced Functional Materials* **2007**, *17*, 1255-1262.

(14) Koh, K.; Wong-Foy, A. G.; Matzger, A. J. *Angew. Chem. Int. Ed.* **2008**, *47*, 677-680.

(15) Koh, K.; Wong-Foy, A. G.; Matzger, A. J. *J. Am. Chem. Soc.* **2009**, *131*, 4184–4185.

(16) Koh, K.; Wong-Foy, A. G.; Matzger, A. J. *J. Am. Chem. Soc.* **2010**, *132*, 15005–15010.

(17) Choi, S. B.; Seo, M. J.; Cho, M.; Kim, Y.; Jin, M. K.; Jung, D.-Y.; Choi, J.-S.; Ahn, W.-S.; Rowsell, J. L. C.; Kim, J. *Cryst. Growth Des.* **2007**, *7*, 2290-2293.

Chapter 4 Developing MOFs for gas storage applications via PSM

4.1 Introduction

There has substantial interest in using H_2 as a clean and efficient energy source to power vehicles.[1,2] Prior to 2010, the Department of Energy (DOE) set an initial target of developing on-board H_2 storage devices that could hold up to 6.0 wt% and 45 g/L of H_2 at ambient temperature.[3] MOFs showed great promise as H_2 storage materials because of their high porosities and good reversibility of guest uptake and release.[3] However, it became evident the weak interaction of H_2 with the framework made it challenging to meet the DOE's desired requirements. Several MOFs were able to meet the DOE capacity standards, but they required cryogenic temperatures and/or high pressures to accomplish high H_2 uptake. Calculation of the isosteric heats of adsorptions (ΔH_{ads}) revealed MOFs had fairly low binding affinities with H_2 on average (10 kJ/mol and below), therefore making it difficult to achieve good gravimetric and volumetric uptake under ambient conditions.[4] As a result, there has been a great interest in developing MOFs with improved isosteric heats of adsorptions (up to 20 kJ/mol) while maintaining large storage capacities.[5-9] Currently, the DOE has set moderate targets for achieving storage materials with 5.2 wt % and 40 g/L of H_2 by 2015.[10] However, the ultimate goal is to reach 7.0 wt % and 70 g/L without resorting to cryogenic temperatures and high pressures.[10]

There are many different approaches for improving H_2 binding affinity in MOFs. Synthesizing MOFs that are catenated or interpenetrated (e.g., two or more interwoven frameworks) is one method for enhancing H_2 binding because there is less void space and H_2 can interact more strongly with the framework.[3] Metal nanoparticle or metal ion cluster impregnation of MOFs has been another preferred route.[11-13] The most common,

and popular, approach for improving H_2 binding affinity in MOFs has involved generating unsaturated metal centers within the framework because H_2 interacts more strongly with metal centers.[14,15] Many groups have used prefunctionalization to design MOFs with specific SBUs that will have unsaturated metal centers, such as frameworks with Mn^{2+} ions and Cu^{2+} ions.[9,14] However, there have been very few reports utilizing PSM to design MOFs for H_2.

Instead of using prefunctionalization to synthesize a MOF with unsaturated metal sites, Hupp and coworkers demonstrated coordinate covalent modification, a form of PSM, as a way to incorporate unsaturated metal sites within a MOF.[16] Coordinate covalent modification involves changes with the coordination environment of the SBUs without interfering with the SBU structure or MOF topology. Hupp and coworkers used ion exchange to enhance the H_2 interactions of their DO-MOF.[17] Modification by ion exchange is possible if the framework is anionic[18] or the organic linkers have pendant groups that can be deprotonated and subsequently metallated. Coordinate covalent modification was used to convert the diol groups of DO-MOF into lithium and magnesium alkoxides using either Li*O*tBu in CH_3CN/THF or $Mg(OMe)_2$ in MeOH (Figure 4-1). From these studies, the amount of metal ion present in the MOF was found to influence H_2 uptake. Higher loadings of either cation (2.62 Li^+ to Zn^{2+} and 2.02 Mg^{2+} to Zn^{2+}) caused the framework to lose crystallinity and porosity. H_2 uptake was also significantly lower than the unmodified DO-MOF. By decreasing the loading amount of Li^+ (0.2 Li^+ to Zn^{2+}) and Mg^{2+} (0.86 Mg^{2+} to Zn^{2+}), the MOF crystallinity was preserved. Higher H_2 uptake was observed for DO-MOF $Li_{0.2}$, which had a slightly higher H_2 weight percent uptake with an average of two additional H_2 molecules per Li^+; however, the H_2

uptake did not improve with DO-MOF $Mg_{0.86}$. Interestingly, both DO-MOF $Li_{0.2}$ and DO-MOF $Mg_{0.86}$ did show heats of adsorption that increased with higher loading, which is not commonly seen in MOFs.

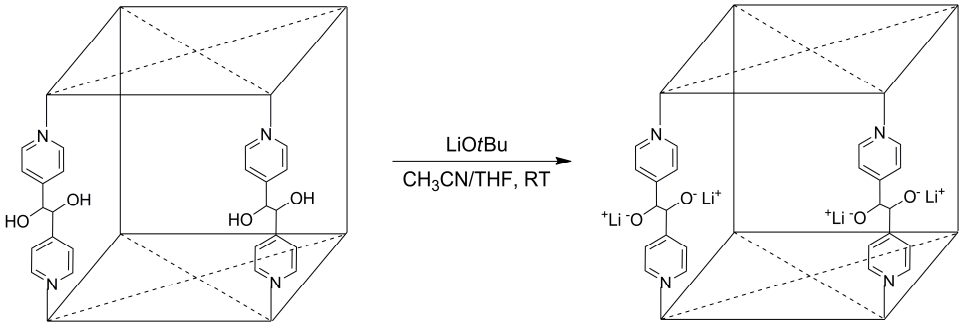

Figure 4-1. PSM of DO-MOF to produce unsaturated metal centers in the form of Li^+ alkoxides via ion exchange with LiO*t*Bu.

While the main focus for H_2 improvement has been on designing MOFs with unsaturated metal sites, there have been very few reports studying how the organic components of the MOF (e.g., organic ligand), could potentially influence H_2 binding.[19,20] Several groups used neutron diffraction and inelastic neutron scattering (INS) spectroscopy to determine the preferred binding sites of H_2 in IRMOF-1.[3,6] The results from these studies indicated that, on average, the strongest binding sites for H_2 were near the Zn_4O SBU. However, interactions with the aromatic ring of the BDC ligand were detected, although they were weak. MOFs with unsaturated metal centers also displayed a similar trend where H_2 was observed to interact with both the SBU and the organic ligands.[3] Overall, aromatic substituents appeared to influence H_2 binding; however, no concise studies were performed in order to elucidate that H_2 binding in MOF could be

improved via the organic ligand without having any unsaturated metal centers present in the framework at all.

This chapter focuses on the development of H_2 storage MOFs by using covalent modification to functionalize the organic ligand with various substituents to improve H_2 binding. Unmodified and modified IRMOF-3, DMOF-1-NH_2, and UMCM-1-NH_2 were examined for H_2 weight % uptake and their isosteric heat of adsorptions (ΔH_{ads}) were calculated. The effects of substituent type, as well as MOF topology, were studied in order to understand how H_2 binding affinities were affected. All modified MOFs were analyzed using ^{1}H NMR analysis, TGA, PXRD, and N_2 sorption analysis. H_2 sorption experiments were conducted at 77 K and 87 K and the isosteric heat of adsorption was calculated using both the virial equation[21] and the Langmuir-Freundlich equation.[22]

4.2 Results and Discussion

4.2.1 Synthesis and characterization of MOFs for H_2 storage

Three topologically diverse MOF systems were prepared for H_2 sorption analysis: IRMOF-3, DMOF-1-NH_2, and UMCM-1-NH_2.[23-25] IRMOF-3, DMOF-1-NH_2, and UMCM-1-NH_2 were modified with benzoic anhydride to yield IRMOF-3-AMPh (70%), DMOF-1-AMPh (63%), and UMCM-1-AMPh (76%) (Figure 4-2). IRMOF-3-URPh and IRMOF-3-AM5, whose syntheses were previously reported, were also prepared with yields of 41% and 86%, respectively.[24,26] All MOFs were digested and analyzed by ^{1}H NMR to confirm their percent modifications (Table 4-1, Figures 4-3 to 4-5), and they were all analyzed by PXRD and BET surface area to ensure the framework remained intact and microporous (Table 4-1, Figures 4-6 to 4-7).

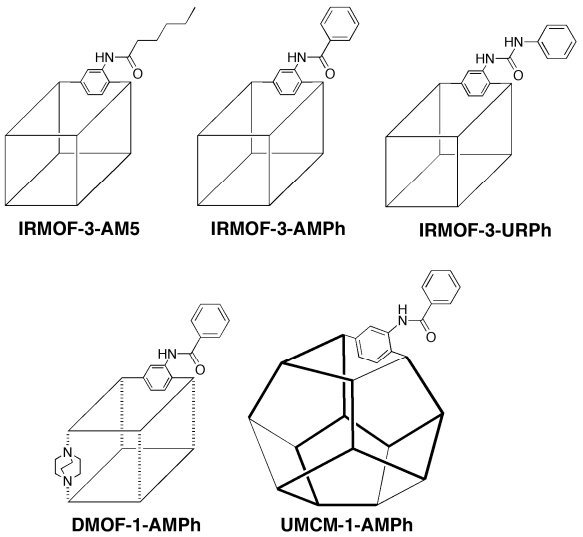

Figure 4-2. Schematic representation of the five modified MOFs utilized in this study.

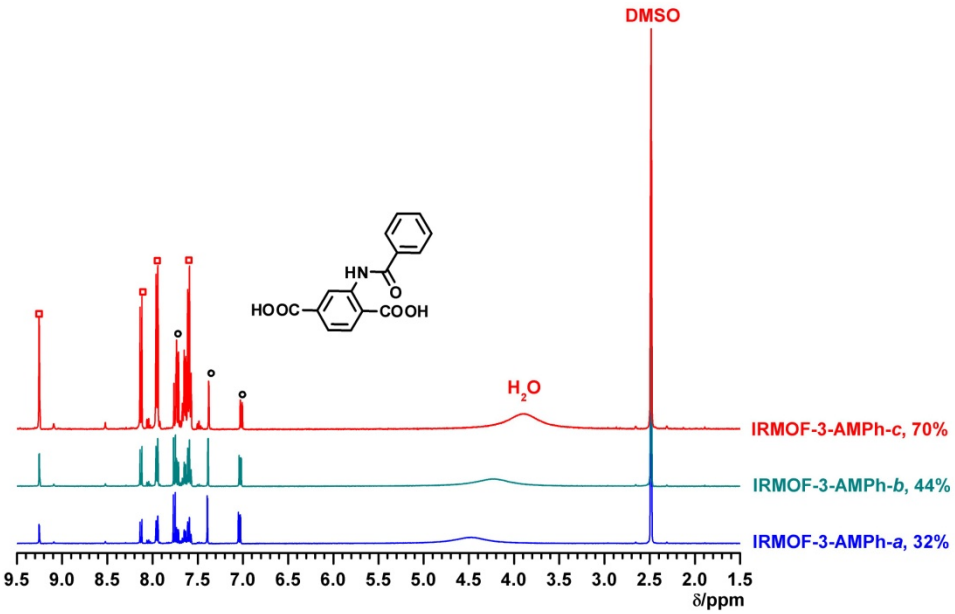

Figure 4-3. ^{1}H NMR spectra of digested IRMOF-3-AMPh samples with different degrees of postsynthetic modification. Unmodified NH_2-BDC and modified NH_2-BDC are indicated by circles and squares, respectively.

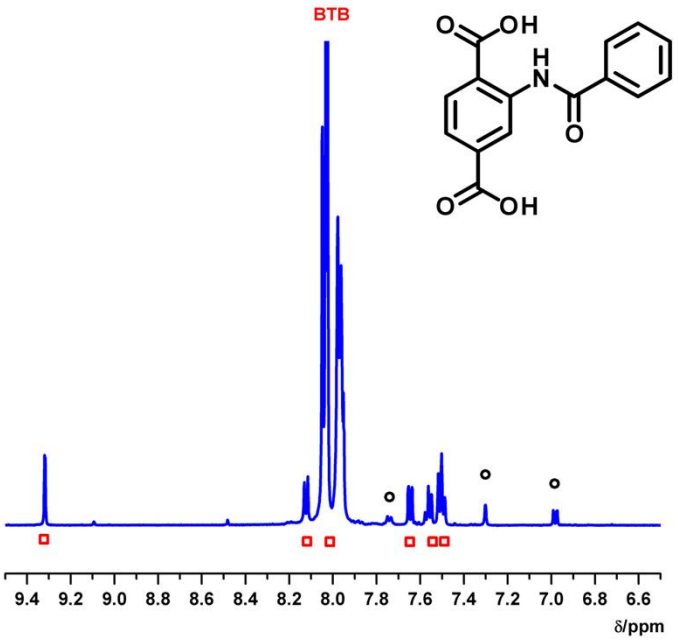

Figure 4-4. [1]H NMR spectra of digested UMCM-1-AMPh. Unmodified NH_2-BDC and modified NH_2-BDC are indicated by black circles and red squares, respectively.

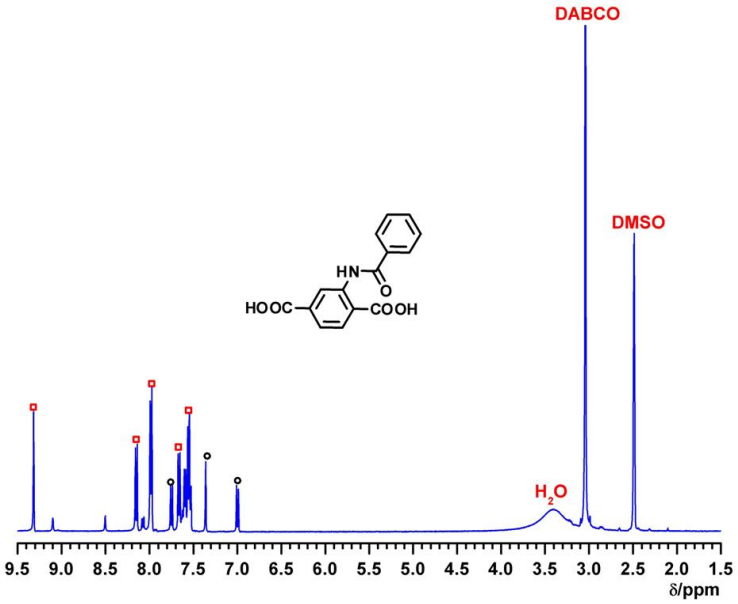

Figure 4-5. [1]H NMR spectra of digested DMOF-1-AMPh. Unmodified NH_2-BDC and modified NH_2-BDC are indicated by black circles and red squares, respectively.

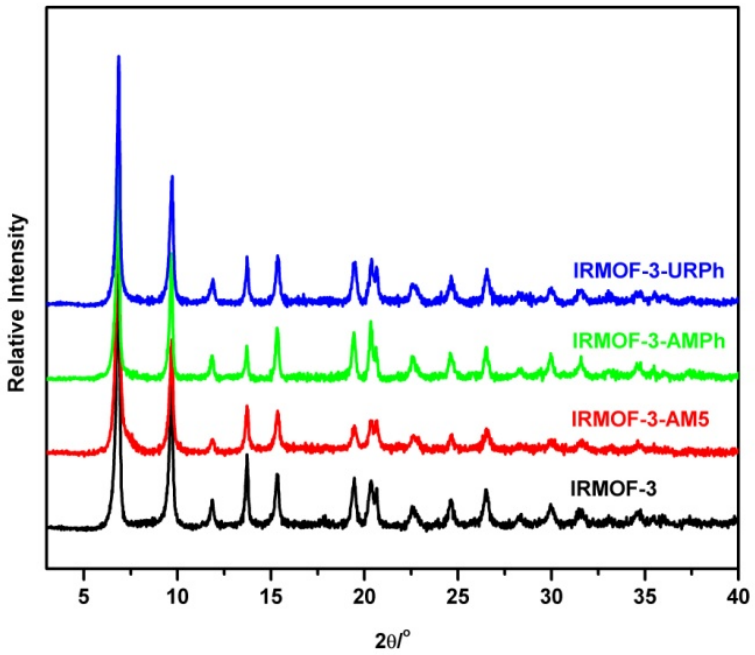

Figure 4-6. PXRD spectra of IRMOF-3, IRMOF-3-AM5, IRMOF-3-AMPh, and IRMOF-3-URPh. All samples were soaked in $CHCl_3$ and briefly air-dried prior to analysis.

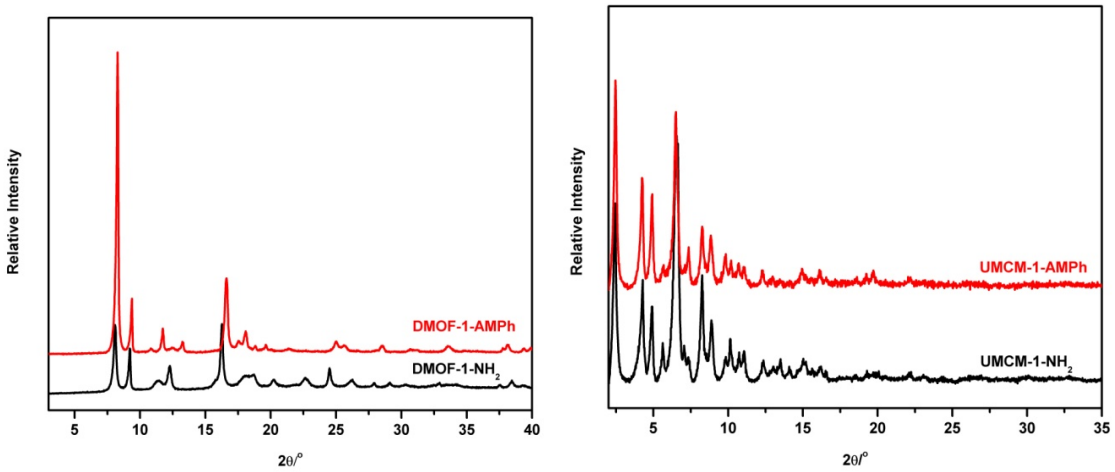

Figure 4-7. PXRD comparison of DMOF-1-NH_2 (black, exchanged with $CHCl_3$) and DMOF-1-AMPh (red) (left) and UMCM-1-NH_2 (black, exchanged with $CHCl_3$) and UMCM-1-AMPh (red) (right).

4.2.2 Modified IRMOF-3 gravimetric uptake results

The H_2 sorption isotherms of IRMOF-3-AMPh and IRMOF-3-URPh samples were measured using a volumetric gas sorption apparatus. Both MOFs show higher gravimetric uptake than unmodified IRMOF-3 at 77 K and 1 atm, with a noticeable increase from 1.51 wt% (IRMOF- 3) to as high as 1.73 wt% (IRMOF-3-AMPh) and 1.54 wt% (IRMOF-3-URPh) (Figure 4-8). In contrast, IRMOF-3-AM5 showed enhanced uptake at low pressure (< 250 mmHg), but overall lower uptake of 1.21 wt %. To ensure the enhancement of H_2 uptake was due to the improved H_2 molecule interactions of the phenyl substituents, and not due to the differences in percent conversions, the reaction conditions of IRMOF-3-AMPh were modified to yield three IRMOF-3-AMPh MOFs with varying percent conversions: IRMOF-3-AMPh-*a* (32%), IRMOF-3-AMPh-*b* (44%), and IRMOF-3-AMPh-*c* (70%) (Figure 4-3). At 1 atm and 77 K, IRMOF-3-AMPh-*a*, -*b*, and -*c* showed similar enhanced gravimetric uptake of H_2 over IRMOF-3 regardless of their different degrees of modification (Figure 4-9). As further evidence, at least 3 independent samples were tested for the other unmodified and modified IRMOF-3, which all gave reproducible results and therefore supported the findings that the aromatic substituents contribute favorably to the enhancement of H_2 sorption on a gravimetric basis (Figures 4-10 to 4-12).

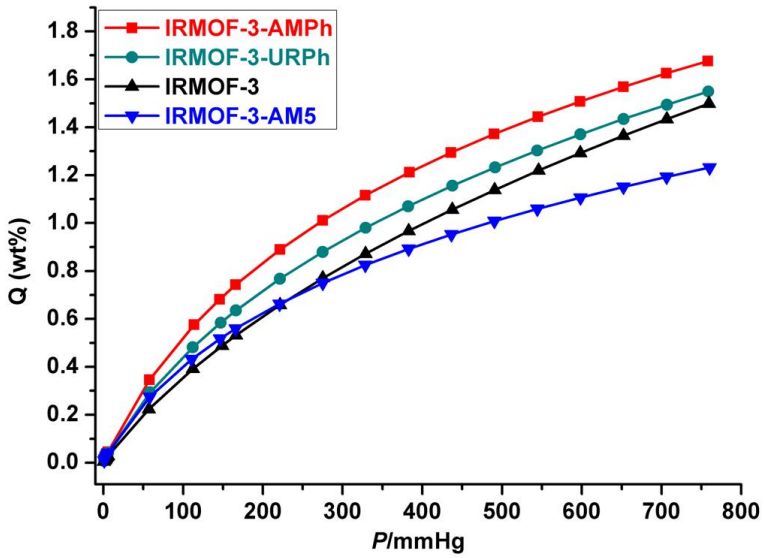

Figure 4-8. H_2 gravimetric uptake for IRMOF-3, IRMOF-3-AMPh, -URPh, and -AM5 at 77 K

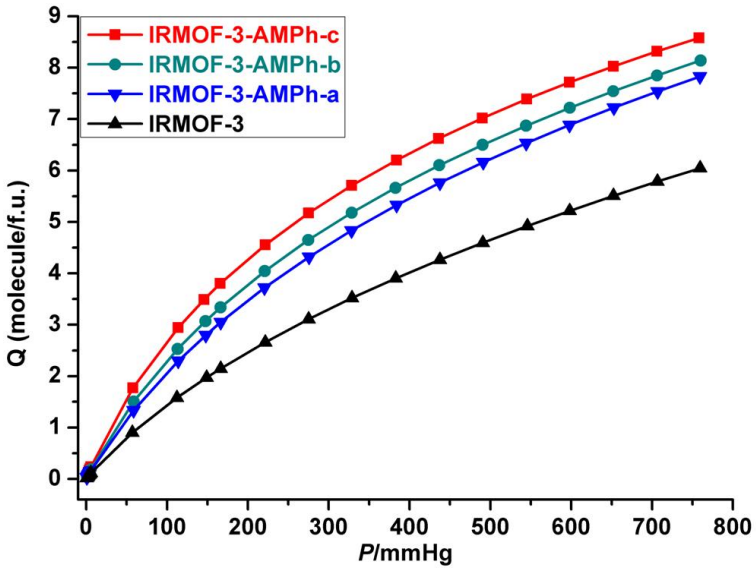

Figure 4-9. Gravimetric uptake of H_2 (wt%) at 77 K for IRMOF-3 and IRMOF-3-AMPh-*a*, -*b*, -*c*

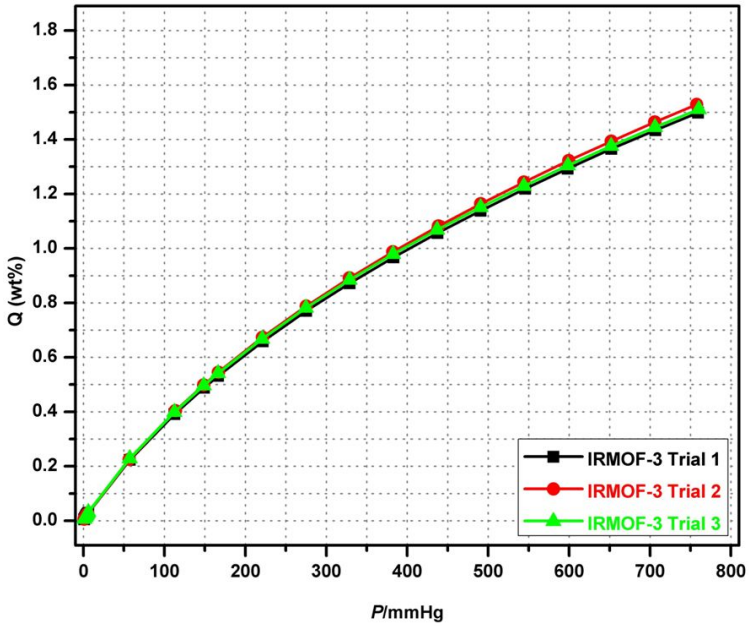

Figure 4-10. Gravimetric uptake of H_2 (wt%) at 77 K for three independent IRMOF-3 samples.

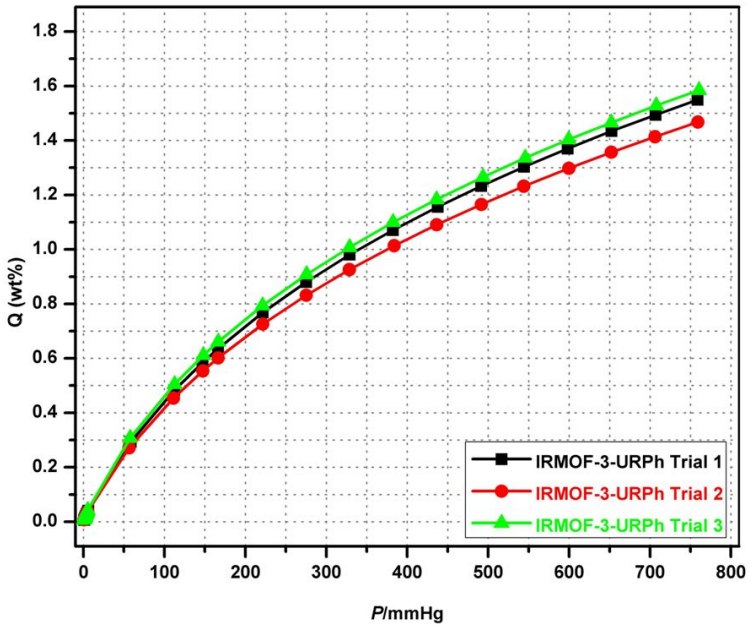

Figure 4-11. Gravimetric uptake of H_2 (wt%) at 77 K for three independent IRMOF-3-URPh samples.

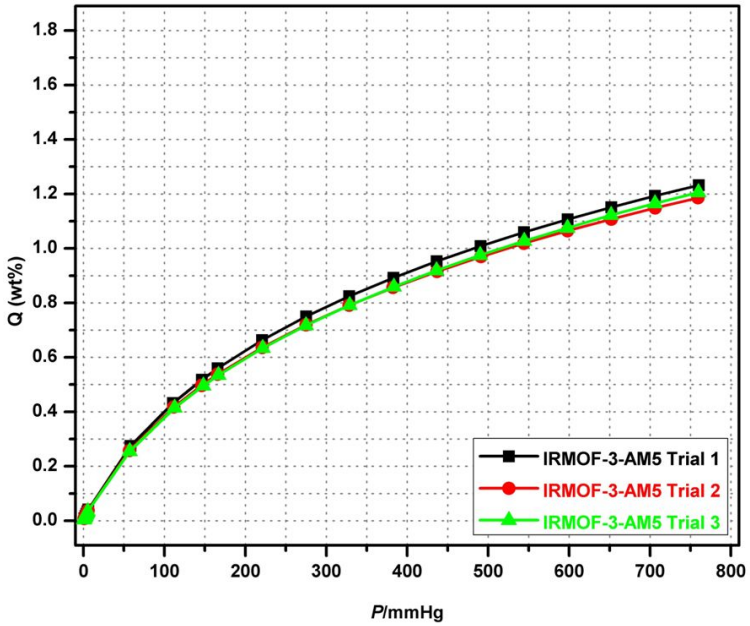

Figure 4-12. Gravimetric uptake of H_2 (wt%) at 77 K for three independent IRMOF-3-AM5 samples.

All three modified MOFs (IRMOF-3-AMPh, -URPh, and -AM5 showed higher uptake on a per molar (and volumetric) basis (Table 4-1, Figure 4-13). This suggests that the decrease in H_2 gravimetric uptake above 250 mmHg for IRMOF-3-AM5 is largely due to an increase in sample mass as a result of PSM. This was also rationalized for the gravimetric uptake values for IRMOF-3-AMPh-*a*, -*b*, and -*c*. On a per molar basis, IRMOF-3-AMPh-*c* had the highest uptake overall, followed by IRMOF-3-AMPh-*b* and -*c* in order of decreasing percent modification (Figure 4-14). Moreover, IRMOF-3-AMPh-*c* had drastically improved volumetric uptake in comparison with IRMOF-3. Overall, the phenyl groups appeared to have better binding affinities with H_2, as indicated by the number of additional 1-2 H_2 molecules per modified ligand in contrast with alkyl chains, where ~ 0.2 H_2 molecules were calculated for each modified ligand of IRMOF-3-AM5. These results seemed to be influenced by well-defined, extra binding sites with the

phenyl modified frameworks. In either scenario, the results highlighted here suggest that the organic components of MOFs may play a more critical role in binding H_2 molecules than previously recognized.[27]

Table 4-1. A summary of hydrogen sorption properties of three distinct MOFs upon postsynthetic modification.

Material	Conversion	SA_{BET} (m^2/g)	H_2 (wt%)[a]	H_2 (per f.u.)[b,c]	$+H_2/L'$[d]	H_2 (g/L)[e]	ΔH_{ads} (kJ/mol)[f]
IRMOF-3	N.A.	2639 ± 61	1.51 ± 0.02	6.07 ± 0.03	N.A.	9.59 ± 0.10	5.3 ± 0.3
AMPh-a	32%	2267	1.73	7.84	1.86	12.30	5.3
AMPh-b	44%	2052	1.73	8.16	1.60	12.80	5.7
AMPh-c	70%	1657	1.68	8.60	1.21	13.49	6.0
URPh	41 ± 5%	1940 ± 52	1.54 ± 0.06	7.33 ± 0.33	1.02 ± 0.23	11.50 ± 0.51	5.7 ± 0.3
AM5	86 ± 3%	1239 ± 46	1.21 ± 0.02	6.40 ± 0.14	0.13 ± 0.06	10.05 ± 0.22	5.7 ± 0.3
UMCM-1-NH_2	N.A.	3917 ±137	1.35 ± 0.05	6.91 ± 0.25	N.A.	5.39 ± 0.21	4.6 ± 0.4
AMPh	76 ± 1%	3770 ± 93	1.54 ± 0.04	8.49 ± 0.18	1.84 ± 0.27	6.61 ± 0.16	5.2 ± 0.2
DMOF-1-NH_2	N.A.	1369 ± 14	2.08 ± 0.01	6.21 ± 0.02	N.A.	18.24 ± 0.08	5.6 ± 0.0
AMPh	63 ± 1%	913 ± 37	1.69 ± 0.05	6.13 ± 0.22	-0.09 ± 0.17	18.00 ± 0.63	7.0 ± 0.1

[a] Gravimetric uptake at 77 K and 1 atm. [b] f.u. (IRMOF-3s): $Zn_4O(L)_{3(1-x)}(L')_{3x}$, x is the conversion, L is NH_2-BDC, and L' is the modified BDC ligand; f.u. (UMCMs): $Zn_4O\ (BTB)_{4/3}(L)_{1-x}(L')_x$; f.u. (DMOFs): $Zn_2(L)_{2(1-x)}(L')_{2x}$ (DABCO). [c] Molar uptake at 77 K and 1 atm. [d] $+H_2/L'$ represents the number of additional H_2 molecules per modified BDC ligand. [e] Volumetric uptake at 77 K and 1 atm, estimated from calculated crystal density. It is assumed that the cell volume, and thus macroscopic volume of the MOF crystals do not change noticeably upon postsynthetic modification.[24] [f] Heat of adsorption at zero coverage calculated from the virial-type equation. [g] Average values and errors based off of three independent experiments. [h] Average values and errors based off of two independent experiments.

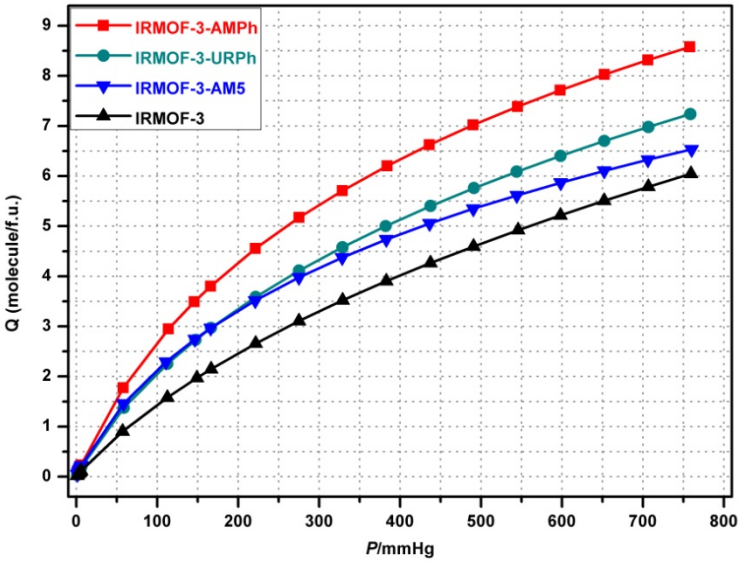

Figure 4-13. Molar uptake of H_2 at 77 K for IRMOF-3, IRMOF-3-AMPh, -URPh and -AM5.

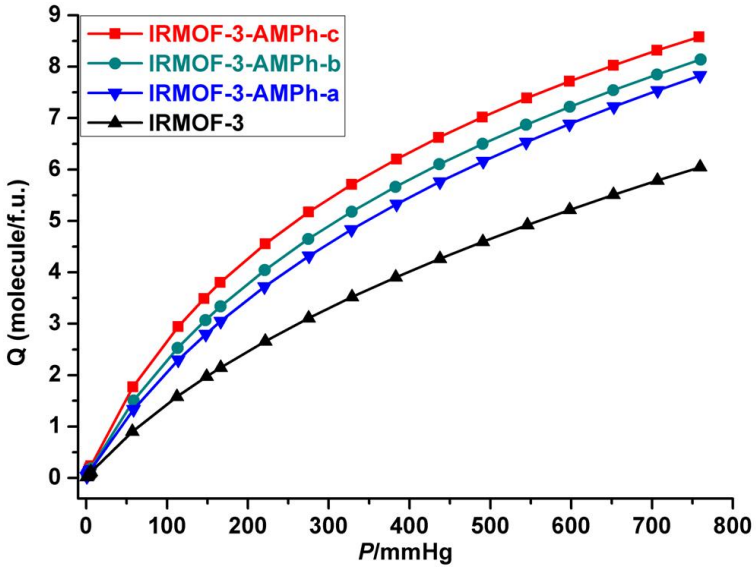

Figure 4-14. Molar uptake of H_2 at 77 K for IRMOF-3 and IRMOF-3-AMPh-*a*, -*b*, and -*c*.

4.2.3 Calculation of heat of adsorption (ΔH_{ads}) using virial type and Langmuir-Freundlich (L-F) model.

The coverage-dependent heat of adsorption for IRMOF-3, IRMOF-3-AMPh, IRMOF-3-URPh, and IRMOF-3-AM5 were calculated using H_2 isotherms at 77 K and 87 K with the viral type[21] and Langmuir–Freundlich[22] (L-F) equations (Figures 4-15 and 4-16, see Experimental Section). These two models are commonly used for calculating the heat of adsorption and give similar results at higher loadings. However, the methods do not agree at near-zero coverage (e.g., low loadings). The L-F model is not very well suited for calculating zero-coverage because it generates a much higher calculated heat of adsorption.[22] Nevertheless, reproducible data was obtained using either model (4-17 to 4-19). With the virial type method, all three modified IRMOF-3 samples showed higher heat of adsorption values over unmodified IRMOF-3 for the entire coverage range with average improved 1 kJ/mol. IRMOF-3-AMPh, IRMOF-3-URPh, and IRMOF-3-AM5 all had heat of adsorption ranging from 5.7 to 6.0 kJ/mol in comparison with a value of 5.3 kJ/mol for unmodified IRMOF-3 (Figure 4-20). In terms of the IRMOF-3-AMPh series, IRMOF-3-AMPh-*c* had the highest heat of adsorption over IRMOF-3-AMPh-*b* and -*a* (Figure 4-21). Based on these results, modification of the pores with organic substituents influences the H_2 binding.

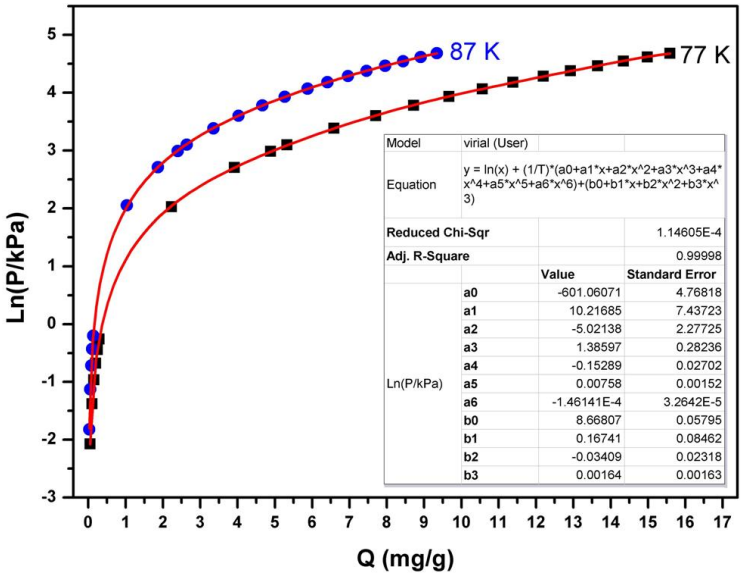

Figure 4-15. Curve fitting of H_2 sorption isotherms (77 K and 87 K) of IRMOF-3 sample using the virial equation.

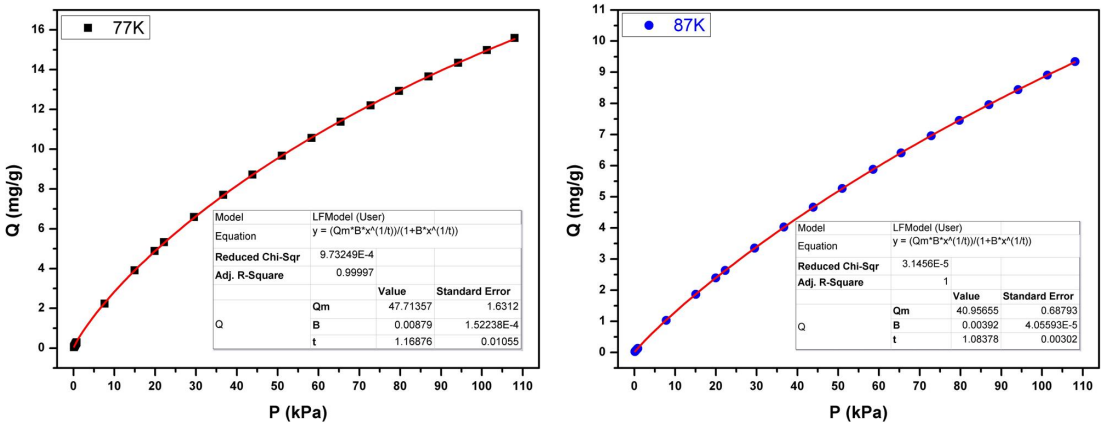

Figure 4-16. Curve fitting of H_2 sorption isotherms (77 K, left and 87 K, right) of IRMOF-3 sample using the Langmuir-Freundlich equation.

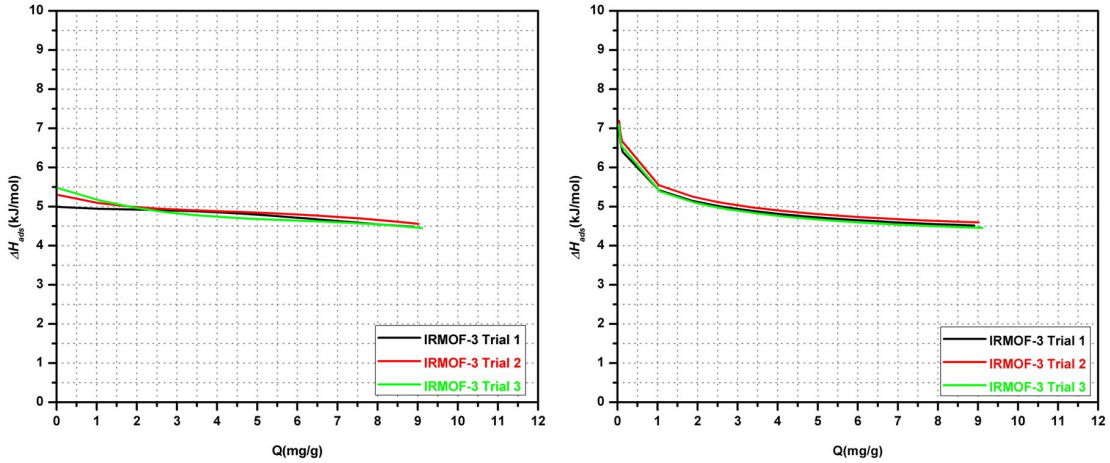

Figure 4-17. Isosteric heat of adsorption as determined by the virial-type equation (left) and the Langmuir-Freundlich method (right) for three independent IRMOF-3 samples.

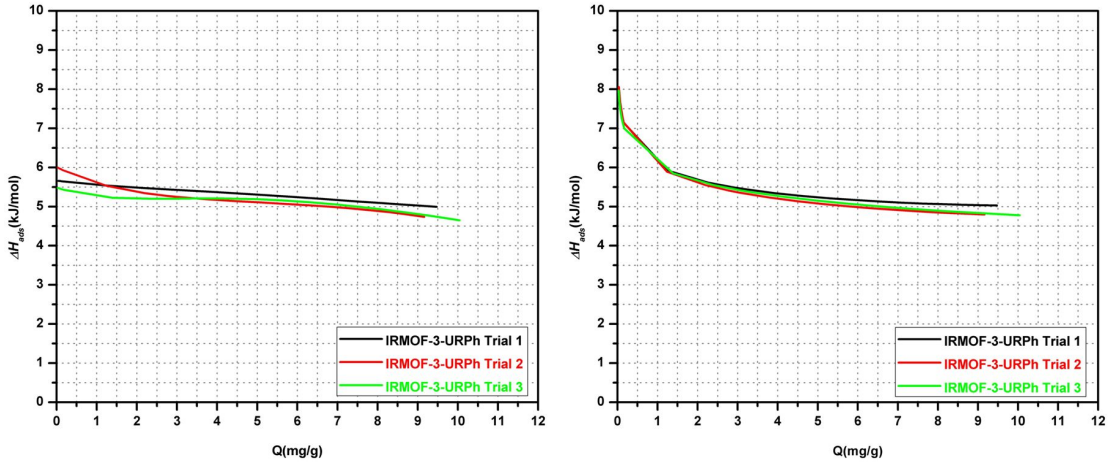

Figure 4-18. Isosteric heat of adsorption as determined by the virial-type equation (left) and the Langmuir-Freundlich method (right) for three independent IRMOF-3-URPh samples.

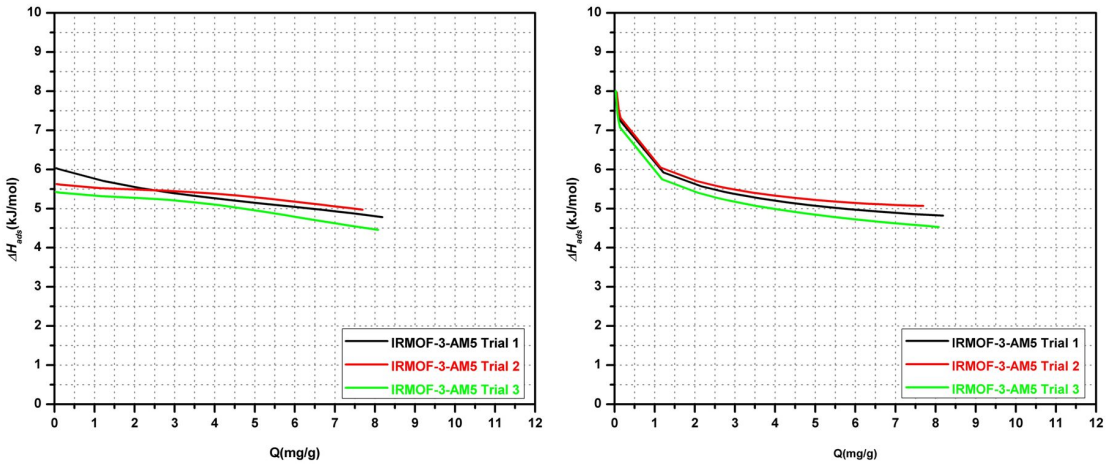

Figure 4-19. Isosteric heat of adsorption as determined by the virial-type equation (left) and the Langmuir-Freundlich method (right) for three independent IRMOF-3-AM5 samples.

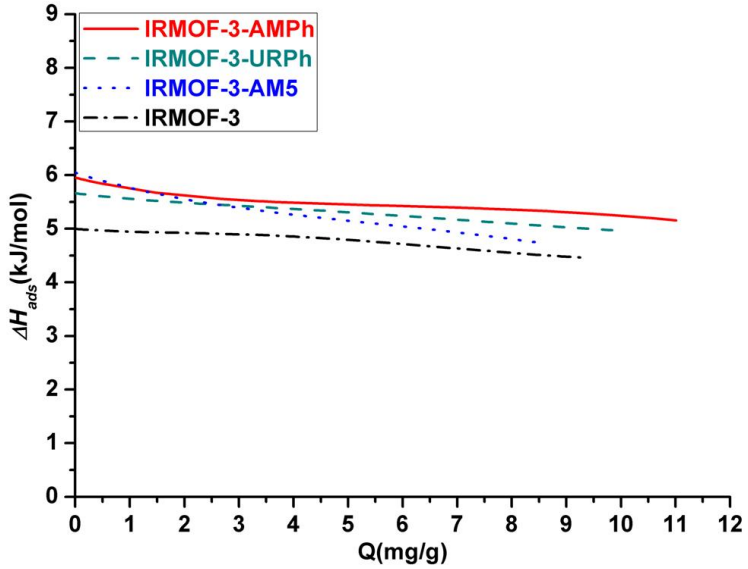

Figure 4-20. Isosteric heat of adsorption for IRMOF-3, IRMOF-3-AMPh, -URPh, and -AM5 at 77 K using the viral equation.

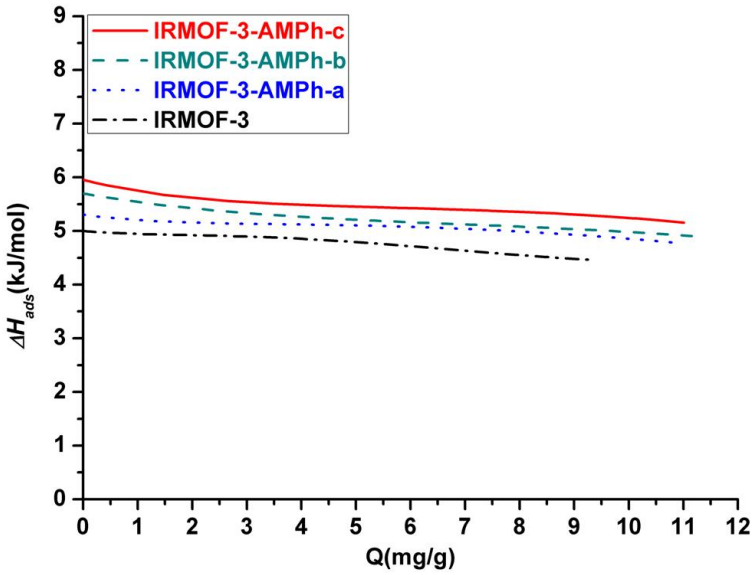

Figure 4-21. Isosteric heat of adsorption for IRMOF-3and IRMOF-3-AMPh-*a*, -*b*, -*c* at 77 K using the viral equation.

4.2.4 Effect of MOF topology on H_2 uptake and heat of adsorption

DMOF-1-AMPh and UMCM-1-AMPh, along with their parent MOFs DMOF-1-NH_2 and UMCM-1-NH_2 were also examined by their H_2 isotherms at 77 K and 87 K at 1 atm. In the UMCM system, the uptake of H_2 by UMCM-1-AMPh was found to be improved over unmodified UMCM-1-NH_2 on both a gravimetric, molar, and volumetric basis (Table 4-1, Figures 4-22 and 4-23). The margin of increase, though, was not very significant in comparison with the IRMOF-3 system. In contrast, DMOF-1-AMPh had much lower uptake than DMOF-1-NH_2 (Figures 4-24 and 4-25). The difference in H_2 sorption behaviors in IRMOF-3-AMPh, UMCM-1-AMPh, and DMOF-1-AMPh were rationalized by their differences in porosity. IRMOF-3 has a BET surface area of 2500 m^2/g while UMCM-1-NH_2 has a surface area of 4000 m^2/g. Both MOFs are porous enough to accommodate both phenyl substituents and H_2 molecules. In contrast, DMOF-1-NH_2, which has a surface area of 1400 m^2/g, has smaller pores and therefore its H_2

uptake may be compromised by due to the modified substituents taking up accessible space within the pores. Interestingly, the trend for the heat of adsorption was reversed for these three MOF systems. UMCM-1-AMPh showed a much smaller increase in heat of adsorption (Figure 4-26). Alternatively, DMOF-1-AMPh achieved an enhanced heat of adsorption comparable to IRMOF-3-AMPh, which seemed reasonable because smaller pores are known to induce higher binding affinities (Figure 4-27).[28] To summarize, H_2 binding affinity (e.g., gravimetric, volumetric, heat of adsorption) is influenced by a combination of functional group type (e.g., phenyl vs. alkyl chain) and the porosity of the framework.

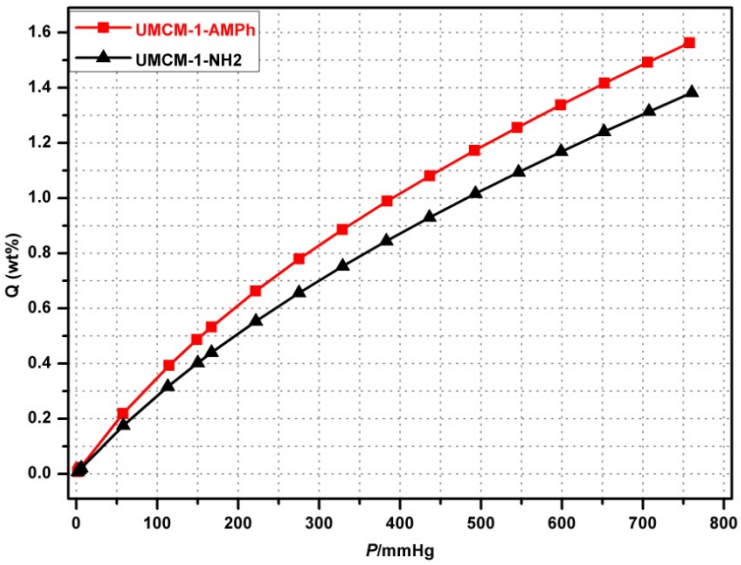

Figure 4-22. Gravimetric uptake of H_2 (wt%) at 77 K for UMCM-1-NH_2 and UMCM-1-AMPh.

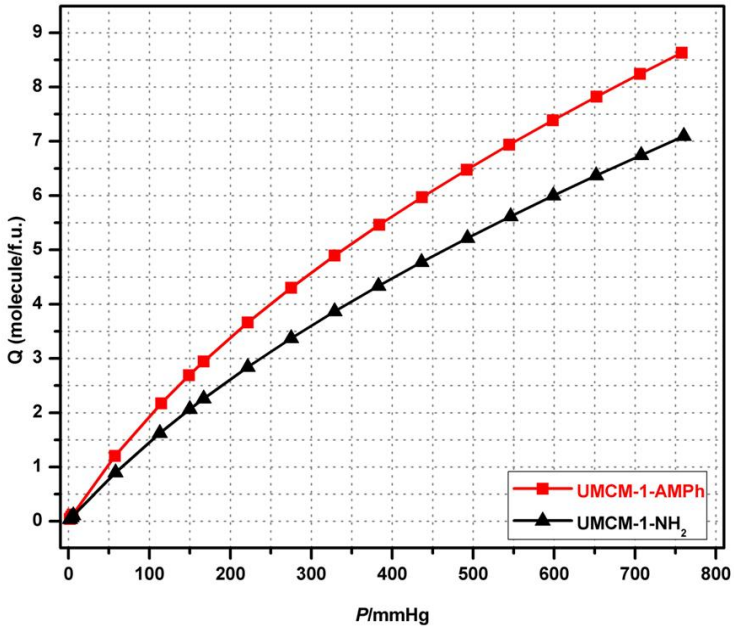

Figure 4-23. Molar uptake of H_2 at 77 K for UMCM-1-NH_2 and UMCM-1-AMPh.

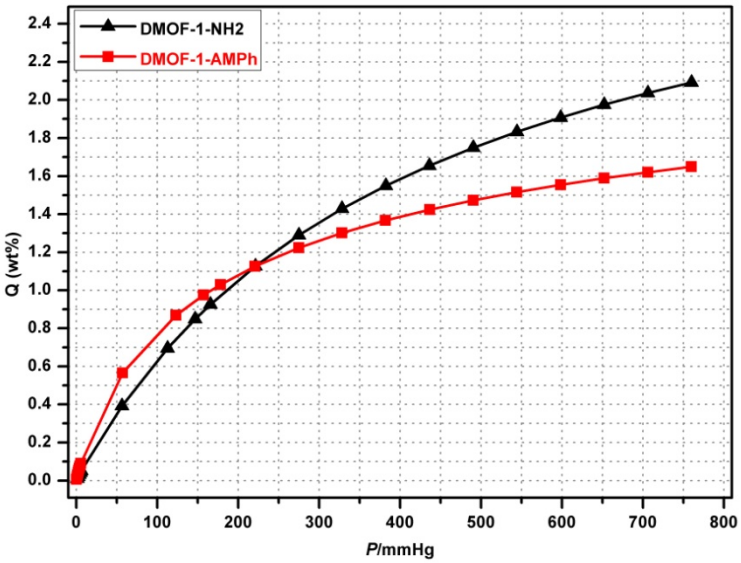

Figure 4-24. Gravimetric uptake of H_2 (wt%) at 77 K for DMOF-1-NH_2 and DMOF-1-AMPh.

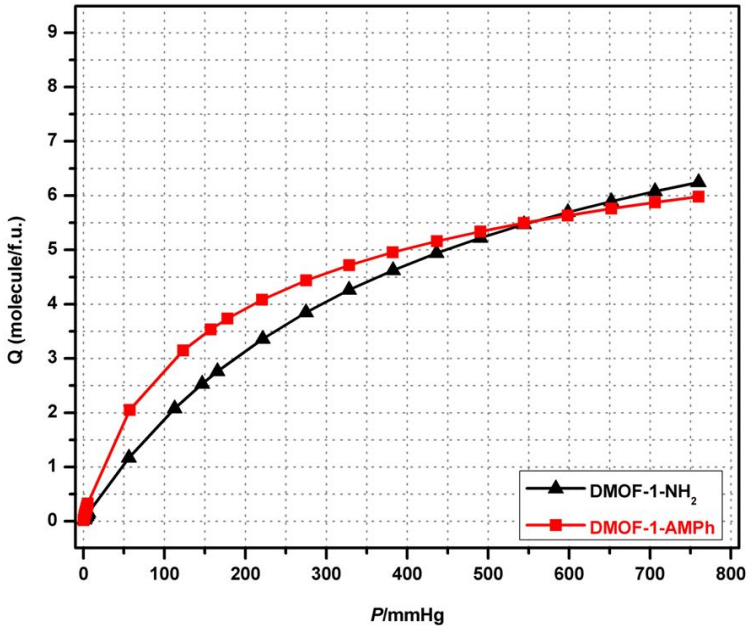

Figure 4-25. Molar uptake of H_2 at 77 K for DMOF-1-NH_2 and DMOF-1-AMPh.

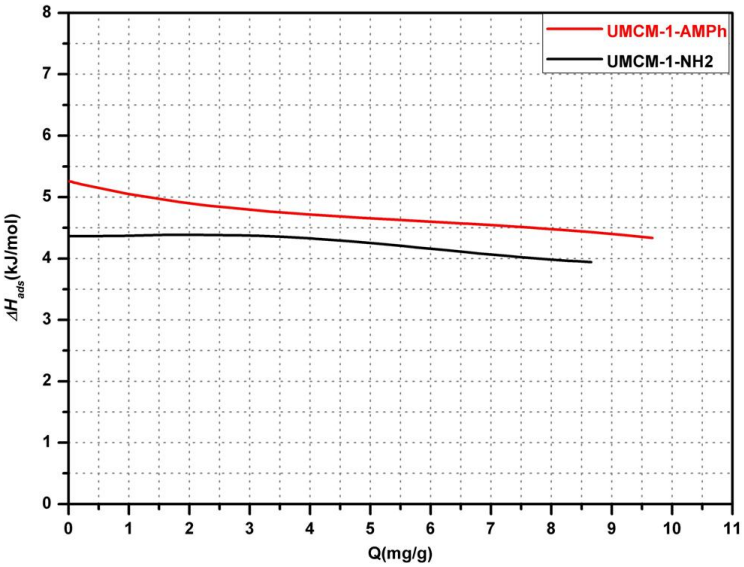

Figure 4-26. Isosteric heat of adsorption as determined by the virial-type equation for UMCM-1-NH_2 and UMCM-1-AMPh samples.

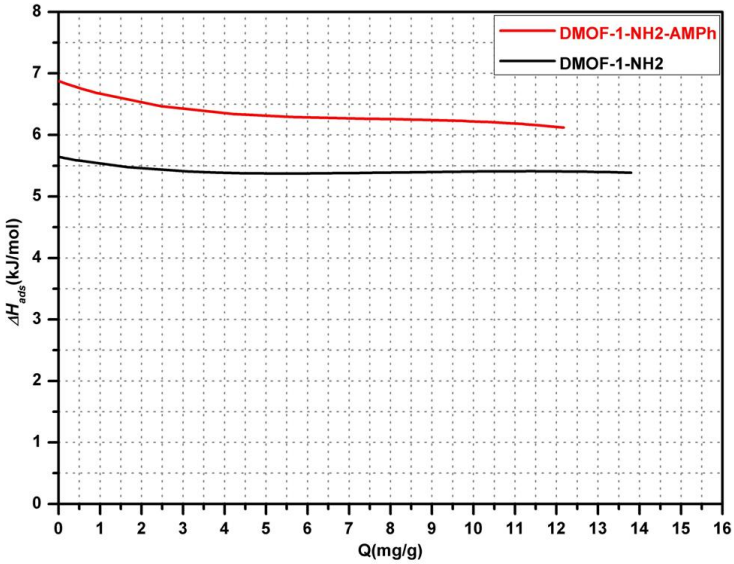

Figure 4-27. Isosteric heat of adsorption as determined by the virial-type equation for DMOF-1-NH_2 and DMOF-1-AMPh samples.

4.3 Conclusions

PSM is a valuable functionalization approach for designing MOFs as potential gas storage. Given the MOF can be modified via its organic ligand or SBU, a variety of functionalized MOFs can be achieved with multiple functionalities with better control over substituent type and degree of modification. Covalent modification was used to modify IRMOF-3, DMOF-1-NH_2, and UMCM-1-NH_2 with phenyl substituents, which were found to influence H_2 uptake and binding affinities The modified phenyl MOFs had higher heats of adsorptions (+1 kJ/mol) and higher H_2 capacities on a per molar and volumetric basis. Close examination of the three modified systems revealed DMOF-1-AMPh and UMCM-1-AMPh to be less optimal H_2 storage materials than IRMOF-3 due to their differences in pore sizes. These results are the first report of using covalent modification to enhance H_2 sorption properties within MOFs.

4.4 Experimental Section

General methods. Starting materials and solvents were purchased and used without further purification from commercial suppliers (Sigma-Aldrich, Alfa Aesar, EMD, TCI, Cambridge Isotope Laboratories, Inc., and others). IRMOF-3, DMOF-1-NH_2, and UMCM-1-NH_2 were synthesized and activated as described previously.[24,25]

IRMOF-3-AM5, -UR5, and -AMPh. For IRMOF-3: IRMOF-3-AM5 and IRMOF-3-URPh were synthesized on a double scale (~120 mg of IRMOF-3, 0.4 mmol equiv of -NH_2) following literature procedures.[24,26] IRMOF-3-AMPh-*a,b,c* were prepared by combining IRMOF-3 crystals (~120 mg, 0.4 mmol equiv of -NH_2) with benzoic anhydride dissolved in $CHCl_3$ (36 mg/mL, 10 mL). The mixtures were allowed to stand at room temperature for a duration of 1 d, 2 d, and 8 d, respectively. For the latter two cases, approximately every 24 h, the solution was decanted and the crystals were washed with 3×6 mL of $CHCl_3$ before a fresh solution of benzoic anhydride (36 mg/mL, 10 mL) was added. At the end of the reaction, the $CHCl_3$ solution was decanted and the crystals were washed with 3×6 mL of $CHCl_3$ before soaking in 10 mL of pure $CHCl_3$ for three days, with fresh $CHCl_3$ added every 24 h. After three days of soaking the crystals were stored in the last $CHCl_3$ solution until needed.

UMCM-1-AMPh. UMCM-1-NH_2 (~112 mg, ca. 0.10 mmol equiv of -NH_2) was combined with 8 equiv (0.80 mmol) of benzoic anhydride in 4 mL of $CHCl_3$. The sample was placed in a 55°C oven for 24h. After removing the sample from the oven, the solution was decanted and the crystals were washed with 3x10mL of $CHCl_3$ before soaking in 10 mL of $CHCl_3$ for 24 h. After repeating the washes and soaks for 3 days, the crystals were stored in the last $CHCl_3$ solution until analyzed.

DMOF-1-AMPh. DMOF-1-NH_2 (~120 mg, ca. 0.40 mmol equiv of -NH_2) was combined with 4 equiv (1.60 mmol) of benzoic anhydride in 4 mL of $CHCl_3$. The sample was placed in a 55°C oven for 24h. After removing the sample from the oven, the solution was decanted and the crystals were washed with 3x6 mL of $CHCl_3$ before soaking in 10 mL of $CHCl_3$ for 24 h. After repeating the washes and soaks for 3 days, the crystals were stored in the last $CHCl_3$ solution until analyzed.

Digestion and Analysis by ^{1}H NMR. ^{1}H NMR spectra were recorded on a Jeol FT-NMR (500MHz) or a Varian FT-NMR spectrometer (400 MHz). Approximately 5 mg of modified MOF (DMOF-1-NH_2, UMCM-1-NH_2, or IRMOF-3) from gas sorption experiments (i.e., thoroughly dried and evacuated; *vide infra*) was digested with sonication in 500 µL of DMSO-d_6 and 100 µL of dilute DCl (23 µL of 35% DCl in D_2O diluted with 1.0 mL of DMSO-d_6).

PXRD Analysis. Approximately 15 mg of modified IRMOF-3, DMOF-1-NH_2, or UMCM-1-NH_2 (typically soaked in $CHCl_3$) was air dried before PXRD analysis. Powder X-ray diffraction (PXRD) data were collected at ambient temperature on a Bruker D8 Advance diffractometer at 40 kV, 40 mA for Cu Kα (λ = 1.5418 Å), with a scan speed of 5 sec/step or 10 sec/step, a step size of 0.02° in 2θ and a 2θ range of 3-40°. The experimental backgrounds were corrected using the Jade 5.0 software package.

H_2 Sorption Analysis. Approximately 100-140 mg of modified IRMOF-3, DMOF-1-NH_2, or UMCM-1-NH_2 was evacuated on a vacuum line for 5-18 h. The sample was then transferred to a preweighed sample tube and degassed at 105 °C for approximately 24 h on an ASAP 2020 or until the outgas rate was <5 µmHg/min. The sample tube was re-weighed to obtain a consistent mass for the degassed modified

IRMOF-3, DMOF-1-NH_2 or UMCM-1-NH_2. For each sample, BET surface area (m^2/g) measurements were collected at 77 K by dinitrogen and at 87 K by argon on an ASAP 2020 using volumetric technique. The sample was then manually degassed on the analysis port overnight at 105 °C for approximately 12h. H_2 sorption isotherms were collected at 77 K. The sample was manually degassed for an additional 1-2h at 105°C prior to collecting H_2 sorption isotherms at 87 K.

Calculation of Isosteric Heat of Adsorption. Two different curve-fitting methods were used in determining the coverage-dependent isosteric heat of adsorption. Hydrogen adsorption isotherms were collected at 77 K and 87 K for each sample. Both the 77 K and 87 K data sets were fitted using the virial-type equation and the Langmuir-Freundlich equation.

Method 1: Virial-type equation

P = Pressure (kPa)

Q = Amount adsorbed (mg/g)

R = 8.314 J mol^{-1} K^{-1}

m and n = Number of coefficients

$$\ln P = \ln Q + \frac{1}{T}\sum_{i=0}^{m} a_i Q^i + \sum_{i=0}^{n} b_i Q^i$$

$$\Delta H_{ads} = -R\sum_{i=0}^{m} a_i Q^i$$

Method 2: Langmuir-Freundlich equation

Q = Amount adsorbed (mg/g)

Q_m = Amount adsorbed at saturation (mg/g)

B and t = Constants

P = Pressure (kPa)

$$\frac{Q}{Q_m} = \frac{B \times P^{(1/t)}}{1 + B \times P^{(1/t)}}$$

The Langmuir-Freundlich equation can be rearranged in terms of solving for P and substituted into a modified version of the Clausius-Clapeyron equation in order to solve for the isosteric heat of adsorption:

$$P = \left(\frac{Q/Q_m}{B - B \times Q/Q_m} \right)^t$$

$$\ln\left(\frac{P_1}{P_2}\right) = \Delta H_{ads} \times \frac{T_2 - T_1}{R \times T_1 \times T_2}$$

$$\Delta H_{ads} = \frac{R \times T_1 \times T_2}{T_2 - T_1} \times \ln \frac{\left(\frac{Q/Q_{m1}}{B_1 - B_1 \times Q/Q_{m1}} \right)^{t_1}}{\left(\frac{Q/Q_{m2}}{B_2 - B_2 \times Q/Q_{m2}} \right)^{t_2}}$$

4.5 Appendix

Table 4-2. A summary of hydrogen sorption properties of postsynthetically modified MOFs.

Material			Conversion	SA_{BET} (m^2/g)	H_2 (wt%)[1]	H_2 (per f.u.)[2,3]	$+H_2/L'$[4]	H_2 (g/L)[5]	ΔH_{ads} (kJ/mol)[6]
IRMOF-3		**Trial 1**	N.A.	2587	1.50	6.05	N.A.	9.50	5.0
		Trial 2	N.A.	2707	1.53	6.06	N.A.	9.70	5.3
		Trial 3	N.A.	2624	1.51	6.10	N.A.	9.58	5.5
	AMPh-*a*		32%	2267	1.73	7.84	1.86	12.30	5.3
	AMPh-*b*		44%	2052	1.73	8.16	1.60	12.80	5.7
	AMPh-*c*		70%	1657	1.68	8.60	1.21	13.49	6.0
	URPh	**Trial 1**	36%	1999	1.55	7.24	1.10	11.36	5.7
		Trial 2	43%	1901	1.47	7.06	0.77	11.08	6.0
		Trial 3	45%	1919	1.59	7.70	1.20	12.07	5.5
	AM5	**Trial 1**	87%	1292	1.23	6.52	0.18	10.24	6.0
		Trial 2	83%	1214	1.19	6.25	0.07	9.80	5.6
		Trial 3	88%	1212	1.21	6.44	0.14	10.10	5.4
UMCM-1-NH_2		**Trial 1**	N.A.	4014	1.38	7.09	N.A.	5.53	4.3
		Trial 2	N.A.	3820	1.31	6.73	N.A.	5.24	4.9
	AMPh	**Trial 1**	75%	3835	1.56	8.61	2.03	6.72	5.3
		Trial 2	76%	3704	1.51	8.36	1.65	6.49	5.0
DMOF-1-NH_2		**Trial 1**	N.A.	1379	2.09	6.22	N.A.	18.30	5.6
		Trial 2	N.A.	1359	2.07	6.19	N.A	18.18	5.6
	AMPh	**Trial 1**	62%	886	1.65	5.97	-0.21	17.55	6.9
		Trial 2	64%	939	1.72	6.28	0.03	18.44	7.0

1: Gravimetric uptake at 77 K and 1 atm.

2: f.u. (IRMOF-3s): $Zn_4O(L)_{3(1-x)}(L')_{3x}$, x is the modification conversion, L is NH_2-BDC, and L' is the modified BDC ligand; f.u. (UMCMs): $Zn_4O(BTB)_{3/4}(L)_{1-x}(L')_x$; f.u. (DMOFs): $Zn_2(L)_{2(1-x)}(L')_{2x}$(DABCO).

3: Molar uptake at 77 K and 1 atm.

4: $+H_2/L'$ represents the number of *additional* H_2 molecules per modified BDC ligand. This can be calculated from the following equation: $+H_2/L' = (N_{H2} - N^0_{H2})/(m*x)$, where N_{H2} is the number of H_2 molecules per f.u. for each modified MOF, N^0_{H2} is the number of H_2 molecules per f.u. for the parent MOF, m is the number of NH_2-BDC per f.u. in the parent MOF, and x is the conversion of modification.

5: Volumetric uptake at 77 K and 1 atm, estimated from calculated crystal density. It is assumed that the cell volume, and thus macroscopic volume of the MOF crystals do not change noticeably upon postsynthetic modification (ref 22).

6: Heat of adsorption at zero coverage calculated from the virial-type equation.

Table 4-3. Hydrogen adsorption data at 77 K and 87 K for three independent IRMOF-3 samples.

IRMOF-3							
Trial 1				**Trial 2**			
77 K		**87 K**		**77 K**		**87 K**	
Pressure (kPa)	H_2 wt%	Pressure (kPa)	H_2 wt%	Pressure (kPa)	H_2 wt%	Pressure (kPa)	H_2 wt%
0.1255	0.0051	0.1620	0.0028	0.1333	0.0059	0.2360	0.0040
0.2521	0.0101	0.3237	0.0055	0.2726	0.0112	0.4769	0.0076
0.3806	0.0150	0.4882	0.0079	0.4143	0.0164	0.7177	0.0110
0.5081	0.0199	0.6512	0.0105	0.5550	0.0215	7.7952	0.1032
0.6421	0.0242	0.8162	0.0130	0.6991	0.0264	15.1164	0.1886
0.7714	0.0289	7.8026	0.1032	7.5468	0.2254	19.9947	0.2416
7.6087	0.2233	15.0505	0.1864	15.1606	0.4036	22.2741	0.2658
14.9730	0.3914	19.9560	0.2395	19.7999	0.4984	29.5285	0.3388
19.8515	0.4884	22.2753	0.2635	22.2317	0.5450	36.6818	0.4069
22.1919	0.5323	29.5159	0.3354	29.5008	0.6733	43.8891	0.4721
29.5196	0.6588	36.6898	0.4027	36.6993	0.7875	50.9886	0.5331
36.6753	0.7703	43.8718	0.4666	43.8020	0.8910	58.5764	0.5949
43.8539	0.8723	50.9923	0.5267	50.9651	0.9875	65.4115	0.6484
51.0569	0.9669	58.5747	0.5878	58.4977	1.0820	72.7975	0.7041
58.3213	1.0564	65.4453	0.6409	65.4507	1.1639	79.7599	0.7552
65.4319	1.1383	72.8264	0.6959	72.5466	1.2433	87.0160	0.8065
72.7705	1.2197	79.7283	0.7455	79.9468	1.3225	94.1481	0.8549
79.7580	1.2925	86.9911	0.7958	86.9397	1.3936	101.3103	0.9022
86.9413	1.3651	94.1201	0.8438	94.1112	1.4637	107.9707	0.9451
94.1958	1.4342	101.3187	0.8907	101.0083	1.5285		
101.2452	1.4985	108.1092	0.9341	108.1719	1.5937		
108.0200	1.5589						

Table 4-3 (continued). Hydrogen adsorption data at 77 K and 87 K for three independent IRMOF-3 samples.

IRMOF-3			
Trial 3			
77 K		**87 K**	
Pressure (kPa)	H_2 wt%	Pressure (kPa)	H_2 wt%
0.1622	0.0066	0.2267	0.0034
0.3271	0.0130	0.4523	0.0069
0.4940	0.0192	0.6778	0.0103
0.6620	0.0253	7.7995	0.1059
0.8182	0.0311	15.0981	0.1929
7.6199	0.2284	20.0140	0.2474
14.9795	0.3991	22.2702	0.2715
19.8075	0.4967	29.4599	0.3452
22.1815	0.5415	36.6943	0.4145
29.4135	0.6679	43.8577	0.4795
36.6427	0.7814	51.0441	0.5415
43.8467	0.8845	58.2149	0.6004
51.0207	0.9794	65.4194	0.6569
58.2383	1.0679	72.5325	0.7111
65.4101	1.1507	79.8201	0.7640
72.5294	1.2292	86.9642	0.8145
79.7901	1.3047	94.1968	0.8638
86.9306	1.3758	101.3379	0.9108
94.1611	1.4451	108.0083	0.9536
101.3608	1.5109		
107.8295	1.5684		

Table 4-4. Hydrogen adsorption data at 77 K and 87 K for three independent IRMOF-3-AMPh samples.

IRMOF-3-AMPh-*a*				**IRMOF-3-AMPh-*b***			
77 K		**87 K**		**77 K**		**87 K**	
Pressure (kPa)	H_2 wt%	Pressure (kPa)	H_2 wt%	Pressure (kPa)	H_2 wt%	Pressure (kPa)	H_2 wt%
0.1244	0.0067	0.2289	0.0046	0.1502	0.0082	0.2245	0.0044
0.2562	0.0127	0.4597	0.0089	0.3022	0.0161	0.4476	0.0087
0.3881	0.0187	0.6937	0.0131	0.4557	0.0240	0.6710	0.0131
0.5190	0.0246	7.7496	0.1265	0.6105	0.0317	7.7343	0.1365
0.6532	0.0303	15.1120	0.2323	0.7673	0.0395	15.1161	0.2488
0.7874	0.0361	19.9769	0.2969	7.8296	0.3196	19.9557	0.3161
7.7968	0.2942	22.2644	0.3261	15.0848	0.5363	22.2692	0.3470
15.1934	0.5066	29.5096	0.4139	19.6578	0.6510	29.4306	0.4367
19.7183	0.6176	36.7190	0.4949	22.1582	0.7080	36.6713	0.5202
22.1953	0.6732	43.8740	0.5704	29.4631	0.8576	43.8166	0.5968
29.3995	0.8215	51.0618	0.6413	36.6231	0.9856	51.0537	0.6688
36.7357	0.9535	58.4199	0.7099	43.8068	1.0986	58.2160	0.7362
43.7477	1.0668	65.5054	0.7726	51.0072	1.2011	65.4294	0.7994
51.2134	1.1763	72.7909	0.8341	58.2247	1.2942	72.5579	0.8589
58.3426	1.2719	79.7643	0.8902	65.3816	1.3786	79.7764	0.9159
65.4787	1.3603	86.9345	0.9457	72.5467	1.4572	86.9532	0.9702
72.5830	1.4422	94.2988	0.9998	79.7732	1.5311	94.1710	1.0223
79.7291	1.5201	101.3117	1.0499	86.9235	1.5995	101.3537	1.0720
87.0097	1.5944	108.2157	1.0975	94.1465	1.6645	108.0194	1.1163
94.2288	1.6641			101.3363	1.7263		
101.2035	1.7283			107.8803	1.7795		
108.0161	1.7885						

Table 4-4 (continued). Hydrogen adsorption data at 77 K and 87 K for three independent IRMOF-3-AMPh samples.

IRMOF-3-AMPh-*c*			
77 K		**87 K**	
Pressure (kPa)	H_2 wt%	Pressure (kPa)	H_2 wt%
0.1206	0.0083	0.2226	0.0053
0.2469	0.0160	0.4517	0.0102
0.3723	0.0239	0.6793	0.0151
0.5032	0.0312	7.6712	0.1471
0.6338	0.0387	15.1338	0.2662
0.7661	0.0459	19.8973	0.3345
7.7038	0.3462	22.2158	0.3658
15.1833	0.5757	29.4796	0.4571
19.4306	0.6819	36.6911	0.5393
22.1214	0.7428	43.8369	0.6141
29.5154	0.8897	51.0720	0.6837
36.6898	1.0109	58.1832	0.7477
43.8012	1.1159	65.5923	0.8096
51.1857	1.2123	72.7754	0.8659
58.1407	1.2943	79.9070	0.9187
65.3450	1.3718	87.0037	0.9683
72.6767	1.4437	94.2049	1.0160
79.7356	1.5076	101.3168	1.0609
86.9577	1.5686	107.9979	1.1010
94.1349	1.6252		
101.0668	1.6763		
108.1014	1.7257		

Table 4-5. Hydrogen adsorption data at 77 K and 87 K for three independent IRMOF-3-URPh samples.

IRMOF-3-URPh							
Trial 1				**Trial 2**			
77 K		**87 K**		**77 K**		**87 K**	
Pressure (kPa)	H_2 wt%	Pressure (kPa)	H_2 wt%	Pressure (kPa)	H_2 wt%	Pressure (kPa)	H_2 wt%
0.1297	0.0070	0.2224	0.0046	0.1099	0.0073	0.1554	0.0036
0.2584	0.0142	0.4483	0.0089	0.2282	0.0137	0.3164	0.0068
0.3910	0.0209	0.6765	0.0131	0.3476	0.0198	0.4798	0.0098
0.5246	0.0276	7.7415	0.1265	0.4654	0.0260	0.6414	0.0129
0.6620	0.0340	15.1087	0.2268	0.5885	0.0318	0.8039	0.0159
0.7974	0.0405	19.9266	0.2860	0.7100	0.0377	7.7711	0.1241
7.7963	0.2936	22.2763	0.3135	7.5100	0.2717	15.1085	0.2198
14.9531	0.4820	29.5278	0.3929	14.8302	0.4536	19.9824	0.2772
19.6121	0.5842	36.7034	0.4649	19.6707	0.5536	22.3026	0.3033
22.1679	0.6356	43.8630	0.5313	22.1814	0.6014	29.4507	0.3784
29.5328	0.7679	50.9597	0.5935	29.5346	0.7257	36.7268	0.4487
36.6720	0.8799	58.4441	0.6543	36.6897	0.8318	43.8263	0.5124
43.8451	0.9804	65.4068	0.7079	43.8070	0.9255	51.0316	0.5730
50.9631	1.0702	72.5800	0.7605	51.1795	1.0136	58.2301	0.6302
58.3472	1.1563	79.9899	0.8118	58.1958	1.0907	65.5818	0.6851
65.4907	1.2329	86.9724	0.8580	65.5451	1.1651	72.5922	0.7348
72.5457	1.3032	94.2332	0.9039	72.5341	1.2318	79.9477	0.7843
79.7676	1.3706	101.3221	0.9472	79.9545	1.2976	86.9301	0.8295
86.9757	1.4347	108.0807	0.9868	86.9492	1.3566	94.2860	0.8750
94.2249	1.4943			94.1613	1.4140	101.3117	0.9165
101.1491	1.5494			101.2087	1.4675	108.0668	0.9554
107.9757	1.6019			107.9996	1.5169		

Table 4-5 (continued). Hydrogen adsorption data at 77 K and 87 K for three independent IRMOF-3-URPh samples.

IRMOF-3-URPh			
Trial 3			
77 K		**87 K**	
Pressure (kPa)	H_2 wt%	Pressure (kPa)	H_2 wt%
0.0775	0.0064	0.0881	0.0029
0.1520	0.0108	0.1744	0.0048
0.2179	0.0152	0.2762	0.0075
0.3009	0.0200	0.3780	0.0102
0.3839	0.0245	0.4834	0.0123
0.4660	0.0291	0.5873	0.0145
0.5499	0.0335	0.6901	0.0170
0.6333	0.0379	7.8193	0.1387
0.7176	0.0425	14.9968	0.2417
7.6794	0.3074	20.0469	0.3070
14.9872	0.5047	22.3485	0.3356
19.7657	0.6117	29.5301	0.4178
22.2145	0.6610	36.7107	0.4934
29.4845	0.7938	43.8812	0.5634
36.7406	0.9084	51.1405	0.6294
43.8447	1.0080	58.8681	0.6953
50.9911	1.0996	65.5016	0.7495
58.1622	1.1837	72.6461	0.8041
65.8083	1.2658	80.3959	0.8615
72.7899	1.3361	87.1910	0.9094
79.9245	1.4039	94.3843	0.9569
86.9380	1.4658	101.7490	1.0042
94.3540	1.5287	108.0984	1.0435
101.4168	1.5849		
108.2973	1.6369		

Table 4-6. Hydrogen adsorption data at 77 K and 87 K for three independent IRMOF-3-AM5 samples.

IRMOF-3-AM5							
Trial 1				**Trial 2**			
77 K		**87 K**		**77 K**		**87 K**	
Pressure (kPa)	H_2 wt%	Pressure (kPa)	H_2 wt%	Pressure (kPa)	H_2 wt%	Pressure (kPa)	H_2 wt%
0.1575	0.0087	0.2478	0.0047	0.1391	0.0078	0.2514	0.0052
0.3188	0.0172	0.4954	0.0094	0.2832	0.0153	0.5061	0.0102
0.4831	0.0255	0.7794	0.0146	0.4326	0.0223	0.7669	0.0149
0.6492	0.0336	7.7038	0.1220	0.5835	0.0293	7.5904	0.1149
0.8036	0.0413	15.1299	0.2159	0.7616	0.0374	15.1038	0.2047
7.7486	0.2743	19.8985	0.2689	7.5511	0.2573	19.9197	0.2555
14.7533	0.4316	22.2584	0.2939	14.8687	0.4174	22.2485	0.2785
19.5139	0.5175	29.4368	0.3629	19.4882	0.4967	29.5059	0.3439
22.1158	0.5598	36.7028	0.4257	22.1134	0.5375	36.6983	0.4022
29.4481	0.6631	43.8541	0.4818	29.4367	0.6363	43.8496	0.4550
36.6612	0.7497	50.9518	0.5335	36.6623	0.7195	51.0177	0.5036
43.7866	0.8248	58.2648	0.5823	43.7558	0.7913	58.2418	0.5491
51.0487	0.8925	65.4101	0.6272	50.9839	0.8566	65.3634	0.5909
58.1845	0.9526	72.5809	0.6698	58.2434	0.9156	72.9063	0.6327
65.3884	1.0081	79.7880	0.7100	65.4778	0.9695	79.7637	0.6687
72.5593	1.0588	86.9208	0.7475	72.5686	1.0187	86.9574	0.7041
79.7738	1.1065	94.1770	0.7839	79.7481	1.0646	94.1565	0.7375
86.9434	1.1509	101.3541	0.8185	86.9466	1.1076	101.3220	0.7693
94.1621	1.1928	108.0222	0.8494	94.1734	1.1484	107.9769	0.7979
101.3555	1.2318			101.2495	1.1859		
107.9980	1.2669			108.1454	1.2209		

Table 4-6 (continued). Hydrogen adsorption data at 77 K and 87 K for three independent IRMOF-3-AM5 samples.

IRMOF-3-AM5			
Trial 3			
77 K		**87 K**	
Pressure (kPa)	H_2 wt%	Pressure (kPa)	H_2 wt%
0.0731	0.0041	0.1323	0.0029
0.1610	0.0087	0.2432	0.0054
0.2504	0.0133	0.3564	0.0073
0.3407	0.0177	0.4682	0.0095
0.4308	0.0221	0.5805	0.0116
0.5222	0.0263	0.6941	0.0134
0.6140	0.0302	7.7674	0.1185
0.7059	0.0343	15.1704	0.2081
7.6130	0.2550	19.9611	0.2595
15.0030	0.4143	22.2028	0.2829
19.7652	0.4961	29.5328	0.3511
22.2267	0.5350	36.6645	0.4113
29.5316	0.6340	43.8031	0.4673
36.6334	0.7172	51.0748	0.5195
43.8547	0.7919	58.3405	0.5683
51.1480	0.8592	65.4881	0.6136
58.1632	0.9189	72.7951	0.6570
65.3609	0.9751	79.8782	0.6974
72.6195	1.0272	86.9739	0.7355
79.7364	1.0754	94.1501	0.7728
86.9342	1.1220	101.3479	0.8081
94.1625	1.1652	107.3546	0.8371
101.3204	1.2060		
108.0746	1.2430		

Table 4-7. Hydrogen adsorption data at 77 K and 87 K for two independent UMCM-1-NH_2 samples.

UMCM-1-NH_2							
Trial 1				**Trial 2**			
77 K		**87 K**		**77 K**		**87 K**	
Pressure (kPa)	H_2 wt%	Pressure (kPa)	H_2 wt%	Pressure (kPa)	H_2 wt%	Pressure (kPa)	H_2 wt%
0.2605	0.0074	0.3477	0.0046	0.2701	0.0082	0.3627	0.0047
0.5290	0.0142	0.6994	0.0086	0.5434	0.0161	0.7350	0.0094
0.7986	0.0208	8.8287	0.0936	0.7910	0.0231	7.8497	0.0884
7.7338	0.1749	15.0829	0.1553	7.7385	0.1818	15.0533	0.1608
15.0579	0.3163	20.0673	0.2026	15.0311	0.3192	20.0054	0.2080
19.9964	0.4023	22.3346	0.2236	19.9005	0.4010	22.2928	0.2292
22.2551	0.4398	29.4165	0.2875	22.1811	0.4373	29.4667	0.2929
29.5445	0.5532	36.7110	0.3504	29.4477	0.5457	36.6819	0.3537
36.6801	0.6560	43.8035	0.4092	36.6300	0.6435	43.8127	0.4113
43.8553	0.7524	51.3062	0.4692	43.8619	0.7347	51.0544	0.4670
51.0706	0.8438	58.1952	0.5225	51.0434	0.8192	58.1656	0.5197
58.1740	0.9292	65.4092	0.5763	58.2303	0.8992	65.3996	0.5715
65.7350	1.0157	72.9251	0.6310	65.4021	0.9750	72.5982	0.6207
72.8407	1.0937	79.7534	0.6796	72.5458	1.0477	79.7969	0.6690
79.8574	1.1679	86.9679	0.7301	79.7848	1.1178	86.9752	0.7160
86.9213	1.2403	94.2931	0.7796	86.9229	1.1847	94.1741	0.7608
94.3295	1.3136	101.5439	0.8272	94.1743	1.2497	101.3292	0.8050
101.3682	1.3816	107.4401	0.8657	101.3482	1.3123	108.0056	0.8458
108.4262	1.4479			107.8749	1.3676		

Table 4-8. Hydrogen adsorption data at 77 K and 87 K for two independent UMCM-1-AMPh samples.

UMCM-1-AMPh							
Trial 1				**Trial 2**			
77 K		**87 K**		**77 K**		**87 K**	
Pressure (kPa)	H_2 wt%	Pressure (kPa)	H_2 wt%	Pressure (kPa)	H_2 wt%	Pressure (kPa)	H_2 wt%
0.2228	0.0080	0.3112	0.0043	0.2716	0.0086	0.3686	0.0048
0.4534	0.0153	0.6237	0.0084	0.5420	0.0172	0.7625	0.0100
0.6866	0.0223	0.9342	0.0125	0.7850	0.0249	7.8448	0.0983
7.6753	0.2182	7.8333	0.0984	7.6536	0.2115	15.1274	0.1821
15.2632	0.3929	15.1326	0.1828	15.0746	0.3773	20.0374	0.2353
19.8657	0.4868	20.0661	0.2368	19.8733	0.4717	22.2388	0.2587
22.2569	0.5327	22.2824	0.2605	22.1249	0.5136	29.5435	0.3322
29.5262	0.6627	29.5181	0.3346	29.4870	0.6403	36.6785	0.4004
36.6891	0.7787	36.6716	0.4037	36.6532	0.7525	43.8701	0.4657
43.8173	0.8858	43.8617	0.4703	43.7825	0.8558	51.0159	0.5281
51.2145	0.9887	51.0016	0.5336	50.9865	0.9531	58.1674	0.5876
58.2178	1.0808	58.3273	0.5958	58.2252	1.0451	65.4461	0.6458
65.6042	1.1726	65.4236	0.6536	65.3970	1.1314	72.5830	0.7008
72.6195	1.2558	72.5790	0.7104	72.5398	1.2132	79.8069	0.7547
79.7932	1.3375	79.7760	0.7655	79.8084	1.2925	86.9711	0.8068
86.9695	1.4162	86.9543	0.8190	86.9536	1.3683	94.1649	0.8575
94.1199	1.4919	94.1244	0.8709	94.1765	1.4416	101.3658	0.9064
101.0457	1.5623	101.2976	0.9213	101.3547	1.5121	108.0094	0.9506
108.0961	1.6321	107.9718	0.9673	107.8300	1.5738		

Table 4-9. Hydrogen adsorption data at 77 K and 87 K for two independent DMOF-1-NH_2 samples.

DMOF-1-NH_2							
Trial 1				**Trial 2**			
77 K		**87 K**		**77 K**		**87 K**	
Pressure (kPa)	H_2 wt%	Pressure (kPa)	H_2 wt%	Pressure (kPa)	H_2 wt%	Pressure (kPa)	H_2 wt%
0.1539	0.0106	0.2729	0.0068	0.1346	0.0089	0.2193	0.0053
0.3159	0.0212	0.5453	0.0135	0.2779	0.0180	0.4380	0.0106
0.4805	0.0316	0.7901	0.0195	0.4229	0.0269	0.6573	0.0159
0.6466	0.0419	7.5241	0.1660	0.5693	0.0358	0.8566	0.0207
0.8012	0.0514	15.0684	0.3115	0.7267	0.0451	7.6569	0.1665
7.4839	0.3919	19.8524	0.3966	7.6988	0.3940	15.0900	0.3083
15.0145	0.6950	22.2210	0.4368	15.1949	0.6901	19.9648	0.3939
19.5586	0.8483	29.5054	0.5534	19.6607	0.8387	22.2468	0.4325
22.0730	0.9253	36.7054	0.6592	22.1300	0.9138	29.5022	0.5478
29.5074	1.1264	43.8351	0.7560	29.5215	1.1120	36.6783	0.6528
36.6514	1.2896	51.0125	0.8465	36.6384	1.2731	43.8547	0.7498
43.7619	1.4282	58.2027	0.9304	43.8124	1.4115	51.0111	0.8397
50.9852	1.5494	65.4079	1.0084	50.9650	1.5315	58.2092	0.9232
58.1484	1.6550	72.5782	1.0811	58.1914	1.6372	65.3835	1.0009
65.3868	1.7491	79.7757	1.1495	65.3969	1.7305	72.5691	1.0736
72.5852	1.8327	86.9415	1.2133	72.5764	1.8135	79.7774	1.1421
79.7973	1.9074	94.1474	1.2737	79.8352	1.8889	86.9648	1.2061
86.9372	1.9747	101.3458	1.3303	86.9630	1.9562	94.1555	1.2666
94.1507	2.0366	107.9864	1.3800	94.1567	2.0178	101.3414	1.3237
101.3409	2.0921			101.3408	2.0741	108.0126	1.3739
107.6838	2.1385			108.0066	2.1230		

Table 4-10. Hydrogen adsorption data at 77 K and 87 K for two independent DMOF-1-AMPh samples.

DMOF-1-AMPh							
Trial 1				**Trial 2**			
77 K		**87 K**		**77 K**		**87 K**	
Pressure (kPa)	H_2 wt%	Pressure (kPa)	H_2 wt%	Pressure (kPa)	H_2 wt%	Pressure (kPa)	H_2 wt%
0.0371	0.0055	0.1780	0.0076	0.0411	0.0070	0.1897	0.0090
0.1232	0.0176	0.3560	0.0151	0.1251	0.0203	0.3804	0.0178
0.2121	0.0295	0.5349	0.0225	0.2125	0.0334	0.5732	0.0266
0.3031	0.0412	0.7160	0.0298	0.3029	0.0464	0.7530	0.0347
0.3959	0.0528	7.4873	0.2465	0.3957	0.0592	7.8178	0.2712
0.4906	0.0643	15.1814	0.4201	0.4906	0.0718	14.9164	0.4371
0.5868	0.0757	19.5263	0.5001	0.5891	0.0845	19.5312	0.5240
0.7126	0.0901	22.0855	0.5424	0.7182	0.1000	22.1198	0.5678
7.6173	0.5657	29.4783	0.6494	7.8355	0.6046	29.4900	0.6766
16.3989	0.8682	36.6167	0.7364	16.0892	0.8973	36.6884	0.7660
20.9508	0.9750	43.8341	0.8122	20.6644	1.0093	43.7922	0.8421
23.7266	1.0299	51.0181	0.8781	23.5711	1.0692	51.0164	0.9095
29.4434	1.1259	58.2337	0.9367	29.3909	1.1721	58.2083	0.9693
36.6789	1.2234	65.4152	0.9889	36.6437	1.2742	65.3422	1.0224
43.7719	1.3015	72.5571	1.0358	43.7763	1.3559	72.5804	1.0713
50.9272	1.3671	79.7747	1.0790	50.9839	1.4249	79.7365	1.1150
58.2082	1.4237	86.9735	1.1184	58.1961	1.4842	86.9569	1.1554
65.3740	1.4723	94.1662	1.1545	65.3958	1.5354	94.1623	1.1926
72.5446	1.5155	101.3368	1.1880	72.5532	1.5810	101.3288	1.2274
79.7763	1.5542	108.0134	1.2175	79.7799	1.6221	108.0238	1.2569
86.9533	1.5889			86.9528	1.6590		
94.1577	1.6204			94.1541	1.6925		
101.3298	1.6492			101.3345	1.7237		
108.0195	1.6740			108.0190	1.7506		

4.6 Acknowledgements

Text, schemes, and figures in this chapter, in part, are reprints of the materials published in the following papers: Wang, Z., Tanabe K. K., Cohen, S. M. "Tuning Hydrogen Sorption Properties of Metal-Organic Frameworks by Postsynthetic Covalent Modification" *Chem. Eur. J.* **2010**, *16*, 212 – 217; Tanabe, K. K., Cohen, S. M. "Postsynthetic Modification of Metal-Organic Frameworks – A Progress Report." *Chem. Soc. Rev.* **2011**, *40*, 498-519. The dissertation author was the primary researcher and either primary or co-author for the data presented. The co-authors listed in these publications also participated in the research. The permissions to reproduce these papers were granted by Wiley-VCH Verlag GmbH & Co. KGaA, Weinheim, copyright 2010; and the Royal Society of Chemistry, copyright 2011.

4.7 References

(1) U. S. Department of Energy. Energy Efficiency and Renewable Energy. http://www1.eere.energy.gov/hydrogenandfuelcells/storage/basics.html

(2) U. S. Department of Energy. Energy Efficiency and Renewable Energy. http://www1.eere.energy.gov/hydrogenandfuelcells/storage/current_technology.html

(3) Murray, L. J.; Dinca, M.; Long, J. R. *Chem. Soc. Rev.* **2009**, *38*, 1294-1314.

(4) Bhatia, S. K.; Myers, A. L. *Langmuir* **2006**, *22*, 1688-1700.

(5) Férey, G.; Latroche, M.; Serre, C.; Millange, F.; Loiseau, T.; Percheron-Guégan, A. *Chem. Commun.* **2003**, 2976-2977.

(6) Rosi, N. L.; Eckert, J.; Eddaoudi, M.; Vodak, D. T.; Kim, J.; O'Keeffe, M.; Yaghi, O. M. *Science* **2003**, *300*, 1127-1129.

(7) Rowsell, J. L. C.; Yaghi, O. M. *Angew. Chem. Int. Ed.* **2005**, *44*, 4670-4679.

(8) Collins, D. J.; Zhou, H.-C. *J. Mater. Chem.* **2007**, *17*, 3154-3160.

(9) Dinca, M.; Long, J. R. *Angew, Chem. Int. Ed.* **2008**, *47*, 6766-6779.

(10) Getman, R. B.; Miller, J. H.; Wang, K.; Snurr, R. Q. *J. Phys. Chem. C* **2011**, *115*, 2066–2075.

(11) Cheon, Y. E.; Suh, M. P. *Angew. Chem. Int. Ed.* **2009**, *48*, 2899-2903.

(12) Dybstev, D.; Serre, C.; Schmitz, B.; Panella, B.; Hirscher, M.; Latroche, M.; Llewellyn, P. L.; Cordier, S.; Molard, Y.; Haouas, M.; Taulelle, F.; Ferey, G. *Langmuir* **2010**, *26*, 11283–11290.

(13) Zlotea, C.; Campesi, R.; Cuevas, F.; Leroy, E.; Dibandjo, P.; Volkringer, C.; Loiseau, T.; Ferey, G.; Latroche, M. *J. Am. Chem. Soc.* **2010**, *132*, 2991–2997.

(14) Dinca, M.; Dailly, A.; Liu, Y.; Brown, C. M.; Neumann, D. A.; Long, J. R. *J. Am. Chem. Soc.* **2006**, *128*, 16876-16883.

(15) Forster, P. M.; Eckert, J.; Heiken, B. D.; Parise, J. B.; Yoon, J. W.; Jhung, S. H.; Chang, J.-S.; Cheetham, A. K. *J. Am. Chem. Soc.* **2006**, *128*, 16846-16850.

(16) Tanabe, K. K.; Cohen, S. M. *Chem. Soc. Rev.* **2011**, *40*, 498-519.

(17) Mulfort, K. L.; Farha, O. K.; Stern, C. L.; Sarjeant, A. A.; Hupp, J. T. *J. Am. Chem. Soc.* **2009**, *131*, 3866–3868.

(18) Mulfort, K. L.; Hupp, J. T. *J. Am. Chem. Soc.* **2007**, *129*, 9604-9605.

(19) Rowsell, J. L. C.; Yaghi, O. M. *J. Am. Chem. Soc.* **2006**, *128*, 1304-1315.

(20) Lin, X.; Telepeni, I.; Blake, A. J.; Dailly, A.; Brown, C. M.; Simmons, J. M.; Zoppi, M.; Walker, G. S.; Thomas, K. M.; Mays, T. J.; Hubberstey, P.; Champness, N. R.; Schroder, M. *J. Am. Chem. Soc.* **2009**, *131*, 2159–2171.

(21) Czepirski, L.; Jagiello, J. *Chem. Eng. Sci.* **1989**, *44*, 797-801.

(22) Yang, R. T. *Gas Separation by Adsorption Processes*; Butterworth: Boston, 1997.

(23) Eddaoudi, M.; Kim, J.; Rosi, N.; Vodak, D.; Wachter, J.; O'Keeffe, M.; Yaghi, O. M. *Science* **2002**, *295*, 469-472.

(24) Tanabe, K. K.; Wang, Z.; Cohen, S. M. *J. Am. Chem. Soc.* **2008**, *130*, 8508-8517.

(25) Wang, Z.; Tanabe, K. K.; Cohen, S. M. *Inorg. Chem.* **2009**, *48*, 296-306.

(26) Dugan, E.; Wang, Z.; Okamura, M.; Medina, A.; Cohen, S. M. *Chem. Commun.* **2008**, 3366-8.

(27) Klontzas, E.; Mavrandonakis, A.; Froudakis, G. E.; Carissan, Y.; Klopper, W. *J. Phys. Chem. C* **2007**, *111*, 13635-13640.

(28) Frost, H.; Duren, T.; Snurr, R. Q. *J. Phys. Chem. B* **2006**, *110*, 9565-9570.

Chapter 5 Developing MOFs for catalysis applications via PSM

5.1 Introduction

Catalysis has been another popular area of interest for MOFs because they exhibit features that might capture the best features of both homogeneous and heterogeneous catalysts.[1-4] MOFs are highly porous, which allows for good mass transport and interaction with substrates, thermally stable, and easy to isolate and reuse.[5-7] Additionally, MOFs have excellent chemical tunability and can be synthesized with various combinations of metal ions and organic ligands to yield a catalyst that is robust, active, and selective. Even though MOFs are very appealing materials for catalysis, exerting precise control over the physical and chemical properties of the framework to improve catalytic activity and selectivity have been an ongoing challenge. Many MOFs have been explored as catalysts for transesterfications,[8] C-C bond forming reactions,[9-12] epoxidations,[13] and many other reactions,[1,14] but there have been very few reports of MOFs that are both selective and robust.[12,15] Overall, the number of reported MOF catalysts has remained somewhat low in comparison to gas sorption studies.

There are several routes for designing MOF catalysts. MOFs can be functionalized via their metal nodes or organic ligands through presynthetic[16,17] or postsynthetic[18] approaches. The metal ion and organic ligand(s) can be carefully chosen to produce a MOF with specific pore apertures, chiral topologies, and unsaturated metal centers. Likewise, the MOF can be further tuned in a postsynthetic fashion through one of three different PSM approaches: covalent, coordinate covalent, or a combination of both covalent and coordinate covalent modification (Figure 5-1).[19] Covalent modification is defined as the chemical modification of the organic ligand of the framework.[19,20] Garibay and Cohen used covalent PSM to modify the amino groups of

MIL-53(Al)-NH_2 with maleic anhydride, which resulted in the generation of free carboxylic acids (Figure 5-2).[21] The modified MIL, MIL-53(Al)-AMMal, was tested as a potential Brønsted acid catalyst and was found to active, recyclable catalyst for the methanolysis of small epoxides (e.g., *cis*-2,3-epoxybutane). Other modified versions of MIL-53(Al)-NH_2 were prepared with crotonic acetic anhydride, crotonic anhydride, and succinic anhydride and tested alongside MIL-53(Al)-AMMal to determine if the functionality type had an influence on the catalytic activity. Out of the four modified MILs, only MIL-53(Al)-AMMal was catalytically active.

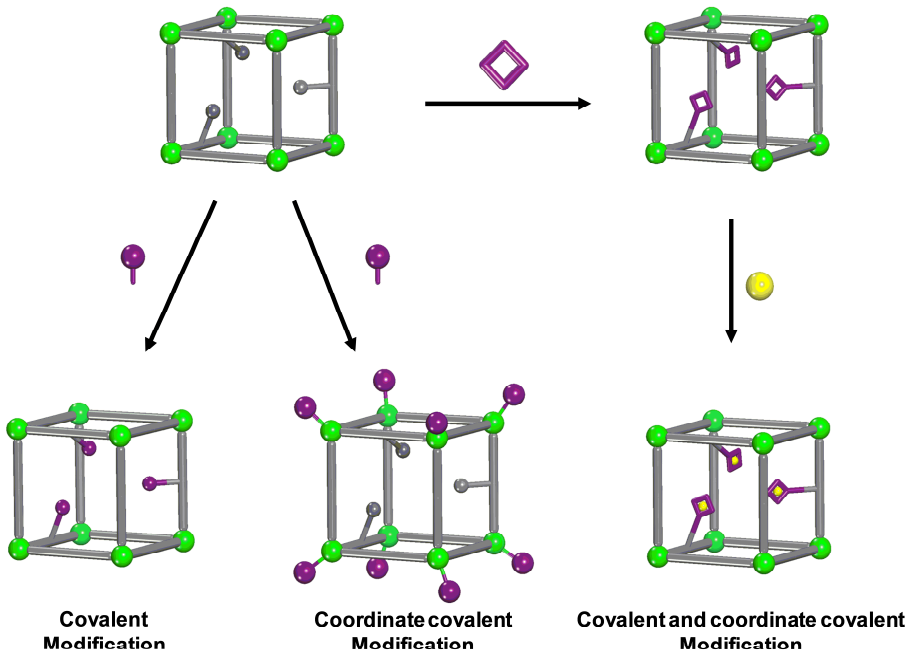

Figure 5-1. Representation of covalent (left), coordinate covalent (middle), and a combination of PSM strategies (right) for PSM of MOFs.

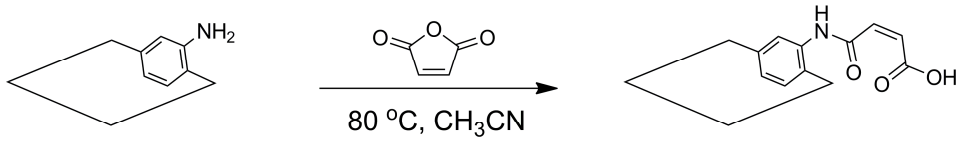

MIL-53(Al)-NH_2 MIL-53(Al)-AMMal

Figure 5-2. Covalent modification of MIL-53(Al)-NH_2 with maleic anhydride. MIL-53(Al)-AMMal was found to be an active, heterogeneous catalyst for methanolysis of epoxides.

Coordinate covalent modification, which was briefly mentioned in Chapter 4, involves modification of the metal centers of the framework. There are two main methods for coordinate covalent modification. In the first route, coordinating ligands, such as alkylamine or pyridines, can be introduced into the framework to bind to unsaturated sites located on the metal nodes of the SBUs.[22-24] Kim and coworkers converted an achiral MOF into an active chiral catalyst by modifying MIL-101(Cr) in a coordinate covalent approach.[11] MIL-101(Cr) has unsaturated metal centers that are generated upon solvent removal. The unsaturated metal centers were coordinated by chiral L-proline derivatives, [(S)-N-(pyridin-3-yl)-pyrrolidine-2-carboxamide] or [(S)-N-(pyridin-4-yl)-pyrrolidine-2-carboxamide], generating CMIL-1 and CMIL-2, respectively (Figure 5-3). CMIL-1 and CMIL-2 were found to be active, chiral catalysts for asymmetric aldol reactions between aldehydes and ketones with yields ranging from 60-90% and with ee's between 55–80%. In the second coordinate covalent modification route, the organic ligand of the MOF may have a binding substituent (e.g., -OH) that does not play a structural role for the framework, and can undergo metalation.[10] One well-known example of the second approach was demonstrated by Lin and coworkers, where they prepared a MOF from Cd^{2+} and (R)-6,6'-dichloro-2,2'-dihydroxy-1,1'-binaphthyl-4,4'-bipyridine and obtained a structure with free, uncoordinated hydroxyl groups that

could be metallated with Ti(O*i*Pr)$_4$ (Figure 5-4).[10] Given the MOF contained a chiral Ti^{4+} site, the MOF was tested as an asymmetric Lewis acid catalyst and was found to be active for $ZnEt_2$ addition to aromatic aldehydes to produce secondary chiral alcohols with high ee's.

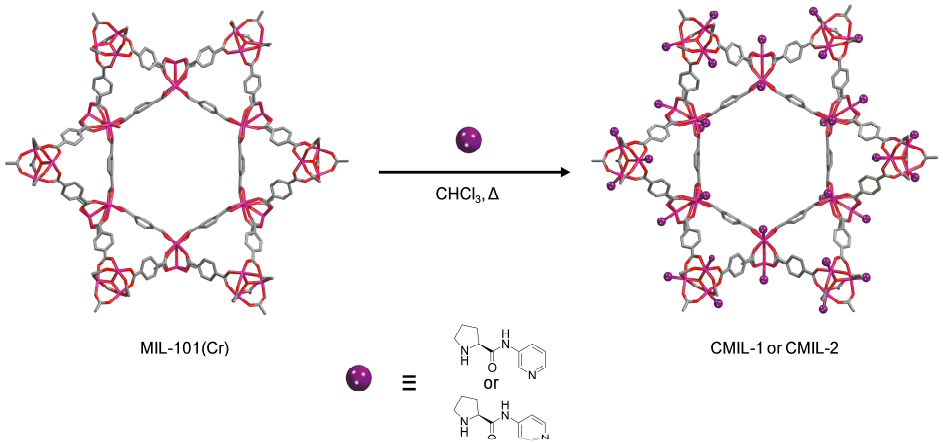

Figure 5-3. Coordinate covalent modification of MIL-101(Cr) with chiral proline ligands. Chiral proline ligands were introduced into the MIL to generate a heterogeneous catalyst.[11]

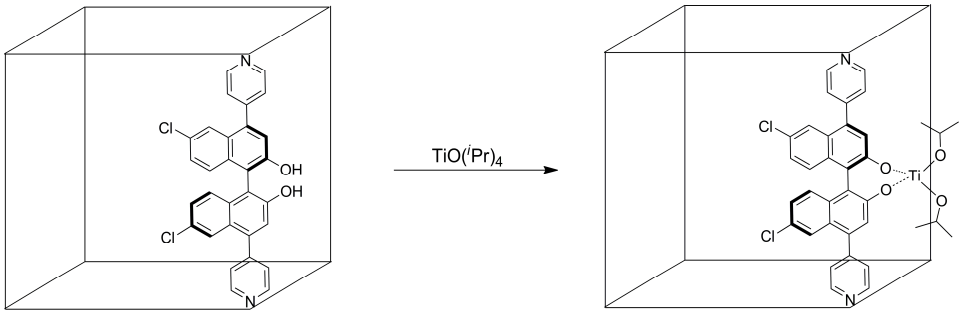

Figure 5-4. Coordinate covalent modification with (R)-6,6'-dichloro-2,2'-dihydroxy-1,1'-binaphthyl-4,4'-bipyridine with Ti(O*i*Pr)$_4$.[10]

The third modification approach involves using both methods in tandem. Synthesizing MOFs with unsaturated metal centers at the SBUs or with metal-binding substituents located on the organic ligand is generally difficult. The SBUs may be coordinately saturated by organic ligands during synthesis. Metal-binding substituents, such as -COOH and –OH, may end up participating in the framework structure. In contrast, a MOF can be covalently modified with a chelating group and subsequently metallated using coordinate covalent modification (Figure 5-1). This approach, termed as covalent and coordinate covalent modification, is advantageous because various combinations of metal chelators (e.g., -OH, -COOH) and metal ions can be introduced to the framework. Very few groups have utilized covalent and coordinate covalent modification as a dual step process. The first example of covalent and coordinate modification was demonstrated by Rosseinsky and coworkers with IRMOF-3 (Figure 5-5). The amino groups of IRMOF-3 were converted into salicylimine chelators with salicylaldehyde, which were metallated with $VO(acac)_2$ to yield IRMOF-3Vsal$_{0.4}$.[25] Rosseinsky and coworkers tested IRMOF-3Vsal$_{0.4}$ as an oxidation catalyst for cyclohexene with *t*BuOOH.[25] Unfortunately, the MOF exhibited low activity and did not appear to be stable.

Hupp and Nguyen *et al.* followed suit by developing a Zn^{2+} paddlewheel MOF (DO-MOF) constructed from 1,2,4,5-tetrakis(4-carboxyphenyl)benzene (TCPB) and DPG (meso-1,2-bis-(4-pyridyl)-1,2-ethanediol) that contained free diol groups.[26] The diol groups of DO-MOF were modified with succinic anhydride, which resulted in the ring opened product with free carboxylic groups that could readily chelate Cu^{2+} ions from a solution of $CuCl_2$ (Figure 5-6). In another report, Yaghi and coworkers modified

UMCM-1-NH_2 with 2-pyridinecarboxyaldehyde and obtained a MOF with iminopyridine moieties that could be metallated with Pd^{2+} ion using [$PdCl_2(CH_3CN)_2$] (Figure 5-7).[27] Both groups demonstrated very nice examples of developing metallated MOFs, but neither group further pursued any applications with their systems.

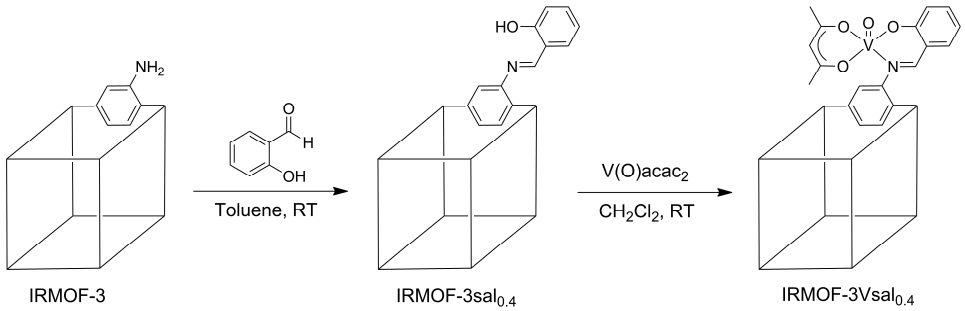

Figure 5-5. Covalent modification of the amino groups of IRMOF-3 with salicylaldehyde, followed by coordinate covalent modification with V(O)$acac_2$.

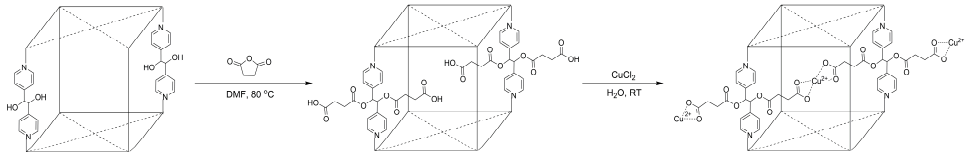

Figure 5-6. Covalent modification of the diol groups of DO-MOF with succinic anhydride, and coordinate covalent modification with $CuCl_2$.

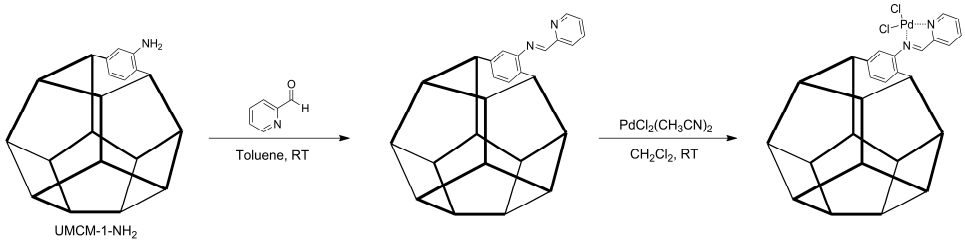

Figure 5-7. Covalent modification of UMCM-1–NH_2 with 2-pyridinecarboxyaldehyde and coordinate covalent modification with $PdCl_2(CH_3CN)_2$.

This chapter focuses on the design of Lewis acid MOF catalysts using covalent and coordinate covalent modification. UMCM-1-NH_2 was modified with two cyclic

anhydrides to generate metal binding sites within the framework, and the two new modified UMCMs were digested and analyzed by ^{1}H NMR. The modified UMCMs were then metallated with metal ions and characterized by TGA, PXRD, atomic absorption (AA) analysis, diffuse reflectance solid-state UV-Vis spectroscopy, and N_2 sorption analysis to determine their metal content and overall stability. The metallated UMCMs were tested as potential Lewis acid catalysts for the Mukaiyama aldol reaction and epoxide ring opening reactions. To confirm their robustness and activity, the UMCM catalysts were recycled several times and examined by PXRD and atomic adsorption (AA) analysis to see if they maintained their structural integrity and metal content.

5.2 Results and Discussion

5.2.1 UMCM-1-AMSal and UMCM-1-AMpz synthesis and characterization

UMCM-1-NH_2 was modified with two different cyclic anhydrides, 2,3-pyrazinedicarboxylic anhydride and 3-hydroxyphthalic anhydride, to produce two new modified MOFs, denoted as UMCM-1-AMpz and UMCM-1-AMsal (Scheme 5-1). To confirm modification occurred, UMCM-1-AMpz and UMCM-1-AMsal were digested and analyzed by ^{1}H NMR, which showed UMCM-1-AMpz was ~50% modified while UMCM-1-AMsal was ~35% modified (Figure 5-8). Both MOFs were examined by TGA and PXRD analysis to determine the overall stability of the modified frameworks. TGA indicated both MOFs remained stable up to ~450 °C and PXRD showed both MOFs maintained their overall bulk crystallinity in comparison with unmodified UMCM-1-NH_2 (Figures 5-9 and 5-10). BET analysis of UMCM-1-AMpz and UMCM-1-AMsal also confirmed microporosity was maintained with surface areas of ~3600 m^2/g.

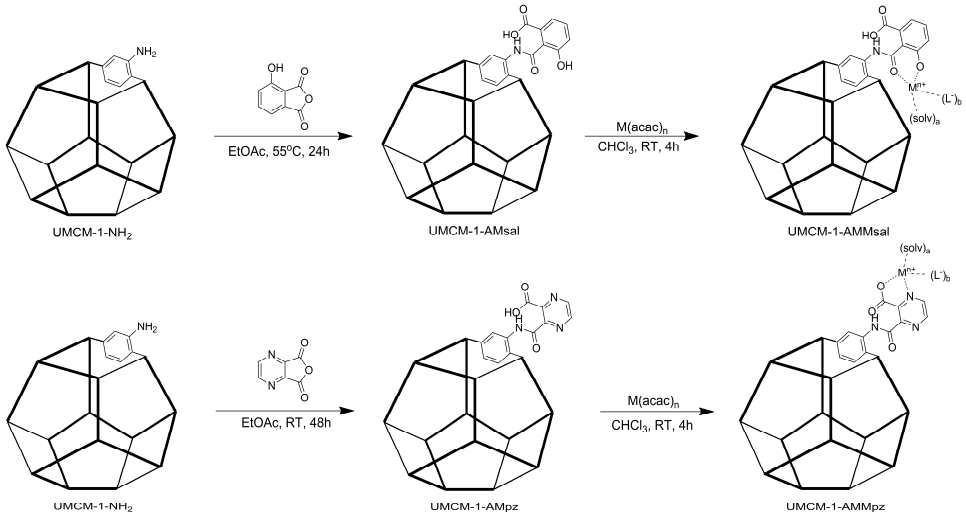

Scheme 5-1. Postsynthetic Modification of UMCM-1-NH_2. UMCM-1-NH_2 is modified with cyclic anhydrides and metallated with metal acetylacetonates (acac, M = Fe^{3+}, Cu^{2+}, In^{3+}) to give UMCM-1-AMMsal (where M = Fe^{3+} or In^{3+}) and UMCM-1-AMMpz (where M = Cu^{2+} or In^{3+}).

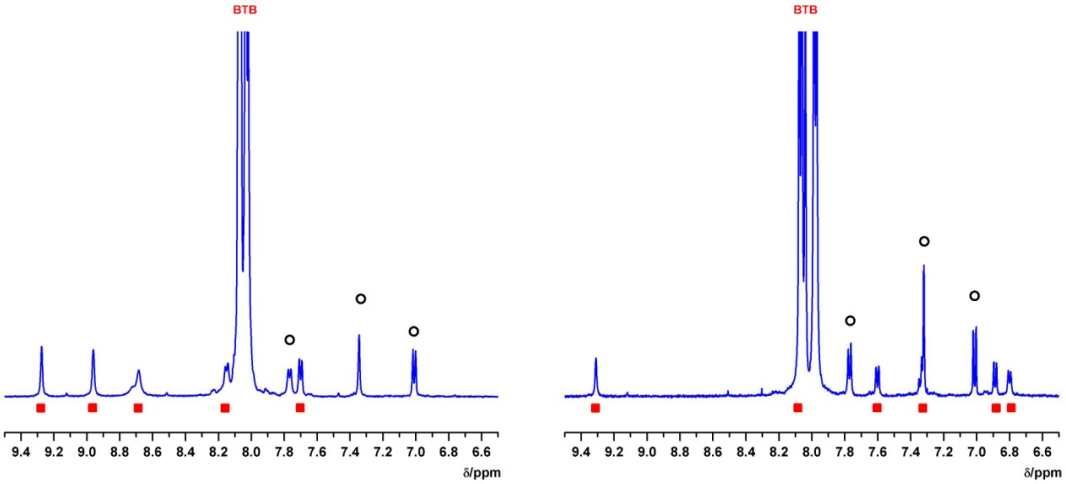

Figure 5-8. ^1H NMR analysis of digested UMCM-1-AMpz (left) and UMCM-1-AMsal (right). Unmodified NH_2-BDC and modified NH_2-BDC are indicated by black circles and red squares, respectively.

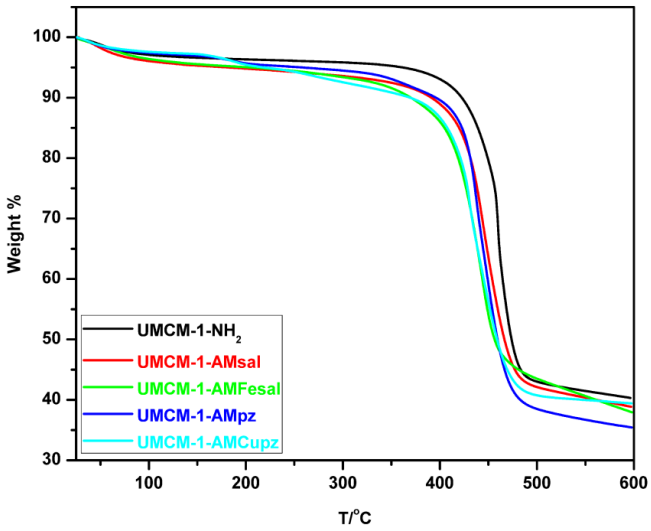

Figure 5-9. TGA traces of unmodified and modified UMCM-1- NH_2.

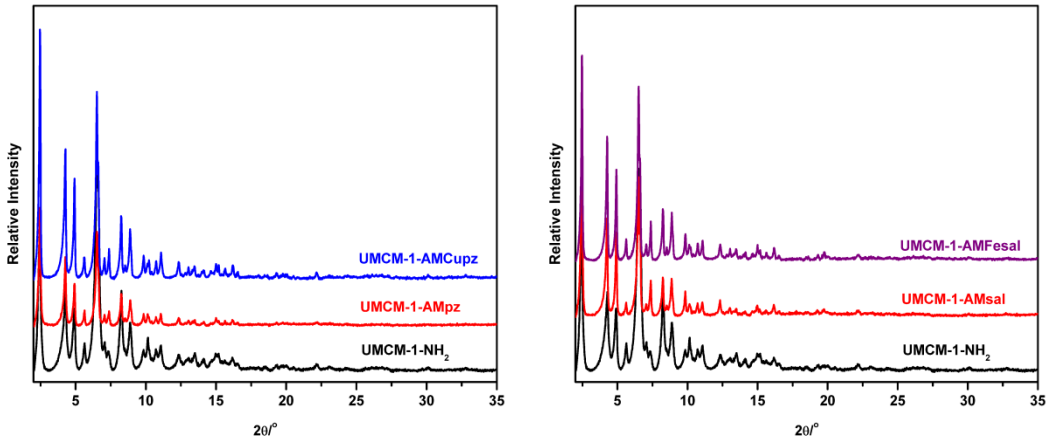

Figure 5-10. PXRD analysis of UMCM-1-NH_2, UMCM-1-AMpz, and UMCM-1-AMCupz (left) and UMCM-1-NH_2, UMCM-1-AMsal, and UMCM-1-Fesal (right).

5.2.2 UMCM-1-AMFesal and UMCM-1-AMCupz synthesis and characterization

Since UMCM-1-AMpz and UMCM-1-AMsal contained metal binding sites, the MOFs were exposed to metal ions. Metal acetylacetonates (e.g., $Fe(acac)_3$ and $Cu(acac)_2$) were selected as the metal source due to their high solubility in $CHCl_3$, and Fe^{3+} and Cu^{2+} were specifically chosen because they exhibit very distinct color changes

in the presence of salicylate and pyrazine moieties, respectively. When UMCM-1-AMpz was subjected to a solution of $Cu(acac)_2$, the pale yellow crystals immediately became blueish-green (Figure 5-11). Similarly, UMCM-1-AMsal, which is also pale yellow, became reddish purple in the presence of $Fe(acac)_3$ (Figure 5-12). TGA and PXRD analysis of UMCM-1-AMCupz and UMCM-1-AMFesal showed no significant changes in thermal or structural stability from their precursors, and BET surface area measurements were found to not change significantly (Table 5-1, Figures 5-13).

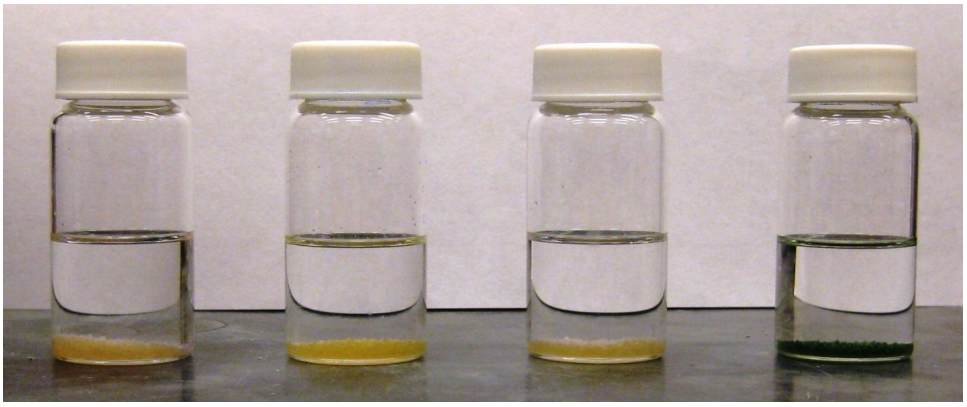

Figure 5-11. From left to right: Photographs of UMCM-1-NH_2 (beige) UMCM-1-AMpz (yellow), UMCM-1-NH_2 treated with $Cu(acac)_2$ (pale yellow) and UMCM-1-Cupz (blueish green).

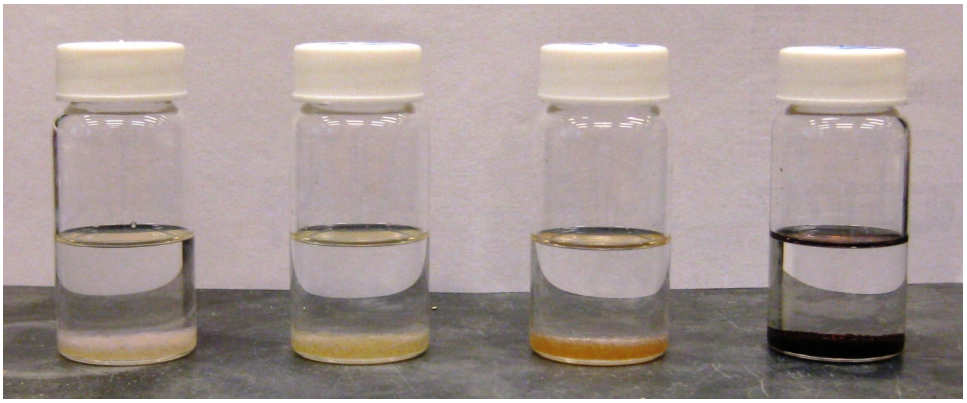

Figure 5-12. From left to right: Photographs of UMCM-1-NH_2 (beige) UMCM-1-AMpz (pale yellow), UMCM-1-NH_2 treated with $Fe(acac)_3$ (pale orange) and UMCM-1-Cupz (reddish purple).

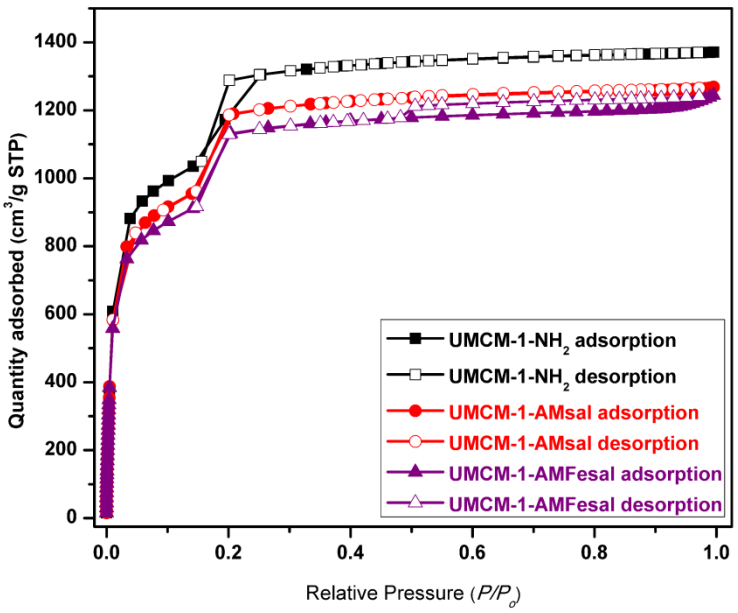

Figure 5-13. N_2 Full isotherm analysis of UMCM-1-NH_2, UMCM-1-AMsal, and UMCM-1-AMFesal at 77 K.

Table 5-1. Brunauer-Emmett-Teller (BET) surface area measurements (m^2/g) under dinitrogen at 77 K. Average values listed were determined from two independent samples.

UMCM-1-	NH_2	AMpz	Cupz	AMsal	AMFesal
BET surface area (m^2/g)	3973	3601	3387	3655	3619

UMCM-1-AMCupz and UMCM-1-AMFesal were further analyzed using diffuse reflectance solid state UV-Vis and atomic absorption (AA) analysis to determine if metal binding was successful. By diffuse reflectance UV-Vis analysis, UMCM-1-AMCupz and UMCM-1-AMFesal showed very distinct absorbances bands at 700 nm and 400 nm, respectively (Figures 5-14 and 5-15). These absorbances were found to be consistent with known Cu-pyrazinecarboxylate[28] and Fe-salicylate[29] compounds. UMCM-1-NH_2, UMCM-1-AMsal, and UMCM-1-AMpz were also examined by diffuse reflectance solid state UV-Vis and showed neglible absorbances above 400 nm. As additional controls,

UMCM-1-NH_2 was treated with either $Fe(acac)_3$ or $Cu(acac)_2$ and was also examined. Visually, UMCM-1-NH_2 underwent a mild color change in the presence of $Cu(acac)_2$ and $Fe(acac)_3$ (Figures 5-11 and 5-12), but did not exhibit any strong absorbances bands above 400 nm. The MOFs exposed to metal acacs were then tested by AA analysis to approximate the metal uptake (Table 5-2). UMCM-1-NH_2 treated with either $Cu(acac)_2$ or $Fe(acac)_3$ contained very low trace amounts of Cu^{2+} and Fe^{3+} at 0.04 wt % and 0.06 wt % on average, respectively. In contrast, UMCM-1-AMCupz was determined to have 1.76 wt% Cu^{2+} and UMCM-1-AMFesal was found to contain 0.77 wt% Fe^{3+}, which corresponds to roughly 50% of the metal binding sites are metallated in both MOF systems. Here, the results indicate the metal species within UMCM-1-AMCupz and UMCM-1-AMFesal are not free metal species and are coordinating to the metal binding sites within the modified frameworks.

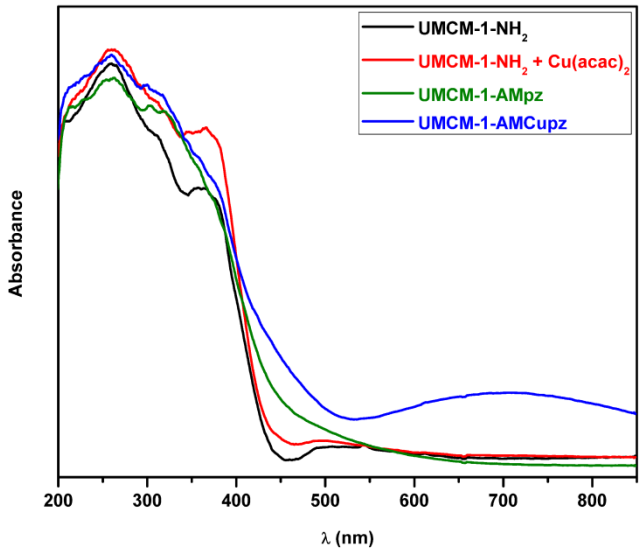

Figure 5-14. Diffuse reflectance solid-state UV-Vis comparison between UMCM-1-NH_2, UMCM-1-NH_2 treated with $Cu(acac)_2$, UMCM-1-AMpz, and UMCM-1-AMCupz.

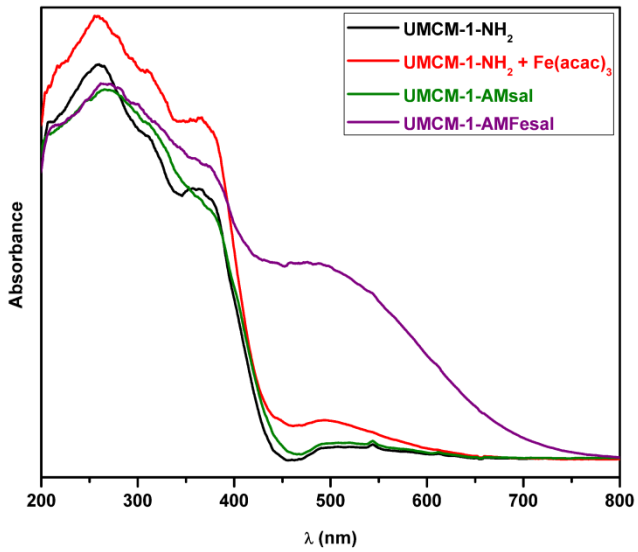

Figure 5-15. Diffuse reflectance solid-state UV-Vis comparison between UMCM-1-NH_2, UMCM-1-NH_2 treated with $Fe(acac)_3$, UMCM-1-AMsal, and UMCM-1-AMFesal.

Table 5-2. AA analysis of metal content in unmodified and modified UMCM-1-NH_2.

MOF[a]	UMCM-1-	NH_2 + Fe^{3+}	AMsal	AMFesal	NH_2 + Cu^{2+}	AMpz	AMCupz
Theoretical[a]	Zn^{2+}	25.26%	23.93%[b]	23.52%[b], [d]	25.26%	23.55%[c],	22.91%[c], [d]
	Cu^{2+}	n.d.	n.d.	n.d.	n.d.	n.d.	2.78%[c], [d]
	Fe^{3+}	n.d.	n.d.	1.76%[b], [d]	n.d.	n.d.	n.d.
Experimental[e]	Zn^{2+}	25.05 ± 0.49%	24.00 ± 0.22%	21.45 ± 0.73%	25.30 ± 0.30%	23.61 ± 0.16%	21.51 ± 0.87%
	Cu^{2+}	n.d.	n.d.	n.d.	0.04%	<0.1%	1.76 ± 0.07%
	Fe^{3+}	0.06 ± 0.03%	<0.1%	0.77 ± 0.04%	n.d.	n.d.	n.d.
Post-catalysis[f], [g]	Zn^{2+}	n.d.	n.d.	20.41 ± 0.80%	n.d.	n.d.	n.d.
	Fe^{3+}	n.d.	n.d.	0.65 ± 0.04%	n.d.	n.d.	n.d.

[a] Determined from f.u. of $Zn_4O(BTB)_{4/3}(L)_{1-x}(L')$; *x* is the conversion, L is NH_2-BDC, and L' is the modified BDC ligand. [b] Based on 35% modification. [c] Based on 50% modification. [d] Assuming all metal binding sites occupied. [e] Three independent samples. [f] Three catalytic cycles. [g] Four independent samples

5.2.3 UMCM-1-AMFesal as a Lewis acid catalyst

Given UMCM-1-NH_2 was successfully modified and metallated with Fe^{3+}, UMCM-1-AMFesal was tested as a potential Lewis acid catalyst for the Mukaiyama aldol reaction. The Mukaiyama aldol reaction involves the carbon-carbon bond formation between an aldehyde and silyl enol and is generally conducted using a Lewis acid catalyst (e.g., $TiCl_4$) under mild conditions (e.g., -78 °C to RT).[30] More importantly, the reaction can be facilitated in CH_2Cl_2, which is a favorable solvent for the UMCM system. As an initial test reaction, UMCM-1-AMFesal, which contains 0.0001 mmol of Fe^{3+}, was suspended in CD_2Cl_2 (or CH_2Cl_2) followed by the addition of aldehyde (mesitaldehyde or 1-naphthaldehyde), and 1-methoxy-2-methyl-1-(trimethylsiloxy)propene (Scheme 5-2). After allowing the reaction to proceed at RT for 24 h, the crude reaction supernatant was analyzed using ^1H NMR (Table 5-3). On average, UMCM-1-AMFesal showed 58% conversion with both aldehydes over three catalytic cycles (Figures 5-16 and 5-17). UMCM-1-AMFesal was found to show higher activity over a Mn^{2+} MOF that been previously tested for the Mukaiyama aldol reaction.[12] UMCM-1-AMFesal had significantly lower catalyst loading (e.g., 0.0001 Fe^{3+} vs. 0.2 mmol Mn^{2+}) and higher activity (24 h vs. 99 h). When UMCM-1-NH_2, UMCM-1-AMsal, and UMCM-1-AMpz were tested under similar conditions, all three MOFs showed little or no reactivity. UMCM-1-NH_2 treated with $Fe(acac)_3$ did show some catalytic activity with 1-naphthaldehyde, but the overall yield was 19% on average and considerably lower than UMCM-1-AMFesal.

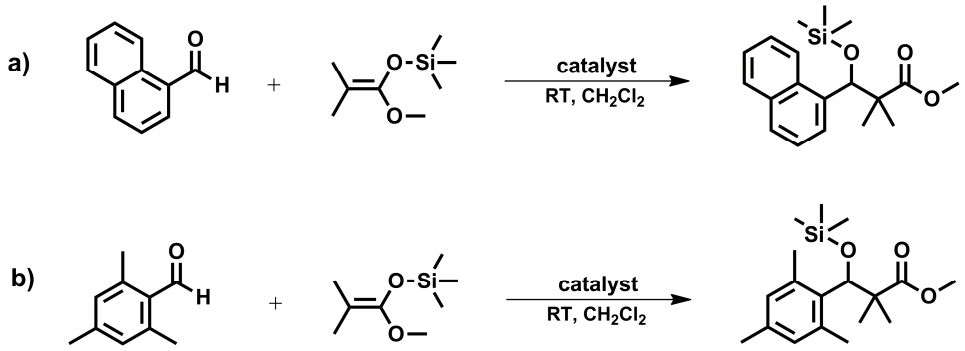

Scheme 5-2. Mukaiyama-aldol reactions with 1-naphthaldehyde (top) and mesitaldehyde (bottom) that were catalyzed by UMCM-1-AMFesal.

Table 5-3. Results from Mukaiyama-aldol reactions with UMCM-1-AMFesal catalyst and control reactions (after 24 h).

Aldehyde	MOF	Cycle 1[a]	Cycle 2[a]	Cycle 3[a]	Overall Average
1-Naphthaldehyde	No MOF	No rxn	n.d.	n.d.	n.d.
	UMCM-1-NH_2	<10%	n.d.	n.d.	n.d.
	UMCM-1-AMsal	<10%	n.d.	n.d.	n.d.
	UMCM-1-NH_2/Fe(acac)$_3$	27%	15%	14%	19 ± 7%
	UMCM-1-AMFesal	70 ± 11%[b]	56 ± 12%[b]	52 ± 12%[b]	58 ± 14%[b]
Mesitaldehyde	No MOF	No rxn	n.d.	n.d.	n.d.
	UMCM-1-NH_2	<5%	n.d.	n.d.	n.d.
	UMCM-1-AMsal	<5%	n.d.	n.d.	n.d.
	UMCM-1-NH_2/Fe(acac)$_3$	<5%	n.d.	n.d.	n.d.
	UMCM-1-AMFesal[c]	53 ± 18%[c]	55 ± 5%[c]	65 ± 8%[c]	58 ± 12%[c]

[a] After 24 h. [b] Based on 4 trials. [c] Based on 3 trials.

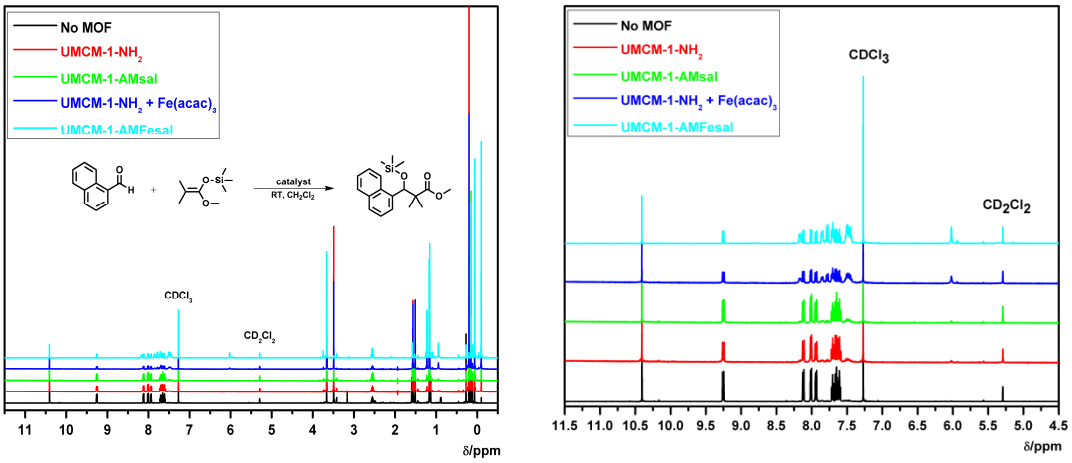

Figure 5-16. ^{1}H NMR spectra of supernatant from the reaction of 1-naphthaldehyde and 1-methoxy-2-methyl-1-(trimethylsiloxy)propene after 24 h at RT without MOF (black) and with UMCM-1-NH_2 (red),UMCM-1-AMsal (green), UMCM-1-NH_2 treated with $Fe(acac)_3$ (blue), or UMCM-1-AMFesal (cyan).

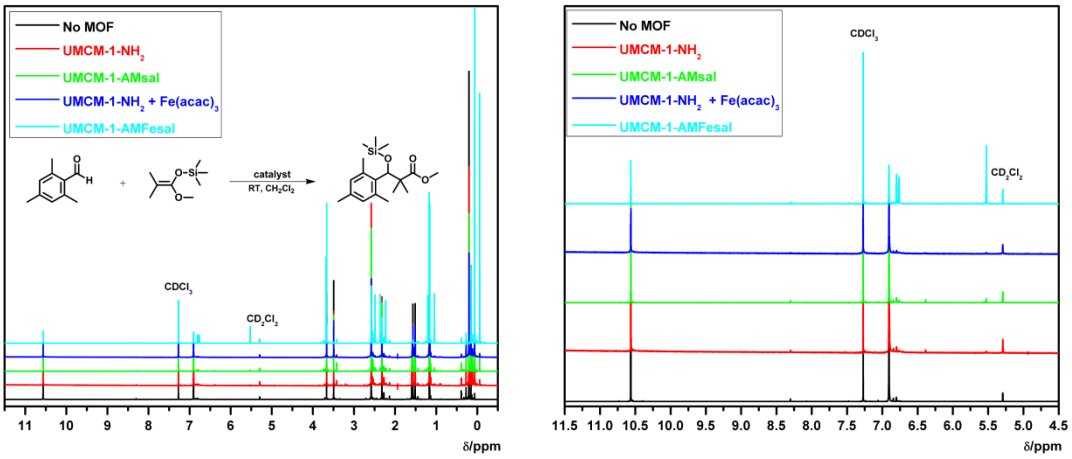

Figure 5-17. ^{1}H NMR spectra of supernatant from the reaction of mesitylaldehyde and 1-methoxy-2-methyl-1-(trimethylsiloxy)propene after 24 h at RT without MOF (black) and with UMCM-1-NH_2 (red), UMCM-1-AMsal (green), UMCM-1-NH_2 treated with $Fe(acac)_3$ (blue), or UMCM-1-AMFesal (cyan).

Several other tests were performed with UMCM-1-AMFesal to pinpoint its catalytic activity and overall stability. Size selectivity studies were performed by switching 1-methoxy-2-methyl-1-(trimethylsiloxy)propene for a larger silyl enol, 1-*tert*-

butylvinyloxy)trimethylsilane, and testing it with 1-napthaldehyde and mesitylaldehyde (Figure 5-18). After 24 h at RT, neither aldehyde underwent carbon-carbon formation with the sily enol. This indicated the silyl enol was too bulky to interact with the aldehydes and confirmed catalysis was indeed taking place within the pores of the framework. Filtration of UMCM-1-AMFesal from the reaction supernatant completely stopped the reaction from proceeding any further, providing additional evidence that UMCM-1-AMFesal was the main catalytic source of the reaction and the catalysis was not being promoted by free soluble species. AA analysis of UMCM-1-AMFesal after 3 catalytic cycles confirmed the former results, showing that the MOF retained 0.65 wt% of Fe^{3+} from its original 0.77 wt% and leached very little Fe^{3+} (Table 5-2). UMCM-1-AMFesal was also found to remain stable, as confirmed by PXRD analysis after 3 catalytic cycles (Figure 5-19).

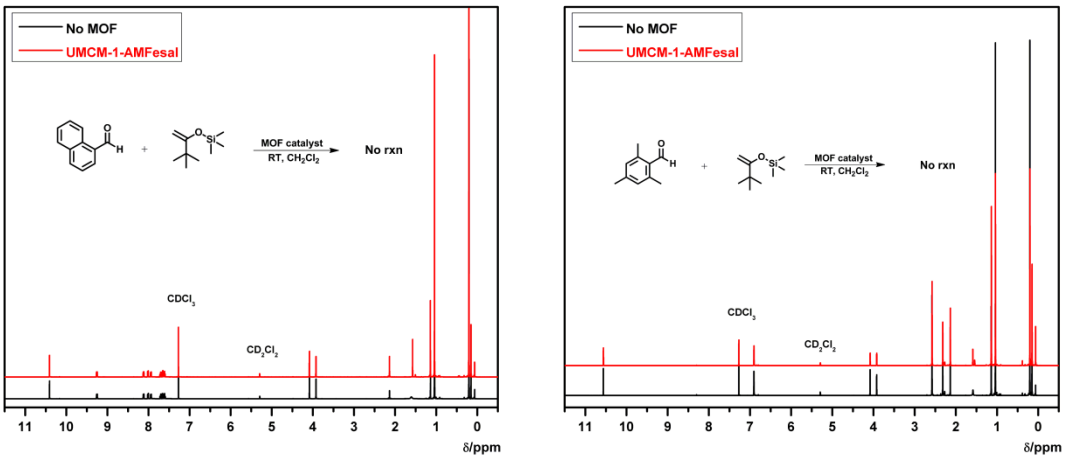

Figure 5-18. ^{1}H NMR spectra of supernatant of 1-naphthaldehyde (top) and mesitaldehyde (bottom) with (1-*tert*-butylvinyloxy)trimethylsilane after 24 h at RT without MOF (black) and with UMCM-1-AMFesal (red). No reaction is observed in either system.

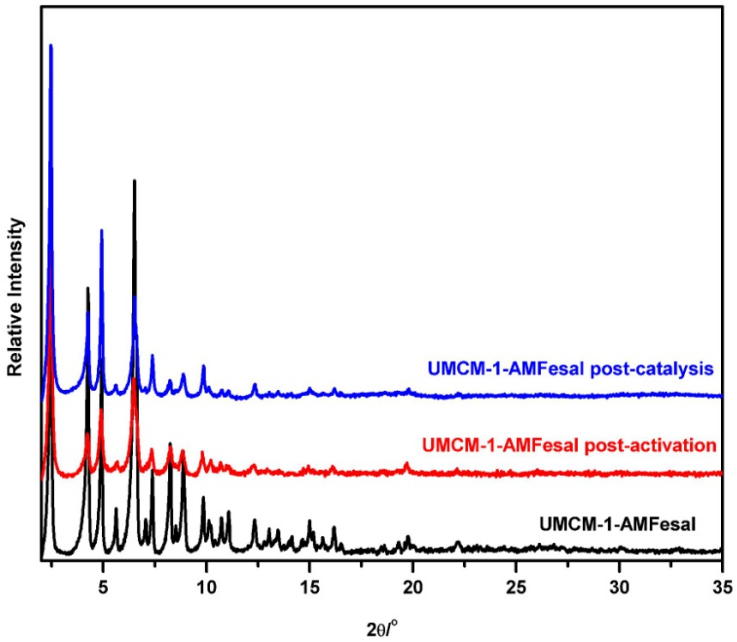

Figure 5-19. PXRD comparisons of UMCM-1-AMFesal pre-activation (black), post-activation (red), and post-catalysis (blue).

5.2.4. Characterization of UMCM-1-AMInpz and UMCM-1-AMInsal

Since UMCM-1-AMFesal showed promising results as a Lewis acid catalyst, additional attempts were made to produce different metallated UMCMs that could be further explored for catalysis. After examining different metal sources, In^{3+} versions of UMCM-1-AMpz and UMCM-1-AMsal were successfully obtained from $In(acac)_3$, resulting in UMCM-1-AMInpz and UMCM-1-AMInsal. AA analysis was used to determine the overall metal binding within UMCM-1-AMInpz and UMCM-1-AMInsal, and with UMCM-1-NH_2 treated with $In(acac)_3$ (Table 5-4). The overall In^{3+} averages for UMCM-1-NH_2 treated with $In(acac)_3$, UMCM-1-AMInpz, and UMCM-1-AMInsal were determined to be 0.5 wt%, 2.96 wt%, and 3.76 wt%. The wt % for UMCM-1-AMInpz and UMCM-1-AMInsal correspond to 70 % of the metal binding sites being metallated with In^{3+}.

Table 5-4. Atomic Absorption (AA) analysis of UMCM-1-NH_2 treated with $In(acac)_3$, UMCM-1-AMInpz, and UMCM-1-AMInsal.

MOF (UMCM-1)	Metal	Theoretical	Experimental
-NH_2 + $In(acac)_3$[a]	Zn^{2+}	25.26	24.30 ± 0.55
	In^{3+}	N/A	0.50 ± 0.28
-AMInpz[b,c]	Zn^{2+}	22.40	21.48 ± 0.77
	In^{3+}	4.92	3.76 ± 0.56
-AMInsal[b,d]	Zn^{2+}	23.09	22.41 ± 0.46
	In^{3+}	3.55	2.96 ± 0.25

[a]Based on three independent samples. [b]Based on six independent samples. [c]Assuming 50% modification. [d]Assuming 35% modification.

TGA and PXRD analysis show no significant structural differences upon In^{3+} binding (Figure 5-20). Single crystal X-ray diffraction data was collected for UMCM-1-AMInpz, which revealed the expected UMCM topology with Zn_4O SBUs coordinated by four BTB and two NH_2-BDC ligands (Figures 5-21 and 5-22).[31,32] The cell parameters were found to be similar to the original UMCM-1-NH_2 structure (space group = $P6_3/m$; $a = b$ = 41.3685 Å, c = 17.5097 Å; α = β= 90°, γ = 120°; V = 25950 $Å^3$). Interestingly, a nitrogen atom was located and assigned on the BDC ligand; however, no electron density was found for the modified pz substituent or for In^{3+}, which is most likely due to incomplete modification of the sites and positional disorder of the modified NH_2-BDC ligand. BET surface areas for UMCM-1-AMInpz and UMCM-1-AMInsal reflected the high uptake of In^{3+}, resulting in lower BETs of ~3200 m^2/g in comparison with UMCM-1-AMCupz and UMCM-1-AMFesal.

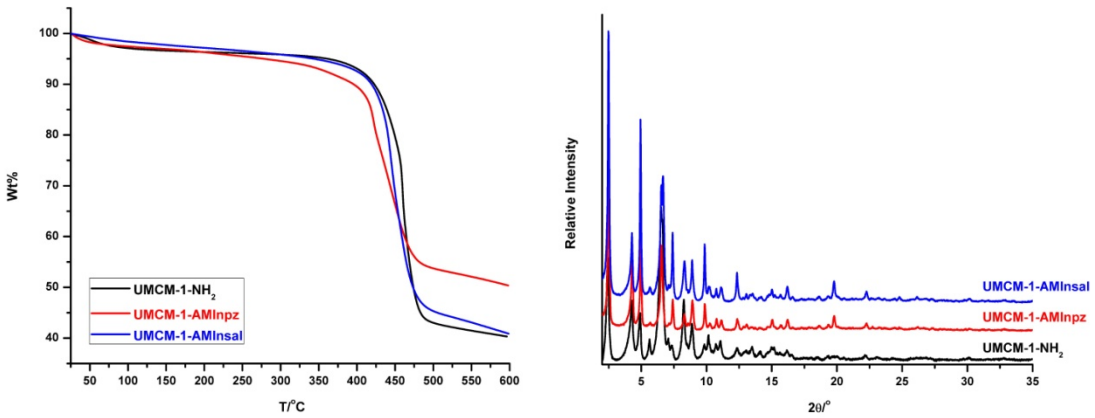

Figure 5-20. TGA trace (left) and PXRD (right) comparison of UMCM-1-NH_2 (black), UMCM-1-AMInpz (red), and UMCM-1-AMInsal (blue).

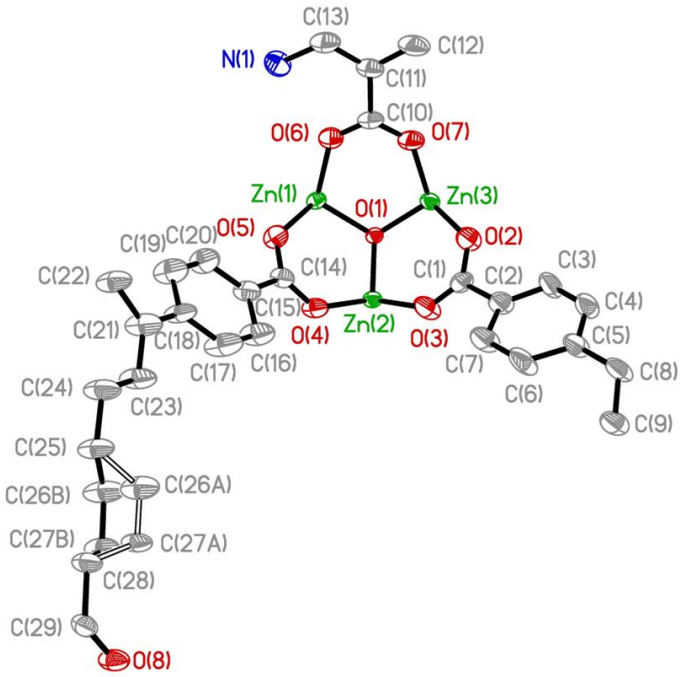

Figure 5-21. Asymmetric unit of UMCM-1-AMInpz with 50% probability ellipsoids and atom numbering scheme.

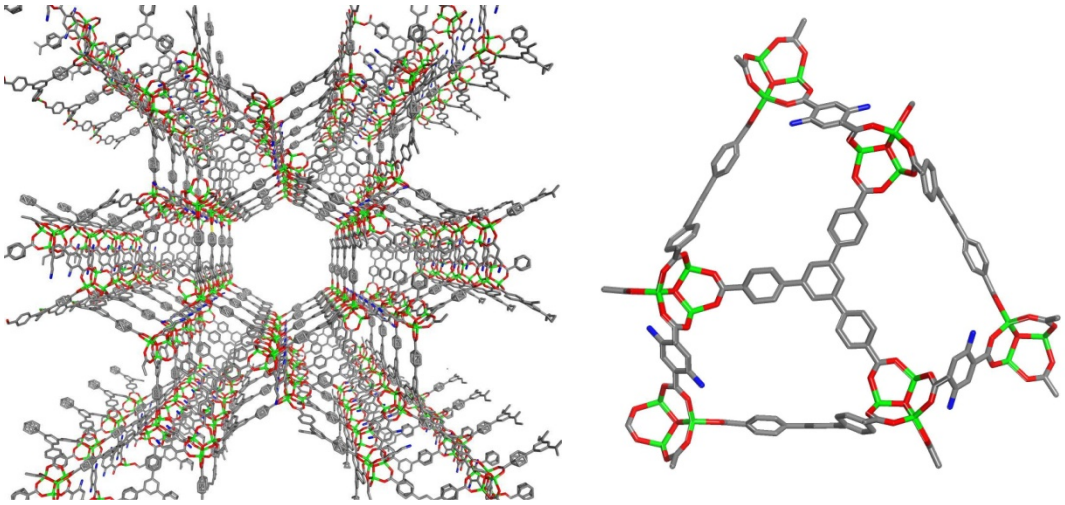

Figure 5-22. UMCM-1-AMInpz single crystal X-ray structure of framework (left) and small pore (right).

5.2.5 Epoxide ring opening catalysis

As a follow-up to the Mukaiyama aldol catalysis study, UMCM-1-AMFesal, UMCM-1-Cupz, UMCM-1-AMInpz, and UMCM-1-AMInsal were examined as potential catalysts for epoxide ring opening reactions. Epoxide ring-opening was targeted for three main reasons: 1) it is an important process for generating stereocontrolled organic intermediates for natural product synthesis[33,34]; 2) it generally involves a Lewis acid catalyst (e.g., metal salen complexes with Cr^{3+}, Co^{2+}, or Mn^{2+})[33,35] and a nucleophile (e.g., thiols, alcohols, aromatic amines) under mild conditions[36,37], which are ideal with a MOF system; and 3) there have not been many reported MOF catalysts for epoxide ring opening, especially those that are robust, have large pores, and are recycable.[38-40]

The general epoxide ring opening conditions involved taking UMCM-1-AMFesal, UMCM-1-AMCupz, UMCM-1-Insal, or UMCM-1-AMInpz, suspending the MOF in $CDCl_3$, adding epoxide and nucleophile, and letting the reaction proceed at RT for 24 h. Afterwards, the crude reaction supernatant was directly analyzed by ^1H NMR to

determine the percent substrate conversion. For this experiment, five epoxides (*cis*-2,3-epoxybutane, cyclopentene oxide, styrene oxide, *cis*- and *trans*-stilbene oxide) and two nucleophiles ($TMSN_3$ and aniline) were examined with each MOF (Schemes 5-3 and 5-4). $TMSN_3$ had never been tested for epoxide ring opening for MOF catalysis. In contrast, aniline had been previously examined with different MOF systems and chosen as a comparison control. UMCM-1-NH_2, UMCM-1-NH_2 treated with $In(acac)_3$, UMCM-1-AMsal, and UMCM-1-AMpz were tested alongside the metallated MOFs to distinguish the catalytic source of the MOFs.

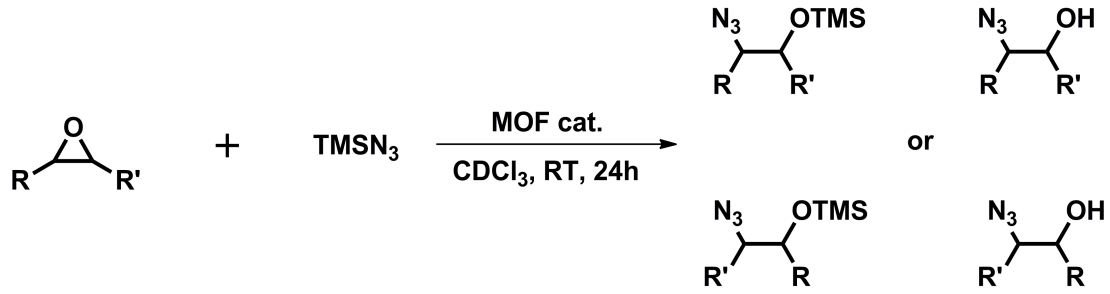

Scheme 5-3. MOF catalyzed epoxide ring opening reactions with $TMSN_3$ as the nucleophile.

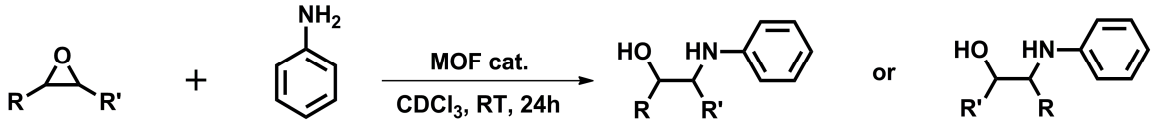

Scheme 5-4. MOF catalyzed epoxide ring opening reactions with aniline as the nucleophile.

cis-2,3-epoxybutane and $TMSN_3$ were examined in the first round of catalysis. *cis*-2,3-epoxybutane has a distinctive multiplet at 3.05 ppm, which is indicative of the *meso* protons, and a doublet at 2.5ppm, which correspond to its methyl groups. After 24 h in the presence of metallated MOF, two new multiplets were observed at 3.6 and 3.8

ppm in addition to a set of new doublets appearing in the upfield region, which corresponded to the ring opened product (Figure 5-23). Interestingly, the product did not match the reported 2-azido-3-(trimethylsilyloxy)butane. A new peak at 2.05 ppm was also present in the crude supernatant spectra that had equivalent integration to the peaks at 3.6 and 3.8 ppm. Closer observation of the product revealed it to be the corresponding β-azido alcohol[36] instead of the TMS protected product, which suggested that in situ deprotection was taking place with the MOF catalyst. UMCM-1-NH_2, UMCM-1-NH_2 treated with $In(acac)_3$, and UMCM-1-AMsal showed very low conversions (< 10%) while UMCM-1-AMInpz had slightly higher yields at ~16% (Figure 4-49). All metallated MOFs catalyzed the reaction between *cis*-2,3-epoxybutane and $TMSN_3$, but with varying turnovers. UMCM-1-AMInpz had the highest conversion at 78%, followed by UMCM-1-AMInsal at 56%, UMCM-1-AMFesal at 30%, and UMCM-1-AMCupz at 11% (Figure 5-24).

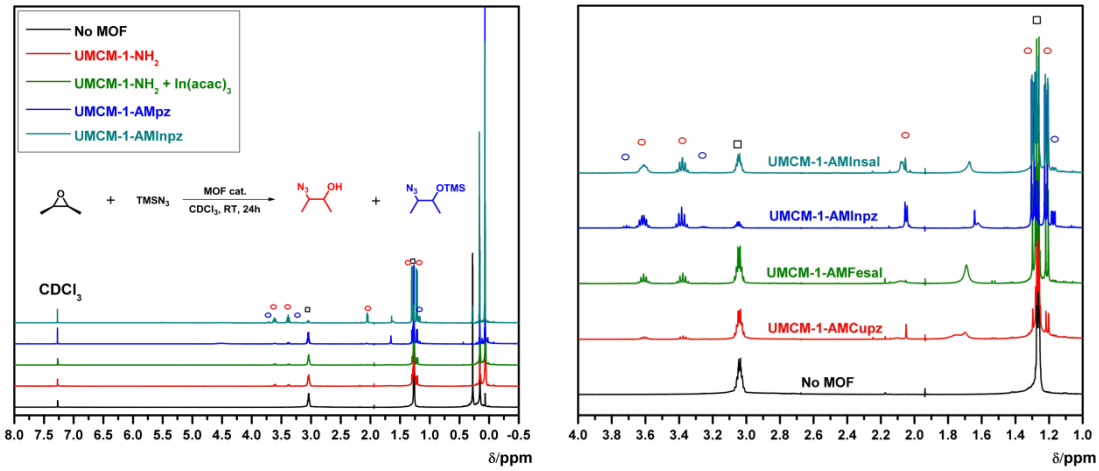

Figure 5-23. No MOF (black), UMCM-1-NH_2 (red), UMCM-1-NH_2 + $In(acac)_3$ (green), UMCM-1-AMpz (blue), and UMCM-1-AMInpz (cyan). Unreacted epoxide is indicated. by black squares, alcohol product is indicated by red circles, and TMS protected product is indicated by blue circles.

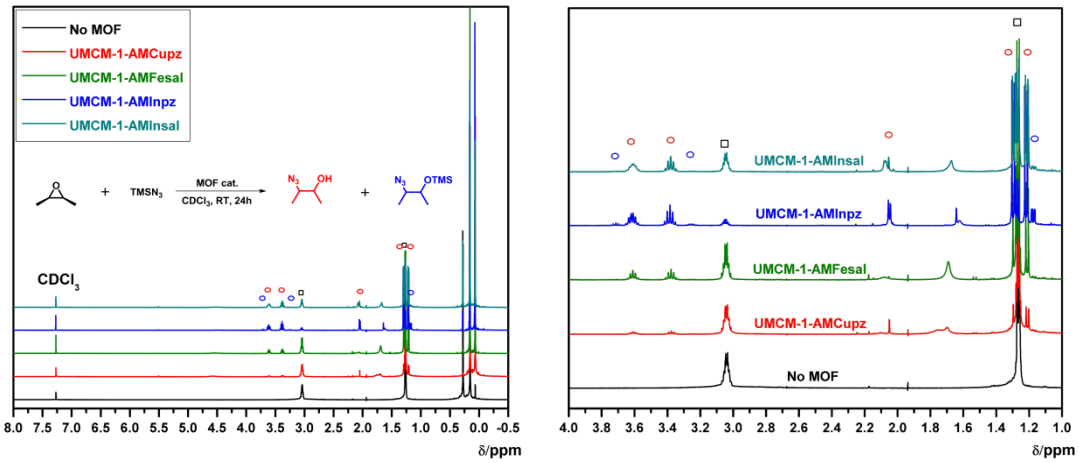

Figure 5-24. ^{1}H NMR supernatant comparison between metallated MOF catalysts with epoxide and $TMSN_3$. Epoxide starting material is indicated by black squares, alcohol product is indicated by red circles, and TMS protected product is indicated by blue circles.

In the second round of the catalysis, $TMSN_3$ was switched with aniline as the nucleophile. The MOFs were treated similarly as the $TMSN_3$ experiment and the reaction supernatants were analyzed after allowing the reaction to go for 24 h at RT. By ^{1}H NMR, two new multiplets appeared at 3.8 and 4.7 ppm along with a new broad peak at 2.6 ppm corresponding to the alcohol group (Figure 5-25). These peaks were found to correlate with the reported β-amino alcohol spectra.[41] UMCM-1-NH_2, UMCM-1-NH_2 treated with $In(acac)_3$, UMCM-1-AMpz, and UMCM-1-AMsal showed little or no reactivity (Figure 5-25). After testing all the metallated MOFs with aniline, UMCM-1-AMInsal turned out to have the highest catalytic activity with 86% conversion. UMCM-1-AMFesal and UMCM-1-AMInpz both had similar conversions at 34% and 30%, respectively, and UMCM-1-AMCupz did not show any activity (Figure 5-26).

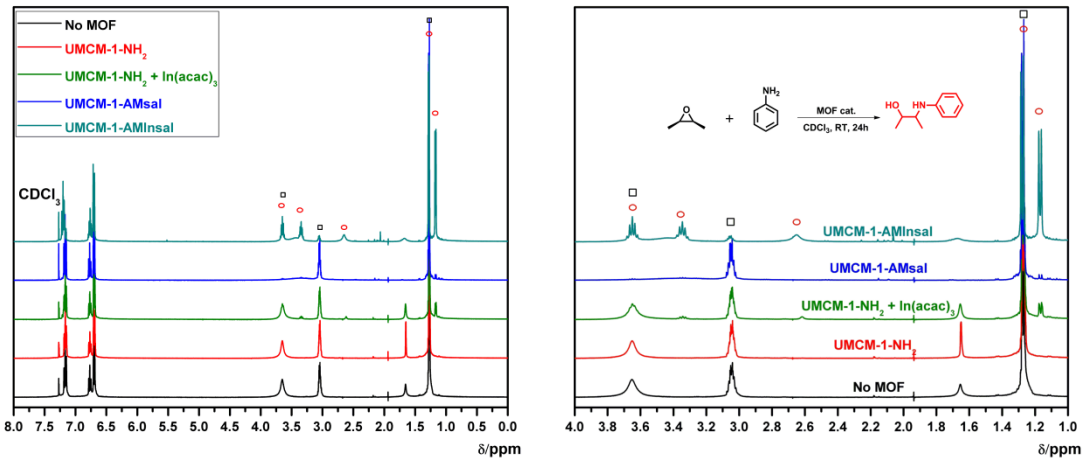

Figure 5-25. No MOF (black), UMCM-1-NH_2 (red), UMCM-1-NH_2 + In(acac)$_3$ (green), UMCM-1-AMsal (blue), and UMCM-1-AMInsal (cyan). Epoxide starting material is indicated by black squares, and the product is indicated by red circles.

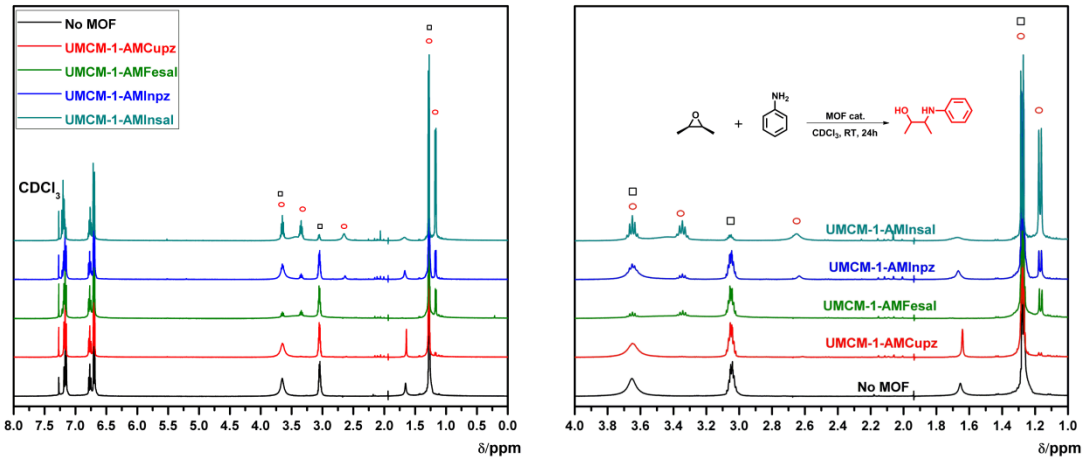

Figure 5-26. ^{1}H NMR supernatant comparison between metallated MOF catalysts with epoxide and aniline. Epoxide starting material is indicated by black squares, and the product is indicated by red circles.

5.2.6 Stability of UMCM-1-AMInpz and UMCM-1-AMInsal

Overall, UMCM-1-AMInpz and UMCM-1-AMInsal were found to be the most active catalysts out of the four metallated MOFs, but for different ring-opening reactions. UMCM-1-AMInpz was highly active for the reaction with $TMSN_3$ while UMCM-1-

AMInsal showed a preference with aniline as the nucleophile. Several tests were performed with UMCM-1-AMInpz and UMCM-1-AMInsal to determine their overall chemical stability postcatalysis. Both MOFs were used for 3 catalytic cycles, with *cis*-2,3-epoxybutane and their respective nucleophiles, and showed no changes in overall reactivity. UMCM-1-AMInpz maintained 76% conversion over three cycles, while UMCM-1-AMInsal gave 82% conversion (Table 5-5). PXRD analysis of both MOFs postcatalysis revealed they maintained their overall structural integrity, and AA analysis showed the MOFs leached < 10% of In^{3+} after three catalytic cycles (Table 5-6, Figure 5-27). To further prove the MOFs were stable and the minimal In^{3+} leaching had no effect on catalyst, UMCM-1-AMInpz or UMCM-1-AMInsal were removed from the reaction supernatant after 6h. Removal of either catalyst completely stopped the reaction, which was confirmed by ^{1}H NMR analysis after completion of the 24h reaction period, thereby justifying the MOFs remained robust and the epoxide ring opening reactions could only proceed if catalyst was present (Table 5-7, Figures 5-28 and 5-29). Additional control tests were performed with $In(acac)_3$ as the catalyst. Despite using 10 mol % catalyst, no catalytic activity was seen, therefore showing $In(acac)_3$ itself had poor catalytic activity for epoxide ring opening.

Table 5-5. Recycling experiment with UMCM-1-AMInpz and UMCM-1-AMInsal. All values are the result of three independent samples.

Cycle	1	2	3	Average
Inpz	76 ± 9	75 ± 5	76 ± 5	76 ± 6
Insal	85 ± 7	83 ± 3	79 ± 3	82 ± 4

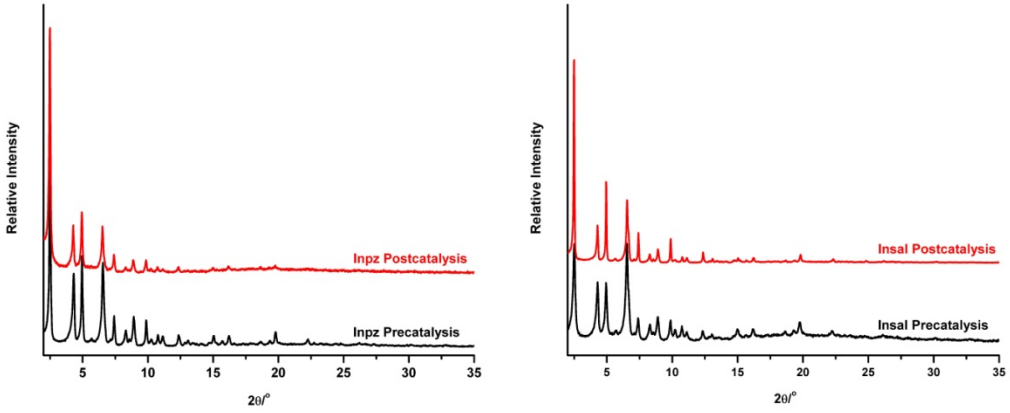

Figure 5-27. PXRD comparison of UMCM-1-AMInpz (left) and UMCM-1-AMInsal (right) before and after 3 catalytic cycles.

Table 5-6. AA analysis of Inpz and Insal before and after 3 catalytic cycles. All values are the result of three independent samples.

MOF	Metal	Precatalysis	Postcatalysis
Inpz	Zn^{2+}	20.97 ± 0.75	20.59 ± 0.59
	In^{3+}	3.33 ± 0.17	3.13 ± 0.19
Insal	Zn^{2+}	22.19 ± 0.21	20.64 ± 0.42
	In^{3+}	3.01 ± 0.01	2.93 ± 0.05

Table 5-7. Leaching experiment with UMCM-1-AMInpz and UMCM-1-AMInsal. Two reaction setups (denoted as A and B) were prepared using the same batch of MOF catalyst. The supernatant of Vial A analyzed after 6 h at RT while Vial B was left undisturbed. Both Vial A and Vial B were then examined by ^{1}H NMR after 24 h from the initial starting time.

Time	UMCM-1-AMInpz	UMCM-1-AMInsal
6h	47%	57%
24h	47%	57%
24h straight	83%	90%

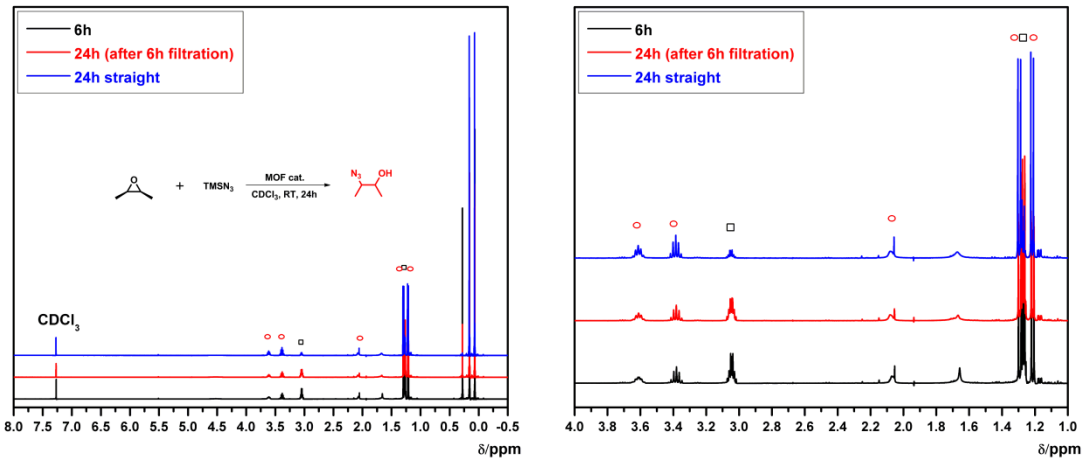

Figure 5-28. Filtration test with UMCM-1-AMInpz at 6 h and 24 h. Epoxide starting material is indicated by black squares and product is indicated by red circles.

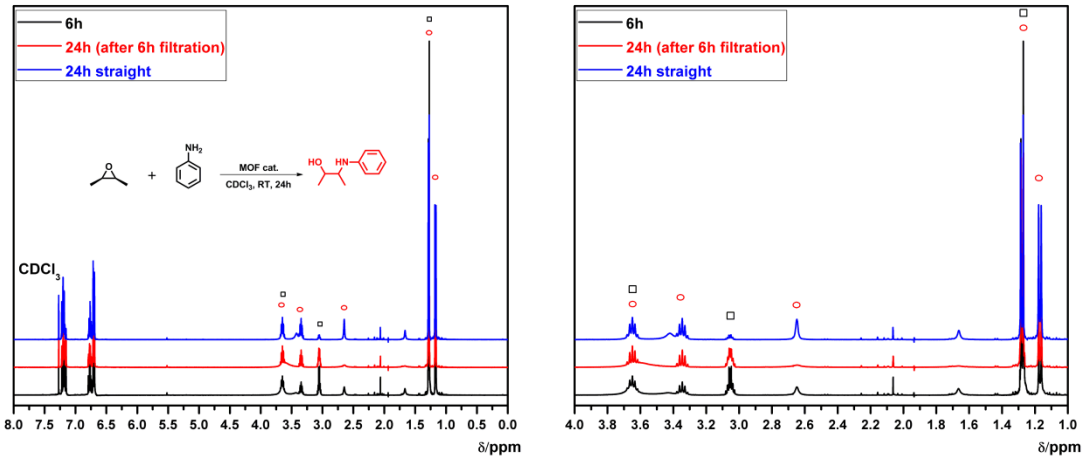

Figure 5-29. Filtration test with UMCM-1-AMInsal at 6 h and 24 h. Epoxide starting material is indicated by black squares and product is indicated by red circles.

5.2.7 Size selectivity - epoxides

The metallated MOFs were tested with other epoxides of various sizes and shapes using the same conditions for *cis*-2,3-epoxybutane. Overall, UMCM-1-AMInpz had the highest conversions with $TMSN_3$ as the nucleophile while UMCM-1-AMInsal dominated with aniline as the nucleophile (Tables 5-8 and 5-9). For $TMSN_3$ and cyclopentene,

UMCM-1-AMInpz had the highest conversion of 53%, followed by UMCM-1-AMInsal with 43%, UMCM-1-AMFesal with 26%, and UMCM-1-AMCupz with < 5% (Figure 5-30). With $TMSN_3$ and styrene oxide, UMCM-1-AMInpz showed 70% and was followed by UMCM-1-AMInsal and UMCM-1-AMFesal with ~53% (Figure 5-31). Surprisingly, UMCM-1-AMCupz had a high conversion of 32%, but the MOF controls also had unexpectedly high conversions up to 40%. The results, though, still indicate the metallated MOFs (e.g., UMCM-1-AMInpz) have the highest activity on average.

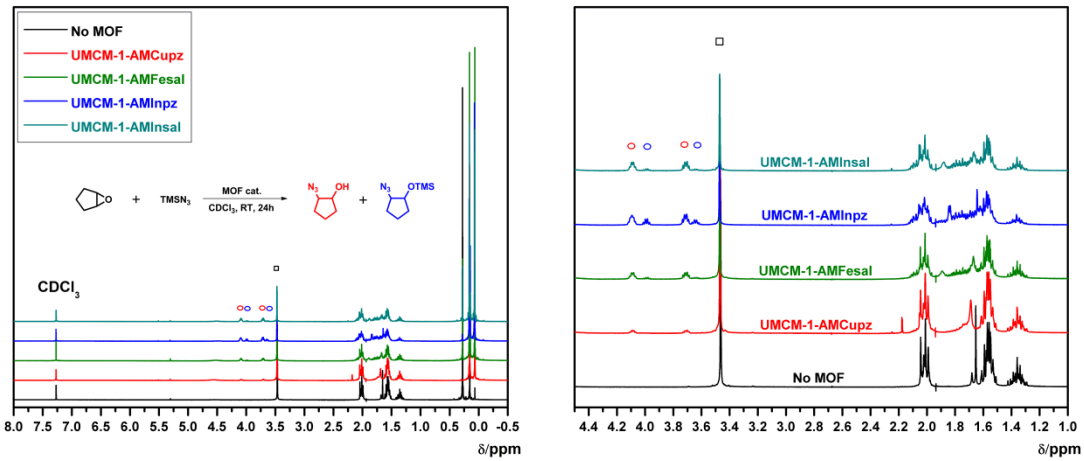

Figure 5-30. ^1H NMR supernatant comparisons of cyclopentene oxide and $TMSN_3$ with all metallated MOFs. Unreacted epoxide is indicated by black squares, alcohol product is indicated by red circles, and TMS protected product is indicated by blue circles.

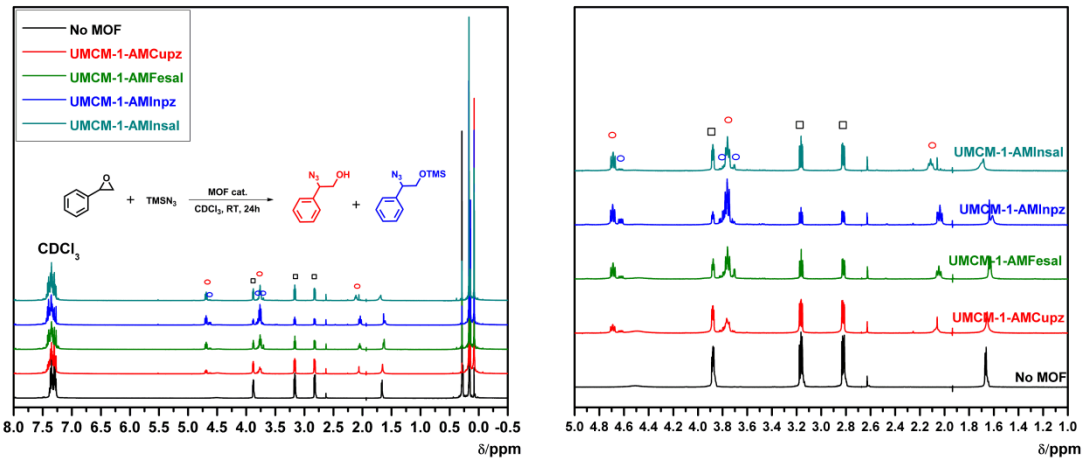

Figure 5-31. ^{1}H NMR supernatant comparisons of styrene oxide and $TMSN_3$ with metallated MOFs. Unreacted epoxide is indicated by black squares, alcohol product is indicated by red circles, and TMS protected product is indicated by blue circles.

Similar results were observed when $TMSN_3$ was switched with aniline. UMCM-1-AMInsal had the highest activity with cyclopentene and aniline at 58% (Figure 5-32). UMCM-1-AMInpz and UMCM-1-AMFesal had percent conversions of ~20% while UMCM-1-AMCupz and the other controls showed < 5% activity. When cyclopentene was switched to styrene oxide, all the MOFs showed an increase in activity (Figure 5-33). UMCM-1-AMCupz and the control MOFs had conversions as high as ~20%; however, the other metallated MOFs still had higher activity (43% for UMCM-1-AMFesal and 49% for UMCM-1-AMInpz). Interestingly, UMCM-1-AMInsal was a very good catalyst for the reaction between styrene oxide and aniline and resulted in the formation of 2 products. The major product was determined to be 2-phenylamino-2-phenylethanol and the minor was identified as the bis-alkylated product, 2,2'(phenylazanediyl)bis(2-phenylethanol).[42-44] The identity of both products was confirmed by ^{1}H and ^{13}C NMR, and high resolution mass spectrometry. By increasing the ratio of aniline to styrene from

1:1 to 4:1, the 2-phenylamino-2-phenylethanol was obtained at ~90% yield. Alternatively, increasing the ratio of styrene to aniline to 2:1 increased production of 2,2'-(phenylazanediyl)bis(2-phenylethanol). *cis*- and *trans*-stilbene oxide were also examined with all the MOFs. The yields were noticeably reduced due to the size and sterics of the stilbene oxides. With $TMSN_3$ as the nucleophile, UMCM- 1-AMInpz had 48% conversion while UMCM-1-AMInsal, UMCM-1-AMFesal, and UMCM-1-AMCupz had 17%, 9%, and 4%, respectively (Table 5-8). When $TMSN_3$ was switched with aniline, only UMCM-1-AMInsal showed any significant activity at 6%. Upon changing the epoxide to *trans*-stilbene oxide, the activity was completely shut down for all the metallated MOFs, and all the control MOFs showed little or no activity regardless of the stilibene oxide and nucleophile combination (Table 5-9).

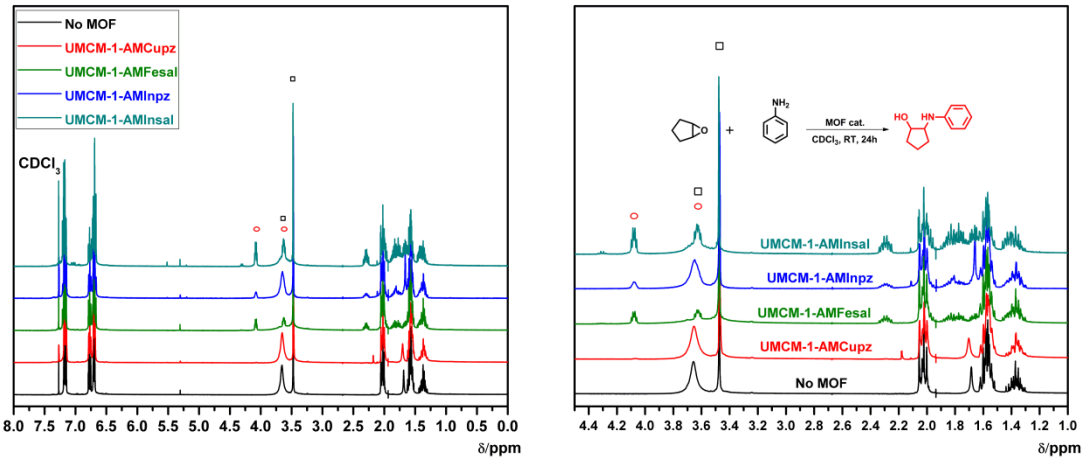

Figure 5-32. ^1H NMR supernatant comparisons of cyclopentene oxide and aniline with metallated MOFs. Unreacted epoxide is indicated by black squares and alcohol product is indicated by red circles.

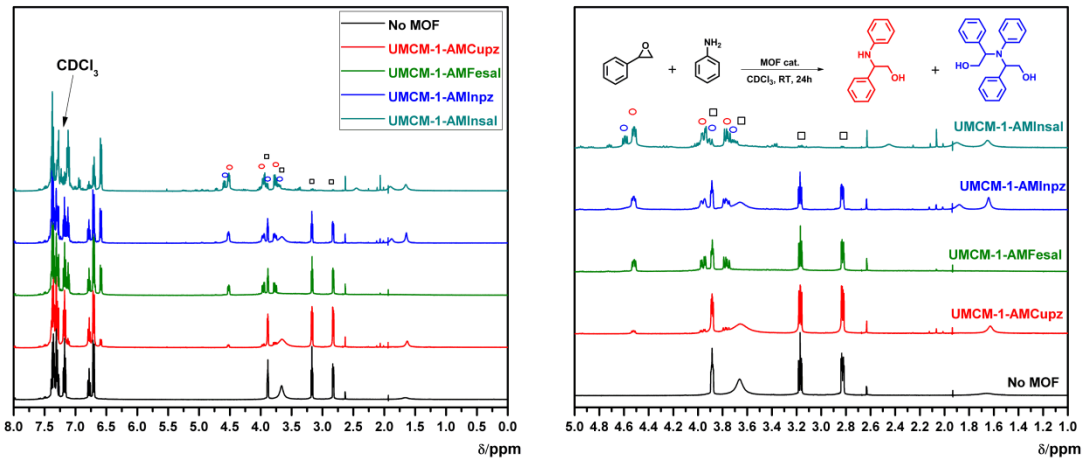

Figure 5-33. ^{1}H NMR supernatant comparisons of styrene oxide and aniline with metallated MOFs. Unreacted epoxide is indicated by black squares and alcohol product is indicated by red circles.

Table 5-8. Percent conversions of MOF catalyzed reactions between different epoxides and $TMSN_3$. All values are the result of three independent experiments.

Epoxide		No MOF	UMCM-1-NH_2	UMCM-1-NH_2 + In^{3+}	UMCM-1-AMpz	UMCM-1-AMsal	UMCM-1-AMInpz	UMCM-1-AMInsal	UMCM-1-AMCupz	UMCM-1-AMFesal
R	R'									
Me	Me	No rxn	8 ± 6	10 ± 4	16 ± 7	7 ± 4	78 ± 9[a]	56 ± 2[a]	11 ± 5	35 ± 14[a]
-$(CH_2)_3$-		No rxn	2 ± 1	4 ± 3	4 ± 2	5 ± 4	53 ± 3[a]	43 ± 5[a]	3 ± 4	26 ± 3
H	Ph	No rxn	19 ± 8	27 ± 7	41 ± 9	19 ± 11	70 ± 2	54 ± 6	32 ± 7	53 ± 1
Ph	Ph[b]	No rxn	2 ± 2	1 ± 1	1 ± 1	3 ± 1	48 ± 8	17 ± 10	4 ± 2	9 ± 2
Ph	Ph[c]	No rxn	No rxn	No rxn	No rxn	No rxn	No rxn	No rxn	No rxn	No rxn

[a]Based on four independent trials. [b]Cis [c]Trans

Table 5-9. Percent conversions of MOF catalyzed reactions between different epoxides and aniline. All values are the result of three independent experiments.

Epoxide		No MOF	UMCM-1-NH_2	UMCM-1-NH_2 + In^{3+}	UMCM-1-AMpz	UMCM-1-AMsal	UMCM-1-AMInpz	UMCM-1-AMInsal	UMCM-1-AMCupz	UMCM-1-AMFesal
R	R'									
Me	Me	No rxn	No rxn	9 ± 7	8 ± 6	13 ± 2	30 ± 7	86 ± 11	1 ± 2	34 ± 6
-$(CH_2)_3$-		No rxn	No rxn	1 ± 1	2 ± 2	1 ± 1	20 ± 7	58 ± 12	No rxn	22 ±8
H	Ph	No rxn	5 ± 4	14 ± 3	20 ± 1	12	49 ± 1	~99	16 ± 1	43 ± 1
Ph	Ph[b]	No rxn	No rxn	No rxn	No rxn	No rxn	No rxn	6 ± 2	No rxn	No rxn
Ph	Ph[c]	No rxn	No rxn	No rxn[a]	No rxn[a]	No rxn	No rxn[a]	No rxn	No rxn[a]	No rxn

[a]Based on two independent experiments. [b]Cis [c]Trans

5.2.8 Size selectivity – aniline derivatives

Different aniline derivatives were also examined with the metallated MOFs, in particular with UMCM-1-AMInsal. UMCM-1-AMInsal readily catalyzed the reaction between *cis*-2,3-epoxybutane and aniline up to 78%. As a starting point, UMCM-1-AMInsal was tested with *cis*-2,3-epoxybutane and different aniline derivatives (aniline, 2-methylaniline, 2,6-dimethylaniline) under similar reaction conditions. After 24 h at RT, all three aniline derivatives were found to give moderate percent conversions at 86%, 93%, and 56% for aniline, 2-methylaniline, and 2,6-dimethylaniline, respectively (Figure 5-34). Given all three anilines were turned over despite their size differences, UMCM-1 AMInsal appeared to be relatively tolerant of derivatized nucleophiles.

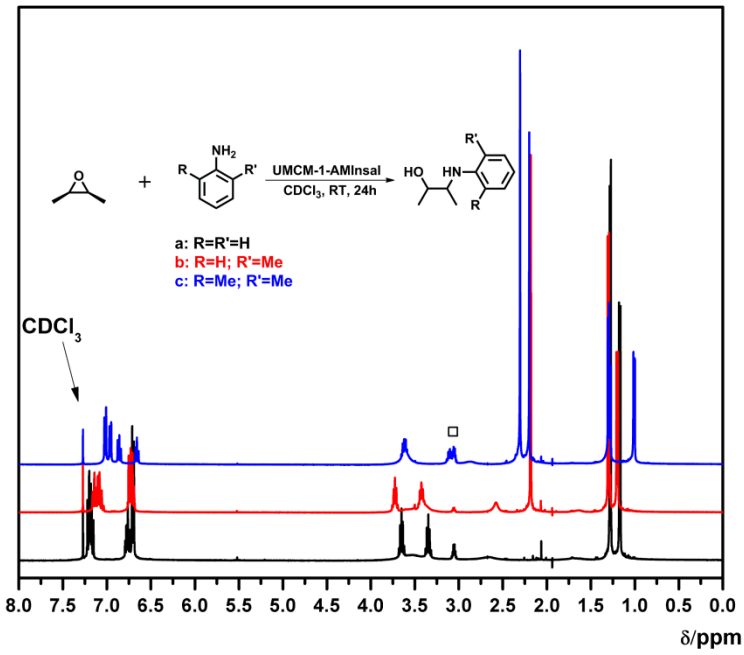

Figure 5-34. ^{1}H NMR comparison between *cis*-2,3-epoxybutane and aniline derivatives (aniline, 2-methylaniline, or 2,6-dimethylaniline). Unreacted *cis*-2,3-epoxybutane is indicated by the black square.

5.2.9 Catalytic selectivity of UMCM-1-AMInpz and UMCM-1-AMInsal

Overall, UMCM-1-AMInpz and UMCM-1-Insal had the highest activity for epoxide ring opening, but showed specificity with certain nucleophiles. UMCM-1-AMInpz proved to be a better catalytic with $TMSN_3$ while UMCM-1-AMInsal exhibited higher catalytic activity with aniline as the nucleophile. This trend was consistent regardless of the epoxide. On a molecular level, both MOFs have similar In^{3+} loadings and the same topology, but it appears the metal binding groups, pyrazinedicarboxylate vs. salicylate, as well as the type of metal ion (Fe^{3+} vs. Cu^{2+} vs. In^{3+}) has a significant influence on the catalytic activity of the MOF. Previous studies with UMCM-1-NH_2 indicated that the efficiency of PSM is influenced by a combination of both pore and

reagent size/shape. The metal-ligand combination seems to play a major role in epoxide ring opening catalysis. The results obtained here show that catalysis can be similarly affected. The orientation and accessibility of the catalytic site is dependent on how the metal-ligand unit fits within the pore based on the size and shape of the chelating ligand, the metal ion coordination geometry, and the size and shape of the pore. The position of the catalytic site can affect how the substrates (e.g., epoxide and nucleophiles) interact with the catalytic site and with each other. Catalytic activity can also be affected by the orientation and accessibility of the catalytic sites (e.g., metal-ligand combinations) within the framework. For example, UMCM-1-AMInpz and UMCM-1-AMInsal were good catalysts for these epoxide ring opening reactions, but UMCM-1-AMCupz and UMCM-1-AMFesal had the opposite outcome.

Interesting selectivity was observed amongst the metallated MOFs when *cis*- and *trans*-stilbene oxide was used. *cis*-stilbene oxide was readily turnover with $TMSN_3$ as the nucleophile, but *trans*-stilbene oxide was completely shut out. To rule out the possibility *trans*-stilbene oxide might be poisoning the catalyst, UMCM-1-AMInpz and UMCM-1-AMInsal were recycled after being used for the *trans*-stilbene oxide reaction and were shown to still be competent for the reaction between *cis*-2,3-epoxybutane and both nucleophiles ($TMSN_3$ with UMCM-1-AMInpz and aniline with UMCM-1-AMInsal). Based on these results, the shape of the stilbene oxides appears to influence its interactions with the catalytic sites within the MOFs. More specifically, *cis*-stilbene oxide seems to interact more favorably with the MOF catalytic sites over *trans*-stilbene oxide, especially with UMCM-1-AMInpz. UMCM has two types of pores: a large hexagonal pore and a smaller pore. Based on the crystal structure of UMCM-1-AMInpz

the catalytic site can exist in either the hexagonal or smaller pore. Given *cis* and *trans* have different conformations, their structural differences may affect how it can interact with the catalytic site. While trans-stilbene may be able to access the interior of the MOF, it may be (a) sterically unable to interact with the metal site, or it (b) can interact with the metal site, but is in an orientation that makes nucleophilic attack unfavorable.

To test this theory, a known homogeneous catalyst (Cr(salen)Cl) was tested with the stilbene oxides. In one report, Cr(salen)Cl was found to catalyze ring opening of *cis*- and *trans*-stilbene oxide with aniline up to 90% conversion.[41,45] Cr(salen)Cl was used as a catalyst for *cis*-and *trans*-stilbene oxide with either $TMSN_3$ or aniline. Under similar reaction conditions adapted from the MOF catalyst experiment, Cr(salen)Cl was found to turnover both stilbene oxides with either nucleophile. With $TMSN_3$, *cis*- and *trans*-stilbene oxide gave yields of 94% and 68%, respectively. Changing $TMSN_3$ to aniline resulted in conversions of 43% for *cis*-stilbene oxide and 60% for *trans*-stilbene oxide. UMCM-1-AMInpz and Cr(salen)Cl were then studied side by side to see how they compared as catalysts for stilbene oxide. $CDCl_3$ solutions were prepared with 1:1 ratios of *cis*- and *trans*-stilbene oxide with $TMSN_3$ as the nueclophile. *cis*- and *trans*-stilbene oxide have distinct proton shifts at 4.38 ppm and 3.89 ppm, respectively, which allows for easy monitoring. As expected, Cr(salen)Cl readily catalyzed the conversion of both *cis*- and *trans*-stilbene (Figure 5-35), but UMCM-1-AMInpz only catalyzed the ring-opening of *cis*-stilbene oxide (Figure 5-36). As an additional experiment, a 1:1 ratio of *cis*- and *trans*-2,3-epoxybutane were prepared and tested with both catalysts. With Cr(salen)Cl, both *cis* and *trans* were ~99% converted. In the UMCM-1-AMInpz system, both epoxides were catalyzed, but *cis* was ~90% converted while only 20% of *trans* was

reacted. Based on these results, the UMCM-1-AMInpz catalyst shows unique, stereochemistry-based substrate selectivity due to its metal-ligand combination.

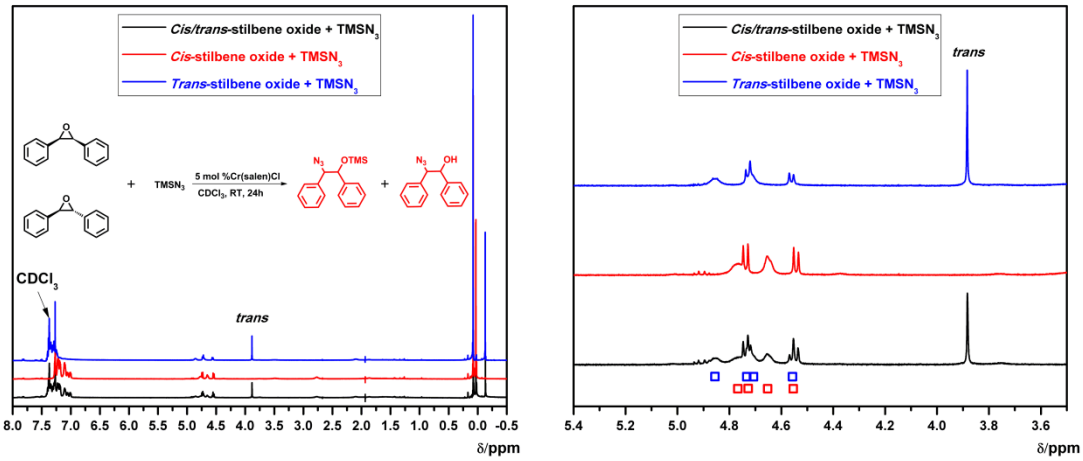

Figure 5-35. ^{1}H NMR of 1:1 mixture *cis*/*trans*-stilbene oxide and $TMSN_3$ with Cr(salen)Cl as the catalyst. The peaks are slightly broadened due to the presence of Cr^{3+}. *cis*-stilbene oxide was ~99% converted to a mixture of TMS azido and β-azido alcohol products (red squares). *trans*-stilbene oxide was ~70% converted to a mixture of TMS azido and β-azido alcohol products (blue squares).

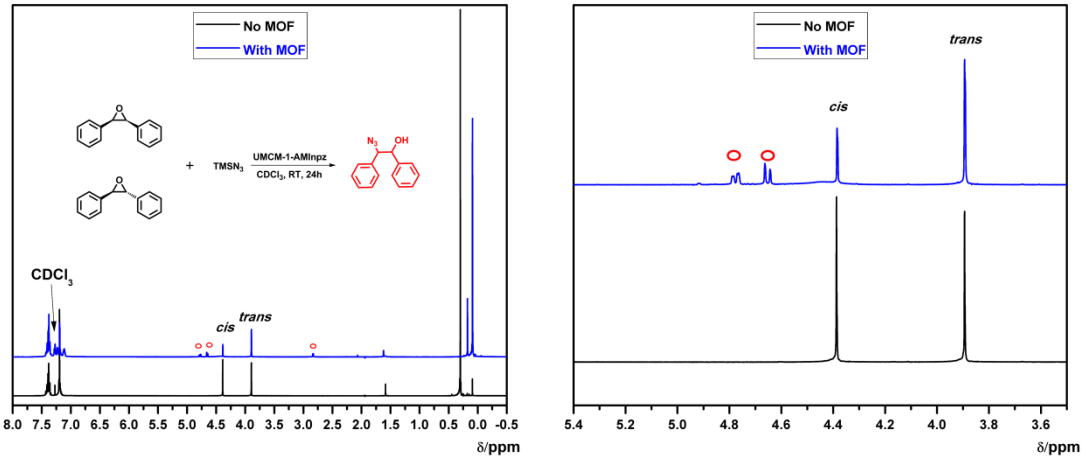

Figure 5-36. ^{1}H NMR of 1:1 mixture *cis*:*trans*-stilbene oxide and $TMSN_3$ before and after addition of UMCM-1-AMInpz.

5.3 Conclusions

UMCM-1-NH_2 was modified with two types of metal binding groups (pyrazinedicarboxylate and salicylate) and metallated with three metal ions (Fe^{3+}, Cu^{2+}, and In^{3+}) resulting in four single site MOF catalysts. All four MOF catalysts remained isostructural to one another and had similar thermal stabilities; however, the MOFs displayed different catalytic activity based on their metal ion and organic ligand combination. UMCM-1-AMFesal was an active, robust catalyst for the Mukaiyama aldol reaction while UMCM-1-AMInpz and UMCM-1-AMInsal were found to be very active catalysts for epoxide ring opening. UMCM-1-AMInpz and UMCM-1-AMInsal displayed unique substrate selectivity in comparison with homogeneous catalysts due to their different pore environments. This highlights the advantages of using PSM to decorate the MOF pores with specific functionalities (e.g., metal and ligand combinations) to enhance their selectivity and activity. Lastly, all MOF catalysts underwent three catalytic cycles without degradation, as confirmed by PXRD and AA analysis. These catalytic results represent the first systematic study of designing Lewis acid MOF catalysts through covalent and coordinate covalent modification.

5.4 Experimental Section

General methods. Starting materials and solvents were purchased and used without further purification from commercial suppliers (Sigma-Aldrich, Alfa Aesar, EMD, TCI, Cambridge Isotope Laboratories, Inc., and others). Methylene chloride was dried using molecular sieves. Samples were submitted to Robertson Microlit Laboratories for atomic absorption (AA) analysis. IRMOF-3, DMOF-1-NH_2, and

UMCM-1-NH_2 were synthesized and activated as described previously.[32,46] Formation of the corresponding TMS protected, β-azido alcohol, and β-amino alcohol products were confirmed by comparison with reported literature spectra.[36,41,43,44,47-50]

UMCM-1-AMsal. UMCM-1-NH_2 (ca. 56 mg, 0.05 mmol equiv of -NH_2) was combined with 2 mL of a 0.05 M solution of 3-hydroxyphthalic anhydride in EtOAc and transferred to a 55 °C oven. After 24h, the supernatant was decanted and the crystals were washed with EtOAc (3 x 10mL). After the last wash, 10 mL of $CHCl_3$ was added to the vial and the crystals were left to soak overnight. The crystals were washed with $CHCl_3$ (3 x 10 mL) and soaked in $CHCl_3$ overnight for an additional 2 days. Following the last overnight soak, the crystals were immediately used for metallation. Yield: 35±2% (based on three independent samples).

UMCM-1-AMFesal. $Fe(acac)_3$ (18 mg, 0.05 mmol) was added to a vial of UMCM-1-AMsal in 2 mL of $CHCl_3$. Within minutes, the crystals became a dark purple red. After 4 h at RT, the supernatant was decanted and the crystals were profusely washed with $CHCl_3$ (5 x 10 mL minimum). The crystals were soaked in 10 mL of $CHCl_3$ overnight and the process was repeated for a minimum of 3 days or until the supernatant was colorless. The crystals were stored in the final $CHCl_3$ wash.

UMCM-1-AMpz. UMCM-1-NH_2 (ca. 56 mg, 0.05 mmol equiv of -NH_2) was combined with 4 mL of a 0.006 M solution of 2,3-pyrazinedicarboxylic anhydride in EtOAc. After 24 h at RT, the supernatant was decanted and the crystals were washed with EtOAc (3 x 10 mL). An additional 4 mL of anhydride solution was added back to the vial and the reaction was left at RT for another 24 h. At the end of day 2, the supernatant was decanted and the crystals were washed with EtOAc (3 x 10mL). After

the last wash, 10 mL of $CHCl_3$ was added to the vial and the crystals were left to soak overnight. The crystals were washed with $CHCl_3$ (3 x 10 mL) and soaked in $CHCl_3$ overnight for an additional 2 days. The crystals were stored in the final $CHCl_3$ wash until metallation. Yield: 49±1% (based on three independent samples).

UMCM-1-AMCupz. $Cu(acac)_2$ (13 mg, 0.05 mmol) was added to a vial of UMCM-1-AMpz in 2 mL of $CHCl_3$. Within minutes, the crystals became bluish green. After 4 h at RT, the supernatant was decanted and the crystals were washed profusely with $CHCl_3$ (5 x 10 mL minimum). The crystals were soaked in 10 mL of $CHCl_3$ and the process was repeated for a minimum of 3 days or until the supernatant was colorless. The crystals were stored in the final $CHCl_3$ wash.

UMCM-1-AMInpz and UMCM-1-AMInsal. $In(acac)_3$ (21 mg, 0.05 mmol) was added to a vial of either UMCM_1-AMpz or UMCM-1-AMsal in 2 mL of $CHCl_3$. The mixture was left to stand at room temperature (RT) for 4 h. After 4 h at RT, the supernatant was decanted and the crystals were washed profusely with $CHCl_3$ (4 x 10 mL minimum). The crystals were soaked in 10 mL of $CHCl_3$ and the process was repeated for a minimum of 3 days. The crystals were stored in the final $CHCl_3$ wash.

UMCM-1-NH_2 treated with $Fe(acac)_3$, $Cu(acac)_2$, or $In(acac)_3$. Metal sources ($Fe(acac)_3$ or $Cu(acac)_2$, 0.05 mmol) were added to UMCM-1-NH_2 (ca. 56 mg, 0.05 mmol equiv of -NH_2) in 2 mL of $CHCl_3$. After 4 h at RT, the supernatant was decanted and the crystals were washed profusely with $CHCl_3$ (5 x 10 mL minimum). The crystals were soaked in 10 mL of $CHCl_3$ overnight and the process was repeated for a total of 3 days or until the supernatant was colorless. The crystals were stored in the final $CHCl_3$ wash.

Digestion and Analysis by ^{1}H NMR. ^{1}H NMR spectra were recorded on a Jeol 500 or Varian FT-NMR spectrometer (400 MHz). Approximately 5 mg of modified UMCM-1-NH_2 material was dried under vacuum at RT and digested with sonication in 500 µL of DMSO-d^6 and 100 µL of dilute DCl (23 µL of 35% DCl in D_2O diluted with 1.0 mL of DMSO-d^6).

PXRD Analysis. Approximately 15 mg of modified UMCM-1-NH_2 (typically soaked in $CHCl_3$) was air dried before PXRD analysis. Powder X-ray diffraction (PXRD) data were collected at ambient temperature on a Bruker D8 Advance diffractometer at 40 kV, 40 mA for Cu Kα (λ = 1.5418 Å), with a scan speed of 5 or 10 sec/step, a step size of 0.02° in 2θ, and a 2θ range of 2-35°. The experimental backgrounds were corrected using the Jade 5.0 software package.

Thermal Analysis. Approximately 10-20 mg of MOF sample was used for TGA measurements. Samples were analyzed under a stream of dinitrogen using a TA Instrument Q600 SDT running from room temperature to 600 °C with a scan rate of 5 °C/min.

BET Surface Area Analysis. Approximately 40-60 mg of modified UMCM-1-NH_2 (stored in $CHCl_3$) was evacuated on a vacuum line for 2 h at RT. The sample was then transferred to a preweighed sample tube and degassed at 25 °C on an Micromeritics ASAP 2020 Adsorption Analyzer for a minimum of 12 h or until the outgas rate was <5 µmHg. The sample tube was re-weighed to obtain a consistent mass for the degassed MOF sample. BET surface area (m^2/g) measurements were collected at 77 K with dinitrogen on an Micromeritics ASAP 2020 Adsorption Analyzer using volumetric technique.

Solid State UV-Vis analysis. Approximately 15-20 mg of modified UMCM-1-NH_2 (typically soaked in $CHCl_3$) was air dried before UV-Vis analysis. Solid state spectra were collected using an StellarNet EPP2000C spectrometer with a diffuse reflectance probe.

Activation of UMCM-1-NH_2, UMCM-1-NH_2 treated with $Fe(acac)_3$, and UMCM-1-AMsal for the Mukaiyama aldol reaction. UMCM-1-NH_2 and UMCM-1-NH_2 treated with $Fe(acac)_3$ were dried under vacuum at 90 °C for 4-5 h. Both samples were used immediately afterwards. UMCM-1-AMsal was dried at RT for 4-5 h.

Activation of UMCM-1-AMFesal. UMCM-1-AMFesal was dried under vacuum at 90 °C for 1-2 h. 10 mL of $CHCl_3$ was immediately added to the crystals. The crystals were washed 3x with $CHCl_3$ before being soaked in 10 mL of $CHCl_3$ overnight. After soaking the crystals overnight, the supernatant was decanted and the crystals were washed an additional 3x with $CHCl_3$ before being dried under vacuum again. The process was repeated for a total of three times. The crystals were dried one more time under vacuum at 90 °C for 4-5 h and used immediately afterwards.

Mukaiyama aldol reaction. Dried modified UMCM-1-NH_2 (15 mg) was transferred to a 4 mL dram vial and 1 mL of CH_2Cl_2 (or CD_2Cl_2) was added. 1-Methoxy-2-methyl-1-(trimethylsiloxy)propene (0.2 mmol) and aldehyde (0.1 mmol) were subsequently added and the contents of the vial were lightly agitated to ensure thorough mixing. The vials were left at RT for 24 h. 50μL (or 100μL if CD_2Cl_2) of the supernatant was diluted in 500 μL of $CDCl_3$ and analyzed by ^1H NMR. The supernatant was decanted from the catalyst and the catalyst was washed with $CHCl_3$ (3 x 3 mL) before being soaked in pure $CHCl_3$ (3 mL) overnight. The supernatant was decanted the

following morning and the catalyst was washed 3 times before being left in pure $CHCl_3$ until needed.

Epoxide ring opening catalysis with MOFs. UMCM-1-NH_2, UMCM-1-NH_2 treated with $In(acac)_3$, UMCM-1-AMCupz, UMCM-1-AMInpz, and UMCM-1-AMInsal were dried under vacuum at 90 °C for 4-5 h. UMCM-1-AMpz and UMCM-1-AMsal were dried at room temperature for 4-5 h. UMCM-1-AMFesal was activated as previously reported.[51] Dried MOF samples (15 mg, 0.014 mmol based on -NH_2) were placed into 4 mL dram vials. The MOF was immersed in 1 mL of $CDCl_3$, followed by epoxide (0.1 mmol), and $TMSN_3$ (0.1 mmol) or aniline (0.1 mmol). The reaction mixture was left standing at room temperature for 24 h and the supernatant was analyzed by ^1H NMR.

Recycling Experiment with UMCM-1-AMInpz and UMCM-1-AMInsal. UMCM-1-AMInpz or UMCM-1-AMInsal (15 mg, 0.014 mmol based on -NH_2), *cis*-2,3-epoxybutane (0.1 mmol), nucleophile ($TMSN_3$ for UMCM-1-AMInpz, aniline for UMCM-1-AMInsal, 0.1 mmol), were placed in a 4 mL dram vial with 1 mL $CDCl_3$ for 24 h at RT. The reaction supernatant was directly analyzed by ^1H NMR without further purification. The MOF catalyst was washed with $CHCl_3$ (3x 3 mL) and left to soak in fresh $CHCl_3$ overnight. After washing the catalyst with $CHCl_3$ again (3x 3 mL), the catalyst was dried at 90 °C under vacuum for 1-2h and then reused.

Leaching experiment with UMCM-1-AMInpz and UMCM-1-AMINsal. UMCM-1-AMInpz or UMCM-1-AMINsal (15 mg each, 0.014 mmol based on –NH_2). *cis*-2,3-epoxybutane (0.1 mmol), nucleophile ($TMSN_3$ for UMCM-1-AMInpz, aniline for UMCM-1-AMInsal, 0.1 mmol), were placed in a 4mL dram vial with 1 mL $CDCl_3$ for 24

h at RT. Two reaction setups (denoted as A and B) were prepared using the same batch of MOF catalyst. The supernatant of Vial A was removed and filtered through sand and a glass wool plug after 6 h at RT. The reaction supernatant was directly analyzed by ^{1}H NMR without further purification and stored at RT. Vial B was left undisturbed. Both Vial A and Vial B were then examined by ^{1}H NMR after 24 h from the initial starting time.

Epoxide ring opening catalysis with UMCM-1-Insal and aniline derivatives. UMCM-1-AMInsal (15 mg, 0.014 mmol based on -NH_2), *cis*-2,3-epoxybutane (0.1 mmol), and nucleophile (aniline, 2-methylaniline, or 2,6-dimethylaniline, 0.1 mmol) were placed in a 4 mL dram vial with 1 mL $CDCl_3$ at RT for 24 h. The reaction supernatant was directly analyzed by ^{1}H NMR without further purification.

In(acac)$_3$ Control Reactions. In(acac)$_3$ (23 mg, 0.056 mmol) was dissolved in 4 mL of $CDCl_3$ followed by the addition of ligand (3-hydroxyphthalic anhydride, 2,3-pyrazinedicarboxylic anhydride, or salicylamide, 0.042 mmol). The mixture was sonicated for 15 min and was left to sit overnight. A portion (1 mL) of the $CDCl_3$ solution was transferred to a 4 mL dram vial followed by *cis*-2,3-epoxybutane (0.1mmol) and nucleophile ($TMSN_3$ or aniline, 0.1 mmol). The reaction mixture was left standing at room temperature for 24 h and the supernatant was analyzed by ^{1}H NMR.

Epoxide ring opening catalysis with Cr(salen)Cl. The experiments described were adapted from a literature procedure.[45] *Cis* or *trans*-stilbene oxide (0.1 mmol) and 5 mol % (*R*,*R*)-*N*,*N'*-bis(3,5-di-*tert*-butylsalicylidene)-1,2-cyclohexanediaminochromium(III) chloride (Cr(salen)Cl) were dissolved in 50 µL of $CDCl_3$ in a 4 mL dram vial. $TMSN_3$ or aniline (0.1 mmol) was added and the vials were

placed on a shaker for 24 h at room temperature. The reaction mixture was directly analyzed by ^{1}H NMR without further purification.

Epoxide ring opening catalysis with Cr(salen)Cl and 1:1 cis/trans-stilbene oxide. A 1:1 mixture of *cis*/*trans*-stilbene oxide (0.05 mmol each) and 5 mol % (*R*,*R*)-*N*,*N*'-bis(3,5-di-*tert*-butylsalicylidene)-1,2-cyclohexanediaminochromium(III) chloride (Cr(salen)Cl) were dissolved in 50 µL of $CDCl_3$ in a 4 mL dram vial. $TMSN_3$ or aniline (0.1 mmol) was added and the vials were placed on a shaker for 24 h at room temperature. The reaction mixture was directly analyzed by ^{1}H NMR without further purification.

Epoxide ring opening catalysis with UMCM-1-AMInpz and 1:1 mixture of cis/trans-stilbene oxide. UMCM-1-AMInpz (15 mg, 0.014 mmol based on -NH_2), *cis*/*trans*-stilbene oxide (0.05 mmol each), and $TMSN_3$ (0.1 mmol) were placed in a 4 ML dram vial with 1 mL $CDCl_3$ for 24 h at RT. The reaction supernatant was directly analyzed by ^{1}H NMR without further purification.

5.5 Acknowledgements

Text, schemes, and figures in this chapter, in part, are reprints of the materials published in the following papers: Tanabe, K. K., Cohen, S. M. "Engineering a Metal–Organic Framework Catalyst by using Postsynthetic Modification" *Angew. Chem. Int. Ed.* **2009**, *48*, 7424-7427; Tanabe, K. K., Cohen, S. M. "Modular, Active, Robust Lewis Acid Catalyst supported on a Metal-Organic Framework." *Inorg. Chem.* **2010**, *49*, 6766-6774; Tanabe, K. K., Cohen, S. M. "Postsynthetic Modification of Metal-Organic Frameworks – A Progress Report." *Chem. Soc. Rev.* **2011**, *40*, 498-519. The dissertation

author was the primary researcher and author for the data presented. The co-authors listed in these publications also participated in the research. The permissions to reproduce these papers were granted by the American Chemical Society, copyright 2009; Wiley-VCH Verlag GmbH & Co. KGaA, Weinheim, copyright 2009; the American Chemical Society, copyright 2010; and the Royal Society of Chemistry, copyright 2011.

5.6 References

(1) Lee, J.; Farha, O. K.; Roberts, J.; Scheidt, K. A.; Nguyen, S. T.; Hupp, J. T. *Chem. Soc. Rev.* **2009**, *38*, 1450-1459.

(2) Ma, L.; Abney, C.; Lin, W. *Chem. Soc. Rev.* **2009**, *38*, 1248-1256.

(3) Farrusseng, D.; Aguado, S.; Pinel, C. *Angew. Chem. Int. Ed.* **2009**, *48*, 7502 - 7513.

(4) Corma, A.; Garcia, H.; Llabres i Xamena, F. X. *Chem. Rev.* **2010**, *110*, 4606-4655.

(5) Forster, P. M.; Cheetham, A. K. *Topics in Catalysis* **2003**, *24*, 79-86.

(6) Li, C. *Catal. Rev. Sci. Eng.* **2004**, *46*.

(7) Czaja, A. U.; Trukhan, N.; Muller, U. *Chem. Soc. Rev.* **2009**, *38*, 1284-1293.

(8) Seo, J. S.; Whang, D.; Lee, H.; Jun, S. I.; Oh, J.; Jeon, Y. J.; Kim, K. *Nature* **2000**, *404*, 982-986.

(9) Fujita, M.; Kwon, Y. J.; Washizu, S.; Ogura, K. *J. Am. Chem. Soc.* **1994**, *116*, 1151-1152.

(10) Wu, C.-D.; Hu, A.; Zhang, L.; Lin, W. *J. Am. Chem. Soc.* **2005**, *127*, 8940-8941.

(11) Banerjee, M.; Das, S.; Yoon, M.; Choi, H. J.; Hyun, M. H.; Park, S. M.; Seo, G.; Kim, K. *J. Am. Chem. Soc.* **2009**, *131*, 7524-7525.

(12) Horike, S.; Dinca, M.; Tamaki, K.; Long, J. R. *J. Am. Chem. Soc.* **2008**, *130*, 5854-5855.

(13) Cho, S.-I.; Ma, B.; Nguyen, S. T.; Hupp, J. T.; Albrecht-Schmitt, T. E. *Chem. Commun.* **2006**, 2563-2565.

(14) Burrows, A. D.; Frost, C. G.; Mahon, M. F.; Richardson, C. *Chem. Commun.* **2009**, 4218-4220.

(15) Garibay, S. J.; Cohen, S. M. *Inorg. Chem.* **2010**, *49*, 8086-8091.

(16) Deng, H.; Doonan, C.; Furukawa, H.; Ferreira, R. B.; Towne, J.; Knobler, C. B.; Wang, B.; Yaghi, O. M. *Science* **2010**, *327*, 846 - 850.

(17) Devic, T.; Horcajada, P.; Serre, C.; Salles, F.; Maurin, G.; Moulin, B.; Heurtaux, D.; Clet, G.; Vimont, A.; Greneche, J.-M.; Ouay, B. L.; Moreau, F.; Magnier, E.; Filinchuk, Y.; Marrot, J.; Lavalley, J.-C.; Daturi, M.; Ferey, G. *J. Am. Chem. Soc.* **2010**, *132*, 1127–1136.

(18) Wang, Z.; Cohen, S. M. *Chem. Soc. Rev.* **2009**, *38*, 1135-1329.

(19) Tanabe, K. K.; Cohen, S. M. *Chem. Soc. Rev.* **2011**, *40*, 498-519.

(20) Wang, Z.; Cohen, S. M. *J. Am. Chem. Soc.* **2007**, *129*, 12368-12369.

(21) Garibay, S. J.; Cohen, S. M. *Inorg. Chem.* **2010**, *49*, 8086-8091.

(22) Farha, O. K.; Mulfort, K. L.; Hupp, J. T. *Inorg. Chem.* **2008**, *47*, 10223-10225.

(23) Hwang, Y. K.; Hong, D.-Y.; Chang, J.-S.; Jhung, S. H.; Seo, Y.-K.; Kim, J.; Vimont, A.; Daturi, M.; Serre, C.; Férey, G. *Angew. Chem. Int. Ed.* **2008**, *47*, 4144-4148.

(24) Bae, Y.-S.; Farha, O. K.; Hupp, J. T.; Snurr, R. Q. *J. Mater. Chem.* **2009**, *19*, 2131-2134.

(25) Ingleson, M. J.; Barrio, J. P.; Guilbaud, J. B.; Khimyak, Y. Z.; Rosseinsky, M. J. *Chem. Commun.* **2008**, 2680-2682.

(26) Gadzikwa, T.; Farha, O. K.; Mulfort, K. L.; Hupp, J. T.; Nguyen, S. T. *Chem. Commun.* **2009**, 3720-3722.

(27) Doonan, C. J.; Morris, W.; Furukawa, H.; Yaghi, O. M. *J. Am. Chem. Soc.* **2009**, *131*, 9492–9493.

(28) Yseilel, O. Z.; Mutlu, A.; Buyukgungor, O. *Polyhedron* **2009**, *28*, 437-444.

(29) Cohen, S. M.; Petoud, S.; Raymond, K. N. *Chem. Eur. J.* **2000**, *7*, 272-279.

(30) Mukaiyama, T.; Banno, K.; Narasaka, K. *J. Am. Chem. Soc.* **1974**, *96*, 7503-7509.

(31) Koh, K.; Wong-Foy, A. G.; Matzger, A. J. *Angew. Chem. Int. Ed.* **2008**, *47*, 677-80.

(32) Wang, Z.; Tanabe, K. K.; Cohen, S. M. *Inorg. Chem.* **2009**, *48*, 296-306.

(33) Martinez, L. E.; Leighton, J. L.; Carsten, D. H.; Jacobsen, E. N. *J. Am. Chem. Soc.* **1995**, *117*, 5897-5898.

(34) Bergmeier, S. C. *Tetrahedron* **2000**, *56*, 2561-2576.

(35) Jacobsen, E. N. *Acc. Chem. Res.* **2000**, *33*, 421-431.

(36) Yamashita, H. *Bull. Chem. Soc. Jpn.* **1988**, *61*, 1213-1220.

(37) Paterson, I.; Berrisford, D. J. *Angew. Chem. Int. Ed.* **1992**, *31*, 1179-1180.

(38) Ingleson, M. J.; Barrio, J. P.; Bacsa, J.; Dickinson, C.; Park, H.; Rosseinsky, M. J. *Chem. Commun.* **2008**, 1287-9.

(39) Jiang, D.; Mallat, T.; Krumeich, F.; Baiker, A. *J. Catalysis* **2008**, 390-395.

(40) Jiang, D.; Urakawa, A.; Yulikov, M.; Mallat, T.; Jeschke, G.; Baiker, A. *Chem. Eur. J.* **2009**, 12255-12262.

(41) Kureshy, R. I.; Prathap, K. J.; Agrawal, S.; Khan, N.-u. H.; Abdi, S. H. R.; Jasra, R. V. *Eur. J. Org. Chem.* **2008**, 3118-3128.

(42) Bedore, M. W.; Zaborenko, N.; Jensen, K. F.; Jamison, T. F. *Organic Process Research & Development* **2010**, *14*, 432-440.

(43) Fleming, E. M.; Quigley, C.; Rozas, I.; Connon, S. J. *J. Org. Chem.* **2008**, *73*, 948-956.

(44) Shivarkar, A. B.; Gupte, S. P.; Chaudhari, R. V. *Synlett.* **2006**, *9*, 1374-1378.

(45) Bartoli, G.; Bosco, M.; Carlone, A.; Locatelli, M.; Massaccesi, M.; Melchiorre, P.; Sambri, L. *Org. Lett.* **2004**, *6*, 2173-2176.

(46) Tanabe, K. K.; Wang, Z.; Cohen, S. M. *J. Am. Chem. Soc.* **2008**, *130*, 8508-8517.

(47) Ami, E. i.; Ohrui, H. *Biosci. Biotechnol. Biochem.* **1999**, *63*, 2150-2156.

(48) Negron, G.; Guerra, N.; Lomas, L.; Gavino, R.; Cardena, J. *ARKIVOC* **2003**, *11*, 179-184.

(49) Sahasrabudhe, K.; Gracias, V.; Furness, K.; Smith, B. T.; Katz, C. E.; Reddy, S.; Aube, J. *J. Am. Chem. Soc.* **2003**, *125*, 7914-7922.

(50) Schaus, S. E.; Larrow, J. F.; Jacobsen, E. N. *J. Org. Chem.* **1997**, *62*, 4197-4199.

(51) Tanabe, K. K.; Cohen, S. M. *Angew. Chem. Int. Ed.* **2009**, *48*, 7424-7427.

Chapter 6 Postsynthetic Deprotection

6.1 Introduction

In Chapter 1, two methods for synthesizing functionalized MOFs were introduced: prefunctionalization and PSM. Prefunctionalization was described as the direct preparation of a functionalized MOF from a specific metal ion and functionalized organic ligand combination under solvothermal conditions.[1-3] PSM was defined as the chemical modification of a MOF after the framework had been synthesized.[4,5] During the course of PSM, a third approach, named postsynthetic deprotection (PSD), was introduced as a combination of the prefunctionalization and PSM strategy (Figure 6-1). PSD involves protecting the functional group of interest, using the protected ligand to synthesize a MOF, and then removing the protecting group within the framework afterwards. In theory, PSD utilizes the prefunctionalization approach first to synthesize the MOF with the protected functionality, and then the PSM approach afterward to reveal the functional group.

In 2009, Yamada and Kitagawa made an early observation that free, uncoordinated -OH groups could potentially be incorporated into MOFs through PSD. As an initial test, they attempted to protect 2,5-dihydroxy-1,4-benzenedicarboxylic acid (dhBDC), synthesize a MOF with the protected ligand, and then remove the protecting groups afterwards (Figure 6-2).[6] dhBDC was protected using acetic anhydride to yield 2,5-diacetoxy-1,4-benzendicarboxylic acid and was combined with Zn^{2+} ions and bipyridine (bpy) in an attempt to the form the protected MOF. Surprisingly, the acetyl groups were removed in situ, resulting in a MOF with free uncoordinated -OH groups. No explanation could be made for the unexpected result aside from the conclusion that the acetyl deprotection took place during framework synthesis. However, the results

foreshadowed that the protection and deprotection strategy of functional groups was a valuable method for obtaining MOFs with more complex functionalities.

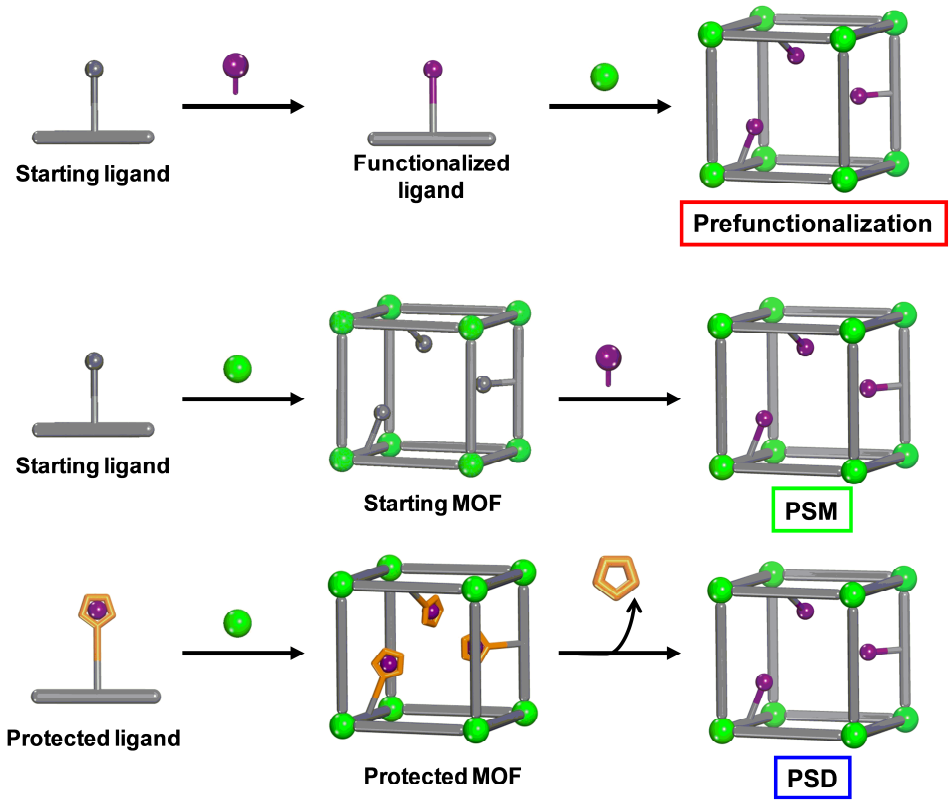

Figure 6-1. Three different methods for obtaining functionalized MOFs: Prefunctionalization (top), PSM (middle), and PSD (bottom). The green spheres represent the metal source, the purple spheres represent the functional group, and the orange pentagon refers to the protecting group.

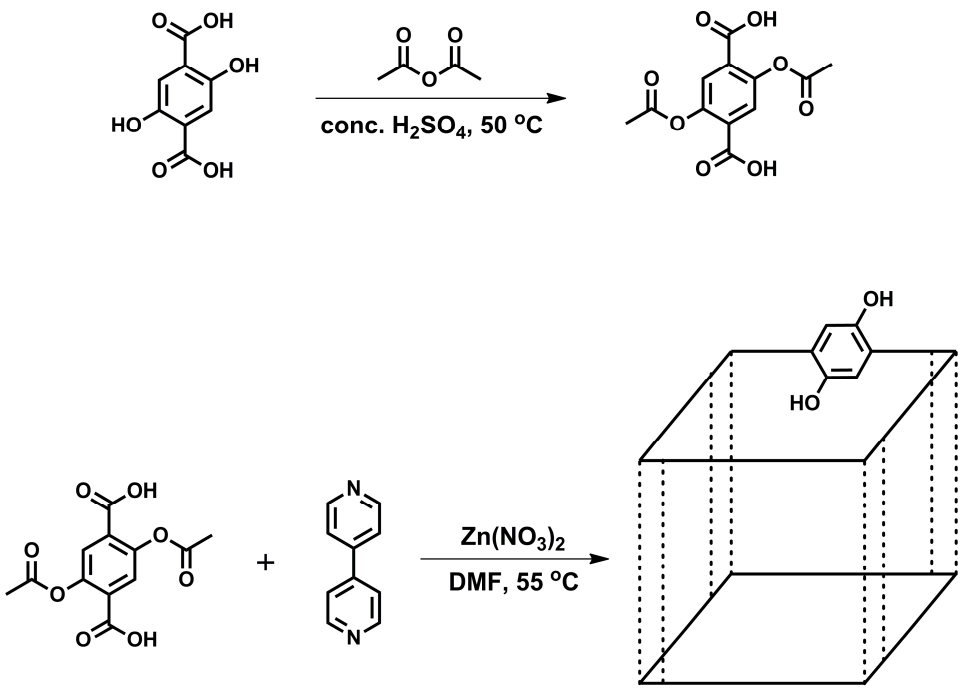

Figure 6-2. Synthesis of 2,5-diacetoxyterephthalic acid from 2,5-dihydroxyterephthalic acid and acetic anhydride (top). MOF synthesis with 2,5-diacetoxyterephthalic acid, bipyridine, and $Zn(NO_3)_2$ in DMF. Bipyridine is represented by the dashed lines.

Hupp and Nguyen *et al.* performed chemical PSD on TMS protected alkyne-containing MOFs.[7,8] Trimethylsilyl (TMS) groups are known to undergo deprotection in the presence of fluoride to yield the terminal alkyne. Two types of Zn^{2+} paddlewheel MOFs were prepared from 3-[(trimethylsilyl)ethynyl]-4-[2-(4-pyridinyl)ethenyl]pyridine and either 2,6-naphthalenedicarboxylic acid (NDC) or 1,2,4,5-tetrakis(4-carboxyphenyl)benzene (TCPB). In their first study, Hupp and Nguyen *et al.* exposed their NDC containing MOF to a solution of tetrabutylammonium fluoride (TBAF) and were able to deprotect only the MOF surface, which was attributed to the bulkiness of TBAF.[7] To confirm the deprotection, the newly exposed alkyne groups underwent 'click' chemistry with either ethidium bromide monoazide or *O*-(2-aminoethyl)-*O*-(2-azidoethyl)nonethylene glycol (PEGazide). Both azides were successfully clicked with

the alkyne groups to form their respective triazole products. Matrix-assisted laser desorption ionization time-of-flight (MALDI-TOF) mass spectrometry confirmed that the triazole ligands were present. As further proof of the modification, fluorescence microscopy was used to confirm the ethidium bromide monoazide product while contact angle measurements were used to confirm the newly hydrophilic PEGazide substituent. In their second study, the TCPB containing MOF (TO-MOF) was selectively modified on the surface and interior by utilizing the solubility preference of the deprotection reagents (Figure 6-3).[8] To perform the selective deprotection, TO-MOF was modified with two different fluoride reagents: potassium fluoride (KF) in H_2O and tetraethylammonium fluoride (TEAF) in THF/H_2O. The MOF, which was initially prepared from DMF, was solvent exchanged with $CHCl_3$ and exposed to the KF solution. Only the MOF surface was deprotected due to the insolubility of KF in $CHCl_3$. After coupling the alkyne groups with ethidium bromide monoazide, the MOF was subsequently exposed to the TEAF solution to remove the silyl groups from the MOF interior. Benzyl azide was successfully coupled with the interior alkyne groups, therefore showing that selective deprotection could be accomplished on the surface and interior of the framework.

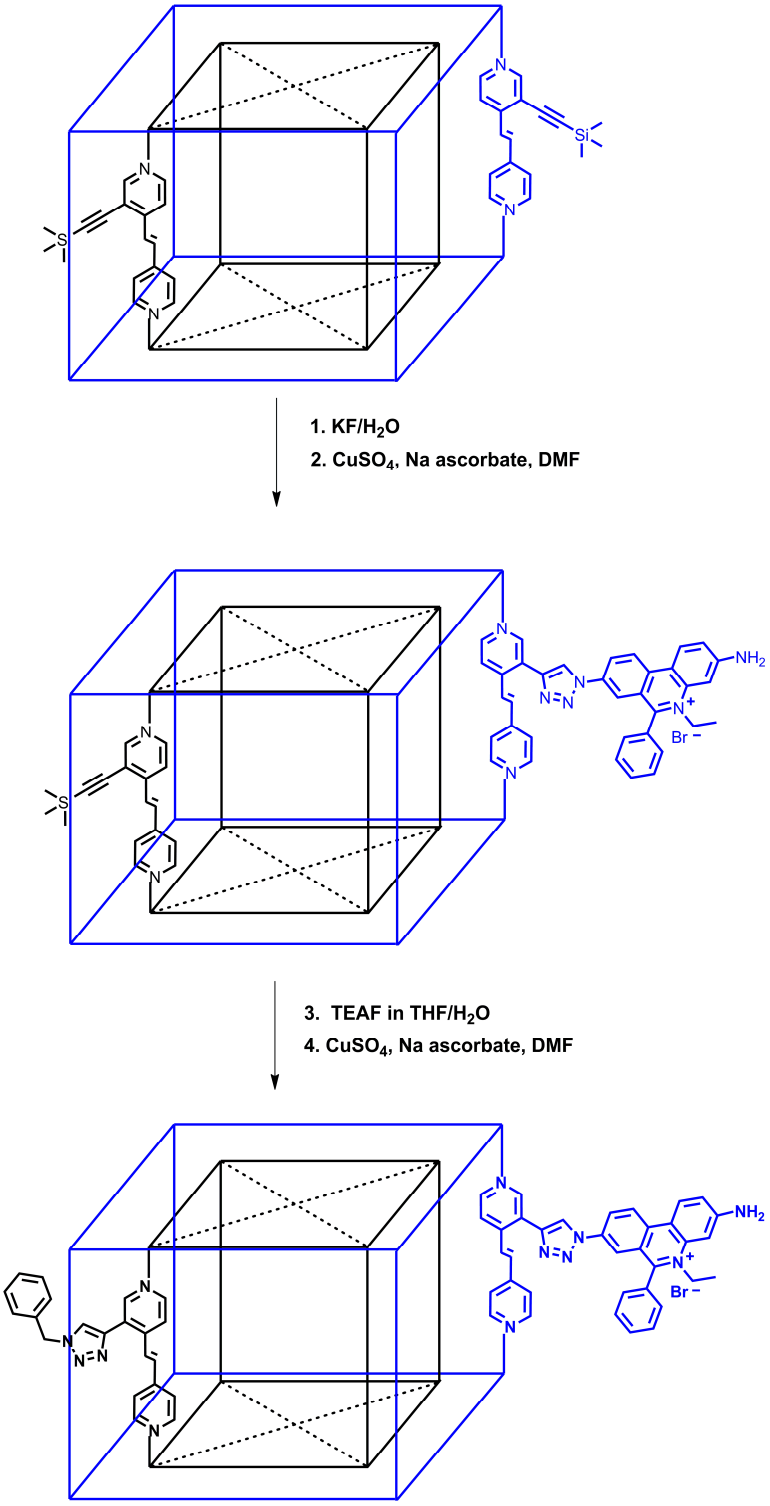

Figure 6-3. Selective modification via Click chemistry with ethidium bromide monoazide on the surface (middle) and benzyl azide in the interior of TO-MOF (bottom). 1,2,4,5-Tetrakis(4-carboxyphenyl) benzene (TCPB) is represented by the dashed lines.

Telfer and coworkers took PSD to the next level by performing a unique study using thermolysis as a deprotection method.[9] For their study, *tert*-butoxycarbonyl (Boc) was selected as the protecting group because: a) it is thermally labile at high temperatures, and 2) it breaks down into CO_2 and isobutylene, which are innocuous side products (Figure 6-4). Boc-protected 2-amino-4,4'-biphenyldicarboxylic acid was synthesized and combined with Zn^{2+} ions in diethylformamide (DEF), which resulted in colorless cubic crystals. Single crystal X-ray diffraction revealed that the product was an analog of IRMOF-9, a 3D cubic lattice with Zn_4O SBUs and biphenyldicarboxylate linkers; however, the Boc-protected substituent could not be detected due to disorder over eight positions of the biphenyl linker. ^{1}H NMR analysis of the digested MOF, though, confirmed the presence of the Boc-protecting group.

To perform the thermal deprotection, the Boc-protected MOF was suspended in DMF and heated between 150-200 °C for several hours. Powder and single crystal X-ray diffraction verified that the thermolysis had no effect on framework stability. Unfortunately, no electron density was present for the resulting amino substituents to unambiguously confirm removal of the Boc groups. However, ^{1}H NMR analysis and TGA both showed the protecting group was completely removed and only the free amino group was present. When the protected MOF is heated, a distinct weight loss is observed between 120- 240 °C (approx. 22%), which corresponds to the Boc-protecting group breaking down into CO_2 and isobutylene. In contrast, the deprotected MOF showed little weight loss around the same region (approx. 5%), therefore confirming the successful deprotection.

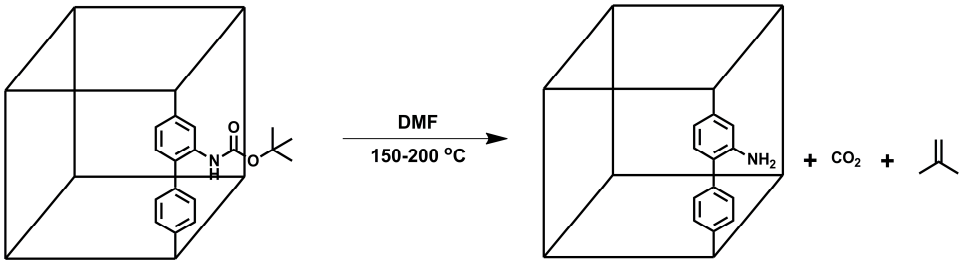

Figure 6-4. Deprotection of an IRMOF-9 analog using a thermally labile Boc protecting group (Boc = *tert*-butoxycarbonyl).

Telfer and coworkers emphasized several interesting advantages by using PSD. Protecting functional groups could prevent these groups from interfering with framework formation. As a control experiment, 2-amino-4,4'-biphenyldicarboxylic acid was directly combined with Zn^{2+} to form a MOF. Surprisingly, no crystals could be obtained despite testing different reaction conditions. Another key point was that use of the bulky Boc-protecting group prevented formation of an interpenetrated framework. IRMOF-9, which is obtained from 4,4'-biphenyldicarboxylic acid, is known to be an interpenetrated framework unless extremely dilute conditions are used.[1] Here, the bulky Boc-protecting group prevented interpenetration presumably due to steric hinderance coming from the size and shape of the Boc group. Lastly, the use of protecting groups could be used to obtain MOFs with expanded pore volumes and greater pore accessibility. Theoretically, removal of the Boc-protecting should result in a higher surface area and larger pore diameters then the as-synthesized material. To test out this theory, the Boc-protected and deprotected MOFs were examined for N_2 sorption analysis. However, the MOFs were found to undergo pore collapse upon solvent removal and no gas sorption surface area measurements could be obtained to confirm the expected increase in porosity.

Regardless, these seminal results indicate the utility of PSD for obtaining more functionalized MOFs with control over framework formation and porosity.

In this chapter, photochemical deprotection was explored as a new method for revealing more complex functionalities within the framework. Two new BDC ligands, 2-((2-nitrobenzyl)oxy)terephthalic acid (NO_2BnO-BDC, **4**) and 2,3-bis((2-nitrobenzyl)oxy)terephthalic acid ((NO_2BnO)$_2$-BDC, **8**) were prepared from hydroxyl-containing BDC ligands and protected using a well-established photolabile protecting group. Two new MOFs, UMCM-1-OBnNO_2 and UMCM-1-(OBnNO_2)$_2$, were successfully synthesized using the protected BDC ligands and underwent photochemical deprotection to yield their hydroxyl analogs. All MOFs were characterized using ^{1}H NMR, TGA, PXRD, single crystal X-ray diffraction, and N_2 sorption analysis. Metalation studies with one of the hydroxyl containing MOFs were conducted and the preliminary results will be discussed. Two other benzyl protected MOFs were synthesized from two new benzyl protected BDC ligands, and both MOFs were fully characterized and tested for photochemical deprotection. Lastly, a new hydroxyl functionalized ligand (4,4',4''-benzene-1,3,5-triyl-tribenzoate, HO-BTB) was synthesized, and the preliminary attempts to prepare the ligand for PSD will be discussed.

6.2 Results and Discussion

6.2.1 Synthesis of UMCM-1-OBnNO_2 and UMCM-1-(OBnNO_2)$_2$

One of the challenges with PSD is to find a protecting group that can be removed under conditions that are compatible with the MOF. Hupp, Nguyen, and Telfer were able to find relatively labile groups that could be removed under mild chemical and thermal

conditions. For this study, light was selected as the deprotection method of interest. There have been a few reports using light to physically and chemically modify MOFs and their properties,[10-12] but there have not been any studies using light as a deprotection method on a MOF. As a starting point, 2-hydroxy-1,4-benzenedicarboxylic acid (HO-BDC, **1**) and 2,3-dihydroxy-1,4-benzenedicarboxylic acid (CAT-BDC, CAT = catechol, **5**) were selected as the ligands of interest and nitrobenzylethers were chosen as the protecting group. MOFs with free, uncoordinated hydroxyl groups are very rare because the hydroxyl groups tend to chelate to metal ions.[2,13] Nitrobenzylethers are well known photolabile protecting groups for amines and alcohols and are easily removed when exposed to UV light.[14] Moreover, the byproduct produced from the deprotection reaction, nitrosobenzaldehyde, is not caustic or reactive.[15] For these reasons, attempts were made to synthesize hydroxyl protected BDC ligands, incorporate them into a MOF, and then remove the protecting groups through photochemical deprotection (Scheme 6-1).

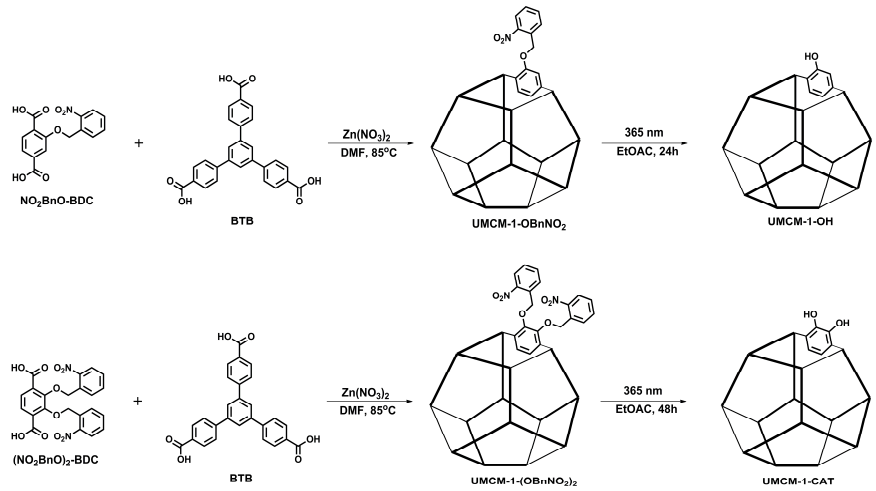

Scheme 6-1. Synthesis and postsynthetic photochemical deprotection of UMCM-1-$OBnNO_2$ (top) and UMCM-1-$(OBnNO_2)_2$ (bottom).

HO-BDC[13] and CAT-BDC[16] were prepared from previously established literature procedures. The carboxylic acid groups were protected via esterification first, and the hydroxyl groups were protected subsequently using *o*-nitrobenzyl bromide in DMF and K_2CO_3. After isolating and purifying the ligands, the fully protected ligands were subjected to a solution of THF/4%KOH followed by acidification with concentrated HCl to yield the nitrobenzyl protected BDC ligands: 2-((2-nitrobenzyl)oxy)terephthalic acid (NO_2BnO-BDC, **4**) and 2,3-bis((2-nitrobenzyl)oxy)terephthalic acid ((NO_2BnO)$_2$-BDC, **8**) (Scheme 6-2).

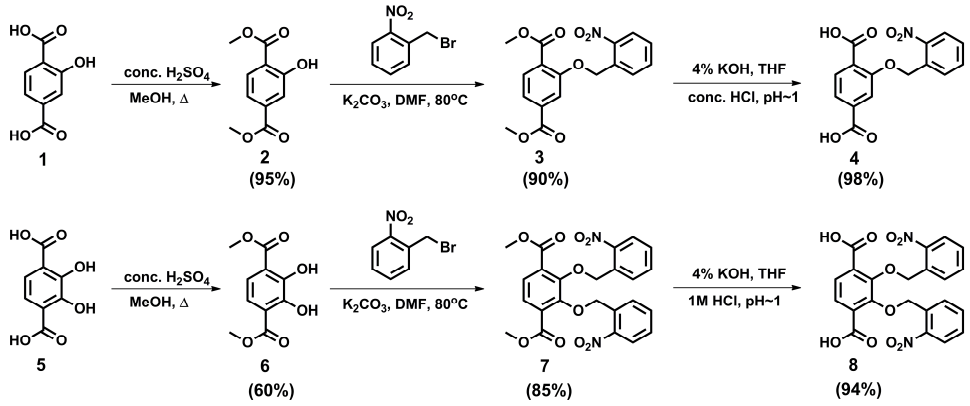

Scheme 6-2. Synthesis of **4** (NO_2BnO-BDC) (top) and **8** ((NO_2BnO)$_2$-BDC) (bottom).

The ligands were used to synthesize two UMCM-1[17] type MOFs (Scheme 6-3). In a general setup, a 3:1 ratio of protected BDC ligand to 4,4',4''-benzene-1,3,5-triyl-tribenzoate[17] (BTB) was dissolved with $Zn(NO_3)_2 \cdot 6H_2O$ in DMF and the solution was heated at 85 °C. After 48 h, both setups yielded colorless needle crystals, which were assumed to be UMCM-1-OBnNO_2 and UMCM-1-(OBnNO_2)$_2$. The crystals were analyzed by several techniques to confirm the composition and structure. PXRD analysis confirmed that both sets of crystals had similar PXRD patterns as UMCM-1 (Figure 6-5).

^{1}H NMR of the digested MOF samples in dilute acid (35% DCl in D_2O/d^6-DMSO) verified the presence of both the BTB and the respective protected ligand, thus indicating that the protecting group remained intact during synthesis (Figure 6-6). As further support, TGA revealed UMCM-1-$OBnNO_2$ and UMCM-1-$(OBnNO_2)_2$ displayed unique weight losses corresponding to the nitrobenzyl moieties (Figure 6-7). UMCM-1-$OBnNO_2$ showed a weight loss of 9% (expected 9%) while UMCM-1-$(OBnNO_2)_2$ displayed a more prominent weight loss of 18% (expected 20%) between 250-400 °C. After 400 °C, both UMCM-1-$OBnNO_2$ and UMCM-1-$(OBnNO_2)_2$ decomposed, which is consistent with previously established UMCM analogs.[17,18] N_2 sorption analysis at 77 K revealed that UMCM-1-$OBnNO_2$ and UMCM-1-$(OBnNO_2)_2$ maintained their high porosities regardless of having bulky substituents located within the pores of the framework. The BET surface area measurements were determined to be 3219±150 m^2/g and 2661±172 m^2/g for UMCM-1-$OBnNO_2$ and UMCM-1-$(OBnNO_2)_2$, respectively. Full isotherm analysis of both MOFs revealed a characteristic step at P/P_o ~0.2, which is typically seen for the UMCM-1 structure type.[17]

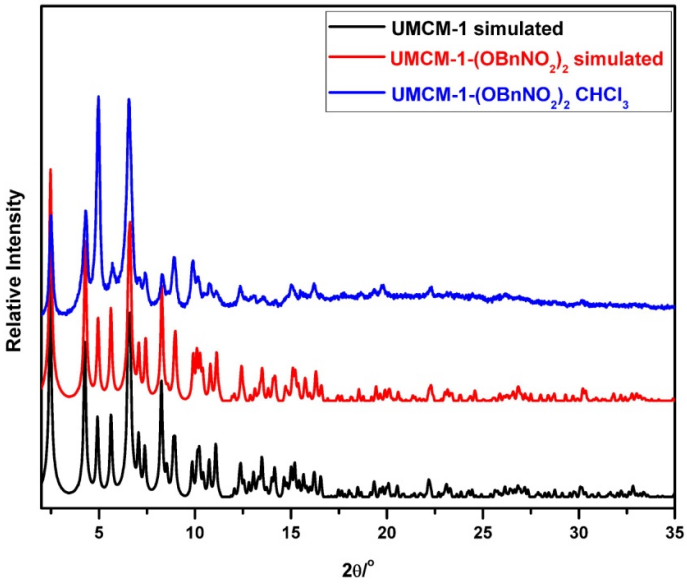

Figure 6-5. PXRD comparison of UMCM-1 (black, simulated), UMCM-1($OBnNO_2$)$_2$ (red, simulated), and UMCM-1-($OBnNO_2$)$_2$ (blue, $CHCl_3$ exch).

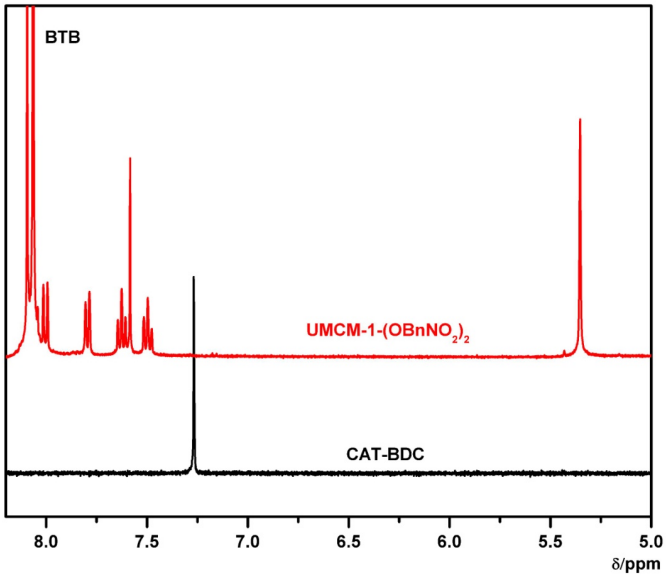

Figure 6-6. ^{1}H NMR comparison between digested UMCM-1-($OBnNO_2$)$_2$ and CAT-BDC ligand.

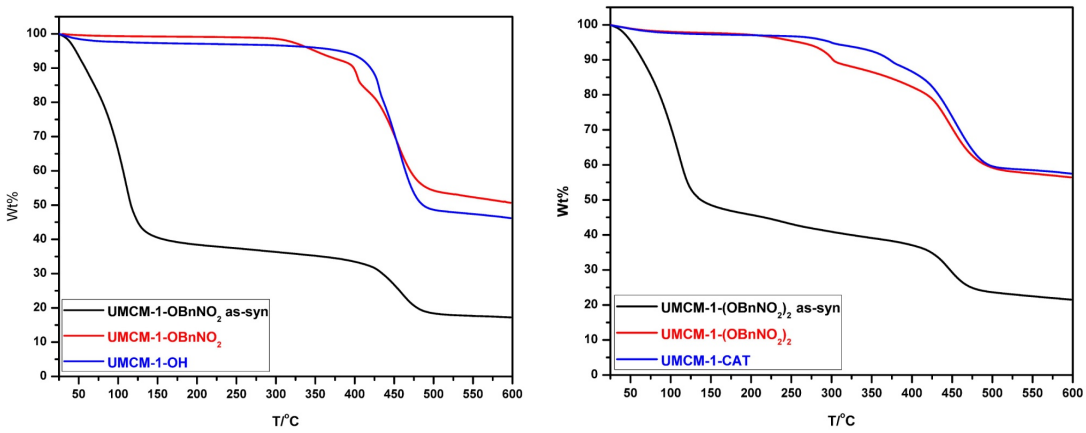

Figure 6-7. TGA comparison between as-synthesized protected UMCM (black, from DMF), protected UMCM (red, $CHCl_3$ exchanged and dried), and deprotected UMCM (blue, $CHCl_3$ exchanged and dried). UMCM-1-$OBnNO_2$/UMCM-1-OH system (left) and UMCM-1-$(OBnNO_2)_2$/UMCM-1-CAT (right).

Single crystal X-ray diffraction provided the most compelling evidence that UMCM-1-$OBnNO_2$ and UMCM-1-$(OBnNO_2)_2$ were indeed isostructural to UMCM-1. Both MOFs were found to have similar cell parameters as UMCM-1 and contained Zn_4O SBUs coordinated by BTB and their respective *o*-nitrobenzyl BDC ligands. UMCM-1-$OBnNO_2$ and UMCM-1-$(OBnNO_2)_2$ both have large hexagonal pores bordered primarily by BTB ligands and smaller pores built from BTB and the nitrobenzyl BDC ligands (Figures 6-8 and 6-9). In the UMCM-1-$OBnNO_2$ structure, no suitable electron density was located for the nitrobenzyl protecting group. An oxygen atom was located off of the benzenedicarboxylate and was found to be disordered over all four positions. In contrast, both oxygen atoms and benzyl groups were located and assigned for UMCM-1-$(OBnNO_2)_2$ (Figure 6-10). The oxygen atoms and benzyl groups were also disordered over all four positions of the benzenedicarboxylate. Nitro groups were located for the benzyl group in the difference map, but suitable electron density could not be assigned due to severe disorder.

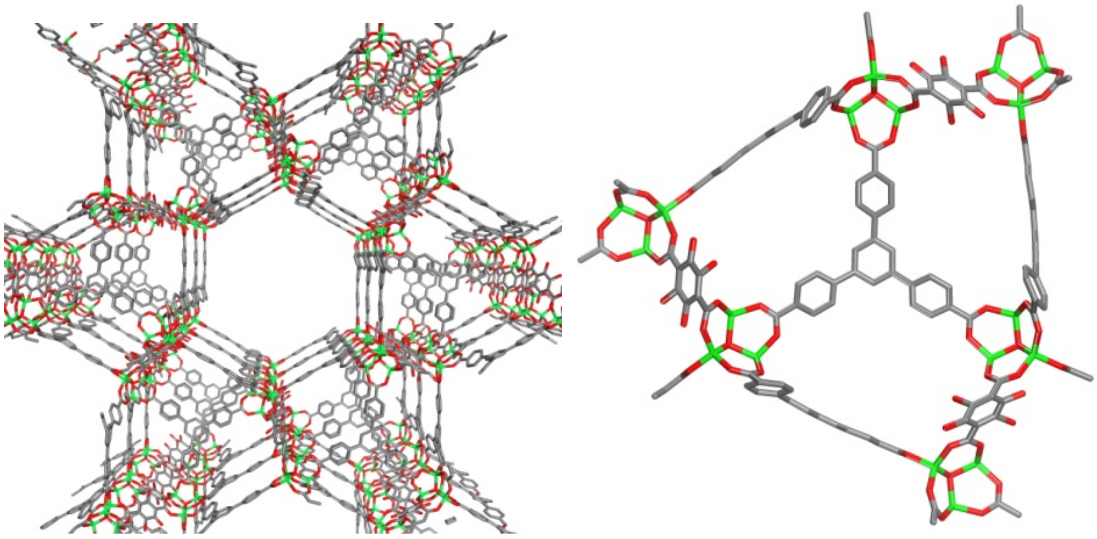

Figure 6-8. Single crystal X-ray structure of UMCM-1-$OBnNO_2$ with view of the framework (left) and small pore (right). Electron density for the oxygen atom of the benzylether group was located and assigned (disordered over four positions).

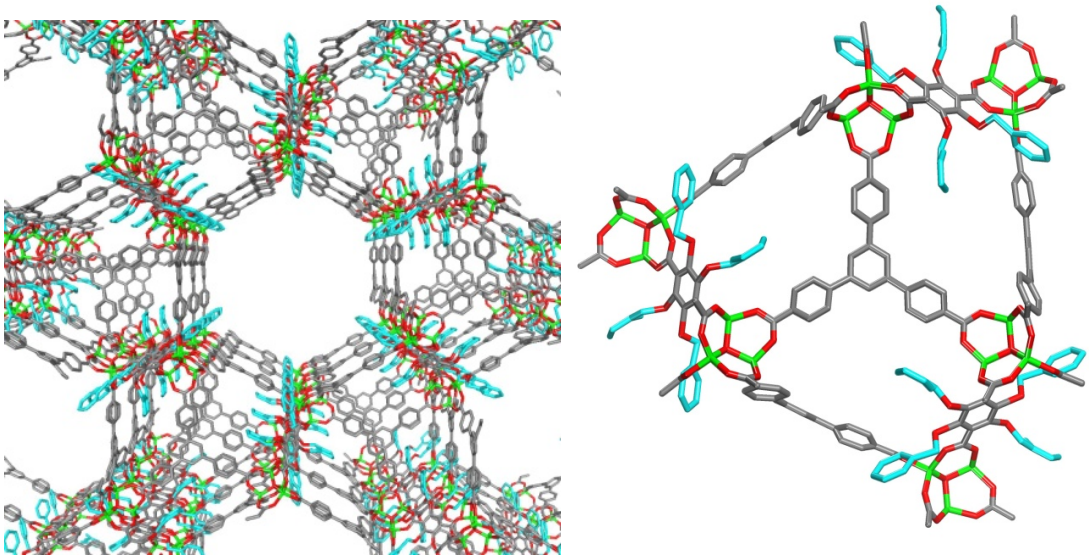

Figure 6-9. Single crystal X-ray structure of UMCM-1-$(OBnNO_2)_2$ with view of the framework (left) and small pore (right). Electron density for the benzylether group was located and assigned (disordered over two positions). The nitrobenzyl groups are highlighted in cyan.

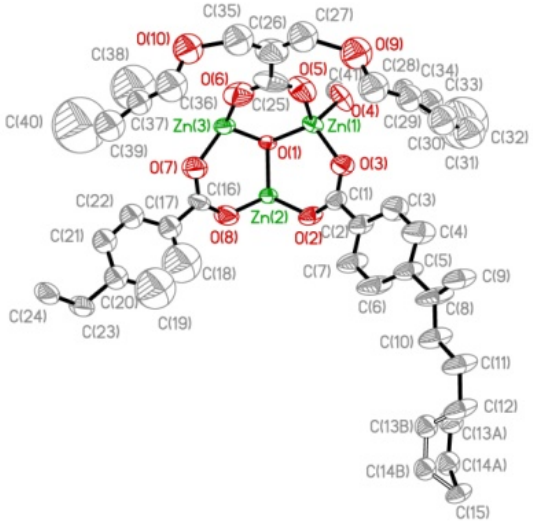

Figure 6-10. Asymmetric unit of UMCM-1-$(OBnNO_2)_2$ with 50% probability ellipsoids and atom numbering scheme.

6.2.2 Synthesis of UMCM-1-$(OBn)_2$ and UMCM-1-$(OBnNO_2(MeO)_2)_2$

Benzyl and 4,5-dimethoxy-2-nitrobenzyl BDC ligand versions were prepared using slightly modified reaction conditions for the nitrobenzyl BDC ligand synthesis. The two benzyl groups were selected for two main reasons: 1) Benzyl is not a photolabile group; and 2) 4,5-dimethoxy-2-nitrobenzyl is photolabile and known to have faster photocleavage rates than the nitrobenzyl group.[14] CAT-BDC was protected using benzyl bromide and 4,5-dimethoxy-2-nitrobenzyl bromide to yield $(BnO)_2$-BDC (**10**, Scheme 6-3) and $((MeO)_2NO_2BnO)_2$-BDC (**12**, Scheme 5-3), respectively. After testing different ratios of BDC:BTB and solvent conditions (e.g., DEF vs. DMF), UMCM-1-$(OBn)_2$ and UMCM-1-$(OBnNO_2(MeO)_2)_2$ were both successfully synthesized from DEF at 85 °C for 48 h. Pale yellow needle clusters were obtained for both MOFs, but the crystals were too small for single crystal X-ray analysis (Figure 6-11). PXRD and gas sorption analysis provided concrete evidence that UMCM-1-$(OBn)_2$ and UMCM-1-$(OBnNO_2(MeO)_2)_2$

were indeed UMCM MOFs. PXRD analysis showed UMCM-1-$(OBn)_2$ and UMCM-1-$(OBnNO_2(MeO)_2)_2$ had similar structures to UMCM-1-$(OBnNO_2)_2$ and UMCM-1 (Figure 5-12). Both MOFs also displayed the characteristic step at P/P_o ~0.2 in their isotherms and had BET surface areas of 2983±50 m^2/g for UMCM-1-$(OBn)_2$ and 2534±23 m^2/g for UMCM-1-$(OBnNO_2(MeO)_2)_2$ (Figure 6-13). ^1H NMR analysis of UMCM-1-$(OBn)_2$ and UMCM-1-$(OBnNO_2(MeO)_2)_2$ showed both the benzyl protected BDC ligand and BTB. The MOFs were found to be stable up to ~450 °C and displayed unique weight losses corresponding to their benzyl groups. A 15% weight loss was observed for UMCM-1-$(OBn)_2$ (15% expected) and a 21% weight loss was calculated for UMCM-1-$(OBnNO_2(MeO)_2)_2$ (27% expected) (Figure 6-14).

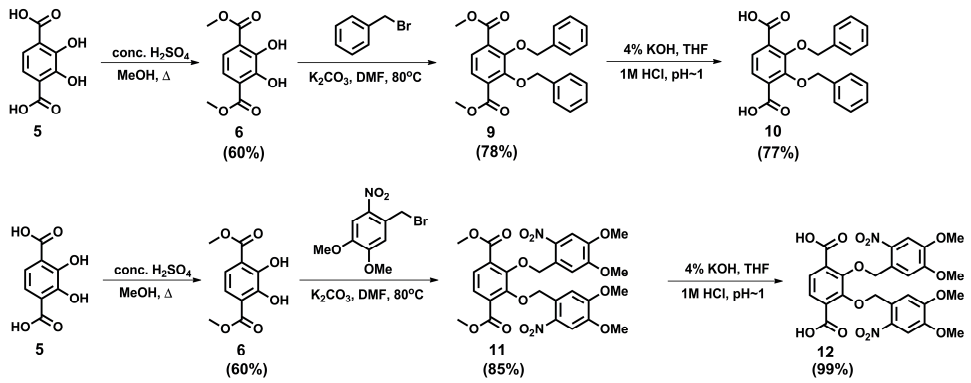

Scheme 6-3. Synthesis of **10** ($(BnO)_2$-BDC) (top) and **12** ($(MeO)_2NO_2BnO)_2$-BDC (bottom).

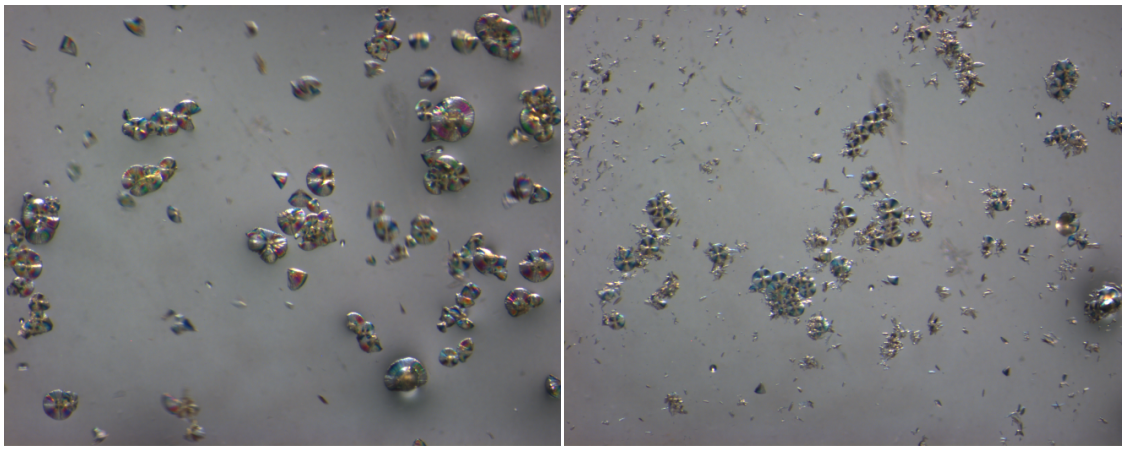

Figure 6-11. Photographs of UMCM-1-$(OBn)_2$ (left) and UMCM-1-$(OBnNO_2(MeO)_2)_2$ at 4× magnification.

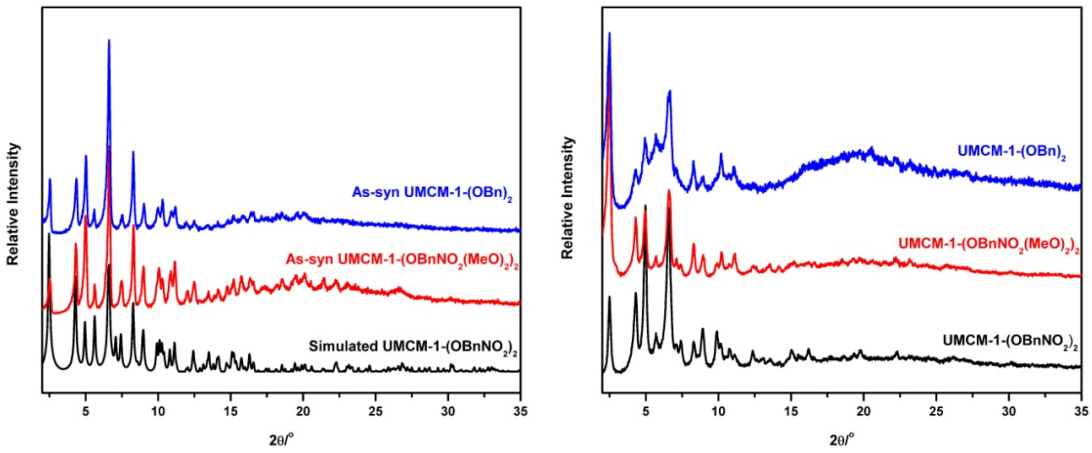

Figure 6-12. PXRD analysis of UMCM-1-$(OBn)_2$ and UMCM-1-$(OBnNO_2)(MeO)_2)_2$ as-synthesized from DEF (left) and $CHCl_3$ exchanged (right).

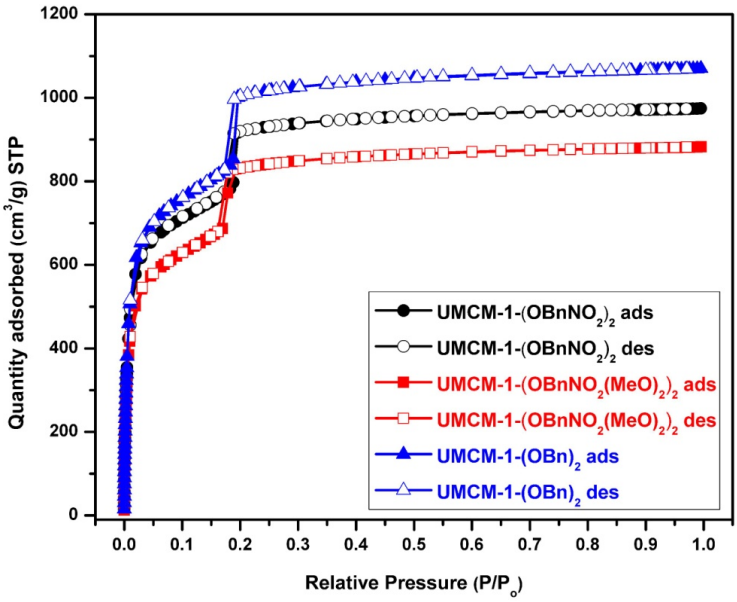

Figure 6-13. N_2 isotherms of UMCM-1-$(OBnNO_2)_2$, UMCM-1-$(OBnNO_2(MeO)_2)_2$, and UMCM-1-$(OBn)_2$ at 77 K.

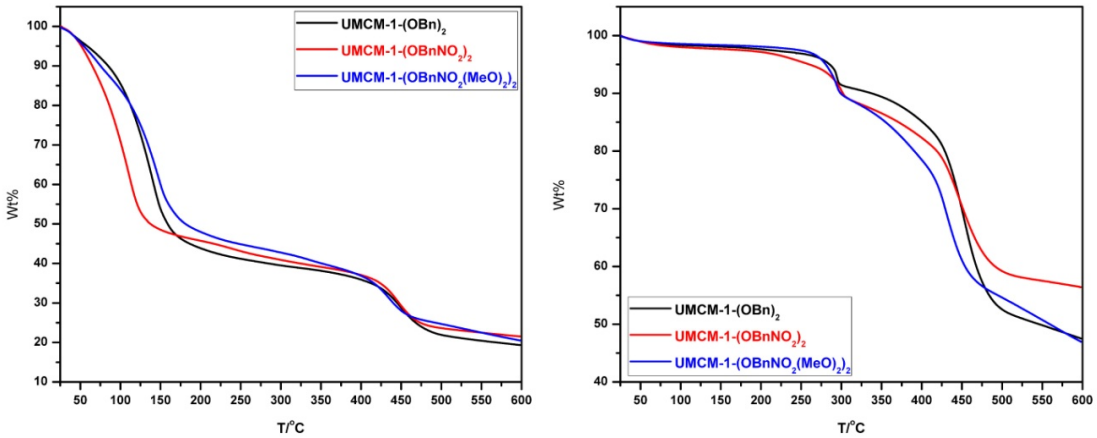

Figure 6-14. TGA comparison of UMCM-1-$(OBnNO_2)_2$, UMCM-1-$(OBnNO_2(MeO)_2)_2$, and UMCM-1-$(OBn)_2$ as-synthesized (left) and $CHCl_3$ exchanged and dried (right).

6.2.3 Photochemical deprotection

Initial tests were conducted with UMCM-1-$OBnNO_2$ and UMCM-1-$(OBnNO_2)_2$ to determine suitable reaction conditions for photochemical deprotection. The crystals were suspended in $CHCl_3$, EtOAc, and DMF and exposed to 365 nm to see if solvent had

any effect on the deprotection rate and MOF stability. The MOFs, which are initially colorless, were found to undergo a color change upon exposure to the light, thus indicating that a reaction was occurring. In $CHCl_3$, the crystals became red and were visually opaque, therefore signaling a loss of crystallinity. Alternatively, when DMF was used as the solvent, crystals turned light orange and remained crystalline, but were clearly cracked. EtOAc was found to be the best solvent for the photochemical reaction, where the crystals were found to maintain their crystallinity.

To perform the photochemical deprotection, UMCM-1-$OBnNO_2$ and UMCM-1-$(OBnNO_2)_2$ were suspended in EtOAc and irradiated at 365 nm for 24-48 h. Both MOFs underwent a distinct color change from colorless to orange, which was indicative of the photochemical reaction occurring (Figures 6-15 and 6-16). After 24 h, UMCM-1-$OBnNO_2$ was quantitatively converted into UMCM-1-OH, as determined by ^{1}H NMR analysis of the digested sample (Figure 6-17). Only the aromatic peaks associated with the HO-BDC were seen in the ^{1}H NMR spectra. UMCM-1-CAT was achieved at 75% after 48 h and was found to contain a mixture of both singly protected (approx. 12%) and doubly protected (approx. 12%) CAT-BDC (Figure 6-18). The percent deprotection was determined by taking the singlet aromatic peak of CAT-BDC and dividing it by the summation of the integrated singlet peak and the two integrated methylene peaks corresponding to the singly and doubly product CAT-BDC ligands. The difference in deprotection between the singly and doubly protected UMCMs can be explained by the concentration of protecting groups present and their crystal morphology. Initial solution state studies with **4** and **8** in d^6-DMSO showed **4** underwent deprotection at a much faster rate than **8**, presumably due to having only one photocleavable substituent. This trend

was found to be consistent with UMCM-1-$OBnNO_2$ and UMCM-1-$(OBnNO_2)_2$. All the protecting groups were removed from UMCM-1-$OBnNO_2$, as expected, but UMCM-1-$(OBnNO_2)_2$ could not undergo complete deprotection even when exposed to UV light for up to 72 h. Both MOFs form as needles, but UMCM-1-$(OBnNO_2)_2$ consists of tightly packed needle clusters while UMCM-1-$OBnNO_2$ forms as distinct, single needles (Figures 6-15 and 6-16). The UV light appears to penetrate UMCM-1-$OBnNO_2$ without any problem, but the morphology of UMCM-1-$(OBnNO_2)_2$ may prevent the UV light from reaching the center of the crystal clusters. This possibly explains why complete deprotection cannot be achieved regardless of extending the exposure time. To confirm this speculation, the crystal clusters of UMCM-1-$(OBnNO_2)_2$ were lightly crushed to increase surface area exposure to UV light. After optimizing the setup conditions, a maximum 85% deprotection yield was achieved, therefore indicating the morphology of UMCM-1-$(OBnNO_2)_2$ has a profound effect on the deprotection rate.

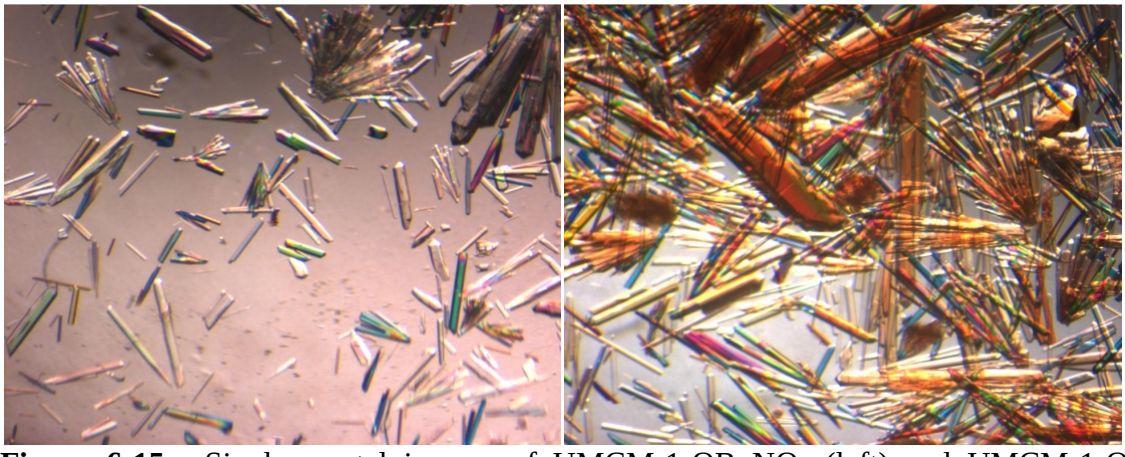

Figure 6-15. Single crystal images of UMCM-1-$OBnNO_2$ (left) and UMCM-1-OH (right).

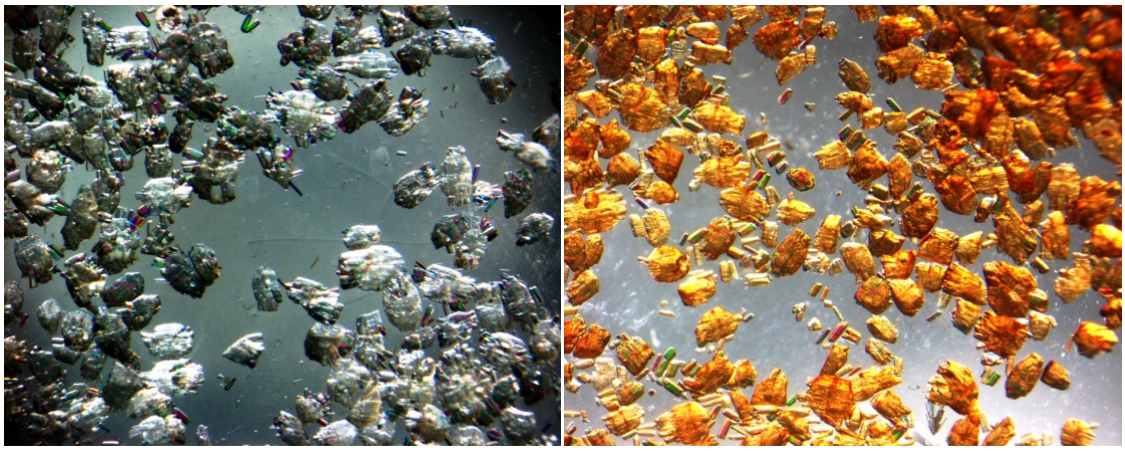

Figure 6-16. Single crystal images of UMCM-1-$(OBnNO_2)_2$ (left) and UMCM-1-CAT (right).

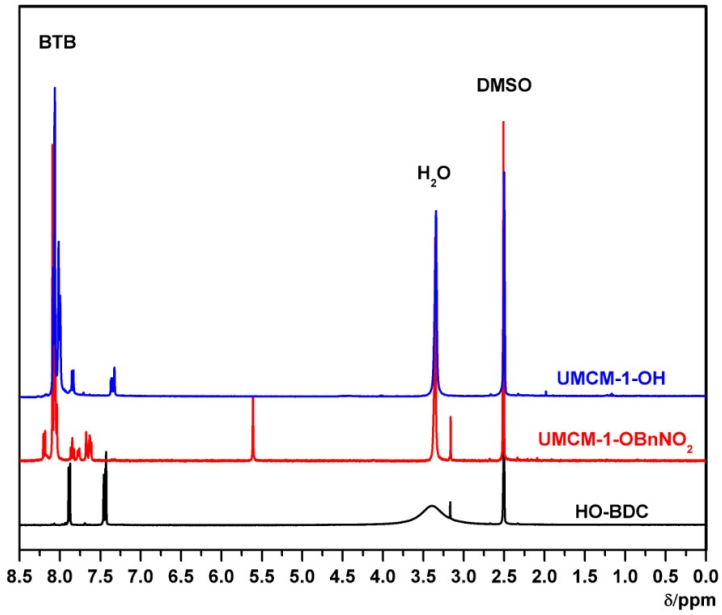

Figure 6-17. ^1H NMR comparison of HO-BDC (black), digested UMCM-1-$OBnNO_2$ (red), and digested UMCM-1-OH (blue).

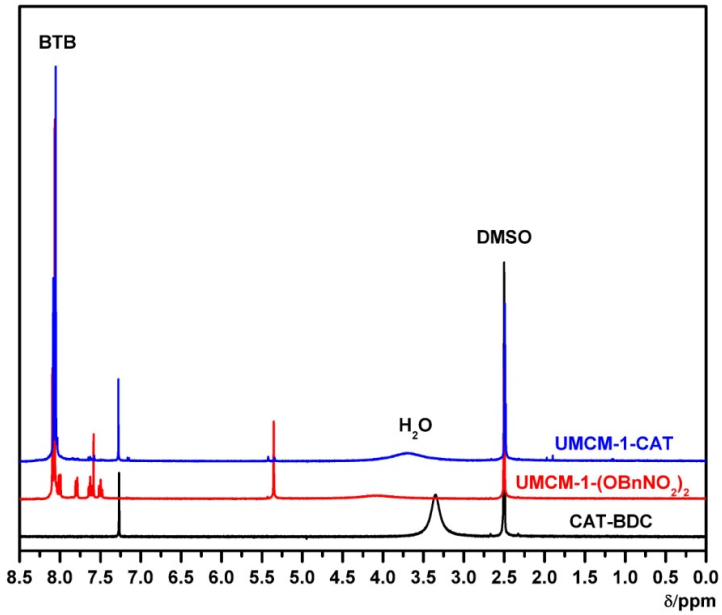

Figure 6-18. ^{1}H NMR comparison of CAT-BDC (black), digested UMCM-1-$(OBnNO_2)_2$ (red), and digested UMCM-1-CAT (blue). Based on the NMR spectrum, UMCM-1-CAT is comprised of ~75% CAT-BDC, ~12 % $(NO_2BnO)_2$-BDC, and ~12% of a BDC ligand with a single 2-nitrobenzyl group removed.

TGA, PXRD, and single crystal X-ray diffraction provided additional evidence that the MOFs had undergone successful photochemical deprotection. By TGA, UMCM-1-OH showed no significant weight loss, therefore confirming all the nitrobenzyl groups had been completely deprotected (Figure 6-7). Since UMCM-1-CAT was not fully deprotected, a weight loss was still detected (~13%), but was lower than the fully protected MOF. Both MOFs showed no significant structural anomalies as a result of UV exposure, as confirmed by PXRD and single crystal X-ray analysis. Single crystal X-ray analysis of UMCM-1-OH revealed the framework was isostructural to UMCM-1-$OBnNO_2$ (Figures 6-19 and 6-20). For UMCM-1-CAT, single crystal X-ray analysis showed complete disappearance of the nitrobenzyl protecting groups, thus indicating that the photochemical deprotection was indeed successful (Figures 6-19 and 6-21). Oxygen

atoms were only located off of the benzenedicarboxylate and no electron density was present for the nitrobenzyl groups.

N_2 sorption analysis of UMCM-1-OH and UMCM-1-CAT also gave compelling evidence for the loss of the protecting groups. As mentioned previously, UMCM-1-$OBnNO_2$ and UMCM-1-$(OBnNO_2)_2$ have surface areas around ~3200 and 2600 m^2/g, respectively. After deprotection, large increases in surface area were seen for both MOFs. The BET surface area for UMCM-1-OH was found to be 3705±177 m^2/g, which is an increase of 500 m^2/g from its protected analog, and UMCM-1-CAT was determined to be 3541±38 m^2/g, which is an increase of 900 m^2/g from its protected version. Previous PSM studies have shown that incorporating substituents into MOFs via PSM results in a decrease in BET surface area.[19] Likewise, the increase in surface area for UMCM-1-OH and UMCM-1-CAT appear to be consistent with the removal of the nitrobenzyl protecting groups. Geometric calculations of UMCM-1-$(OBnNO_2)_2$ and UMCM-1-CAT infer they should have BETs of 3493 and 4120 m^2/g, respectively.[20,21] Full isotherm analysis of both deprotected MOFs showed their overall uptake capacities were substantially higher. Their average pore size distributions were also found to increase from 7.5 to 7.9 Å using the Horvath-Kawazoe (H-K) model.

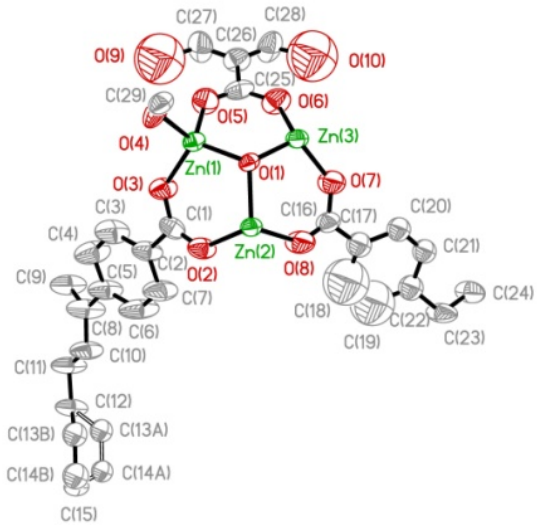

Figure 6-19. Asymmetric unit of UMCM-1-CAT with 50% probability ellipsoids and atom numbering scheme.

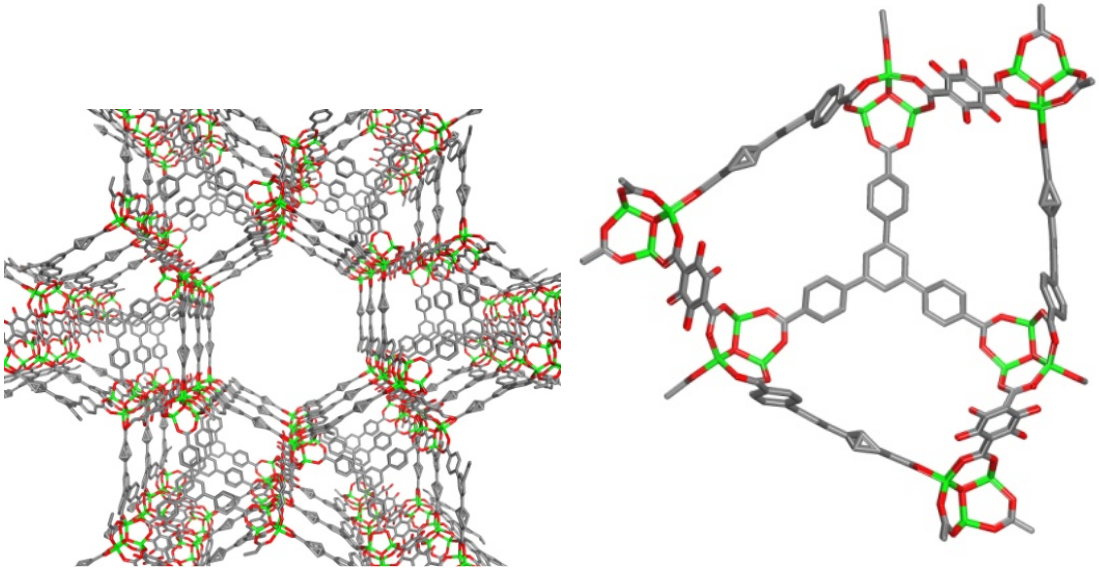

Figure 6-20. Single crystal X-ray structure of UMCM-1-OH with view of the framework (left) and small pore (right). Electron density for the oxygen atom of the hydroxyl group was located and assigned (disordered over four positions).

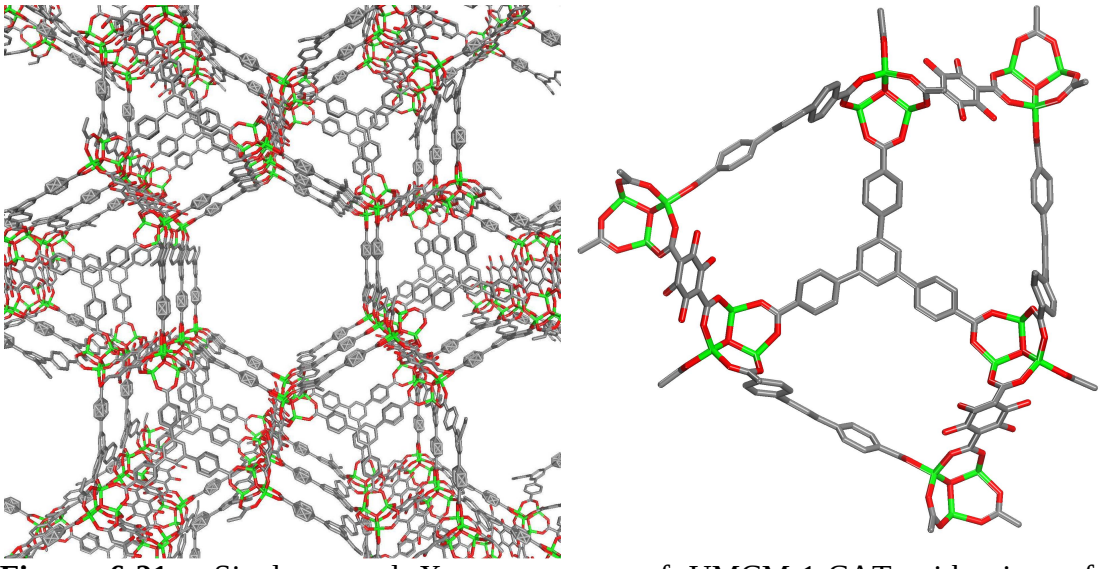

Figure 6-21. Single crystal X-ray structure of UMCM-1-CAT with view of the framework (left) and small pore (right). Electron density for the oxygen atoms of the hydroxyl groups was located and assigned (disordered over two positions).

UMCM-1-$(OBn)_2$ and UMCM-1-$(OBnNO_2(MeO)_2)_2$ were also suspended in EtOAc and exposed to 365 nm under similar conditions as UMCM-1-$(OBnNO_2)_2$. After 24 h, UMCM-1-$(OBn)_2$ did not undergo any significant color changes, but UMCM-1-$(OBnNO_2(MeO)_2)_2$ crystals did turn orange. ^{1}H NMR analysis of the digested frameworks showed no changes for UMCM-1-$(OBn)_2$ (Figure 6-22), but some reactivity was found for UMCM-1-$(OBnNO_2(MeO)_2)_2$, which was calculated to be <30% (Figure 6-23). After 48 h, the BnO-BDC ligand for UMCM-1-$(OBn)_2$ had significantly decomposed and only trace amounts could be seen in the ^{1}H NMR spectra. In contrast, UMCM-1-$(OBnNO_2(MeO)_2)_2$ appeared to remain intact, but deprotection was still <30%. Based on these results, it is clear that photochemical deprotection only occurs with a photolabile group, which was demonstrated with UMCM-1-$(OBn)_2$, but it appears that the MOF is not stable for prolonged periods under UV light. Alternatively, it was anticipated that UMCM-1-$(OBnNO_2(MeO)_2)_2$ would react more quickly than UMCM-1-

$(OBnNO_2)_2$, but instead the reaction was very slow. This suggests several possibilities: 1) the MOF morphology may not be ideal for efficient deprotection; 2) the nitrosbenzaldehyde byproduct may be lingering within the pores of the framework and preventing UV light from reaching further into the crystal. Since these studies are preliminary, optimization of the crystal quality (e.g., size and morphology) and photochemical deprotection conditions of UMCM-1-$(OBnNO_2(MeO)_2)_2$ should be conducted in order to develop a better understanding of how MOF morphology (and topology) plays a crucial role in the choice of protecting groups used.

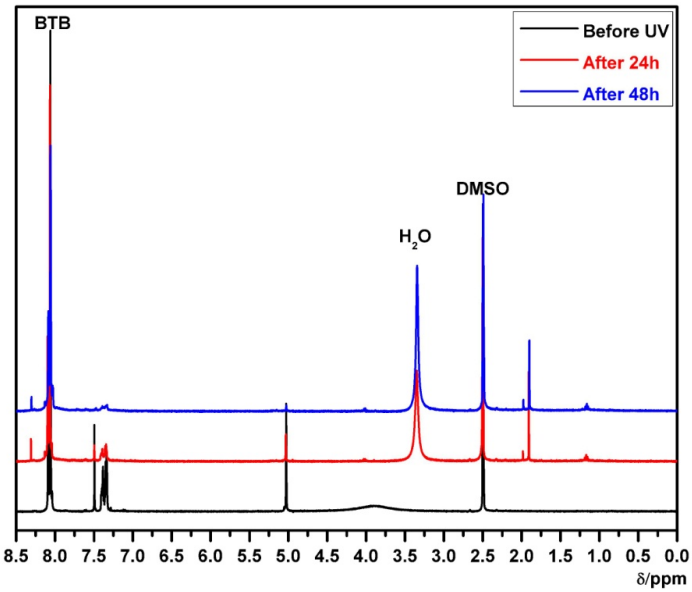

Figure 6-22. ^1H NMR comparison between digested UMCM-1-$(OBn)_2$ before UV exposure (black), digested UMCM-1-$(OBn)_2$ after 24 h in the photoreactor (red), and digested UMCM-1-$(OBn)_2$ (blue) after 48 h in the photoreactor.

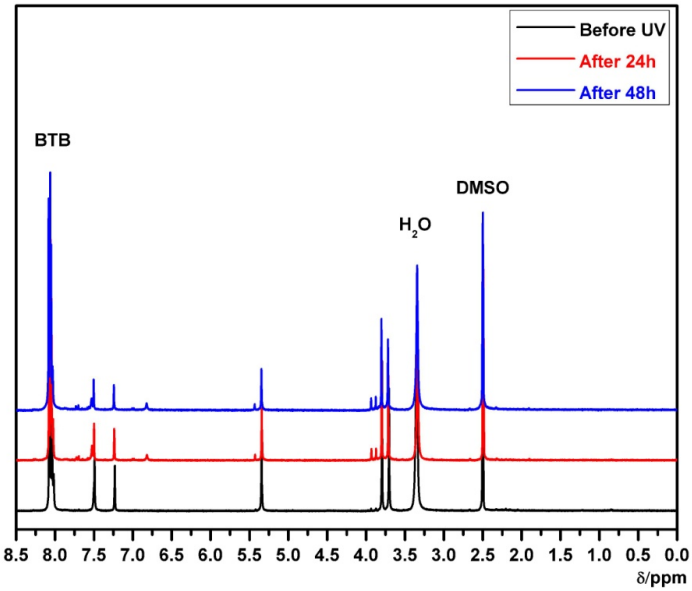

Figure 6-23. ^{1}H NMR comparison between digested UMCM-1-($OBnNO_2(MeO)_2)_2$ before UV exposure (black), digested ($OBnNO_2(MeO)_2)_2$ after 24 h in the photoreactor (red), and digested ($OBnNO_2(MeO)_2)_2$ (blue) after 48 h in the photoreactor.

6.2.4 Metallation attempts with UMCM-1-CAT

As further proof that free uncoordinated hydroxyl funcitonalities were obtained within the MOF, UMCM-1-CAT was metallated with $Fe(acac)_3$. Exposure of UMCM-1-CAT to a solution of $Fe(acac)_3$ in EtOAc resulted in a distinct color change from orange to red-purple. The change in color was found to be consistent with known Fe^{3+} catechol complexes (Figure 6-24).[22,23] When protected UMCM-1-($OBnNO_2)_2$ was subjected to $Fe(acac)_3$, the crystals turned pale orange, but did not exhibit the intense color change as UMCM-1-CAT. Metallated, and as well non-metallated, UMCM-1-($OBnNO_2)_2$ and UMCM-1-CAT were analyzed by diffuse reflectance solid-state electronic spectroscopy. UMCM-1-($OBnNO_2)_2$ did not show any significant absorbance above 400 nm. In contrast, UMCM-1-CAT had a distinct shoulder around 400 nm, which was indicative of

the catechol substituent. When UMCM-1-CAT and UMCM-1-$(OBnNO_2)_2$ were exposed to $Fe(acac)_3$, both MOFs showed a new absorbance band around 500 nm. The absorbance band was found to be more prominent for UMCM-1-FeCAT, and the catechol absorbance band around 400 nm was significantly reduced as a result of metal binding (Figure 6-25).

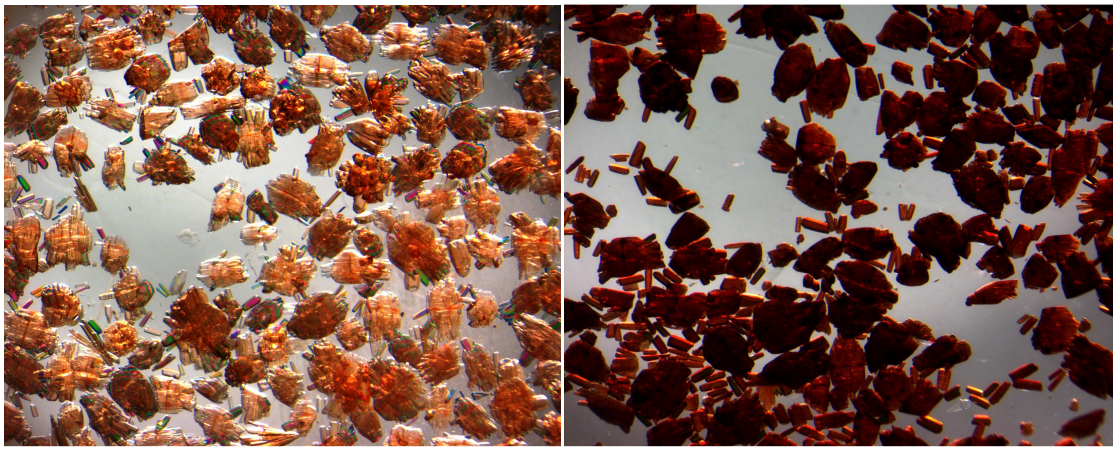

Figure 6-24. Single crystals of UMCM-1-$(OBnNO_2)_2$ treated with $Fe(acac)_3$ (left) and UMCM-1-FeCAT (right).

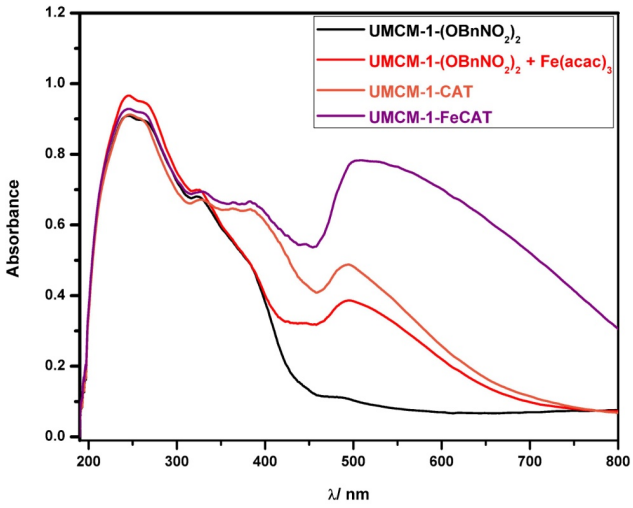

Figure 6-25. Diffuse reflectance solid-state UV-Vis spectra of UMCM-1-$(OBnNO_2)_2$, UMCM-1-$(OBnNO_2)_2$ treated with $Fe(acac)_3$, UMCM-1-CAT, and UMCM-1-FeCAT.

Several attempts were made to try and obtain a single crystal structure of UMCM-1-FeCAT. Unfortunately, no trace of Fe^{3+} electron density was located in the difference map, therefore suggesting metal binding within UMCM-1-FeCAT was much lower than anticipated. UMCM-1-FeCAT does contain Fe^{3+} ions, which can be seen by eye and by diffuse reflectance UV-Vis, but $Fe(acac)_3$ does not appear to be successfully diffusing through the pores of the framework. Closer inspection of the crystals revealed the expected Fe-catecholate color was not very intense, especially when the crystals were cracked open. Prolonged soaking in $Fe(acac)_3$ solutions (e.g., up to 3 days) and with heating (e.g., 55°C) did not seem to improve metal binding. Other attempts were made using $Fe(OTf)_3$ and $FeCl_3$ as the metal salts dissolved in either EtOAc or 10% MeOH in $CHCl_3$; however, the crystal quality was greatly reduced and were not suitable for powder or single crystal X-ray diffraction. Other metal salts were tested with the UMCM-1-CAT system, including Cp_2TiCl_2, $Al(acac)_3$, $Al(OTf)_3$, $Zr(acac)_4$, $Mg(acac)_2$, $Mg(OTf)_2$, $Cu(OTf)_2$, and $Cu(acac)_2$. Distinct color changes were observed with Cp_2TiCl_2 (red black) and $Cu(OTf)_2$ (brown), which suggested successful metal binding was occurring. Unfortunately, the single crystallinity was diminished, and BET surface area measurements for the samples were noticeably reduced from 3500 m^2/g to 1700 m^2/g. With the other metal salts, initial metal binding was detected by using a handheld UV lamp. UMCM-1-CAT fluoresces blue (λ_{ex} = 365 nm), which is characteristic of the CAT-BDC ligand and is not observed with UMCM-1-$(OBnNO_2)_2$. The fluorescence was found to change depending on the metal ion, which indirectly suggested metal binding was occurring. However, the crystal quality was not very good, as indicated by PXRD

analysis, and no single crystal X-ray structure could be obtained with the metal ion chelating to the catechol substituents.

It has proven to be fairly difficult to metalate the majority of catechol groups even though the protecting groups have been clearly removed in UMCM-1-CAT and the MOF has remained highly porous. Metal ions should have no problems diffusing within the pores of UMCM-1-CAT, but this seems to be the opposite case. UMCM-1-CAT has a large hexagonal pore bordered primarily by BTB and a smaller pore consisting of BTB and CAT-BDC. Metal ions should easily diffuse into the larger hexagonal pore; however, the size and shape of the smaller pore may affect metal ion accessibility of the catechol substituents. The smaller pore has two CAT-BDC ligands adjacent to each other, and it is possible that both catechol substituents may be too close in proximity to one another, which could make it more difficult for chelation to occur.[18]

6.2.5 Synthesis of functionalized BTB ligand

The UMCM system is built from two similar, yet different ligands: BDC, which is a ditopic ligand, and BTB, which is a tritopic ligand. Many different UMCM structures have been reported using various functionalized BDC ligands, including BDC, NH_2-BDC, 1,4-naphthalenedicarboxylic acid (NDC), thiophenedicarboxylic acid (TDC), and the benzyl protected BDC ligands presented earlier in this chapter.[27] Alternatively, there has only been one report of a functionalized BTB ligand. Recently, Kaskel and coworkers developed a BTB ligand with pendant chiral oxazolidinones groups and were able to synthesize a MOF.[28] After completing the PSD studies, it was hypothesized that a UMCM MOF could be constructed with a ligand that could undergo PSM and another

ligand that could undergo PSD. There have been no reports of a bifunctionalized UMCM, and no reports utilizing PSM and PSD in tandem. Herein, attempts were made to develop a hydroxyl functionalized BTB ligand and protect the hydroxyl group with a photolabile protecting group (Scheme 6-4).

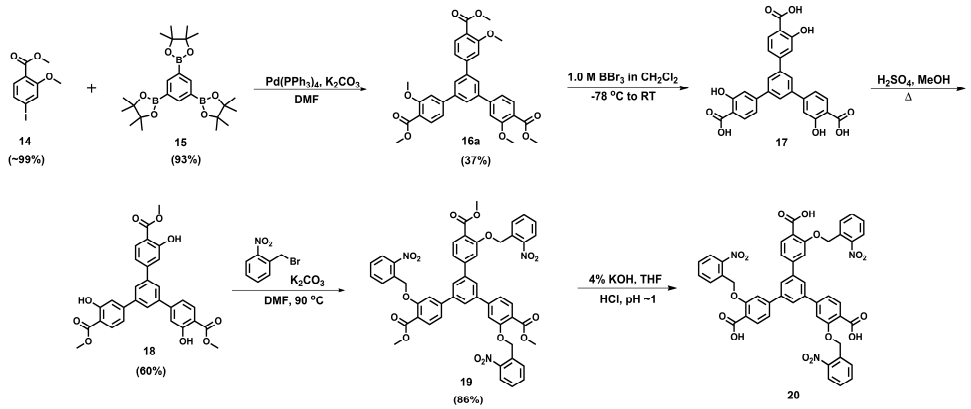

Scheme 6-4. Synthetic scheme for **20**.

Several different synthetic schemes were developed to synthesize **20**. The initial plan was to protect methyl-4-iodo-2-hydroxybenzoate with 2-nitrobenzyl bromide, perform a Suzuki coupling between **13** and **14** to obtain **19**, and hydrolyze the methyl esters to obtain **20** (Scheme 6-5). After performing the Suzuki coupling under different reaction conditions, it became apparent that the nitrobenzyl group was not compatible with the Suzuki coupling conditions and was being removed in situ. Therefore, **14** was synthesized and then coupled with **15** to form the tritopic ligand (**16a**). After purifying the crude mixture, the **16a** was isolated as a beige solid at 30-40% yield. In addition to obtaining the tritopic ligand, **14** underwent homocoupling with itself and its ditopic form (**16b**) was isolated as an orange solid in 10% yield (Scheme 6-6). ^{1}H NMR analysis and ESI-MS confirmed the identities of the two products. **16a** was subjected to BBr_3 and the

methyl ester and methoxy groups were removed to yield crude **17**. Direct esterification of crude **17** resulted in pure methyl ester product (**18**) in 60% yield over two steps.

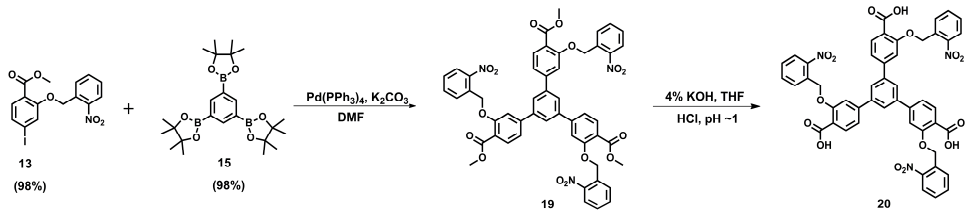

Scheme 6-5. Initial proposed synthetic scheme for **20**.

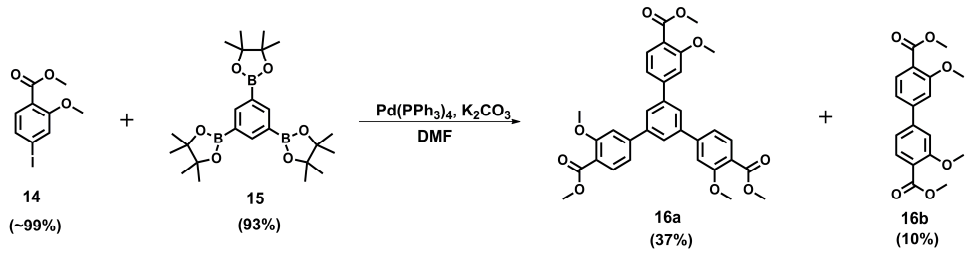

Scheme 6-6. Synthesis of **16a** and **16b**.

19 was prepared from **18** and *o*-nitrobenzyl bromide in moderate yield (80%). Unfortunately, **19** was found to be highly insoluble in polar solvents (e.g., MeOH, THF), which made it very difficult to hydrolyze the methyl esters and obtain **20**. Prolonged stirring at RT did not improve the solubility of **19**. Refluxing **19** in THF:4% KOH caused the ligand to become soluble, but resulted in the simultaneous removal of the nitrobenzyl groups. Other carboxylic acid protecting groups were tested (e.g., ethyl, Boc), but similar solubility problems were also encountered.

6.2.6 Conclusions and Future Directions

Two ligands, HO-BDC and CAT-BDC, were protected using *o*-nitrobenzyl groups to yield two photolabile ligands, $((NO_2BnO)_2$-BDC and $((NO_2BnO)_2$-BDC. The

ligands were used to synthesize two photolabile MOFs: UMCM-1-$OBnNO_2$ and UMCM-1-$(OBnNO_2)_2$. After exposing both MOFs to UV light, the photolabile groups were removed and two hydroxyl containing MOFs, UMCM-1-OH and UMCM-1-CAT, were obtained. This is the first example of using UV light to remove photolabile groups within MOFs to yield frameworks with hydroxyl functionalities and with increased porosities. More importantly, UMCM-1-CAT is the first report of MOF containing a catechol substituent.

Preliminary metalation studies were conducted with UMCM-1-CAT; however, UMCM-1-CAT did not undergo quantitative metalation as anticipated. Many different metal sources were explored with UMCM-1-CAT using various reaction conditions. Further studies will be needed to explore the pore environment of UMCM-1-CAT and how the catechol groups affect metal ion diffusion and chelation. For example, solvent activation of the MOF may be more crucial than initially anticipated. As mentioned earlier, photochemical deprotection of UMCM-1-$OBnNO_2$ and UMCM-1-$(OBnNO_2)_2$ was best achieved using EtOAc as the solvent while $CHCl_3$ and DMF affected crystallinity. Similarly, preliminary tests using EtOAc soaked samples for gas sorption analysis resulted in poor BET surface areas. When the solvent was switched back to $CHCl_3$, better quality BET measurements were obtained. Once metalation has been achieved with UMCM-1-CAT, the metallated UMCM-1-CAT may show potential for a variety of different applications ranging from potential H_2 storage,[24] CO_2 capture,[25] and Lewis acid catalysis.[26]

Two other benzyl containing MOFs, UMCM-1-$(OBn)_2$ and UMCM-1-$(OBnNO_2(MeO)_2)_2$, were also prepared and exposed to UV light. UMCM-1-$(OBn)_2$ was

found to not be photolabile, as expected, and decomposed under prolonged UV exposure. UMCM-1-($OBnNO_2(MeO)_2)_2$ unfortunately did not undergo complete photochemical deprotection despite containing a more photolabile protecting group in comparison with UMCM-1-($OBnNO_2)_2$. Further studies should be conducted with UMCM-1-($OBnNO_2(MeO)_2)_2$ in order to understand the difference in photochemical deprotection rates. This may require revisiting the synthesis of UMCM-1-($OBnNO_2(MeO)_2)_2$ and improving the crystal growth (e.g., morphology) and then optimizing the photochemical deprotection conditions (e.g., time, solvent).

Lastly, a new hydroxyl BTB ligand was synthesized with the goal of developing a bifunctionalized UMCM MOF. Synthesis of **18** was accomplished, but **20** could not be achieved. After protecting **18** with *o*-nitrobenzyl, **19** proved to have very poor solubility, and therefore could not undergo hydrolysis to yield **20**. Its precursors, **17**/**18**, are still promising ligands that can be protected with other hydroxyl protecting groups or other functional substituents. Ultimately, the goal would be to protect the hydroxyl groups of **18**, and as a starting point, mix the ligand with NH_2-BDCand $Zn(NO_3)_2$ to yield a UMCM MOF that can undergo PSM and PSD. The amino groups would be modified first, and then the photolabile groups would be removed afterwards to unmask the hydroxyl functionality. This dual postsynthetic approach has great potential because it would allow for two different functionalities to be present within the framework. The overall distribution and location of the functional groups would be known since they are situated on similar, but different ligands (e.g., tritopic vs. ditopic). Modification of either functionality can be controlled via the reaction conditions. Moreover, having a

bifunctional system may lead to the discovery of new materials for various applications, such as MOFs catalysts that resemble biomimetic systems.

6.3 Experimental Methods

General. Starting materials and solvents were purchased and used without further purification from commercial suppliers (Sigma-Aldrich, Alfa Aesar, EMD, TCI, Cambridge Isotope Laboratories, Inc., and others). $^{1}H/^{13}C$ NMR spectra were recorded on a Varian FT-NMR spectrometer (400 or 500 MHz). Elemental analysis was performed by NuMega Resonance Laboratories, San Diego, CA. 4,4',4''-Benzene-1,3,5-triyl-tribenzoic acid[29] (BTB) was synthesized as reported in Chapter 3. 2-hydroxy-1,4-benzenedicarboxylic acid (**1**), and 2,3-dihydroxy-1,4-benzenedicarboxylic acid (**5**) were synthesized according to literature procedures.[13,16]

Dimethyl 2-hydroxyterephthalate (2). **1**[13] (2.42 g, 13.3 mmol) was dissolved in 250 mL of MeOH. Conc. H_2SO_4 (5 mL) was added and the solution was refluxed overnight (~18 h). Upon cooling the reaction to room temperature, the MeOH was removed under vacuum. The remaining solution was neutralized with saturated $NaHCO_3$ (aq) solution and the product was extracted with CH_2Cl_2 (3×50 mL). The organic layer was isolated, washed with brine (4×15 mL), and the CH_2Cl_2 was removed under vacuum to obtain a white solid. Yield: 2.65 g (95%). ^{1}H NMR ($CDCl_3$, 400 MHz, 25°C): δ 3.92 (s, 3H; CO_2CH_3), 3.98 (s, 3H; CO_2CH_3), 7.52 (dd, 3*J*(H,H)=8 Hz, 4*J*(H,H)=1.6 Hz, 1H; ArH), 7.63 (d, 4*J*(H,H)=1.6 Hz, 1H; ArH), 7.90 (d, 3*J*(H,H)=8.4 Hz, 1H; ArH). ^{13}C NMR ($CDCl_3$, 100 MHz, 25 °C): *δ* 52.5, 52.6, 115.7, 118.8, 119.7, 130.0, 136.4, 161.2, 165.9, 169.9. ESI-MS(+): *m/z* 209.23 $[M-H]^-$.

Dimethyl 2-((2-nitrobenzyl)oxy)terephthalate (3). **2** (1.83 g, 8.7 mmol) was dissolved in 40 mL of DMF. 2-nitrobenzyl bromide (2.26 g, 10.4 mmol) and K_2CO_3 (2.4g, 17.3 mmol) were added and the mixture was stirred at 85 °C for 2 h. After cooling to room temperature, the K_2CO_3 was filtered off, and the solvent removed under vacuum to reveal a slightly orange solid. Yield: 2.74 g (90%). ^{1}H NMR ($CDCl_3$, 400 MHz, 25°C): δ 3.95 (s, 3H; CO_2CH_3), 3.95 (s, 3H; CO_2CH_3), 5.62 (s, 2H, CH_2) 7.52 (t, 3*J*(H,H)=8 Hz, 5*J*(H,H)=0.8 Hz,1H; ArH), 7.74 (q, 3*J*(H,H)=7.6 Hz, 4*J*(H,H)=1.2 Hz, 3H; ArH), 7.92 (d, 2*J*(H,H)=8 Hz, 1H; ArH), 8.22 (t, 3*J*(H,H)=8 Hz, 4*J*(H,H)=1.2 Hz, 2H; ArH). ^{13}C NMR ($CDCl_3$, 100 MHz, 25 °C): *δ* 52.3, 52.6, 67.7, 114.0, 122.0, 124.2, 124.9, 128.4, 128.8, 131.9, 133.1, 134.3, 134.8, 146.6, 157.3, 165.7, 165.9. ESI-MS(+): *m/z* 345.87$[M+H]^+$, 362.79$[M+NH4]^+$, 368.07$[M+Na]^+$.

2-((2-nitrobenzyl)oxy)terephthalic acid (4). **3** (2.47 g, 7.1 mmol) was dissolved in 80 mL THF followed by the addition of 4% KOH (aq) (80 mL). After stirring the solution at room temperature for 2 h, the solution was diluted with water (50 mL) and washed with diethyl ether twice (25 mL). The aqueous layer was collected and acidified to pH~1 with concentrated HCl to precipitate out an off white solid. The solid was collected via vacuum filtration, washed with H_2O, and dried under vacuum with heat. Yield: 2.2 g (98%). ^{1}H NMR (*d6*-DMSO, 400 MHz, 25°C): δ 5.60 (s, 2H; CH_2), 7.62 (m, 3H; ArH), 7.78 (d, 3*J*(H,H)=8 Hz, 1H; ArH), 7.82 (t, 3*J*(H,H)=7.6 Hz, 4*J*(H,H)=1.2 Hz, 1H; ArH), 8.06 (d, 3*J*(H,H)=8 Hz, 1H; ArH), 8.16 (dd, 3*J*(H,H)=8 Hz, 4*J*(H,H)=1.2 Hz, 1H; ArH). ^{13}C NMR (d^6-DMSO, 100 MHz, 25 °C): *δ* 67.4, 114.2, 122.1, 125.3, 126.0, 129.2, 129.4, 131.4, 133.1, 134.6, 135.2, 147.2, 146.8, 166.9, 167.1. ESI-MS(-): *m/z* 316.17$[M-H]^-$.

Preparation of UMCM-1-OBnNO$_2$. $Zn(NO_3)_2 \cdot 6H_2O$ (3.26 g, 10.9 mmol), 4,4',4''-benzene-1,3,5-triyl-tribenzoic acid (0.4 g, 0.91 mmol), and **4** (0.87 g, 2.75 mmol) were dissolved in 100 mL DMF. The solution was sonicated and divided into 10 mL portions and transferred to 10 scintillation vials (20 mL capacity each). The vials were placed in a sand bath and the bath was placed in an isothermal oven heated at 85 °C for 48 h. Clear needle clusters were found in each vial. Once the vials were cooled to room temperature, the mother liquor was decanted and the crystals were washed with DMF (3×10 mL), rinsed with $CHCl_3$ (2×10 mL) and left to sit for 3 days with fresh $CHCl_3$ added every 24 h. The crystals were stored in $CHCl_3$ until needed. The average yield of dried UMCM-1-OBnNO$_2$ per vial was approximately 40 mg (37% based on BTB, 0.038 mmol per ligand). Anal. Calcd for $Zn_4O(C_{27}H_{15}O_6)_{1.33}$ ($C_{15}H_9NO_7$): C, 52.18; H, 2.49; N, 1.20. Found: C, 52.09; H, 3.78; N, 1.27. *Upon photochemical deprotection to UMCM-1-OH:* Anal. Calcd for $Zn_4O(C_{27}H_{15}O_6)_{1.33}$ ($C_8H_4O_5$): C, 50.87; H, 2.33; N, 0. Found: C, 50.99; H, 3.23; N, 0.43.

UMCM-1-OH Direct Synthesis Attempt. **1** (0.51 g, 2.8 mmol), BTB (0.4 g, 0.91 mmol), and $Zn(NO_3)_2 \cdot 6H_2O$ (3.26 g, 10.9 mmol) were dissolved in 100 mL DMF. The solution was sonicated, divided into 10 mL portions, and transferred to 10 scintillation vials (20 mL capacity each). The vials were placed in a sand bath and the bath was placed in an oven and heated to 85 °C for 48 h. No solid products were generated.

Dimethyl-2,3-dihydroxyterephthalate (6). **5**[16] (10 g, 50 mmol) was dissolved in 250 mL MeOH. Conc. H_2SO_4 (~2 mL) was added and the solution was refluxed overnight. After cooling the reaction to room temperature, MeOH was removed under

vacuum to yield a brown solid. The crude solid was neutralized with sat. $NaHCO_3$ and the product was extracted using CH_2Cl_2. The organic layers were combined, dried with $MgSO_4$, filtered, and concentrated under vacuum to yield a light beige solid. Yield: 6.9 g (60%). ^{1}H NMR ($CDCl_3$, 400 MHz, 25°C): δ 3.99 (s, 6H), 7.34 (s, 2H), 10.94 (s, 2H). ^{13}C NMR ($CDCl_3$, 100 MHz, 25 °C): *δ* 52.9, 116.0, 118.5, 151.7, 170.3. ESI-MS(+): *m/z* 227.05 $[M+H]^+$, 243.93 $[M+NH_4]^+$.

Dimethyl-2,3-bis(nitrobenzyl(oxo))terephthalate (7). **6** (2.0 g, 8.8 mmol) was dissolved in 60 mL DMF. 2-nitrobenzyl bromide (4.2 g, 19 mmol, 2.2 eq) and K_2CO_3 (5.1 g, 37 mmol, 4.2 eq) were subsequently added and the mixture was left to stir at 80 °C for 2 h. After cooling the mixture to room temperature, H_2O was added to the solution to precipitate out the crude product. A pale yellow solid was isolated by vacuum filtration and was washed with copious amounts of H_2O to remove K_2CO_3 and DMF. The solid was then washed with MeOH to remove any unreacted nitrobenzyl bromide. An off white solid was obtained and dried under vacuum. Yield: 3.7 g (85%). ^{1}H NMR ($CDCl_3$, 400 MHz, 25°C): δ 3.84 (s, 6H), 5.47 (s, 4H), 7.35 (dt, 2H, *J* = 0.8 Hz, 7.8 Hz), 7.54 (dt, 2H, *J* = 1.2 Hz, 7.6 Hz), 7.68 (s, 2H), 7.90 (dd, 2H, *J* = 1 Hz, 7.8 Hz), 7.99 (dd, 2H, *J* = 1.2 Hz, 8 Hz). ^{13}C NMR ($CDCl_3$, 100 MHz, 25 °C): *δ* 52.8, 72.9, 124.7, 126.5, 128.1, 128.2, 130.0, 134.0, 134.3, 146.3, 152.7, 165.5. ESI-MS(+): *m/z* 519.17 $[M+NH_4]^+$, 520.19 $[M+Na]^+$.

2,3-bis(nitrobenzyl(oxo)terephthalic acid (8). **7** (2.0 g, 4.0 mmol) was dissolved in 80 mL of THF. 4% KOH (aq) (80 mL) was added to the solution and the reaction was left stirring at room temperature for 2 h. After removing THF under vacuum, the solution was filtered and washed once with diethyl ether. The solution was

subsquently acidified to pH~1 using a 1M HCl solution resulting in an off white solid. The off white solid was collected by vacuum filtration, washed with copious amounts of H_2O, and dried under vacuum with heat. Yield: 1.7 g (94%). ^{1}H NMR (d^6-DMSO, 400 MHz, 25°C): δ 5.36 (s, 4H), 7.50 (t, 2H, *J* = 7.6 Hz), 7.58 (s, 2H), 7.63 (t, 2H, *J* = 7.6 Hz), 7.79 (d, 2H, *J*= 8 Hz), 8.00 (d, 2H, *J* = 8.4 Hz). ^{13}C NMR (d^6-DMSO, 100 MHz, 25 °C): *δ* 72.9, 125.0, 126.3, 129.1, 129.2, 131.3, 133.5, 134.5, 146.9, 151.7, 166.9. ESI-MS(+): *m/z* 466.92 $[M+H]^+$.

UMCM-1-($OBnNO_2$)$_2$ synthesis. **8** (1.26 g, 2.7 mmol), BTB (0.34 g, 0.78 mmol), and $Zn(NO_3)_2 \cdot 6H_2O$ (3.22 g, 10.8 mmol) was dissolved in 100 mL of DMF by sonication. The solution was split into 10 mL portions and placed into 20 mL scintillation vials. The vials were then transferred to an isothermal oven at 85 °C for 48 h. Colorless needle clusters were found in all vials. The needle clusters were washed with DMF (3×10 mL) and soaked in $CHCl_3$ (12 mL) overnight. After 24 h, the $CHCl_3$ was decanted from the vial and fresh $CHCl_3$ was added. The solution was replaced with fresh $CHCl_3$ every 24 h for a total of 3 days and the crystals were stored in $CHCl_3$ until further used. Yield: 50 mg (49% based on BTB, 0.04 mmol per ligand). Anal. Calcd for $Zn_4O(C_{27}H_{15}O_6)_{1.33}(C_{22}H_{14}N_2O_{10})$: C, 52.57; H, 2.59; N, 2.12. Found: C, 51.71; H, 3.95; N, 2.24. *Upon photochemical deprotection to UMCM-1-CAT:* Anal. Calcd for $Zn_4O(C_{27}H_{15}O_6)_{1.33}$ $(C_8H_4O_6)_{0.75}(C_{15}H_9NO_8)_{0.125}(C_{22}H_{14}N_2O_{10})_{0.125}$: C, 50.65; H, 2.36; N, 0.48. Found: C, 48.49; H, 3.82; N, 0.85.

UMCM-1-CAT Direct Synthesis Attempt. **5** (0.053 g, 0.027 mmol), BTB (0.034 g, 0.078 mmol), and $Zn(NO_3)_2 \cdot 6H_2O$ (0.322 g, 1.23 mmol) were dissolved in either 10 mL of DEF or DMF with sonication. The vials were then transferred to an oven

and heated at 85 °C for 48 h. A dark orange-brown solid was found in reaction mixtures using either DEF or DMF as solvent. PXRD analysis of the products indicated that neither material was UMCM-1-CAT.

Dimethyl-2,3-bisbenzyl terephthalate (9). **6** (1.0 g, 4.4 mmol) was dissolved in 30 mL DMF. Benzyl bromide (2.1 mL, 17.6 mmol, 4 eq) and K_2CO_3 (3 g, 21.7 mmol, 5 eq) were subsequently added and the mixture was left to stir at 80 °C for 1 h. After cooling the mixture to room temperature, the crude product was extracted using brine and $CHCl_3$. The $CHCl_3$ layer was isolated, dried with $MgSO_4$, filtered, and concentrated by vacuum to yield an orange oil. After allowing the oil to cool down back to RT, MeOH was added and an off white solid precipitated. The solid was isolated by vacuum filtration and washed with MeOH. The filtrate was then reisolated and concentrated until solid precipitated again. The solid was isolated by vacuum filtration and combined with the previous product. Yield: 1.4 g (78%). ^{1}H NMR ($CDCl_3$, 400 MHz, 25°C): δ 3.88 (s, 6H), 5.13 (s, 4H), 7.35-7.43 (m, 12H), 7.56 (s, 2H). ESI-MS(+): *m/z* 407.17 $[M+H]^+$, 423.93 $[M+NH_4]^+$, 429.10 $[M+Na]^+$.

2,3-bisbenzyl(oxo)terephthalic acid (10). **9** (1.0 g, 4.0 mmol) was dissolved in 20 mL of THF. 4% KOH (aq) (20 mL) was added to the solution and the reaction was left stirring at room temperature for 2 h. After removing THF under vacuum, the solution was filtered and washed once with diethyl ether. The solution was subsequently acidified to pH~1 using a 1M HCl solution resulting in a white solid. The white solid was collected by vacuum filtration, washed with copious amounts of H_2O, and dried under vacuum with heat. Yield: 0.71 g (77%). ^{1}H NMR (*d*^{6}-DMSO, 400 MHz, 25°C): δ 5.03 (s, 4H), 7.34-7.39 (m, 12H), 7.50 (s, 2H). ESI-MS(-): *m/z* 377.00 $[M-H]^-$.

UMCM-1-(OBn)$_2$ synthesis. **10** (0.51 g, 1.3 mmol), BTB (0.17 g, 0.39 mmol), and $Zn(NO_3)_2 \cdot 6H_2O$ (1.60 g, 5.4 mmol) was dissolved in 50 mL of DEF by sonication. The solution was split into 5 mL portions and placed into 10 mL scintillation vials. The vials were then transferred to an isothermal oven at 85 °C for 48 h. Pale yellow clusters were found in all vials. The clusters were washed with DMF (3×10 mL) and soaked in $CHCl_3$ (12 mL) overnight. After 24 h, the $CHCl_3$ was decanted from the vial and fresh $CHCl_3$ was added. The solution was replaced with fresh $CHCl_3$ every 24 h for a total of 3 days and the crystals were stored in $CHCl_3$ until further used. Yield: 25 mg (52% based on BTB, 0.02 mmol per ligand).

Dimethyl-2,3-bis((4,5-dimethoxy-2-nitrobenzyl)oxy)terephthalate (11). **6** (1.0 g, 4.4 mmol) was dissolved in 30 mL DMF. 4,5-dimethoxy-2-nitrobenzyl bromide (2.7 g, 9.6 mmol, 2.2 eq) and K_2CO_3 (2.6 g, 18.8 mmol, 4.2 eq) were subsequently added and the mixture was left to stir at 80 °C for 1 h. After cooling the mixture to room temperature, H_2O was added to the solution to precipitate out the crude product. A yellow solid was isolated by vacuum filtration and was washed with copious amounts of H_2O to remove K_2CO_3 and DMF. The solid was then washed with MeOH to remove any unreacted benzyl bromide. A pale solid was obtained and dried under vacuum. Yield: 2.3 g (85%). ^{1}H NMR ($CDCl_3$, 400 MHz, 25°C): δ 3.87 (s, 6H), 3.89 (s, 6H), 3.92 (s, 6H), 5.49 (s, 4H), 7.35 (s, 2H), 7.60 (s, 2H), 7.70 (s, 2H). ESI-MS(+): *m/z* 634.13 $[M+NH_4]^+$, 639.16 $[M+Na]^+$, 655.10 $[M+K]^+$.

2,3-bis((4,5-dimethoxy-2-nitrobenzyl)oxy)terephthalic acid (12). **11** (1.0 g, 1.6 mmol) was dissolved in 40 mL of THF. 4% KOH (aq) (40 mL) was added to the solution and the reaction was left stirring at room temperature for 2 h. After removing THF under

vacuum, the solution was filtered and washed once with diethyl ether. The solution was subsequently acidified to pH~1 using a 1M HCl solution resulting in a pale yellow solid. The pale yellow solid was collected by vacuum filtration, washed with copious amounts of H_2O, and dried under vacuum with heat. Yield: 0.93 g (99%). ^{1}H NMR ($CDCl_3$, 400 MHz, 25°C): δ 3.75 (s, 6H), 3.81 (s, 6H), 5.34 (s, 4H), 7.27 (s, 2H), 7.52 (s, 2H), 7.58 (s, 2H). ESI-MS(-): *m/z* 587.12 $[M-H]^-$.

UMCM-1-($OBnNO_2(MeO)_2)_2$ synthesis. **12** (1.58 g, 2.7 mmol), BTB (0.42 g, 0.96 mmol), and $Zn(NO_3)_2 \cdot 6H_2O$ (3.22 g, 10.8 mmol) was dissolved in 100 mL of DEF by sonication. The solution was split into 10 mL portions and placed into 20 mL scintillation vials. The vials were then transferred to an isothermal oven at 85 °C for 48 h. Pale yellow clusters were found in all vials. The clusters were washed with DMF (3×10 mL) and soaked in $CHCl_3$ (12 mL) overnight. After 24 h, the $CHCl_3$ was decanted from the vial and fresh $CHCl_3$ was added. The solution was replaced with fresh $CHCl_3$ every 24 h for a total of 3 days and the crystals were stored in $CHCl_3$ until further used. Yield: 43 mg (31% based on BTB, 0.03 mmol per ligand).

Methyl-4-iodo-2-((2-nitrobenzyl)oxy)benzoate (13). Methyl-4-iodosalicyate (1.0 g, 3.6 mmol) was dissolved in 20 mL of DMF. K_2CO_3 (1.0 g, 7.6 mmol) and *o*-nitrobenzyl bromide (0.86 g, 4.0 mmol) was added and the mixture was placed in a preheated 80 °C oil bath. After heating for 2 h, the mixture was cooled down to RT and H_2O was added to precipitate out the crude orange product. The solid was washed with H_2O several times followed by MeOH washes to remove any unreacted nitrobenzyl bromide. A pale orange solid was obtained and was left to dry on the house vacuum.

Yield: 1.2 g (80%). ^{1}H NMR ($CDCl_3$, 400 MHz, 25°C): δ 3.91 (s, 3H), 5.53 (s, 2H), 7.41 (d, 1H, *J* = 7.2 Hz), 7.45 (s, 1H), 7.52 (t, 1H, *J* = 7.6 Hz), 7.59 (d, 1H, *J* = 8 Hz), 7.78 (t, 1H, *J* = 7.6 Hz), 8.22 (dd, 2H, *J* = 8 Hz).

Methyl-4-iodo-2-methoxybenzoate (14). The procedure was adapted from literature.[30] Methyl-4-iodosalicyate (4.8 g, 17.3 mmol) was dissolved in 20 mL of DMF. K_2CO_3 (9.6 g, 69.6 mmol) and methyl iodide (2.1 mL, 34.5 mmol) was added and the mixture was left to stir at RT for 2 h. The reaction was found to go to completion by TLC. K_2CO_3 was filtered from the reaction and the DMF solution was used without further purification for the next step. ^{1}H NMR ($CDCl_3$, 400 MHz, 25°C): δ 3.82 (s, 3H), 3.84 (s, 3H), 7.30 (s, 1H), 7.34 (d, 1H, *J* = 8.4 Hz), 7.45 (d, 1H, *J* = 8.4 Hz). ESI-MS(+): *m/z* 292.82 $[M+H]^+$.

1,3,5-tris(4,4,5,5-tetramethyl-1,3,2-dioxaborolan-2-yl)benzene (15). DMF (20 mL) was added to a flask containing 1,3,5-tribromobenzene (2.0 g, 6.4 mmol), bis(pinacolato)diboron (5.1 g, 20.1 mmol), $PdCl_2$(dppf) CH_2Cl_2 (0.164 g, 0.2 mmol), and KOAc (3.76 g, 38.3 mmol). The reaction mixture was placed in preheated oil bath at 90 °C and left stirring under N_2 overnight. The dark brown mixture was removed from the oil bath and left to cool to RT. H_2O was added to the flask and a light grayish brown solid was isolated by vacuum filtration. The crude product was washed with H_2O several times and was used without further purification. Yield: 2.7 g (93%). ^{1}H NMR ($CDCl_3$, 400 MHz, 25°C): δ 1.32 (s, 36 H), 8.36 (s, 3H). ESI-MS(+): *m/z* 474.09 $[M+NH_4]^+$.

Dimethyl-3,3''-dimethoxy-5'-(3-methoxy-4-(methoxycarbonyl)phenyl)-[1,1':3',1''-terphenyl]-4,4''-dicarboxylate (16a). The procedure was adapted from literature.[31] **15** (2.2 g, 4.8 mmol), $Pd(PPh_3)_4$ (1.6 g, 1.4 mmol), and K_2CO_3 (10.4 g, 75

mmol) were added to the **14** DMF solution followed by an additional 20 mL of DMF. The flask was placed in a preheated oil bath at 90 °C under N_2 and left stirring overnight. The flask was removed from the oil bath to cool down to RT. H_2O was added to the mixture, which caused a dark red brown solid to precipitate. The dark red brown solid was isolated by vacuum filtration and was redissolved in CH_2Cl_2. The CH_2Cl_2 was dried with $MgSO_4$, filtered, and then concentrated to yield a dark red oil. The red oil was purified twice via column chromatography (SiO_2, CH_2Cl_2, 10% EtOAc/CH_2Cl_2) to yield the pure product as a beige solid. Yield: 1.0 g (37%). ^{1}H NMR ($CDCl_3$, 400 MHz, 25°C): δ 3.91 (s, 3H), 3.98 (s, 3H), 7.21 (s, 1H, *J* = 1.6 Hz), 7.27 (dd, 1H, *J* = 1.6, 8 Hz), 7.78 (s, 1H), 7.93 (d, 1H, *J* = 8 Hz). ESI-MS(+): *m/z* 570.99 $[M+H]^+$.

Dimethyl-3,3'-dimethoxy-[1,1'-biphenyl]-4,4'-dicarboxylate (16b). The orange solid was isolated before **16a** eluted off the column. Yield: 0.3 g (10%). ^{1}H NMR ($CDCl_3$, 400 MHz, 25°C): δ 3.91 (s, 6H), 3.98 (s, 6H), 7.14 (s, 2H), 7.18 (d, 2H, *J* = 8 Hz), 7.88 (d, 2H, *J* = 8 Hz). ESI-MS(+): *m/z* 474.09 $[M+NH_4]^+$.

5'-(4-carboxy-3-hydroxyphenyl)-3,3''-dihydroxy-[1,1':3',1''-terphenyl]-4,4''-dicarboxylic acid (17). The procedure was adapted from literature.[30] **16a** (1 g, 1.75 mmol) was dissolved in dry CH_2Cl_2 and cooled to -78 °C in a dry ice/isopropanol bath under N_2. 1.0 M BBr_3 in CH_2Cl_2 (16 mL) was added to the pale yellow solution, which resulted in turning the solution red-brown. The solution was left to stir overnight while slowly warming up to RT. A yellow-orange solid was present in the flask and MeOH was slowly added to the mixture to quench any remaining BBr_3. After letting the reaction stir for several minutes, the solvent was removed under vacuum. The yellowish solid was redissolved in MeOH and the solvent was removed again. H_2O was then added to the

solid, and a crude off white solid was isolated by vacuum filtration, which was washed with H_2O several times. The crude solid was generally used directly in the esterification step. Attempts to purify the crude solid involved heating in hot EtOAc and isolating the white solid by vacuum filtration. No yields were obtained for either step. ^{1}H NMR ($CDCl_3$, 400 MHz, 25°C): δ 7.46 (d, 1H, *J* = 8 Hz), 7.52 (s, 1H), 7.86 (d, 1H, *J* = 8.4 Hz), 8.02 (s, 1H). ESI-MS(-): *m/z* 242.10 $[M-2H]^{2-}$, 484.95 $[M-H]^-$.

Dimethyl-3,3''-dihydroxy-5'-(3-hydroxy-4-(methoxycarbonyl)phenyl)-[1,1':3',1''-terphenyl]-4,4''-dicarboxylate (18). Crude **17** was dissolved in 100 mL of MeOH and ~2 mL of conc. H_2SO_4 and was refluxed for 24 h. During the reflux, an off white solid precipitated from solution, providing indirect confirmation that the methyl ester product had formed. The solution was cooled to RT and the MeOH was removed under vacuum. The solid was dissolved in CH_2Cl_2 and sat. $NaHCO_3$ was slowly added to the vigorously stirring solution until the solution became basic. The CH_2Cl_2 layer was then isolated and dried with $MgSO_4$, filtered, and then concentrated under vacuum to yield a pale yellow solid. Yield: 0.65 g (60%). ^{1}H NMR ($CDCl_3$, 400 MHz, 25°C): δ 3.99 (s, 9H), 7.20 (d, 3H, *J* = 8 Hz), 7.30 (s, 3H), 7.84 (s, 3H), 7.93 (d, 3H, *J* = 8.4 Hz), 10.85 (s, 3H).

Dimethyl-5'-(4-(methoxycarbonyl)-3-((2-nitrobenzyl)oxy)phenyl)-3,3''-bis((2-nitrobenzyl)oxy)-[1,1':3',1''-terphenyl]-4,4''-dicarboxylate (19). **18** (0.53 g, 1.0 mmol) was dissolved in 10 mL DMF and placed in a 90 °C oil bath. K_2CO_3 (0.9 g, 6.5 mmol) was added followed by the addition of *o*-nitrobenzyl bromide (0.72 g, 3.3 mmol). The mixture was stirred for 2 h and was cooled to RT. H_2O was added to precipitate out

the crude product as a pale yellow solid. The solid was washed with H_2O followed by MeOH to remove any unreacted *o*-nitrobenzyl bromide, resulting in a very light beige solid. Yield: 0.8 g (86%). ^{1}H NMR ($CDCl_3$, 400 MHz, 25°C): δ 3.97 (s, 9H), 5.69 9 (s, 6H), 7.35 (d, 3H, *J* = 8 Hz), 7.39 (s, 3H), 7.51 (t, 3H, *J* = 7.2 Hz), 7.79 (t, 3H, *J* = 8 Hz), 7.80 (s, 3H), 8.05 (d, 3H, *J* = 8 Hz), 8.16 (d, 3H, *J* = 8.4 Hz), 8.34 (d, 3H, *J* = 8 Hz).

MOF Synthesis Attempt with 18. Purified **18** (22 mg, 0.045 mmol) was dissolved in either 5 mL of DMF or DEF with $Zn(NO_3)_2 \cdot 6H_2O$ (94 mg, 0.32 mmol). The vials were transferred to an 85 °C oven and heated for 48 h. Orange crystalline spheres were present in the DMF vial while yellow powder was found in the DEF vial. PXRD analysis showed both products were different from one another and did not resemble MOF-177. Although the DMF vial did produce crystalline material, the crystals were not well formed and were not suitable for single crystal X-ray diffraction.

Digestion and Analysis by ^{1}H NMR. Approximately 5 mg of protected and deprotected UMCM was dried under vacuum at RT (or used immediately after BET analysis) and digested with sonication in 500 μL of d^6-DMSO and 100-200 μL of dilute DCl (23 μL of 35% DCl in D_2O diluted with 1.0 mL of d^6-DMSO).

Digestion and Analysis by ESI-MS. ESI-MS was performed using a ThermoFinnigan LCQ-DECA mass spectrometer, and the data was analyzed using the Xcalibur software suite. Samples for analysis by ESIMS were prepared by either 10 μL of digested ^{1}H NMR solution diluted in 0.5~1 mL of MeOH or by digesting protected and deprotected UMCM crystals (0.1~1 mg) in 1 mL of MeOH with sonication.

Thermal Analysis. Approximately 8-15 mg of protected and deprotected UMCM (dried after gas sorption analysis) was used for TGA measurements. Samples

were analyzed under a stream of dinitrogen using a TA Instrument Q600 SDT running from room temperature to 600 °C with a scan rate of 5 °C/min.

PXRD Analysis. Approximately 15 mg of as-synthesized UMCM (in DMF or EF), UMCM-1-$OBnNO_2$ and UMCM-1-OH (soaked in DMF), UMCM-1-$(OBnNO_2)_2$, UMCM-1-$(OBn)_2$, and UMCM-1-$(OBnNO_2(MeO)_2)_2$ (soaked in $CHCl_3$), or UMCM-1-CAT (soaked in toluene) was air dried before PXRD analysis. Powder X-ray diffraction (PXRD) data were collected at ambient temperature on a Bruker D8 Advance diffractometer at 40 kV, 40 mA for Cu Kα (λ = 1.5418 Å), with a scan speed of 3 or 5 sec/step, a step size of 0.02° in 2θ, and a 2θ range of 2-35°. The experimental backgrounds were corrected with either Eva 14 from the Bruker DIFFRACplus basic evaluation package or the Jade 5.0 software package.

BET Surface Area Analysis. Approximately 35-60 mg of protected and deprotected UMCM (previously soaking in $CHCl_3$) was evacuated on a vacuum line for a minimum of 2 h (protected UMCM) or a minimum of 5 min (deprotected UMCM) at RT. The sample was then transferred to a preweighed sample tube and degassed at 25 °C on an Micromeritics ASAP 2020 Adsorption Analyzer for a minimum of 12 h or until the outgas rate was <5 μmHg. The sample tube was re-weighed to obtain a consistent mass for the degassed protected or deprotected UMCM. BET surface area (m^2/g) measurements were collected on three independent samples of each MOF at 77 K by dinitrogen on an Micromeritics ASAP 2020 Adsorption Analyzer using volumetric technique. Pore size distribution was determined using the Horvath-Kawazoe model.

Single Crystal X-ray Diffraction. Single crystals of protected and deprotected UMCM in $CHCl_3$ were mounted on nylon loops with Paratone oil and placed under a

nitrogen cold stream (200 K). Data was collected on a Bruker Apex diffractometer using Mo Kα radiation (λ = 0.71073 Å) controlled using the APEX 2010 software package. A semiempirical method utilizing equivalents was employed to correct for absorption. All data collections were solved and refined using the SHELXTL suite. All protected and deprotected UMCM were treated with the "squeeze" protocol in PLATON to account for electron density associated with the nitrobenzyl substituents and for partially occupied or disordered solvent (e.g., $CHCl_3$) within the porous framework. Structural details are available at the CCDC under deposition numbers 786348, 786349, 786350, and 786351.

Photochemical deprotection - UMCM-1-OH. One vial of UMCM-1-$OBnNO_2$ (40 mg) was rinsed with EtOAc (3×10 mL) and transferred to a quartz vessel with 20 mL capacity. The solution was decanted and EtOAc (8 mL) was added. The vessel was placed inside a Rayonet RPR-200 photoreactor with 365 nm lamps. After irradiating the samples for 3 h, the yellow supernatant was decanted and the light orange crystals were rinsed with EtOAc (3×5 mL). Fresh EtOAc (8 mL) was added and the vessel was placed back inside the photoreactor chamber. This rinsing process was repeated once more at 20 h. After 24 h, the crystals were washed with EtOAc (3×10 mL) and exchanged back into $CHCl_3$ (2×10 mL) and soaked overnight in fresh $CHCl_3$ (10 mL).

Photochemical deprotection - UMCM-1-CAT. One vial of UMCM-1-$(OBnNO_2)_2$ (50 mg) was split into 10-15 mg portions and transferred to four scintillation vials (20 mL capacity). EtOAc (15 mL) was added to each vial and all four vials were placed inside a Rayonet RPR-200 photoreactor with 365 nm lamps. After irradiating the samples for 1-2 h the yellow supernatant was decanted. Fresh EtOAc (15 mL) was added to each vial and the vials were placed back inside the photoreactor chamber. In a typical

24 h period, the crystals were rinsed with $CHCl_3$ and resoaked in fresh EtOAc twice within a 12 hour span and were agitated once inbetween to ensure equal exposure. After 48 h, the four vials were recombined and the crystals were washed with EtOAc (3 x 10 mL). Samples for metallation were kept in EtOAc while gas sorption samples were washed with $CHCl_3$ (3 x 10 mL) and soaked overnight in fresh $CHCl_3$ (12 mL).

Photochemical deprotection - UMCM-1-CAT optimized: EtOAc (15 mL) was added to one vial of UMCM-1-$(OBnNO_2)_2$ and a glass plunger was used to lightly crush the needle clusters. The vial was then placed inside a Rayonet RPR-200 photoreactor with 365 nm lamps. After irradiating the sample for 1 h, the yellow supernatant was decanted and fresh EtOAc (15 mL) was added to the vial. Any remaining crystal clusters were lightly crushed with the glass plunger again and the sample was transferred back into the photoreactor chamber. The crystals were then resoaked in fresh EtOAc (15 mL) after another 1-2 h. In a typical 24 h period, the supernatant was replaced with fresh EtOAc 2-3 times. After 48 h, the crystals were washed with EtOAc (3 x 10 mL), washed with $CHCl_3$ (3 x 10 mL), and soaked overnight in fresh $CHCl_3$ (12 mL). ^1H NMR analysis of UMCM-1-CAT showed an improved ~85% deprotection.

UMCM-1-$(OBnNO_2)_2$ treated with $Fe(acac)_3$. $Fe(acac)_3$ (14 mg, 0.04 mmol) was added to UMCM-1-$(OBnNO_2)_2$ in 2 mL of EtOAc. After 24 h at RT, the supernatant was decanted and the crystals were washed profusely with EtOAc (4×10 mL). The crystals were soaked in 10 mL of EtOAc overnight and the process was repeated for a total of 3 days or until the supernatant was colorless. The crystals were washed with $CHCl_3$ (3×10 mL) and stored in $CHCl_3$ (12 mL) until further needed.

UMCM-1-FeCAT treated with $Fe(acac)_3$. Fe(acac)3 (14 mg, 0.04 mmol) was added to UMCM-1-CAT (40 mg) in 2 mL of EtOAc. After 24 h at RT, the supernatant was decanted and the crystals were washed profusely with EtOAc (4×10 mL). The crystals were soaked in 10 mL of EtOAc overnight and the process was repeated for a total of 3 days or until the supernatant was colorless. The crystals were washed with $CHCl_3$ (3×10 mL) and stored in $CHCl_3$ (12 mL) until further needed.

Solid State UV-Vis analysis. Approximately 15-20 mg of protected and deprotected UMCM (typically soaked in $CHCl_3$) was air dried before UV-Vis analysis. Solid state spectra were collected using an StellarNet EPP2000C spectrometer with a diffuse reflectance probe.

Geometric Calculation of Surface Areas. The accessible surface area of each structure was calculated from a simple Monte Carlo integration technique described previously (K.S. Walton, R.Q. Snurr, "Applicability of the BET method for determining surface areas of microporous metal-organic frameworks," *J. Am. Chem. Soc.* **129**, 8552-8556 (2007); T. Düren, F. Millange, G. Ferey, K.S. Walton, R.Q. Snurr, "Calculating geometric surface areas as a characterization tool for metal-organic frameworks," *J. Phys. Chem. C* **111**, 15350-15356 (2007)) where a probe molecule is effectively "rolled" over the framework surface. Briefly, a probe molecule was randomly inserted around each of the framework atoms in turn and checked for overlap with other framework atoms. The fraction of probe molecules that did not overlap with other framework atoms was then used to calculate the accessible surface area. The probe diameter was taken as the van der Waals diameter of nitrogen, 3.72 Å. By this method the calculated BET surface areas for UMCM-1-$(OBnNO_2)_2$ and UMCM-1-CAT were 3493 and 4120 m^2/g, respectively.

6.4 Acknowledgements

Text, schemes, and figures in this chapter, in part, are reprints of the materials published in the following papers: Tanabe, K. K., Allen, C. A., Cohen, S. M. "Photochemical Activation of a Metal–Organic Framework to Reveal Functionality" *Angew. Chem. Int. Ed.* **2010**, *49*, 9730-9733; Tanabe, K. K., Cohen, S. M. "Postsynthetic Modification of Metal-Organic Frameworks – A Progress Report." *Chem. Soc. Rev.* **2011**, *40*, 498-519. The dissertation author was the primary researcher and co-author for the data presented. The co-authors listed in these publications also participated in the research. The permissions to reproduce these papers were granted by Wiley-VCH Verlag GmbH & Co. KGaA, Weinheim, copyright 2010; and the Royal Society of Chemistry, copyright 2011.

6.5 Appendix

Table 6-1. Crystal data and structure refinement for UMCM-1-OBnNO$_2$.

Identification code	UMCM-1-OBnNO$_2$
Empirical formula	C51 H29 N O16 Zn4
Formula weight	1173.23
Temperature	205(2) K
Wavelength	0.71073 Å
Crystal system	Hexagonal
Space group	P 63/m
Unit cell dimensions	a = 41.275(2) Å α= 90°. b = 41.275(2) Å β= 90°. c = 17.5787(10) Å γ = 120°.
Volume	25936(3) Å^3
Z	6
Density (calculated)	0.451 Mg/m^3
Absorption coefficient	0.569 mm^{-1}
F(000)	3540
Crystal size	0.50 x 0.20 x 0.20 mm^3
Theta range for data collection	1.51 to 25.36°
Index ranges	-49<=h<=37, -47<=k<=49, -21<=l<=21
Reflections collected	168049
Independent reflections	16395 [R(int) = 0.0869]
Completeness to theta = 25.00°	99.9 %
Absorption correction	Semi-empirical from equivalents
Max. and min. transmission	0.8947 and 0.7641
Refinement method	Full-matrix least-squares on F^2
Data / restraints / parameters	16395 / 0 / 288
Goodness-of-fit on F^2	1.021
Final *R* indices [I>2σ(I)]	R1 = 0.0600, wR2 = 0.1917
R indices (all data)	R1 = 0.0867, wR2 = 0.2055
Largest diff. peak and hole	2.090 and -0.587 e.Å^{-3}

Table 6-2. Crystal data and structure refinement for UMCM-1-OH.

Identification code	UMCM-1-OH
Empirical formula	C44 H24 O14 Zn4
Formula weight	1038.11
Temperature	200(2) K
Wavelength	0.71073 Å
Crystal system	Hexagonal
Space group	P 63/m
Unit cell dimensions	a = 41.381(13) Å α= 90°. b = 41.381(13) Å β= 90°. c = 17.548(5) Å γ = 120°.
Volume	26023(14) $Å^3$
Z	6
Density (calculated)	0.397 Mg/m^3
Absorption coefficient	0.563 mm^{-1}
F(000)	3120
Crystal size	0.40 x 0.15 x 0.10 mm^3
Theta range for data collection	0.98 to 25.47°
Index ranges	-49<=h<=46, -47<=k<=48, -21<=l<=21
Reflections collected	169995
Independent reflections	16596 [R(int) = 0.1827]
Completeness to theta = 25.00°	100.0 %
Absorption correction	Semi-empirical from equivalents
Max. and min. transmission	0.9459 and 0.8062
Refinement method	Full-matrix least-squares on F^3
Data / restraints / parameters	16596 / 0 / 323
Goodness-of-fit on F^2	0.866
Final *R* indices [I>2σ(I)]	R1 = 0.0533, wR2 = 0.1005
R indices (all data)	R1 = 0.1281, wR2 = 0.1135
Largest diff. peak and hole	0.420 and -0.398 $e.Å^{-3}$

Table 6-3. Crystal data and structure refinement for UMCM-1-$(OBnNO_2)_2$.

Identification code	UMCM-1-$(OBnNO_2)_2$
Empirical formula	C58 H34 N2 O19 Zn4
Formula weight	1324.35
Temperature	200(2) K
Wavelength	0.71073 Å
Crystal system	Hexagonal
Space group	P 63/m
Unit cell dimensions	a = 41.288(2) Å α= 90°. b = 41.288(2) Å β= 90°. c = 17.5402(9) Å γ = 120°.
Volume	25894(2) $Å^3$
Z	6
Density (calculated)	0.510 Mg/m^3
Absorption coefficient	0.574 mm^{-1}
F(000)	4008
Crystal size	0.35 x 0.25 x 0.20 mm^3
Theta range for data collection	1.29 to 25.36°.
Index ranges	-44<=h<=49, -49<=k<=45, -21<=l<=20
Reflections collected	140103
Independent reflections	16358 [R(int) = 0.0797]
Completeness to theta = 25.00°	99.9 %
Absorption correction	Semi-empirical from equivalents
Max. and min. transmission	0.8938 and 0.8243
Refinement method	Full-matrix least-squares on F^2
Data / restraints / parameters	16358 / 0 / 307
Goodness-of-fit on F^2	0.981
Final *R* indices [I>2σ(I)]	R1 = 0.0609, wR2 = 0.1753
R indices (all data)	R1 = 0.0964, wR2 = 0.1861
Largest diff. peak and hole	0.565 and -0.563 $e.Å^{-3}$

Table 6-4. Crystal data and structure refinement for UMCM-1-CAT.

Identification code	UMCM-1-CAT
Empirical formula	C47 H26 N0.40 O15 Zn4
Formula weight	1097.76
Temperature	200(2) K
Wavelength	0.71073 Å
Crystal system	Hexagonal
Space group	P 63/m
Unit cell dimensions	a = 41. 377(3) Å α= 90°. b = 41. 377(3) Å β= 90°. c = 17. 5217(13) Å γ = 120°.
Volume	25979(3) $Å^3$
Z	6
Density (calculated)	0.421 Mg/m^3
Absorption coefficient	0.566 mm^{-1}
F(000)	3305
Crystal size	0.40 x 0.10 x 0.07 mm^3
Theta range for data collection	1.50 to 25.33°.
Index ranges	-49<=h<=49, -49<=k<=47, -21<=l<=15
Reflections collected	117586
Independent reflections	16376 [R(int) = 0.1218]
Completeness to theta = 25.00°	100.0 %
Absorption correction	Semi-empirical from equivalents
Max. and min. transmission	0.9615 and 0.8054
Refinement method	Full-matrix least-squares on F^2
Data / restraints / parameters	16376 / 0 / 286
Goodness-of-fit on F^2	0.839
Final *R* indices [I>2σ(I)]	R1 = 0.0477, wR2 = 0.1067
R indices (all data)	R1 = 0.1075, wR2 = 0.1165
Largest diff. peak and hole	0.451 and -0.471 $e.Å^{-3}$

6.6. References

(1) Eddaoudi, M.; Kim, J.; Rosi, N.; Vodak, D.; Wachter, J.; O'Keeffe, M.; Yaghi, O. M. *Science* **2002**, *295*, 469-472.

(2) Devic, T.; Horcajada, P.; Serre, C.; Salles, F.; Maurin, G.; Moulin, B.; Heurtaux, D.; Clet, G.; Vimont, A.; Greneche, J.-M.; Ouay, B. L.; Moreau, F.; Magnier, E.; Filinchuk, Y.; Marrot, J.; Lavalley, J.-C.; Daturi, M.; Ferey, G. *J. Am. Chem. Soc.* **2010**, *132*, 1127–1136.

(3) Garibay, S. J.; Cohen, S. M. *Chem. Commun.* **2010**, *46*, 7700-7702.

(4) Wang, Z.; Cohen, S. M. *Chem. Soc. Rev.* **2009**, *38*, 1135-1329.

(5) Tanabe, K. K.; Cohen, S. M. *Chem. Soc. Rev.* **2011**, *40*, 498-519.

(6) Yamada, T.; Kitagawa, H. *J. Am. Chem. Soc.* **2009**, *131*, 6312–6313.

(7) Gadzikwa, T.; Lu, G.; Stern, C. L.; Wilson, S. R.; Hupp, J. T.; Nguyen, S. T. *Chem. Commun.* **2008**, *43*, 5493-5495.

(8) Gadzikwa, T.; Farha, O. K.; Malliakas, C. D.; Kanatzidis, M. G.; Hupp, J. T.; Nguyen, S. T. *J. Am. Chem. Soc.* **2009**, *131*, 13613–13615.

(9) Deshpande, R. K.; Minnaar, J. L.; Telfer, S. G. *Angew. Chem. Int. Ed.* **2010**, *49*, 4598-4602.

(10) Kaye, S. S.; Long, J. R. *J. Am. Chem. Soc.* **2008**, *130*, 806-807.

(11) Blake, A. J.; Champness, N. R.; Easun, T. L.; Allan, D. R.; Nowell, H.; George, M. W.; Jia, J.; Sun, X.-Z. *Nature Chem.* **2010**, *2*, 688-694.

(12) Sato, H.; Matsuda, R.; Sugimoto, K.; Takata, M.; Kitagawa, S. *Nat. Mater.* **2010**, *9*, 661-666.

(13) Himsl, D.; Wallacher, D.; Hartman, M. *Angew. Chem. Int. Ed.* **2009**, *48*, 4639-4642.

(14) Mayer, G.; Heckel, A. *Angew. Chem. Int. Ed.* **2006**, *45*, 4900 – 4921.

(15) Il'ichev, Y. V.; Schworer, M. A.; Wirz, J. *J. Am. Chem. Soc.* **2004**, *126*, 4581-4595.

(16) Raymond, K.; Xu, J. In *United States Patent and Trademark Office*; Office, U. S. P. T., Ed.; The Regents of the University of California (Oakland, CA) US, 1999.

(17) Koh, K.; Wong-Foy, A. G.; Matzger, A. J. *Angew. Chem. Int. Ed.* **2008**, *47*, 677-80.

(18) Wang, Z.; Tanabe, K. K.; Cohen, S. M. *Inorg. Chem.* **2009**, *48*, 296-306.

(19) Tanabe, K. K.; Wang, Z.; Cohen, S. M. *J. Am. Chem. Soc.* **2008**, *130*, 8508-8517.

(20) Duren, T.; Millange, F.; Ferey, G.; Walton, K. S.; Snurr, R. Q. *J. Phys. Chem. C.* **2007**, *111*, 15350-15356

(21) Walton, K. S.; Snurr, R. Q. *J. Am. Chem. Soc.* **2007**, *129*, 8552-8556.

(22) Karpishin, T. B.; Stack, T. D. P.; Raymond, K. N. *J. Am. Chem. Soc.* **1993**, *115*, 6115-6125.

(23) Karpishin, T. B.; Stack, T. D. P.; Raymond, K. N. *J. Am. Chem. Soc.* **1993**, *115*, 182-192.

(24) Getman, R. B.; Miller, J. H.; Wang, K.; Snurr, R. Q. *J. Phys. Chem. C* **2011**, *115*, 2066–2075.

(25) Britt, D.; Furukawa, H.; Wang, B.; Glover, T. G.; Yaghi, O. M. *Proc. Natl. Acad. Sci. USA* **2009**, *106*, 20637-20640.

(26) Tanabe, K. K.; Cohen, S. M. *Inorg. Chem.* **2010**, *49*, 6766–6774.

(27) Koh, K.; Wong-Foy, A. G.; Matzger, A. J. *J. Am. Chem. Soc.* **2010**, *132*, 15005–15010.

(28) Gedrich, K.; Heitbaum, M.; Notzon, A.; Senkovska, I.; Fröhlich, R.; Getzschmann, J.; Mueller, U.; Glorius, F.; Kaskel, S. *Chem. Eur. J.* **2011**, *17*, 2099-2106.

(29) Choi, S. B.; Seo, M. J.; Cho, M.; Kim, Y.; Jin, M. K.; Jung, D.-Y.; Choi, J.-S.; Ahn, W.-S.; Rowsell, J. L. C.; Kim, J. *Cryst. Growth. Des.* **2007**, *7*, 2290-2293.

(30) Chowdhury, M. A.; Abdellatif, K. R. A.; Dong, Y.; Das, D.; Yu, G.; Velázquez, C. A.; Suresh, M. R.; Knaus, E. E. *Bioorg. Med. Chem. Lett.* **2009**, *19*, 6855-6961.

(31) Yamashita, K.-i.; Sato, K.-i.; Kawano, M.; Fujita, M. *New J. Chem.* **2009**, *33*, 264-270.